



Consiglio Nazionale delle Ricerche

IV Accordo di Programma MSE/CNR

CONSUNTIVO PAR 2015

“D.3: Processi e Macchinari Industriali”

Relazione Tecnica

A cura del referente Scientifico Ottorino Veneri

Dipartimento di Ingegneria,
ICT e Tecnologie per
l'Energia e i Trasporti

1 gennaio 2017
31 dicembre 2017

PAR 2015 – Relazione Tecnico-Scientifica

D.3: Processi e Macchinari Industriali

Progetto: Efficientamento dei processi di produzione e gestione integrata di utenze energivore con fonti rinnovabili e sistemi di accumulo mediante periferiche ICT in un contesto “Smart District”

Organizzazione del documento

Il manifatturiero è uno dei settori industriali più rilevanti dal punto di vista del consumo energetico: il miglioramento della loro efficienza può dare un contributo importante per raggiungere gli obiettivi contenimento del riscaldamento globale, su cui l'Europa si è impegnata da anni. L'efficientamento di sistemi così complessi richiede un approccio multi-disciplinare su più livelli, in grado di cogliere le opportunità che la tecnologia offre, dal singolo componente, alle macchine, ai sistemi produttivi e, più recentemente, anche nell'interazione con le reti intelligenti di fornitura di energia.

La linea 1 del progetto D.3 Processi e Macchinari industriali segue questa strategia: i cinque Work Packages che la compongono analizzano, con un approccio top-down, rispettivamente:

- il consumo energetico a livello di fabbrica, tenendo conto delle dinamiche di costo della fornitura di energia elettrica odierna. Ottimizzazione model-based rispettando i vincoli di processo, per processi continui caratterizzati da elevato consumo energetico (WP 1.1: Sistemi di controllo fabbrica avanzati model-based per l'ottimizzazione congiunta delle performance produttive e dei consumi energetici [CNR-ITIA])
- ottimizzazione energy-aware delle politiche di gestione dei sistemi produttivi discreti, con focus su macchine utensili e linee transfer (WP 1.2: Metodi di analisi e controllo per l'ottimizzazione congiunta delle performance produttive e dei consumi energetici di sistemi produttivi discreti [POLIMI])
- analisi gerarchica dei consumi di una macchina utensile. Definizione di una strategia di ottimizzazione dei parametri di processo. Proposta di metodologia di assessment per lo standard ISO 14955 “Environmental Evaluation of Machine Tools”. Estensione agli aspetti energetici dell'ontologia per la modellazione dei dati del sistema produttivo (WP 1.3: Efficienza energetica dei beni strumentali: la macchina utensile ed il processo di lavorazione [CNR-ITIA])
- metodologia per la caratterizzazione energetica sperimentale di diverse tipologie di mandrini per macchine utensili. Individuazione dei profili di utilizzo ottimali (WP 1.4: Metodologia per l'analisi dell'efficienza energetica dei moduli principali dei beni strumentali [POLIMI])
- sviluppo di materiali innovativi per la realizzazione di moduli per il recupero del calore tramite la conversione in energia elettrica (WP 1.5: Modulo Polimerico: ottimizzazione del power factor e fabbricazione dei moduli [ICMATE])

Questo documento riporta gli sviluppi della linea progettuale 1, presentati nel seguito suddivisi nei vari WorkPackages (WP): ogni sezione descrive, per il WP, il quadro generale di riferimento, gli obiettivi, lo stato dell'arte, gli sviluppi e i risultati.

Elenco dei Partecipanti al Progetto

- Consiglio Nazionale delle Ricerche – Istituto di Tecnologie Industriali e Automazione (CNR-ITIA)
- Consiglio Nazionale delle Ricerche – Istituto di Chimica della Materia Condensata e di Tecnologie per l'Energia (CNR-ICMATE)
- Politecnico di Milano – Dipartimento di Meccanica (POLIMI)

Si riporta di seguito una breve descrizione dei co-beneficiari Universitari coinvolti in questo progetto.

La sezione di Tecnologia e Produzione del dipartimento di Meccanica del Politecnico di Milano già da anni si occupa di aspetti energetici associati al Manufacturing ed al De-manufacturing. Ha sviluppato competenze sia per gli aspetti sperimentali sviluppando sistemi di misura per l'assessment energetico di macchinari sia per gli aspetti modellistici. Ha lavorato a diversi progetti sia nazionali che Europei (EROD Energy Reduction Oriented Design, Industria 2015, Ministero dello Sviluppo Economico. EMC2 - FoF.NMP.2011-1 - The Eco-Factory: cleaner and more resource-efficient production in manufacturing). Inoltre, questo gruppo di ricerca ha preso parte a circa venti convenzioni di ricerca stipulate con partner industriali, tra cui Ferrari GS, Bonfiglioli Riduttori, Neri Motori. Ha partecipato a due programmi ministeriali PRIN (2005 e 2007), e recentemente al progetto di mobilità elettrica MECCANO (programma Industria 2015), al quale hanno partecipato una quindicina d'aziende guidate dal Centro Ricerche Fiat (TO).

Partecipazione a progetti su tematiche affini

- EMC2-FACTORY: Eco Manufactured transportation means from Clean and Competitive Factory – 7° Framework Project ID: 285363
- Progetto SYMBIOPTIMA: Human-mimetic approach to the integrated monitoring, management and optimization of a symbiotic cluster of smart production units - Ambito: Horizon2020 - periodo: 2015-2018
- Progetto Factory Ecomation: Factory ECO-friendly and energy efficient technologies and adaptive autoMATION solutions - Ambito: FP7 - periodo: 2012-2015
- European Project Estomad "Energy Software Tools for Sustainable Machine Design". EU-FP7-ICT project; Feb/10-Aug/12
- ENEPLAN European Project: Energy Efficient Process Planning System (project No. 285461 FP7-NMP: The Eco-Factory: cleaner and more resource-efficient production in manufacturing), 10/2011 - 10/2014.
- EMVeM Project: Energy efficiency Management for Vehicles and Machines (prog No. 315967; Marie Curie Initial Training Networks (ITN) Call: FP7-PEOPLE-2012-ITN), 01/2013 - 12/2016.

Coordinamento tra le attività del presente PAR e le attività condotte dagli altri due beneficiari (ENEA ed RSE spa) nell'ambito dei rispettivi AdP

Le attività proposte si integrano in modo complementare con le attività proposte dagli altri affidatari dell'accordo di programma.

La linea 1 RSE "Supporto alle politiche energetiche nell'industria" fornisce un quadro generale sullo stato e potenzialità di risparmio dell'intero comparto industriale.

L'attività D.3 del CNR si propone di migliorare l'efficienza energetica dei processi produttivi, tramite metodi per ottimizzare la progettazione e gestione di sistemi di produzione. L'ambito è quindi quello delle attività RSE linea 2 e ENEA attività D.3, ma con obiettivi diversificati e complementari, come evidenziato nel seguito.

La linea 2 RSE, "Tecnologie per l'efficienza energetica nell'industria" propone i seguenti obiettivi:

- Membrane innovative per il contenimento energetico nei processi di produzione di gas tecnici.
- Celle microbiche per la produzione di energia elettrica da reflui: prototipi preindustriali.
- Cogenerazione: analisi dei materiali per impianti con microturbine a gas a combustione esterna – problemi di ossidazione e di erosione da particolato solido.

L'attività D.3 dell'accordo di programma ENEA propone i seguenti obiettivi

- Facility per la validazione delle prestazioni dei motori elettrici fino a 55 kW.
- Laboratorio per il controllo e verifica dell'eco-progettazione nei sistemi per la saldatura elettrica.
- Reattore in scala di laboratorio per la sperimentazione di nuovi materiali (catalizzatori) da utilizzare nella catalisi magnetica per induzione.
- Sistema prototipale ad assorbimento o adsorbimento per il recupero di calore di scarto a bassa temperatura.
- Prototipo di un sistema per l'applicazione di campi elettrici pulsati in un caso pilota.

La linea 1 D3 CNR agisce con un approccio analogo, analizzando però settori industriali e tecnologie diverse, considerando sia i processi continui che discreti, con diverse attività focalizzate su macchine utensili e relativi sistemi di produzione. In tal modo l'azione complessiva del progetto D.3 va a coprire settori industriali di rilevanza energetica, con importanza strategica commerciale per l'Italia.

- Inoltre è stato istituito un tavolo di coordinamento tecnico per le attività PAR 2015 – 2017 del gruppo tematico D3 – Processi e Macchinari industriali, composto dai relativi referenti del CNR, ENEA ed RSE. Tale coordinamento si propone di analizzare le attività proposte dei tre affidatari per il triennio 2015-2017, valutare la non sovrapposizione degli studi proposti e valutare l'azione sinergica delle medesime attività.

Costi

Costo totale del progetto € 400.000,00 (Il dettaglio dei costi è riportato nelle tabelle di rendicontazione)

Linea progettuale 1: Sistemi di controllo avanzati model based e generazione termoelettrica per l'ottimizzazione congiunta delle performance produttive e dei consumi energetici ed efficienza energetica dei beni strumentali.

Elenco dei Partecipanti alle attività

Unità di Ricerca	wp
<ul style="list-style-type: none"> Consiglio Nazionale delle Ricerche – Istituto di Tecnologie Industriali e Automazione (CNR-ITIA) 	1.1; 1.3
<ul style="list-style-type: none"> Politecnico di Milano – Dipartimento di Meccanica (POLIMI) 	1.2; 1.4
<ul style="list-style-type: none"> Consiglio Nazionale delle Ricerche – Istituto di Chimica della Materia Condensata e di Tecnologie per l'Energia (CNR-ICMATE) 	1.5

INDICE DELIVERABLES DEI WORK PACKAGES

WP 1.1: Sistemi di controllo fabbrica avanzati model-based per l'ottimizzazione congiunta delle performance produttive e dei consumi energetici [CNR-ITIA] **PAGG: 5-57**

Unità di ricerca coinvolta: Consiglio Nazionale delle Ricerche – Istituto di Tecnologie Industriali e Automazione (CNR-ITIA)

WP 1.2: Metodi di analisi e controllo per l'ottimizzazione congiunta delle performance produttive e dei consumi energetici di sistemi produttivi discreti [POLIMI] **PAGG: 58-69**

Unità di ricerca coinvolta: Politecnico di Milano – Dipartimento di Meccanica (POLIMI)

WP 1.3: Efficienza energetica dei beni strumentali: la macchina utensile ed il processo di lavorazione [CNR-ITIA] **PAGG: 70-166**

Unità di ricerca coinvolta: Consiglio Nazionale delle Ricerche – Istituto di Tecnologie Industriali e Automazione (CNR-ITIA)

WP 1.4: Metodologia per l'analisi dell'efficienza energetica dei moduli principali dei beni strumentali [POLIMI] **PAGG: 167-201**

Unità di ricerca coinvolta: Politecnico di Milano – Dipartimento di Meccanica (POLIMI)

WP 1.5: Modulo Polimerico: ottimizzazione del power factor e fabbricazione dei moduli [ICMATE] **PAGG:202-226**

Unità di ricerca coinvolta: Consiglio Nazionale delle Ricerche – Istituto di Chimica della Materia Condensata e di Tecnologie per l'Energia (CNR-ICMATE)

Attività WP 1.1: Sistemi di controllo fabbrica avanzati model-based per l'ottimizzazione congiunta delle performance produttive e dei consumi energetici [CNR-ITIA]

Quadro generale di riferimento, obiettivi e stato dell'arte

This document intends to give a detailed description of the model-based control system developed for the Energy-Aware Production Optimization (EAPO) of power-intensive industries based on the concept of Cyber Physical Systems (CPS). This tool not only helps those industries to increase their efficiency but also serves as the main enabler to participate in the energy markets under both dispatchable and non-dispatchable demand response programs and take advantage of their flexibility.

In Europe Demand-Response (DR) access to the deregulated markets is granted through balance responsible parties (BRP) and aggregators. BRPs are financially responsible to balance the expected electricity generation and demand profile for the suppliers and consumers under their jurisdiction. They bid their power profile in the wholesale day-ahead market and subsequently on the real-time market minimize the deviation of real profile from the contracted one. The participation of loads in the day-ahead energy creates a win-win situation for both the TSO and end user. While it helps TSO in balancing the power via BRP/aggregators, consumers can increase their economic welfare by exploiting their consumption flexibility. Furthermore, the consequent growth in the penetration of RES lowers the marginal electricity price by pushing the more expensive fossil fuel power plant out of the market, which is described as "merit-order effect".

The EAPO presented in this report is an optimal control software which can be customized for power-intensive process such as steelmaking and metal casting. The software is composed of two modules: 1: A day-ahead process optimization module, which receive production recipe and operational constraints together with energy price from BRP and produces daylong production setpoint that minimizes the cost of energy consumption. 2: A real-time module based on MPC (Model Predictive Control) approach, whose goal is to modify the day-ahead optimization in the presence of process variations and demand changes such that the committed load is followed as closely as possible. Both of these modules use the same operational constraints but with different objectives and in a different time scale. This difference in time-scale is the result of difference in the level of detail at which the process is required to be modelled based on the certainty of the available data.

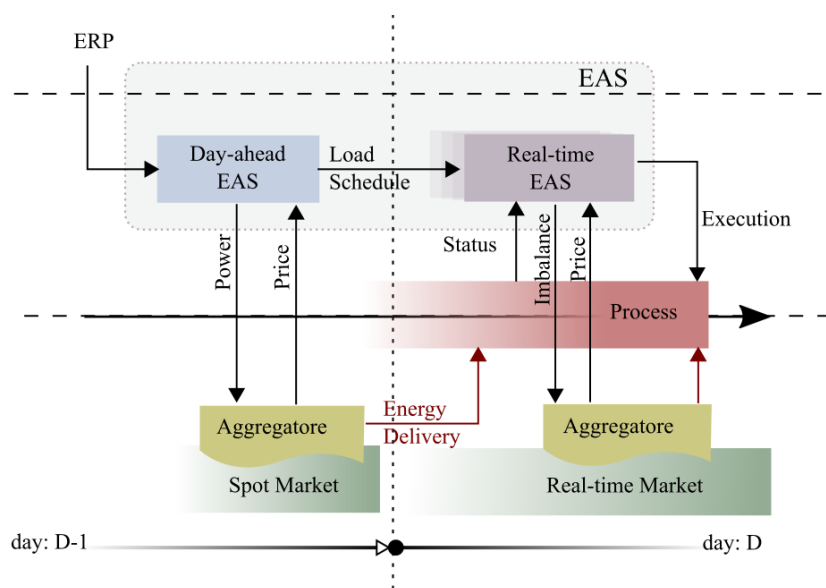


Figure 1 : Schematic view of Energy-Aware Solution modules and their interaction with market

Figure 1 illustrates different modules of EAPO scheme and their interaction with various market elements.

In the day before operation, EAPO involves multiple communications with the cluster aggregator where at each iteration EAPO modules receive the cost of electricity and reports back its consumption profile accordingly. Similarly, in the execution day, after the primary attempt to minimize the deviation from the pre-agreed load, real-time module of EAPO sends a request for additional power in case of negative imbalance, or inform the aggregator of its positive imbalance. Aggregator sums up the entire negative and positive imbalances within the cluster and bids accordingly in the real-time market. In addition, in the case of participation in the dispatchable demand response program, the real-time module should be able to react to a dispatch signal from TSO in an adequate amount of time.

The mathematical modeling approach is very similar for both off-line and on-line optimization. However, while the former focuses on the economic aspects of operation on a daily or weekly basis, the latter is formulated as an MPC to follow the optimal load reference and - if necessary - re-optimize it over a shorter time window.

Subsequently, the modeling process presented here does not differentiate these two modules. From the optimization point of view, the real-time problem can be considered a sub-problem with respect to the off-line version and thus computationally more tractable. Even though a one-shot optimization over an intended horizon (day or week) can produce an optimal result, the rolling horizon concept – similar to the one used for on-line optimization – can be implemented for the off-line optimization to renders the problem computational less expensive by temporal decomposition, which of course is achieved at the cost of compromising optimality. Thus, in the development of the customized model for each application a great deal of effort has been made to make the optimization engine as fast as possible.

In the rest of this report, first we introduce the optimization and control architecture based on Cyber-Physical Systems. Then we give a brief description of EAPO as an optimization engine in both off-line and on-line modules. Subsequently the rolling horizon framework is discussed based on which the MPC module works. At the end, we describe the model development procedure and EAPO adaption for two cases of power intensive processes: steelmaking and metal casting. For each of these cases we show the economic benefits of the proposed control and optimization system. Finally, the report draws some conclusions and remarks on future directions.

CPS-based Architecture

The execution of the Energy-Aware Scheduler requires an interconnection with the physical process and the management of the data flow from (and to) the field.

The interaction with the plant is achieved by the development of a digitalization layer based on the concept of Cyber-Physical Systems (CPS). The architecture of the Energy-Aware Production Optimization (EAPO) is represented in *Figure 2*. Each component of the process is framed as a single Cyber-Physical System, where a CPS is an entity with three main features: communication, computation and control. The physical component, e.g. in the steel application the Electric Arc Furnace, is typically a stand-alone atomic element of the process controlled by its Programmable Logic Control (PLC) unit, where the communication between the process I/O channels and the controller is based on a proprietary protocol (e.g. Modbus, Profibus, analog signals, etc.). This condition makes the components interconnection (or the connection to an external service, like the EAPO) a hard task.

The OPC-UA has been selected to overcome this issue, as an interoperable service-oriented architecture for the data exchange among components. To this aim, an OPC-UA Wrapper has been conceived to enable an

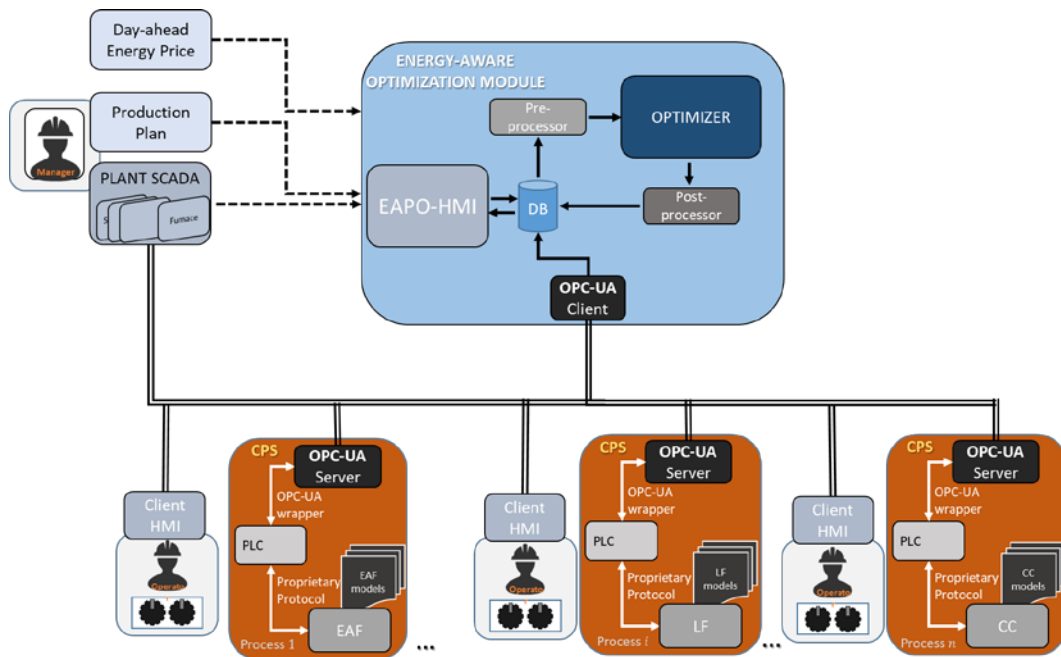


Figure 2 CPS-based architecture for Energy-Aware Production Optimization

OPC-UA Server module for each CPS. The Wrapper maps the PLC variables in the OPC-UA framework, making them available and accessible to other process module where an OPC-UA Client is instantiated.

In the EAPO architecture, the Energy-Aware Optimization module is equipped with the OPC-UA Client, which connects to the OPC-UA Servers existing on the network to fetch updated information about the components status and their variables.

The current information about the systems are stored in a database, which is also a repository of other internal and external data flows. The other external data required by the EAPO are introduced by a front-end application, the EAPO-HMI. This HMI permits the user (e.g. the plant manager) the configuration of the EAPO or the input of production info; moreover it can connect to external services or repositories to retrieve data, like the day-ahead energy price or the task list from the production plan. Additional data can be acquired from the connection with the plant SCADA system.

The optimization of the process is achieved by the solution of a Mixed-Integer Linear Program. The pre-processing module constructs the optimization problem, by fetching data from the internal database and using the process model.

In the CPS framework, the cyber part can contain also a repository of component models, which can be used in the configuration of the EAPO module to construct the overall process model required for the optimization. The solution obtained by the EAPO is stored in the database and sent to the EAPO-HMI after a post-processing phase.

The EAPO-HMI provides the EAPO results to the manager and plant operators. In large and distributed plants, the transmission of the solution to the different users is done through a client human machine interface, made available to every operator.

Model-based Energy-Aware Optimization

The main goal of EAPO is to enable an energy-intensive process plant to realize its demand-side response potential at the production control level, finding a compromise between production delays and the cost of energy. This implies the need of proper day-to-day control of plant operations through proper modelling

techniques capable of exploiting incentive and price based schemes, such as for example intra-day or day-ahead spot market pricing, as changes in the prices of energy might significantly affect the profitability.

Assuming that the goal of a company is to deliver certain amount of products and by-products within a predefined time window, the energy-aware optimization concept seeks to schedule the production in favor of a period with a lower cost of energy procurement, which would be otherwise an under-utilized interval with respect to the production capacity. The exploitation of this surplus capacity could provide the plant manager a degree of freedom in most cases where the due-dates are not so strict. In addition to the economic potential, such as energy cost saving, EAPO helps to lower the emission by reduction of peak generation in the power grid. More importantly, regarding the environmental impact, the flexibility that such scheme offers can serve as the main enabler for the integration of renewable energy sources through financial justification, which would be otherwise challenging considering the intermittent nature of these resources. The peak-time reduction can also decrease the risk of power cut thus improve the reliability of the power grid.

In order to achieve all above-mentioned goals, the EAPO proposed here will go beyond the conventional mono-objective optimization scheme and tries to address all these goals explicitly within a multi-objective scheduling framework. While a mono-objective approach can only offer an exploratory balance of production related objective (e.g. makespan) and the energy costs and emissions footprint, a multi-objective optimization provides as output a set of Pareto optimal alternatives. One of its main advantages is that it allows articulating the decision makers' preferences in the post-optimal analysis of the solutions found. This makes it possible to identify solutions that achieve large production performance improvements at a marginal increase in the energy cost.

However, in reality, a day-ahead EAPO would be very much impractical, as it is developed mainly based on the assumption that the process remain as predicted for a whole day. On the other hand, it is necessary for each company to participate in the day ahead price-based scheme in order to take advantage of an EAPO. To deal with this issue a real-time adjustment concept will be developed as a complementary scheme to the day-ahead scheduling paradigm whose goal is to compensate the effect of unforeseen events and uncertainties.

Uncertainties are a major element in any real-time decision process where the information about the presence and the future unfolds iteratively. The nature of uncertainties can be different in various levels: uncertainties in online scheduling are related to the availability of resources (breakdowns, lack of personnel), uncertain yields or unsuccessful production steps, uncertain durations of operations, and, often most importantly, dynamically changing demands or targets.

The approach that is proposed here to handle uncertainties in scheduling is dynamic re-optimization also called Rolling horizon strategy. In model-based scheduling, the decisions are optimized over a forecast horizon in order to take longer term effects due to the inertia of the system into account, but only a subset of "next" decisions or optimized variables have to be fixed and implemented based upon the available information on the new state of the system and new requirements. Taking into account the real progress of the operations and new information about the production targets, all decisions that can be modified are recomputed iteratively, assuming the system to be perfectly modelled, and the "plant" and the external disturbances to be deterministic. If the computation time required for full re-planning is too long for a frequent online application, reactive planning can approximate it, modifying nominal plans when an unexpected event occurs.

There is a wide range of aspects that need to be considered in developing the scheduling model. The most fundamental of these aspects, which has a direct influence on the complexity of problem, is the development of a simplified, though accurate, representation of the production process. Such a model would eventually serve as the mapping between the real process components, and the decision variable and constraints within

the optimization model. Problem representation serves as the basis on which an effective optimization technique can be developed either using mathematical programming techniques as in MIP or Constraint Logic Programming and Constraint Satisfaction.

The most practiced process layout in the industry is the sequential layout, in which batches are processed either in single or in multiple stages. The required elements to represent such a topology are batch orders and production units belonging to one or more individual production stage. In the case batch size are determined a priori, the scheduling problem would boil down to batch-unit matching, stage sequencing, process timing and fixing the due-date. Otherwise, production orders are utilized instead of batches within the same context.

Time representation is the first aspect needed to be taken into consideration in the problem formulation procedure of scheduling problems, considering industrial process requirements as complexity and required execution time.

The time representation approaches are often divided into two subgroups according to their physical features: discrete and continuous models. The main differences between these two approaches are whether decisions are formulated as variables, constraints or combination of these.

Discrete-time approach divides the time horizon into evenly or non-evenly distributed time grids, at which decisions may take place. In discrete-time approaches, the integration of energy and other material/inventory constraints is straightforward. Nevertheless, the accuracy of the problem representation may be insufficient as the problem complexity and size grow with the number of grid points needed to represent the time axis. Adopting a continuous time formulation, decisions can take place anywhere on a continuous time axis, without adding to problem complexity

The main drawback of continuous-time approaches is the difficulty of formulating balances, as there are no clearly defined balance points. Even though continuous-time models generally outperform discrete-time models, concerning solution efficiency and quality, discrete-time models remain popular for industrial problems, keeping the debate over the effectiveness of discrete versus continuous-time representation open, as both formulations have complementary strengths and the ideal approach should combine the advantages of both. The decision to explore approximate process models (in the context of phenomenological representation of transportation activities between stages) makes sense in the context of a discrete-time formulation, which in general is unable to consider the exact processing times.

The main advantage of discrete time modelling is the knowledge of exact location each time instance, which makes it possible to include the dynamically coupled resources or the exogenous events effecting the underlying process. The main instance of such resources concerning the specific problem in hand is the changing electricity price and availability of the power.

The only downside of a discrete model is the inability to exploit the continuity of time to deliver a globally optimal solution. However, when dealing with even slightly stochastic processes, the optimality obtained through continuous-time approach could ironically leads to a suboptimal or even infeasible solution of the secondary real-time optimization.

In fact, the initial sub-optimality of the discrete approach would exclude feasible spaces in the resource-time space, which can later accommodate the variations due to the stochasticity of process. Such a conservative approach is inevitable but only inherent a conservatism from the upper production planning level when dealing with stochastic processes such as melting in a foundry

On the other hand, it is more straightforward to consider dynamic operational constraint in discrete formulation. Of course, the nature of these constraints may vary from one plant to another depending on furnace technology and the level of automation.

Production Control Scheme

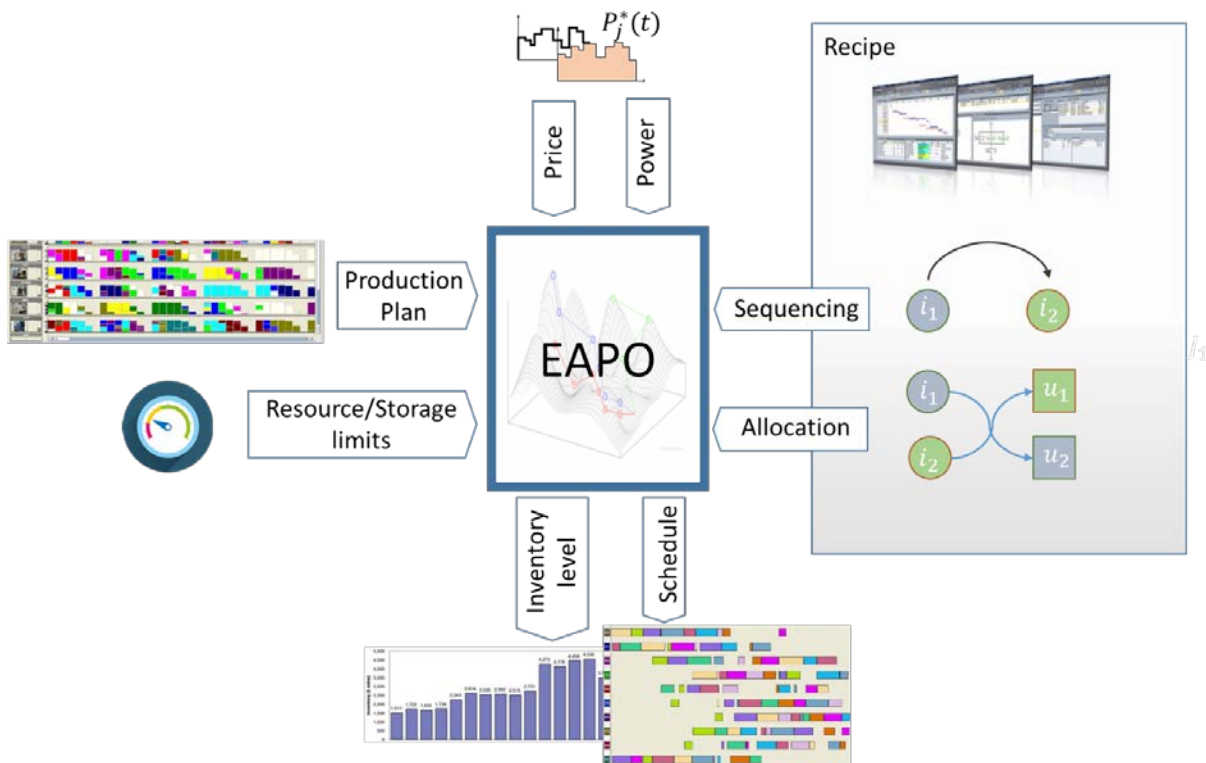


Figure 3 Energy-Aware Process Optimization

As mentioned previously, the main challenge of employing a precedence-based scheduling model, which is inherently defined in continuous domain, within an energy-aware scheduling framework is the inclusion of energy consumption. In order to address this issue a grid-based model is introduced based on the time grid corresponding to the day-ahead electricity price, which is assumed constant for a fixed time interval of one hour. Such a model will enable the optimizer to minimize both the electricity consumption cost and the deviations from the pre-agreed power consumption. While the former minimization can be exploited by DSM during the day-ahead planning to produce an optimal power profile, the latter would allow each company to follow this profile while adjusting in real-time to the unforeseen conditions and change of plans.

Rolling Horizon Framework

In order to take into account unforeseen events and dynamic variations from the nominal process model and - eventually- plan, here we propose a rolling horizon algorithm as the real-time adjustment mechanism. In this scheme, based on the day-ahead plan, optimization is performed within a shifted time window to take into account the corresponding unforeseen circumstances that are unfold with time and produce a new feasible set point.

An important advantage of such a framework is the reduction of problem size by optimizing the process on a relatively short horizon instead of the original daylong horizon. In addition, temporal decomposition method can also be used within the rolling horizon framework to further reduce the solution space. This concept is based on the fact that further you get from the current time (i.e. beginning of the rolling horizon) the less accurate the solution requires to be. In this approach, the control horizon is divided into aggregated

and detailed time periods based on the minimum time interval in which the cost of electricity can be considered constant. Such a reduction in space comes with the cost of compromising the optimality. The longer the length of control horizon, the less optimal is the solution. However, considering the fact that rolling horizon algorithm is going to be implemented only for real-time adjustment where the objective is to follow a previously agreed power profile, such a negative effect on the optimality can be neglected. It should be taken into account that the crucial step in realizing the rolling algorithm is finding an aggregated model, which can solve a relaxed version of the problem and produce a lower bound on the cost function.

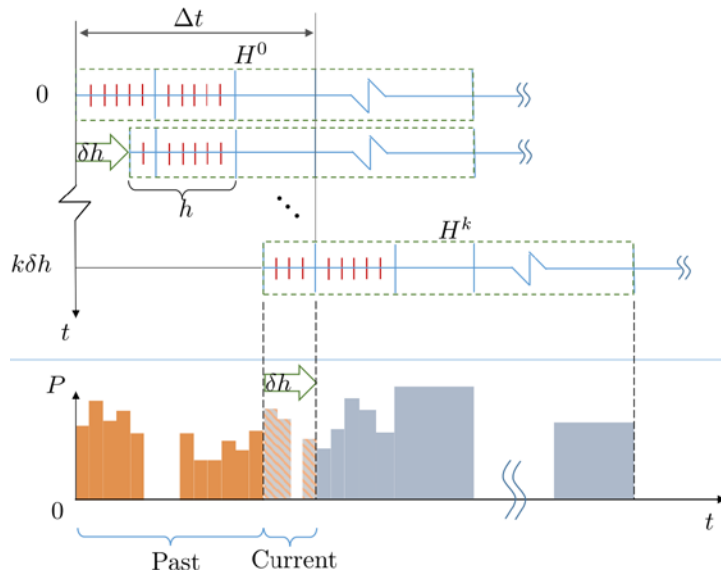


Figure 4: Rolling horizon and temporal decomposition scheme

Figure 4 illustrates how this method is used for real-time adjustment of production plan. Once the process is optimized for the combined horizon the detailed time interval schedule is fixed as the new optimal schedule and the optimization horizon moves forward for the successive optimization, starting from first aggregate time block of previous solution. The new optimization horizon is again divided into detailed and aggregated time blocks and the optimization is carried out iteratively.

Case Studies

In this section, we describe the synthesis of the model-based process control system for joint optimization of production performance and energy consumption for two cases of energy intensive process: steelmaking and metal casting. In each case first a brief description of the plant is given, then the corresponding mathematical model is developed for two different time scales: short-term and medium-term optimization horizon. While the former is designed to control the production within the operation day, the latter aims at a weeklong horizon. Consequently these models have different characteristic and scopes.

Steelmaking Process

Process layout

The steel manufacturing process can be modelled as a flow shop with essentially three main stages: melting of the scrap metal, adjusting the chemical composition and performing thermal processes and continuous casting. The middle stage can contain different sub-processes, depending on steel quality and plant layout. Accordingly, a typical steel plant layout consists of production steps (tasks) as show in the Figure 5

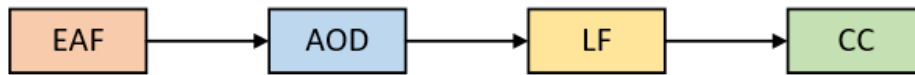



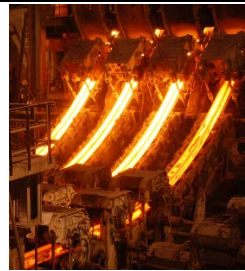


Figure 5 - Steel manufacturing typical flow shop

Solid scrap metal from recycled steel is first molten in the Electric Arc Furnace (EAF), and then further processed in the Argon Oxygen Decarburization unit (AOD) to reduce carbon content. The molten steel is then chemically refined in the Ladle Furnace (LF) and finally transported in ladles to the Continuous Caster (CC) to be casted into slabs or billets (final product).

To sum up:

Unit type	Electric Arc Furnace	Argon Oxygen Decarburizer	Ladle Furnace	Continuous Caster
Tag	EAF	AOD	LF	CC
Picture				
Task	Melting of scrap metal	Reducing carbon content	Adjusting chemical composition	Casting
Power consumption	Huge (50-100 MW)	Very low (1-3 MW)	Very low (1-3 MW)	Low (5-8 MW)

The steel can be characterized by grade, slab width and thickness a/o billet diameter. Different kind of products require different chemical ingredients and different casting procedures. The first three tasks operate in batch mode, which means that a specified amount of metal is processed at a time. Each lot of metal is called a “charge” or a “heat”. On the other hand, the casting stage operates continuously and has some critical processing constraints. Due to the extreme conditions in the caster, it can only process a limited number of heats, after which it needs maintenance, such as changing the tundish and the mold, before further operation. For this reason, several heats sharing the same or very similar grade and shape requirements are casted sequentially in groups or “batches”. The casting order should follow certain rules and cannot be interrupted.

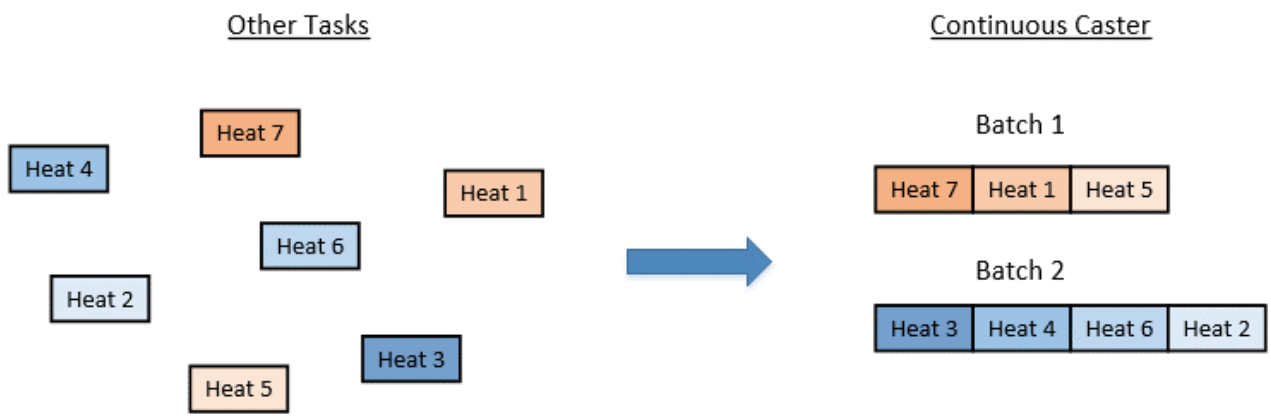


Figure 6 - Heats and batches

The four units of this simplified layout (EAF, AOD, LF and CC) can obviously be arranged into complete or partial parallel lines, possibly changing the path of a single heat but keeping intact the overall pattern of the flow shop. The molten steel is transported from a process unit to the subsequent through ladles, meaning that transport time must be taken into consideration as it lasts for a significant time, subjected to a minimal (technical reason) and maximal (temperature degradation) time span. Following these general framework, this is an example of daily schedule of a single line steel melt shop, with 12 heats divided into 3 batches.

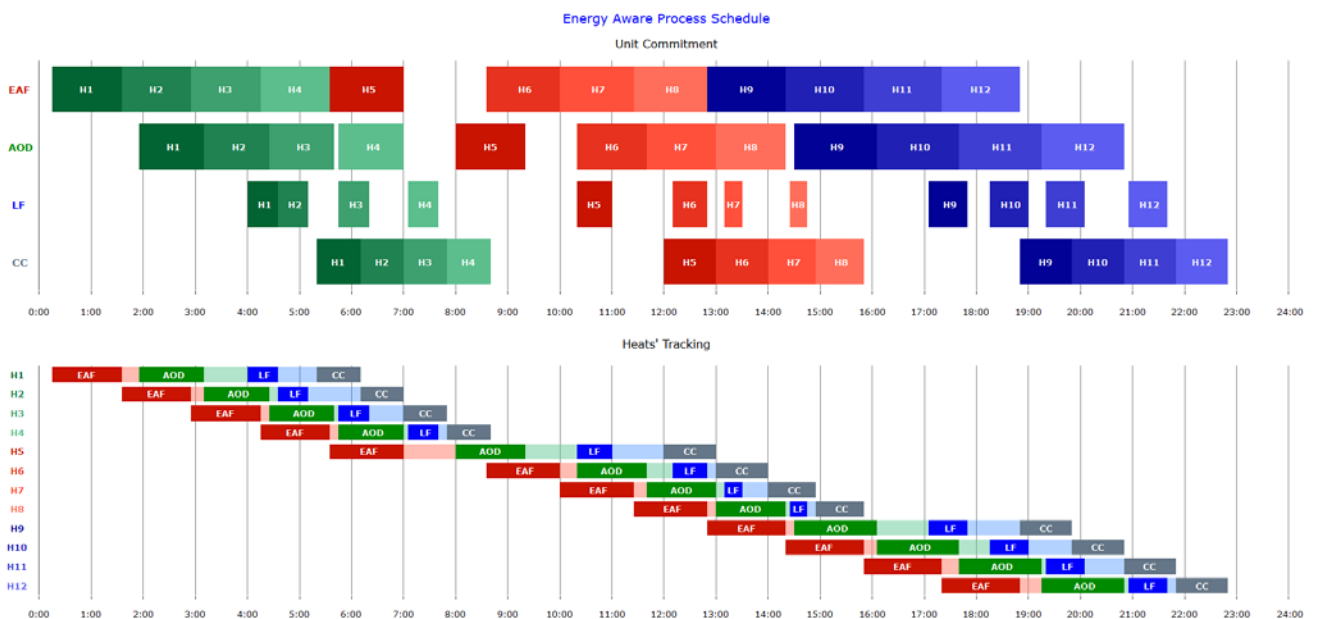


Figure 7 - Example of a feasible daily schedule

At the top, time commitment of the four units (EAF, AOD, LF and CC) has been shown where every rectangle represents a task. Every heat has been identified by a tag and a colour, which remains the same throughout the different stages of process. The first three stages do not have particular constraints, besides the non-overlapping of multiple tasks (single line, in this case). On the other hand, the Continuous Caster operates strictly continuously within groups of heats (batches), known a-priori and sharing similar chemical or geometrical properties, thus the similar colour tone.

At the bottom, the very same schedule is given in the perspective of the heats. (The colours in this graph should be associated with the ones used for distinguishing each heat in the upper pannel)

- EAF (melting) tasks are in red
- AOD (decarburization) tasks are in green
- LF (chemical adjusting) tasks are in blue
- CC (continuous casting) tasks are in grey
- The transportations are in transparent colours

Preface on optimal schedule

Typically, job shop and flow shop scheduling are considered strongly NP-hard problems. To partially reduce complexity, optimization models related to this topic are designed to deal with one of these two issues:

1. How molten steel heats should be arranged in casting groups and in what sequence (sequencing problem)
2. At what time and in which machine to perform every task of the plan (unit commitment)

The first issue is of a combinatorial nature and focus only on the continuous caster sequencing, because it is the bottle-neck of the whole process both due to its continuous nature and its non-flexibility. The second one assumes the casting grouping and sequence as constant and focuses on optimizing the pure unit commitment and timing of the tasks. This documentation will consider only optimization models aiming at the latter issue. As will be further explained, energy cost minimization will be, in some cases, coupled with other production planning goals such as minimization of makespan, delivery time tardiness a/o earliness and CO2 emissions, making the optimization multi-objective.

MILP models for optimal daily schedule

This section discusses in detail a discrete-time model for the daily optimal scheduling of steelmaking process based on Mixed Integer Linear Programming technique. We describe in detail the possible inputs that can be selected by the end user to reflect their priorities for the particular application in hand.

Scheduling Parameters:

The problem data can be divided into 6 categories:

- **Heats and batches**
Contains the list of heats ($H_1 \dots H_H$) to be scheduled, the batch they belong ($B_1 \dots B_B$) and the sequence order within the casting group (batch). Moreover, each heat has a specific the delivery time which it is due and advance and delay fees (€/h)
- **Processing times**
Each heat has a nominal processing time at each unit of the process (EAF, AOD, LF and CC). The nominal processing time is the forecasted process time (in minutes), considering the unit to work constantly at nominal power. In case a unit can operate at variable power (it is flexible), the processing could be different from the nominal one, but the total energy required for the process (computable as nominal power times nominal processing time) is kept constant
- **Units' settings**
Each unit (EAF, AOD, LF and CC) has a nominal power (in MW), a binary representing if it is flexible or not (in term of power consumption rate) and, if it is flexible, minimum and maximum power it can absorb. The set-up time for the Continuous Caster (CC) is required (in minutes)

- **Transports' settings**

The three transfers within the flow shop (from EAF to AOD, from AOD to LF and from LF to CC) should have a minimum and a maximum time range (in minutes)

- **Hourly variable electricity price**

The predicted day-ahead price, which is a set of Hr (number of hours) float numbers (€/MWh) is required, as well as a single contracted fixed price (for economic comparisons)

- **Optimization settings**

A set of parameters to address the general-purpose model to specific needs:

- Time:
 - Hr = number of hours (e.g. 24, for daily schedule)
 - δ = single time step width (minutes)
- Plant layout:
 - U = number of parallel lines, equals to each other (typical value 1)
 - Flexibility = binary denoting the presence of flexible units
 - Flexmode = [*constant power / full flex*] representing the flexibility logic. *Constant power* means that the unit must choose a single power level (within a finite set) and keep it until the task is completed. To compute the set of possible power levels, we assume that each task ends exactly at the interface between two consequent discrete time steps. Therefore, the flexible task can last an integer number of time steps between the steps needed at constant maximum power and the steps needed at constant minimum power. Each of these power levels are called '*modes*'. On the other hand, *full flex* means the power can vary arbitrarily at each time step. As mentioned before, in both flexible cases, the total energy required for the task has to be fulfilled
- Constraints options:
 - Order = binary denoting if the heats should be ordered by delivery time or not (1 is extraordinary faster)
 - Delivery = binary denoting if the delivery time is taken into consideration
 - Slack = binary that allows a delivery time cost-wise overtaking. If delivery = 1 and slack = 0, there's a hard constraint disallowing each heat to finish the process after its delivery time
- Objective:
 - Selectable among '*energy cost*', '*makespan*' or '*best delivery*'
- Solver parameters:
 - Precision = MIPGap (%)
 - TimeLimit = max solving time (in minutes)

Nomenclature:

Sets

Tag	Index	Description
T	t	Discrete time steps (time = $t_1, t_2, t_3, \dots, t_T$)
H	h	Heats to be processed within the time horizon

B	b	Batches (group of heats with similar casting settings)
CO _b	co	Heats' casting order of batch b (example: CO _{B1} = [H ₁ , H ₂ , H ₃ , H ₄])
P	p	Processes (or units): melting (EAF), decarburization (AOD), ladle (LF) and casting (CC)
FU	p	Set of flexible units (or processes)
FU ^{cp}	p	Set of flexible units (or processes) with flexmode 'constant power', FU ^{cp} ⊆ FU
FU ^{ff}	p	Set of flexible units (or processes) with flexmode 'constant power', FU ^{ff} ⊆ FU
TR	tr	Transports from one unit to the next (EAF to AOD, AOD to LF, LF to CC)
I _{p,h}	i	Set of modes (constant power levels) for flexible process p's unit, processing heat h

Constants (parameters)

Tag	Description
δ	Single time step width [minutes] (the model is discrete-time)
Hr	Number of hours to schedule
U	Number of parallel lines (equal to each other)
d _{p,h}	Duration (nominal) of process p for heat h [minutes]
dt _h	Delivery time (or due time) for heat h
af _h	Advance fee for heat h [€/h]
df _h	Delay fee for heat h [€/h]
TT _{tr} ^{min}	Minimum transfer time of transport tr [minutes]
TT _{tr} ^{max}	Maximum transfer time of transport tr [minutes]
CCsut	Continuous caster set-up time [minutes]
PW _p	Nominal power of process p's unit [MW]
PW _p ^{MIN}	Minimum power of flexible process p's unit [MW]
PW _p ^{MAX}	Maximum power of flexible process p's unit [MW]
Etot _{p,h}	Total energy required for process p of heat h [MW*min]
flex _{p,h,i}	Constant power level of mode i for flexible process p's unit processing heat h [MW]
ELprice _t	Electricity price at time step t [€/MWh]
ELfp	Electricity fixed price [€/MWh]

Set T length is computed as follow:

$$T = int\left(\frac{Hr \cdot 60}{\delta}\right)$$

Variables

List of all the variables. Note two things:

- The model is generic: not all of these variable are always present in the model, but some of them depends on specific optimization settings (e.g. units' flexibility, slack)
- Not all the variables are *decision variables* (my bad): many dependant variables have been added to simplify the constraints implementation. In any case, these dependant variables should not slow down the solver

Tag	Description	Type	Lower bound	Upper bound
S _{p,h}	Start of process p for heat h	integer	1	T
F _{p,h}	Finish (or end) of process p for heat h	integer	1	T
TRS _{tr,h}	Start of transport tr for heat h	integer	1	T
TRF _{tr,h}	Finish of transport tr for heat h	integer	1	T
SUS _b	Start of continuous caster set-up at the end of batch b	integer	1	T
SUF _b	Finish of continuous caster set-up at the end of batch b	integer	1	T

$\Omega_{p,t}$	Occupation of process p's unit at time t	integer	0	U
$k_{p,h,t}$	Auxiliary variable to link start of processes to units' occupation	binary		
$w_{p,h,t}$	Auxiliary variable to link start of processes to units' occupation	binary		
$y_{p,h,t}$	Auxiliary variable to link start of processes to units' occupation	integer	-(T+1)	T
EL_t	Electric energy consumed at time t [MWh]	continuous	0	$+\infty$
$mode_{p,h,i}$	Choice of flex mode i by process p of heat h	binary		
$Si_{p,h,i}$	Start of process p of heat h in flex mode i (0 if i not chosen)	integer	0	T
$ki_{p,h,t,i}$	Auxiliary variable to link start of p by h at mode i to Ω	binary		
$wi_{p,h,t,i}$	Auxiliary variable to link start of p by h at mode i to Ω	binary		
$yi_{p,h,t,i}$	Auxiliary variable to link start of p by h at mode i to Ω	integer	-(T+1)	T
sld_h	Slack variable representing time slots of advance in delivery	integer	0	T
sld_h	Slack variable representing time slots of delay in delivery	integer	0	T
$\Omega_{su_{b,t}}$	Occupation of units CC for setup of batch b at time t	integer	0	U
$ksu_{b,t}$	Auxiliary variables to link start of setup to CC unit occupation	binary		
$wsu_{b,t}$	Auxiliary variables to link start of setup to CC unit occupation	binary		
$ysu_{b,t}$	Auxiliary variables to link start of setup to CC unit occupation	integer	-(T+1)	T
$\Omega_{flex_{p,h,t}}$	Occupation of units for flexible process p for heat h at time t	integer	0	U
$Pflex_{p,h,t}$	Flexible power for process p for heat h at time t	continuous	0	PW_p^{MAX}

While almost all the variables' meaning is basically straight forward, here follows a description of auxiliary variables y , k and w , whose task is to logically connect the start and finish of a task (variables) to the occupation of the unit (Ω variable). The y - k - w trio is present in three versions (for a regular task, for a constant power flexible mode task and for the CC setup after a batch is completed), maintaining this common logic:

- y is a positive integer before the start of the task, a negative integer after it and takes exactly the value 0 at the time slot which is the value of variable S
- k is a binary of value 0 before the start of the task and 1 after
- w is a binary of value 1 before the finish of the task and 0 after

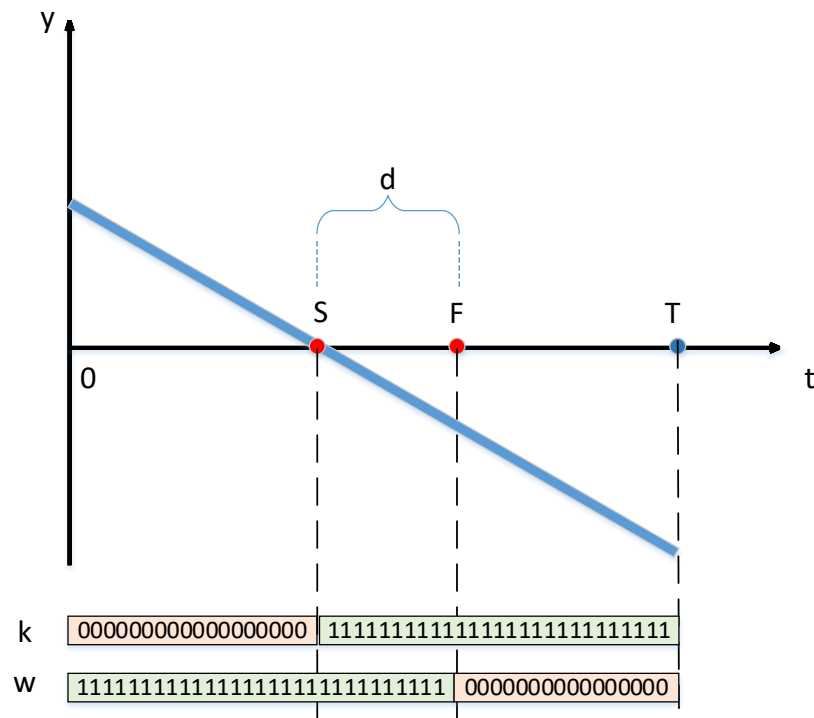


Figure 8 - graphical interpretation of auxiliary variables y , k and w

The set of constraints associated with these three variables will make it Easier to understand them.

Constraints

Time constraints (non-flexible units):

$$F_{p,h} = S_{p,h} + \text{int} \left(\frac{d_{p,h}}{\delta} \right) - 1 \quad \forall p \in (P \setminus FU), \forall h \in H$$

The end of each task $F_{p,h}$ is related to its start $S_{p,h}$ through the specific duration $\frac{d_{p,h}}{\delta}$. In case the task duration (in minutes) is not integrally dividable by δ , the ratio is rounded to next integer

Time constraints (flexible units with flexmode 'constant power'):

$$\sum_{i \in I_{p,h}} \text{mode}_{p,h,i} = 1 \quad \forall p \in FU^{cp}, \forall h \in H$$

$$\sum_{i \in I_{p,h}} Si_{p,h,i} = S_{p,h} \quad \forall p \in FU^{cp}, \forall h \in H$$

$$Si_{p,h,i} \leq \text{mode}_{p,h,i} \cdot T \quad \forall p \in FU^{cp}, \forall h \in H, \forall i \in I_{p,h}$$

$$F_{p,h} = S_{p,h} + \left[\sum_{i \in I_{p,h}} \text{mode}_{p,h,i} \cdot \text{int} \left(\frac{Etot_{p,h}}{\text{flex}_{p,h,i} \cdot \delta} \right) \right] - 1 \quad \forall p \in FU^{cp}, \forall h \in H$$

Only one power level (mode i) can be chosen for each heat and flexible process. The start of this mode $Si_{p,h,i}$ should be equal to $S_{p,h}$ if the mode is chose, 0 otherwise. In this case, the task duration is not completely fixed, but chosen within a set, consequent to the ratio between the total energy needed for the task $Etot_{p,h}$ and the power level $\text{flex}_{p,h,i}$ of mode i

Time constraints (flexible units with flexmode 'full flex'):

$$F_{p,h} = S_{p,h} + \sum_{t \in T} \Omega \text{flex}_{p,h,t} - 1 \quad \forall p \in FU^{ff}, \forall h \in H$$

In this case, the task duration is not fixed, but depends on the occupation (in full flexible mode) of the unit. Obviously, Ωflex will be further constrained

Transports constraints:

$$TRF_{tr,h} \geq TRS_{tr,h} + \text{int} \left(\frac{TT_{tr}^{min}}{\delta} \right) - 1 \quad \forall tr \in TR, \forall h \in H$$

$$TRF_{tr,h} \leq TRS_{tr,h} + \text{int} \left(\frac{TT_{tr}^{max}}{\delta} \right) - 1 \quad \forall tr \in TR, \forall h \in H$$

The end of each transport must be within minimum and maximum transfer time distance from its start

Process order of each heat (flow shop):

$$TRS_{EAF-AOD,h} = F_{EAF,h} + 1 \quad \forall h \in H$$

$$S_{AOD,h} = TRF_{EAF-AOD,h} + 1 \quad \forall h \in H$$

$$TRS_{AOD-LF,h} = F_{AOD,h} + 1 \quad \forall h \in H$$

$$S_{LF,h} = TRF_{AOD-LF,h} + 1 \quad \forall h \in H$$

$$TRS_{LF-CC,h} = F_{LF,h} + 1 \quad \forall h \in H$$

$$S_{CC,h} = TRF_{LF-CC,h} + 1 \quad \forall h \in H$$

Set of constraints to respect processes' and transports' order. Every consecutive process starts exactly after the previous has ended

Continuous Caster (CC) constraints:

$$S_{CC,g} = F_{CC,(g-1)} + 1 \quad \forall b \in B, \forall g \in CO_b \wedge g \neq CO_b[first]$$

$$SUS_b = F_{casting,CO_b[last]} + 1 \quad \forall b \in B$$

$$SUF_b = SUS_b + int\left(\frac{CCsut}{\delta}\right) - 1 \quad \forall b \in B$$

The first constraint aim to ensure batches' casting order and that casting tasks are executed immediately one after another. The other two force the caster's setup to be placed after the last heat of each batch

Delivery time constraints:

Case delivery = 1 and slack = 0

$$F_{CC,h} \leq dt_h \quad \forall h \in H$$

Heat h's whole process must be finished before its delivery time (due time). dt_h must be converted into time slots

Case delivery = 1 and slack = 1

$$F_{CC,h} = dt_h + sld_h - sla_h \quad \forall h \in H$$

In this case, the difference between the completion of h and its delivery time must be equal to the slack variables. Two opposite slack variables has been chosen (delay slack sld_h and advance slack sla_h) to keep their value positive for cost considerations

Heats' order constraints:

Case order = 1 and U = 1

$$S_{p,h} \geq F_{p,h-1} + 1 \quad \forall p \in P, \forall h \in H^* \quad , \text{ with } H^* \text{ equal to set H ordered by delivery time}$$

Case order = 1 and U > 1

$$S_{p,h} \geq S_{p,h-1} \quad \forall h \in H^* \quad , \text{ with } H^* \text{ equal to set } H \text{ ordered by delivery time}$$

In case of single line ($U = 1$), each heat's process must start after previous-in-order heat has completed it. In case of multiple parallel lines, the order is manifested only on the starts of processes (which can eventually start simultaneously)

Units occupation constraints (non-flexible units):

$$y_{p,h,t} = S_{p,h} - t \quad \forall p \in (P \setminus FU), \forall t \in T, \forall h \in H$$

y has a positive value before process p of heat h starts and a negative value after. This equation leads to the straight line in Figure 4

$$y_{p,h,t} \geq -k_{p,h,t} \cdot T + 1 \quad \forall p \in (P \setminus FU), \forall t \in T, \forall h \in H$$

$$y_{p,h,t} \leq (1 - k_{p,h,t}) \cdot T \quad \forall p \in (P \setminus FU), \forall t \in T, \forall h \in H$$

Big-M constraints that ensure that k is equal to 1 from the time step in which process p of heat h starts

$$y_{p,h,t} \leq w_{p,h,t} \cdot T - \text{int} \left(\frac{d_{p,h}}{\delta} \right) \quad \forall p \in (P \setminus FU), \forall t \in T, \forall h \in H$$

$$y_{p,h,t} \geq (w_{p,h,t} - 1) \cdot T - \text{int} \left(\frac{d_{p,h}}{\delta} \right) + 1 \quad \forall p \in (P \setminus FU), \forall t \in T, \forall h \in H$$

Big-M constraints that ensure that w is equal to 0 from the time step in which process p of heat h ends

$$\Omega_{p,t} = \left[\sum_{h \in H} (k_{p,h,t} + w_{p,h,t}) \right] - H \quad \forall p \in (P \setminus FU), \forall t \in T$$

Occupation or process p 's at time step t is found by doing $k + w - 1$, as you can see in Figure 4. This has to be true for all heats h simultaneously

Units occupation constraints (flexible units with flexmode 'constant power'):

$$yi_{p,h,t,i} = Si_{p,h,i} - t \quad \forall p \in FU^{cp}, \forall t \in T, \forall h \in H, \forall i \in I_{p,h}$$

$$yi_{p,h,t} \geq -ki_{p,h,t} \cdot T + 1 \quad \forall p \in FU^{cp}, \forall t \in T, \forall h \in H, \forall i \in I_{p,h}$$

$$yi_{p,h,t} \leq (1 - ki_{p,h,t}) \cdot T \quad \forall p \in FU^{cp}, \forall t \in T, \forall h \in H, \forall i \in I_{p,h}$$

$$yi_{p,h,t} \leq wi_{p,h,t} \cdot T - \text{int} \left(\frac{Etot_{p,h}}{flex_{p,h,i} \cdot \delta} \right) \quad \forall p \in FU^{cp}, \forall t \in T, \forall h \in H, \forall i \in I_{p,h}$$

$$yi_{p,h,t} \geq (wi_{p,h,t} - 1) \cdot T - \text{int} \left(\frac{Etot_{p,h}}{flex_{p,h,i} \cdot \delta} \right) + 1 \quad \forall p \in FU^{cp}, \forall t \in T, \forall h \in H, \forall i \in I_{p,h}$$

$$\Omega_{p,t} = \sum_{h \in H} \sum_{i \in I_{p,h}} ki_{p,h,t,i} + wi_{p,h,t,i} - 1 \quad \forall p \in FU^{cp}, \forall t \in T$$

Same constraints block as before (see Figure 4), but with the modes concept

Units occupation constraints (flexible units with flexmode 'full flex'):

$$y_{p,h,t} = S_{p,h} - t \quad \forall p \in FU^{ff}, \forall t \in T, \forall h \in H$$

$$y_{p,h,t} \geq -k_{p,h,t} \cdot T + 1 \quad \forall p \in FU^{ff}, \forall t \in T, \forall h \in H$$

$$y_{p,h,t} \leq (1 - k_{p,h,t}) \cdot T \quad \forall p \in FU^{ff}, \forall t \in T, \forall h \in H$$

$$y_{p,h,t} \leq w_{p,h,t} \cdot T - \sum_{t \in T} \Omega flex_{p,h,t} \quad \forall p \in FU^{ff}, \forall t \in T, \forall h \in H$$

$$y_{p,h,t} \geq (w_{p,h,t} - 1) \cdot T - \sum_{t \in T} \Omega flex_{p,h,t} + 1 \quad \forall p \in FU^{ff}, \forall t \in T, \forall h \in H$$

$$\Omega_{p,t} = \left[\sum_{h \in H} (k_{p,h,t} + w_{p,h,t}) \right] - H \quad \forall p \in FU^{ff}, \forall t \in T$$

Same constraints block as before (see Figure 4), but with the task duration represented by $\sum_{t \in T} \Omega flex_{p,h,t}$

$$\Omega flex_{p,h,t} = k_{p,h,t} + w_{p,h,t} - 1 \quad \forall p \in FU^{ff}, \forall t \in T, \forall h \in H$$

$$\Omega_{p,t} = \sum_{h \in H} \Omega flex_{p,h,t} \quad \forall p \in FU^{ff}, \forall t \in T$$

Additional constraints to link $\Omega_{p,t}$ to $\Omega flex_{p,h,t}$ making sure that the latter is strictly linked to the task duration (relationship with k and w)

$$Pflex_{p,h,t} \leq \Omega flex_{p,h,t} \cdot PW_p^{max} \quad \forall p \in FU^{ff}, \forall t \in T, \forall h \in H$$

$$Pflex_{p,h,t} \geq \Omega flex_{p,h,t} \cdot PW_p^{min} \quad \forall p \in FU^{ff}, \forall t \in T, \forall h \in H$$

Bounds for flexible power

CC setup time location constraints:

$$ysu_{b,t} = SUS_b - t \quad \forall b \in B, \forall t \in T$$

$$ysu_{b,t} \geq -ksu_{b,t} \cdot T + 1 \quad \forall b \in B, \forall t \in T$$

$$ysu_{b,t} \leq (1 - ksu_{b,t}) \cdot T \quad \forall b \in B, \forall t \in T$$

$$ysu_{b,t} \leq wsu_{b,t} \cdot T - int\left(\frac{CCsut}{\delta}\right) \quad \forall b \in B, \forall t \in T$$

$$ysu_{b,t} \geq (wsu_{b,t} - 1) \cdot T - int\left(\frac{CCsut}{\delta}\right) + 1 \quad \forall b \in B, \forall t \in T$$

$$\Omega su_{b,t} = ksu_{b,t} + wsu_{b,t} - 1 \quad \forall b \in B, \forall t \in T$$

Same constraints block as before (see Figure 4), but with the CC setup task

Parallel lines limit:

$$\Omega_{p,t} \leq U \quad \forall p \in (P \setminus CC), \forall t \in T$$

$$\Omega_{CC,t} + \sum_{b \in B} \Omega_{su_{b,t}} \leq U \quad \forall t \in T$$

Process p's unit occupation at each time step t must not exceed the number of parallel lines available (U). In case of continuous caster (CC), the unit is considered to be occupied also when the set-up is ongoing

Energy consumption constraint:

$$EL_t = \left(\frac{\delta}{60}\right) \cdot \left\{ \left[\sum_{p \in (P \setminus FU)} \Omega_{p,t} \cdot PW_p \right] + \left[\sum_{p \in FU^{cp}} \sum_{h \in H} \sum_{i \in I_{p,h}} (ki_{p,h,t,i} + wi_{p,h,t,i} - 1) \cdot flex_{p,h,i} \right] + \left[\sum_{p \in FU^{ff}} \sum_{h \in H} Pflex_{p,h,t} \right] \right\} \quad \forall t \in T$$

Electricity consumption at time step t is equal to the sum of three contribution:

- non-flexible unit power consumption computed with unit occupation multiplied by unit nominal power
- flexible unit power consumption (flexmode 'constant power') computed with unit occupation in mode i multiplied by its correspondent power level
- flexible unit power consumption (flexmode 'full flex') which is already a variable

a coefficient ($\delta/60$) is multiplied to convert power (MW) to energy (MWh)

Objective function

Makespan:

$$\text{minimize } \sum_{h \in H} F_{CC,h}$$

All heats must finish the process as soon as possible

Best delivery:

$$\text{minimize } \sum_{h \in H} (F_{CC,h} - dt_h)^2$$

The difference between the end of a heat's process must be as near as possible to its delivery time (due time)

Energy cost:

Case delivery = 1 and slack = 1

$$\text{minimize } \left\{ \sum_{t \in T} EL_t \cdot ELprice_t + \sum_{h \in H} \left[(sld_h \cdot df_h + sla_h \cdot af_h) \cdot \left(\frac{\delta}{60} \right) \right] \right\}$$

Electricity price must be added to advances and delays of all heats, weighted by their cost coefficients

Otherwise

$$\text{minimize } \sum_{t \in T} EL_t \cdot ELprice_t$$

Simulation and results

The developed MILP model can be solved efficiently using commercial solvers such as CPLEX, XPRESS or GUROBI. In this case, we used the latter through Python API. The input data is extracted from a properly structured access database. To do so it uses the public library pypodbc that provide the driver to connect to the database, it makes multiple queries to the database using SQL syntax and stores the data inside a multiple Python keys dictionary.

Prior to optimization some pre-processing and organization is performed if the data (for example computing the power levels (or modes) in the time-flexible units, if present). In addition, in order to reduce the computational expenses, the search spaced can be reduced by trimming the infeasible solution. For the problem in hand, the complementary unreachable region is defined by the most energetically compact solution for all other stages and jobs.

For the simulation, we have used real data from a steelmaking process. *Table 1* presents the list of heats to be processed for a specific day along with theirs delivery time, delay fee and advanced fee.

Table 1 Heats to be scheduled for a specific day

ID	Heat Name	ID_Batch	Delivery Time	Delay Fee	Advance Fee
1	H1	1	10:30:00	120	60
2	H2	1	11:00:00	180	72
3	H3	1	11:30:00	240	36
4	H4	1	12:00:00	148	96
5	H5	2	14:00:00	180	120

6	H6	2	14:30:00	180	24
7	H7	2	15:00:00	360	108
8	H8	2	15:30:00	240	36
9	H9	3	20:00:00	168	84
10	H10	3	21:00:00	0	0
11	H11	3	22:00:00	145	84
12	H12	3	23:00:00	132	36

An the specification of the processing units are presented in the *Table 2*

Table 2 specification of processing units

ID	Unit Name	Unit Type	Nominal Power	Flexible	Max Power	Min Power	Setup Time
1	EAF1	Electric Arc Furnace	85	Yes	95	75	
2	AOD1	Argon Oxygen Decarburization	2	No			
3	LF1	Ladle Furnace	2	No			
4	CC1	Continuous Caster	7	No	10	5	70

The optimization model was solved in an Intel Core i7 machine at 2.40 GHz with 16 GB RAM. The average CPU time for the day-ahead scheduling reported in this section was 256 s, subsequently reduced to a total of 51 s using space reduction technique. Using the rolling horizon approach the CPU has been reduced to under 10 seconds for a 6-hour long window, which is well within the time limit imposed by the real-time production control scheme (for a $\delta h = 30$ sec as in *Figure 4*)

The results of the simulation is reported in *Figure 9* where the objection of the optimization is set to be the cost of energy consumption. At the top, the prices of electricity is shown both for fixed and forecasted day-ahead. In the middle, power consumption is presented in yellow and hourly overall energy consumption in light blue. In this case, time discretization (δ) is set to 5 minutes. At the bottom, it is shown the hourly energy cost both in the case of fixed price and in the case of variable price. The difference between the two costs, hour by hour, is written above in green if it is a money saving and in red if otherwise.

As expected, it can be notices that the optimal schedule tends to avoid the power consumption when the energy price is at its peak and vice-versa.

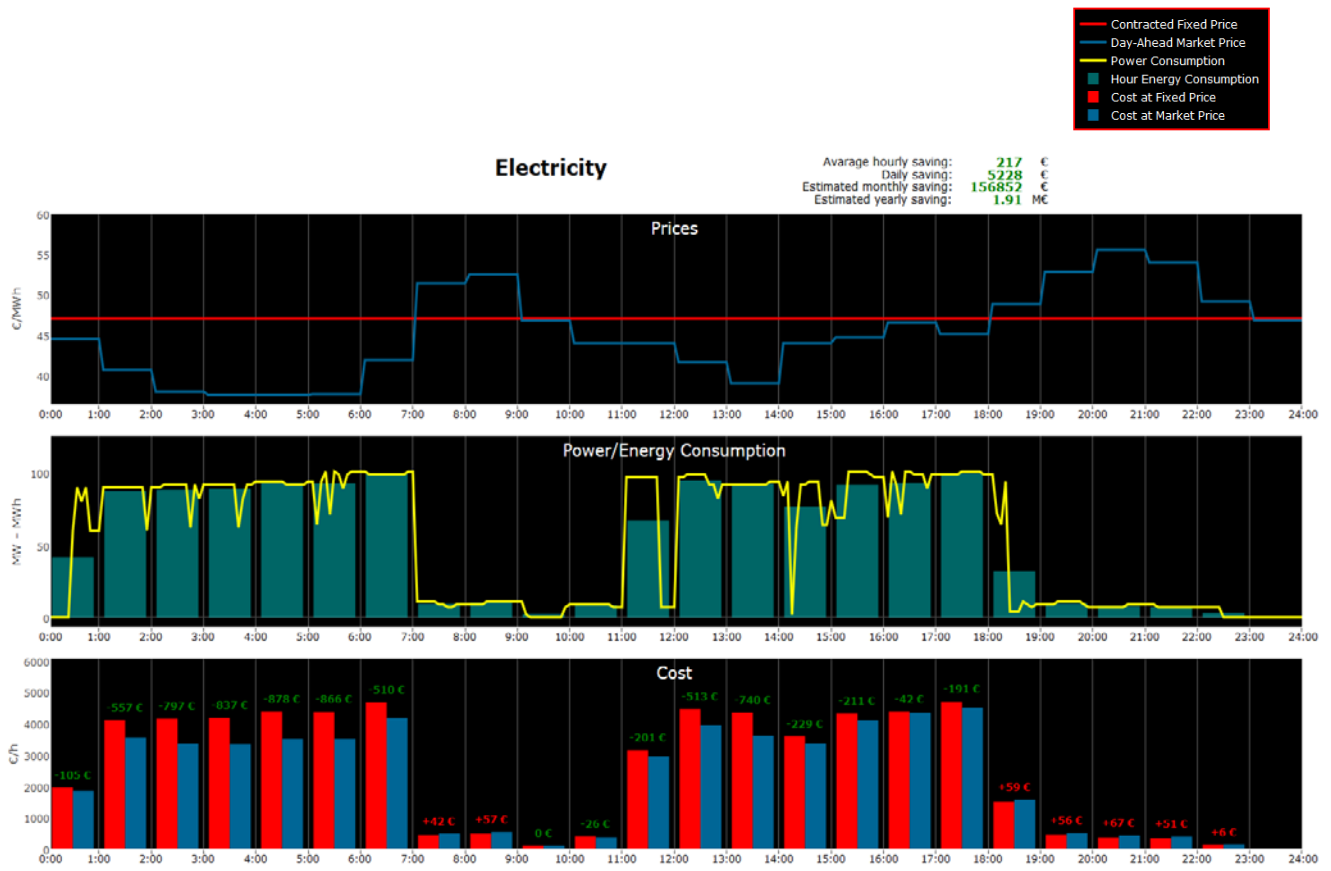


Figure 9 Results of Energy aware scheduling for a steel making process

SCADA

In this section we discuss the connection of the optimization model with Movicon Next SCADA. Using this interface, it is possible to fill the model parameters (problem data) through user-friendly screen and fields, launch the optimization and see statistics and plots. Inside the Movicon project, some VB.net scripts have been implemented to store the data from Movicon variables to the database of the Energy-aware scheduler with the proper structure that will feed a custom instance of the general model described above, once the optimization is launched. The results are automatically stored in another database, which will eventually be opened by other scripts to display some statistics a/o plots. The SW homepage for a melt shop is shown in Figure 10.

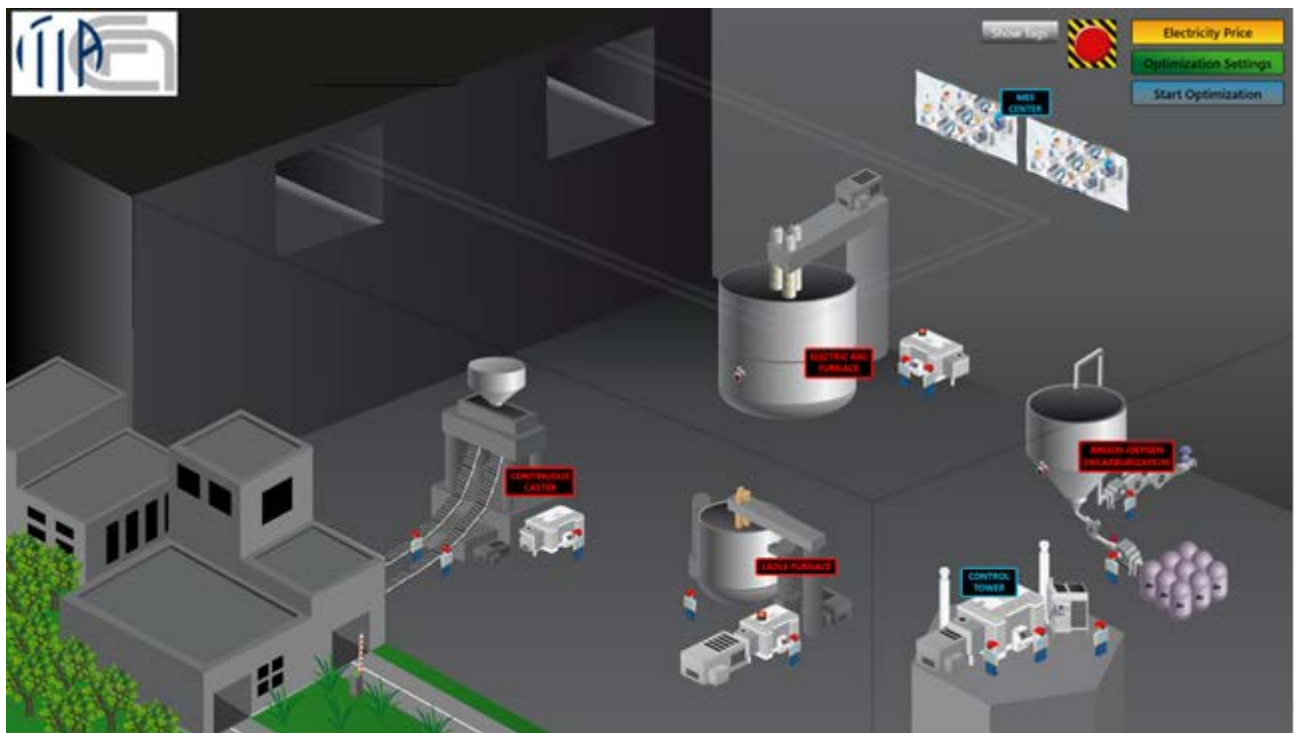


Figure 10 - Movicon interface SW main screen

Ladles carrying steel, firstly in solid scrap form then in molten metal form, move around the plant via ceiling rail in clockwise sense, stopping at every stage as the process evolves.

Pressing on the “control tower” a window will pop (Figure 11) up enabling the user to insert the suitable settings and constraints concerning units (power consumption, flexibility) and transports (times).



Figure 11 - The Control Tower screen

In the “MES center” (**Errore. L'origine riferimento non è stata trovata.**) it is possible to set the daily orders of the plant. The amount of steel to produce is divided and organized in batches (called “heats”) and groups (called “batches”), the latter indicating the possibility of gather multiple similar heats during the continuous casting process, limiting the caster set-up times only when a new group has to be dealt with.

Daily Orders

Batch #	Heat #	Processing times [mins]				Timetable		
		Melting From (hrs)	Decarburizing From (hrs)	Ladling From (hrs)	Casting From (hrs)	Timetable	Advance fee (k€)	Delay fee (k€)
1	1	65	60	35	60	7:30	60	120
	2	60	60	35	35	8:30	72	180
	3	65	55	40	40	9:30	36	240
	4	65	60	35	35	10:30	96	148
2	5	80	70	45	65	12:00	120	180
	6	90	85	55	80	13:00	24	180
3	7	45	50	25	50	17:00	108	390
	8	45	50	30	45	18:30	36	240
	9	50	55	30	45	19:30	84	168
	10	50	55	25	50	20:30	0	0
	11	55	40	25	55	21:30	84	545
4	12	65	55	35	60	22:00	36	132
	13	65	65	30	60	22:30	30	200
	14	70	60	35	55	23:00	90	365
	15	70	60	30	55	23:30	70	345

Figure 12 The MES Center screen

Every heat must be qualified with the estimation of the process time needed at each stage and eventually with indication of the pre-scheduled delivery time and relative costs of deviation from it.

The contracted electricity price and the day-ahead market prices should be uploaded into the “Electricity Price” section (Figure 13).

Inside the “Optimization settings” section (Figure 14) the user will define the mathematical problem:

- **Objective function:** choice between minimization of energy costs, minimization of the whole daily order makespan or best delivery time fitting
- **Solution accuracy (MIP gap) and time limit:** this are the limit criteria at which the optimization will stop and display a partially optimal solution. The default optimality tolerance is anyway 0.001% MIP Gap
- **Hours:** time horizon (set to daily)
- **Minimum time interval:** represents the discretization time (brief intervals lead to more accurate solutions but worsens the computational effort)
- **Number of parallel lines:** set to 1 for the problem in hand
- **Number of heats:** automatically taken from the daily orders

Some optional heuristic logics help to address specific optimization needs:

- **Delivery time:** it helps to reduce the mathematical problem’s magnitude. If not selected the heats’ delivery times are set to the end of the time horizon (h 24:00)
- **Cost-wise shifting:** delay and advance fees are taken into account to design a multi-objective optimization (minimize energy costs considering heats’ delivery time fitting)
- **Execution order:** to process the heats in order (from 1 to N) boosts the solution time

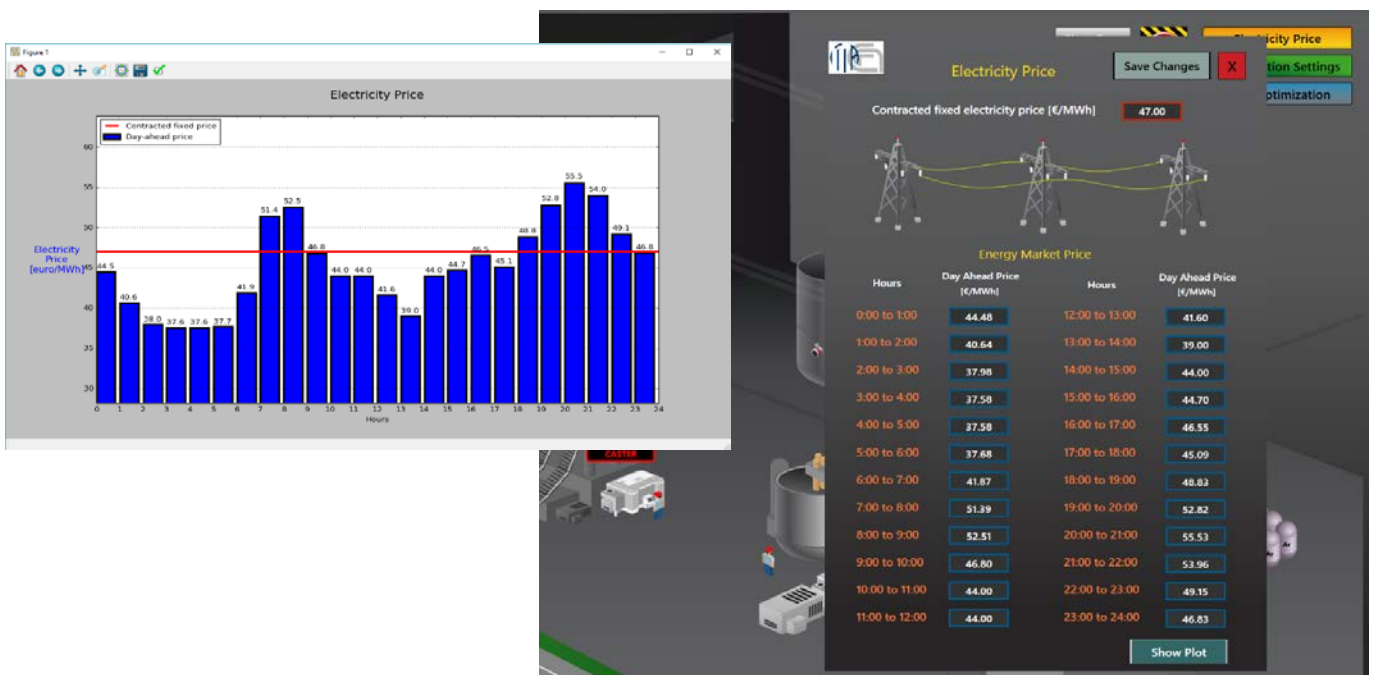


Figure 13 - The electricity price screen

- **Units' power flexibility:** to consider the power flexibility of some of the units (with bounds specified in the control tower section). Two modes are available: "constant power" means that for each heat the optimal power consumption is computed and maintained throughout the task, "full flex" enables the solver to change the power consumption at every time step.

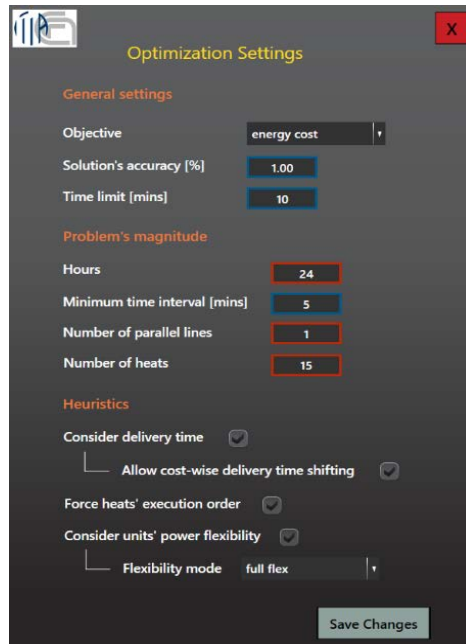


Figure 14 - The optimization settings screen

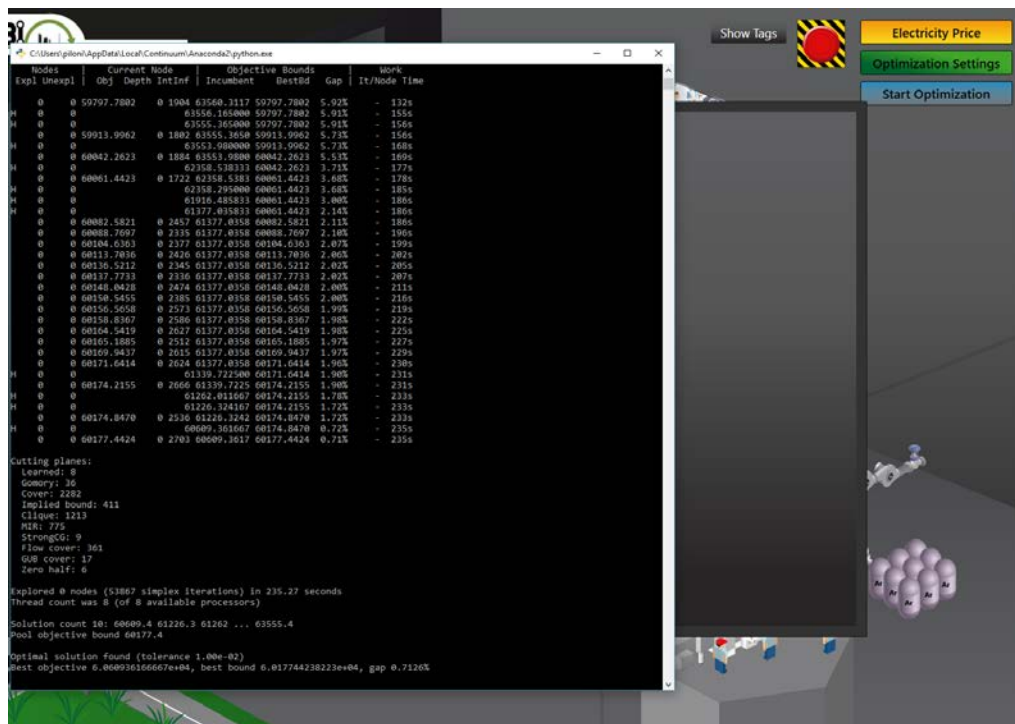


Figure 15 - Optimization has been launched

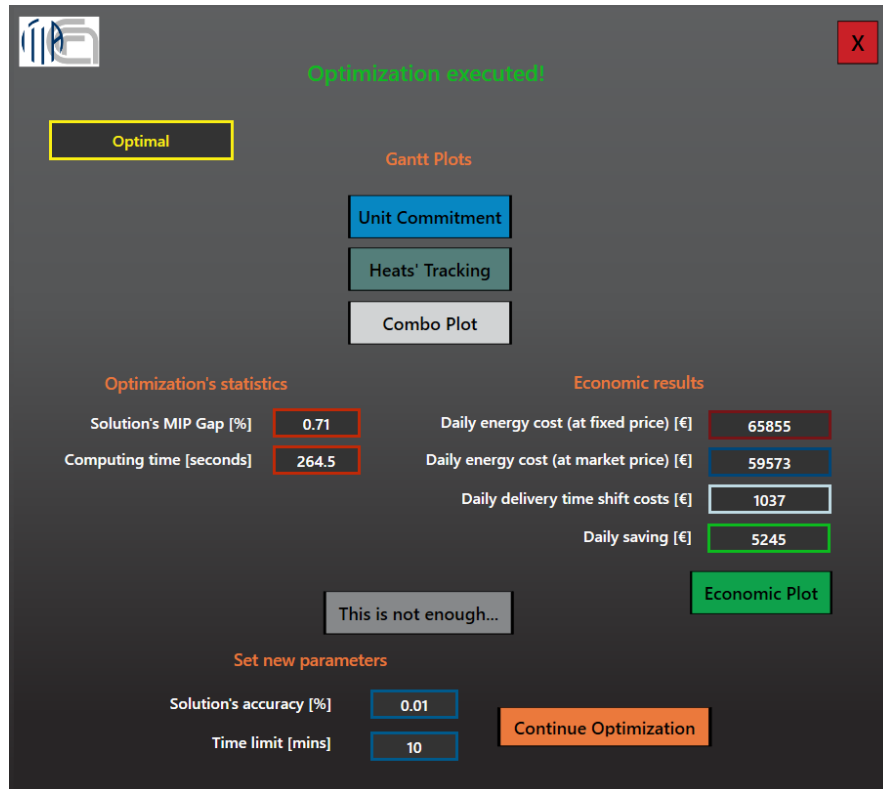


Figure 16 - The results screen

After everything is set and saved, the user can press “Start Optimization”. A python console will pop up and display the solving progress (Figure 15Figure 16).

When the optimization ends, a window opens with results, plots and statistics (Figure 16).

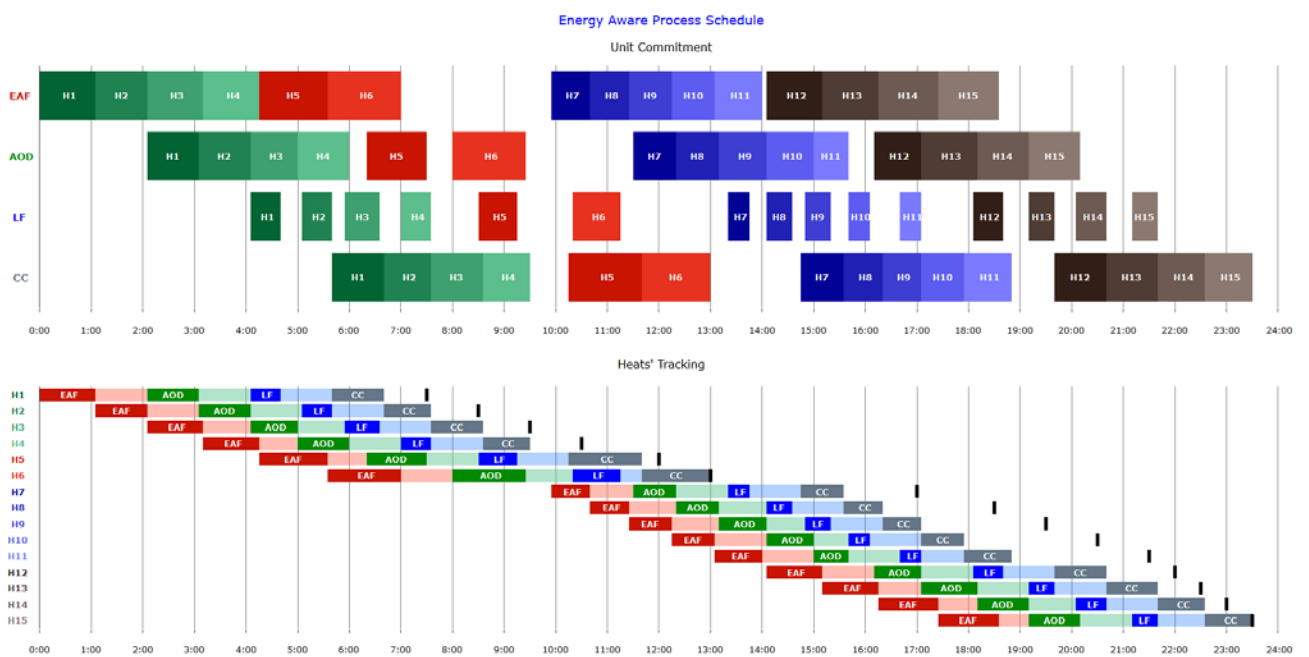


Figure 17 - Combo plot

The “Combo Plot” (Figure 17 - Combo plot) displays the previous two Gantt plots joined together. The first one displays the optimal schedule of each unit (EAF, AOD, LF and CC). Note that the heats are grouped in batches by similar colour tones (4 in this case). All batch’s heats performs the continuous caster process altogether and some time is dedicated to the caster’s set up between batches.

The second plot (Figure 18 - The electricity plot) shows the very same schedule but with the heats’ perspective. Each heat performs the 4 tasks in order: melting (EAF, red), decarburization (AOD, green), ladle furnace (LF, blue), continuous caster (CC, grey). The transports between units are shown with transparent colours.

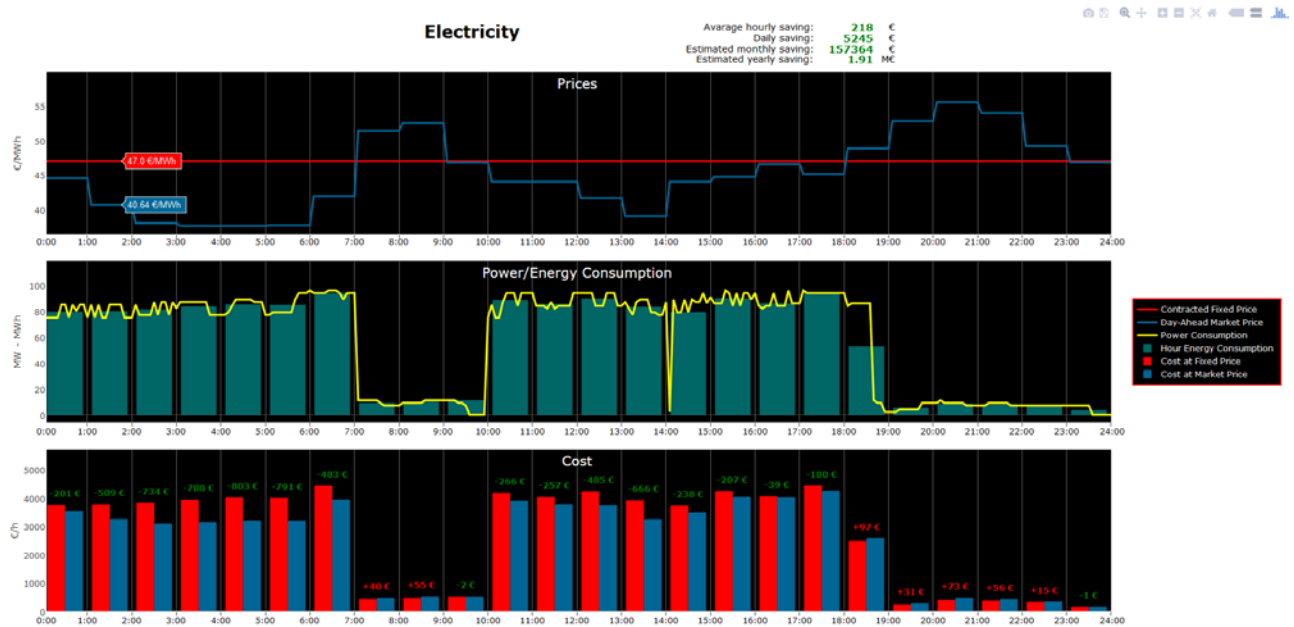


Figure 18 - The electricity plot

The “Economic Plot” pictures the electricity prices, the plant power and energy consumption end the resulting hourly energy costs. Note that the optimal schedule tends to concentrate the plant electricity consumption (water-green in the middle subplot) when the market price is lower than the fixed one. The third subplot shows the hourly difference between energy costs at fixed price (red bars) end variable price (blue bars), the delta is displayed above. Even if in some hours the balance is slightly negative, the overall effect is clearly a positive saving, as can be seen from the average projections written at the top.

MILP models for optimal weekly schedule

In this section we use the same technique to derive a model which is more fit to for a weekly scheduling of steelmaking process. This model is designed for a high-level production plan of short-to-mid-term, potentially helping the MES to organize and deploy the orders within different days. To do so three cost components are taken into consideration:

- **Electric energy cost**

The forecasted day-ahead hourly price for a whole week is needed. Since the forecast on this relatively long term could not be precise in an absolute way, it is important to note that:

- The curve shape of the day ahead price is periodic in some fashion
- It is only important to localize the time spans with peaks and valleys

- Some predictions on average daily price is related to some exogenous variables such as day of the week, atmospheric weather, period of the year, social-economic events
- **Heats delivery time**
Similarly that for the daily schedule, every batch has a contracted delivery time (due time). The batch process could end exactly on its delivery timetable or could end:
 - Earlier, being subjected to a batch-specific advance fee, representing the storage costs
 - Later, being subjected to a batch-specific delay fee
- **Makespan**
As for the daily schedule, to minimize the makespan of the whole process is a synonym of using the highest possible production rate, hence maximum profitability. To quantify the makespan in a comprehensive cost function it is possible to take as reference the average process time and revenue of a typical batch and compute the 'addable batches' of a solution, in the hypothesis to fill the leftover time with new batches

Preamble

The typical solving time of the daily schedule for energy cost minimization, with a time discretization of 5 minutes and performing the commitment of 10-15 heats, is around 300-500 seconds. Extending the daily schedule model to a weekly time horizon, involving 70-100 heats, would lead to such a huge number of variables and constraints that make the subsequent optimization intractable in reasonable time. Moreover, this level of precision does not fit the logical aim of this tool, which is suitable to ease mid-term high-level decisions on time unit commitment. Therefore, this kind of problem needs a new model that should be conceptually simpler (less variables, less constraints) than the daily one, hence should contain a certain degree of approximation.

While the last two cost components are straightforward and easily computable, the electric energy cost surprisingly hides some pitfalls in terms of MILP modelling. The key difference is that makespan and delivery time costs can be evaluated using only variables not indexed in time (i.e. as in variables $S_{p,h}$ and $F_{p,h}$) because its time information is contained inside the value they take. On the contrary, to evaluate the precise energy cost, the time mapping of the unit occupation (and so the resource consumption) is needed. Referring to the previous model (for daily schedule), every variable that has a t index (discrete-time variable value), in the hypothesis of considering 5 minutes as a time step ($\delta = 5$), in a weekly time horizon results into 2016 variables. The magnitude is also becoming bigger since the number of heats (and tasks) to schedule is significantly higher. For example with $\delta = 5$, $H = 100$, $T =$ a week, the variable $k_{p,h,t}$ has a length of 806400 values, alone, the whole model reaching several millions variables.

Again, is a task starting time shift of five minutes important for a high-level scheduler? Is the actual precise value of the energy price (forecasted, moreover) important? The high-level approach should mainly focus on avoiding negative peak price zones and produce at full rate in periods of forecasted favourable energy price. After these high-level results, the actual precise daily schedule can be refined feeding the daily schedule model.

Simplification hypothesis

Based on the considerations of previous section, the change of perspective is now clarified explaining the main hypothesis of this model, aiming to reduce the problem size:

1. The only process unit to be considered in energy price cost consideration is the EAF (Electric Arc Furnace), since it is by far the greatest power consumer of the whole melt shop
2. All units have constant power consumption, so every task has a fixed duration, known a-priori
3. The plant layout is made of a single line ($U = 1$)
4. The delivery timetable is now for the whole batch, not for every single heat as in the daily model. Since the tasks are now at constant power (fixed duration) and the batch composition and order is fixed, this procedure does not change any accuracy to the model
5. The hourly energy price is divided into price ranges, 7 in this case ()

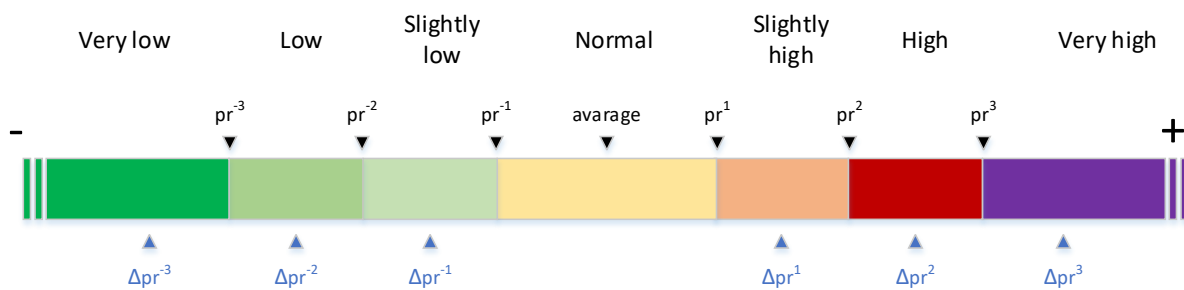


Figure 19 - Price ranges

To define these ranges 6 prices has to be declared:

- pr^1 , pr^2 , pr^3 must be strictly increasing and higher than the price average
- pr^{-1} , pr^{-2} , pr^{-3} must be strictly decreasing and lower than the price average

For the MILP model, every range will have a single 'grade' or cost coefficient, which can be arbitrary (since we are approximating the real cost function). In this case, I have chosen 6 delta coefficient (Δpr^x) meaning the difference between the average price of the range and the overall average price, so that the range 'Normal price' will have a cost coefficient equal to 0. This approach will lead to put cost-wise consideration only on hours where the price is 'abnormal'. This sub-set of hours, which are the most important, has been called '**extreme price**', referring both to hours with high and low prices.

6. Either a melting task can 'escape' an element of **extreme price** or 'being trapped' inside it, these two conditions will be represented by a binary variable. If the task escapes a highly priced hour (variable will have value 1) it will gain points with a coefficient of Δpr^x being a positive number; on the contrary if a task escapes a lowly priced hour it will gain points with a

coefficient of Δpr^x being a negative number, hence lose points. This key concept is depicted below.

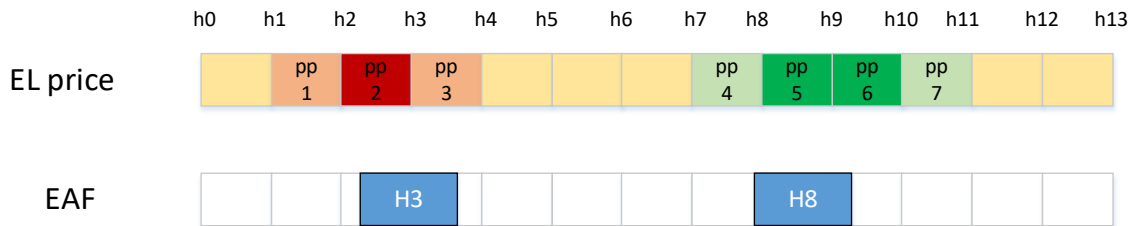


Figure 20 - Model approximation of melting tasks time location

Of these 13 hourly time slots, only 7 belong to the **extreme price** list. Based on the tasks time location in Figure 7:

- Heat H3 melting escapes extreme price 1, 4, 5, 6 and 7 but it is trapped in both extreme price 2 and 3
- Heat H8 melting escapes extreme price 1, 2, 3 and 7 but it is trapped in extreme price 4, 5 and 6

Constants

The problem data can be divided into 6 categories:

- **Heats and batches**

Contains the list of heats ($H_1 \dots H_H$) to be scheduled, the batch they belong ($B_1 \dots B_B$) and the sequence order within the casting group (batch). Moreover, each heat has a specific the delivery time which it is due and advance and delay fees (€/h)

- **Processing times**

Each heat has a nominal processing time at each unit of the process (EAF, AOD, LF and CC). The nominal processing time is the forecasted process time (in minutes), considering the unit to work constantly at nominal power.

- **Units' settings**

Each unit (EAF, AOD, LF and CC) has a nominal power (in MW). The set-up time for the Continuous Caster (CC) is required (in minutes)

- **Transports' settings**

The three transfers within the flow shop (from EAF to AOD, from AOD to LF and from LF to CC) should have a minimum and a maximum time range (in minutes)

- **Hourly variable electricity price**

The forecasted day-ahead price, which is a set of H_r (number of hours) float numbers (€/MWh) is required, as well as a single contracted fixed price (for economic comparisons). In addition, the prices of the range interfaces and cost coefficients are required (pr^x and Δpr^x in Figure 16)

- **Optimization settings**

A set of parameters to address the general-purpose model to specific needs:

- Time:
 - Hr = number of hours (e.g. 24, for daily schedule)
 - δ = single time step width (minutes). As mentioned before, this model will not have variables indexed by time, so this parameter does not influence the magnitude of the problem, but still influences the precision of task durations. For example, if a task duration is 43 minutes, if $\delta = 5$, then the task duration is rounded to 9 time-spans (45 minutes). It also influences the precision of time location system (see Figure 17). It is by default set to 1 (minute)
- Constraints options:
 - Order = binary denoting if the heats should be ordered by delivery time or not (1 is extraordinary faster)
- Objective:
 - Selectable among 'energy', 'makespan', 'delivery' or a combination of more than one of these 3 (in this last case, objective must be a list of strings).
- Solver parameters:
 - Precision = MIPGap (%)
 - TimeLimit = max solving time (in minutes)

Nomenclature:

Sets

Tag	Index	Description
H	h	Heats to be processed within the time horizon
B	b	Batches (group of heats with similar casting settings)
CO _b	co	Heats' casting order of batch b (example: CO _{B1} = [H ₁ , H ₂ , H ₃ , H ₄])
P	p	Processes: melting (EAF), decarburization (AOD), ladle (LF) and casting (CC) but also transports (EAF to AOD, AOD to LF, LF to CC)
AP	p	Active processes (EAF, AOD, LF and CC), AP ⊂ P
R	r	Price ranges (7 in the case of Figure 16)
PP	pp	Extreme price , set of time locations where the price is ab-normal (significantly high or low)

For the sake of clarity, the model is not discrete-time, but still a discrete-time grid (of width δ) is in the background, to help conceiving simpler constraints. The **extreme price** set is a list of times in the discrete-time grid reference (δ minutes). To pass from peak price hour to a single time step, this conversion is applied:

$$PP(h) = \frac{(h \cdot 60) + 30}{\delta}$$

The half-hour addition helps computing the distance from a extreme price hour, since the relative reference is located in the middle of such hour. For example, if $\delta = 1$ and there is an highly priced hour at hour number 11, the correspondent extreme price value is 690, meaning there is an ab-normal price within a half-hour neighbourhood of time step 690.

Constants (parameters)

Tag	Description
δ	Single time step width [minutes] (the model is not discrete-time)
Hr	Number of hours to schedule
T	Total time horizon (in a hypothetical discrete-time grid)
$d_{p,h}$	Duration (nominal) of process p for heat h [minutes], $p \in AP$
dt_b	Delivery time (or due time) for batch b
af_b	Advance fee for batch b [€/min]
df_b	Delay fee for batch b [€/min]
TT_p^{\min}	Minimum transfer time of transport p [minutes], $p \in (P \setminus AP)$
TT_p^{\max}	Maximum transfer time of transport p [minutes], $p \in (P \setminus AP)$
CCsut	Continuous caster set-up time [minutes]
PW_{EAF}	Nominal power of Electric Arc Furnace (melting unit)
pr^r	Ranges price interfaces (see Figure 16)
Δpr^r	Ranges cost coefficients (see Figure 16)
$\Delta price^{PP}$	Cost coefficients of an element of extreme price
ELfp	Electricity fixed price [€/MWh]
btime	Avarage batch process time
bvenue	Avarage batch process revenue

The total time horizon is computed as follow:

$$T = int\left(\frac{Hr \cdot 60}{\delta}\right)$$

Variables

List of all the variables. Note that not all the variables are *decision variables* (my bad): some dependant variables have been added to simplify the constraints implementation. In any case, these dependant variables should not slow down the solver.

Tag	Description	Type	Lower bound	Upper bound
$S_{p,h}$	Start of process p for heat h	continuous	1	T
$F_{p,h}$	Finish (or end) of process p for heat h	continuous	1	T
$\alpha_{p,h,h'}$	Unit non overlapping variable, $p \in (AP \setminus CC)$	binary		
$\beta_{b,b'}$	CC non overlapping variable	binary		
δ_b^+	Slack variable representing the delay in delivery of batch b	continuous	0	T
δ_b^-	Slack variable representing the advance in delivery of batch b	continuous	-T	0
Ω_b	Auxiliary variable for choosing delay or advance in delivery of batch b	binary		
$dx_{h,pp}$	Slack variable representing the delay of the melting task of heat h in respect to extreme price pp	continuous	0	T

$SX_{h,pp}$	Slack variable representing the advance of the melting task of heat h in respect to extreme price pp	continuous	-T	0
$\omega_{h,pp}$	Auxiliary variable for choosing delay or advance in melting task of heat h in respect to extreme price pp	binary		
$Z_{h,pp}$	Escape/entrapment of melting task of heat h in respect to extreme price pp	binary		
$grade_h$	Grade of heat h in escaping/being trapped within extreme price	continuous	$-\infty$	$+\infty$

Constraints

Time constraints:

$$F_{p,h} = S_{p,h} + d_{p,h} - 1 \quad \forall p \in AP, \forall h \in H$$

The end of each task $F_{p,h}$ is related to its start $S_{p,h}$ through the specific duration $d_{p,h}$

$$S_{p,h} \geq F_{p-1,h} + 1 \quad \forall p \in (P \setminus EAF), \forall h \in H$$

The start of each task $S_{p,h}$ must be immediately after the end of the same heat previous-in-order process $F_{p-1,h}$. This is valid both for active processes and transports

Transports constraints:

$$F_{p,h} \geq S_{p,h} + TT_p^{min} - 1 \quad \forall p \in (P \setminus AP), \forall h \in H$$

$$F_{p,h} \leq S_{p,h} + TT_{tr}^{max} - 1 \quad \forall p \in (P \setminus AP), \forall h \in H$$

The end of each transport must be within minimum and maximum transfer time distance from its start

Heats' order constraints:

Case order = 1

$$S_{p,h} \geq F_{p,h-1} + 1 \quad \forall p \in P, \forall h \in H^* \quad , \text{ with } H^* \text{ equal to set } H \text{ ordered by delivery time of the batch they belong}$$

Each heat's process must start after previous-in-order heat has completed it

Unit non-overlapping constraints:

$$S_{p,h} \geq F_{p,h'} + \alpha_{p,h,h'} - (1 - \alpha_{p,h,h'}) \cdot T \quad \forall p \in (AP \setminus CC), \forall h, h' \in H$$

$$F_{p,h} \leq S_{p,h'} + \alpha_{p,h,h'} \cdot T - (1 - \alpha_{p,h,h'}) \quad \forall p \in (AP \setminus CC), \forall h, h' \in H$$

If binary variable $\alpha_{p,h,h'}$ is equal to 1, then the heat h will start after the end of heat h' . On the contrary, if binary variable $\alpha_{p,h,h'}$ is equal to 0, then heat h finishes before the start of heat h' . This approach is valid for all active processes except the continuous casting, that will follow other constraints

Continuous Caster (CC) constraints:

$$S_{CC,g} = F_{CC,(g-1)} + 1 \quad \forall b \in B, \forall g \in CO_b \wedge g \neq CO_b[first]$$

Constraint to ensure batches' casting order and that casting tasks are executed immediately one after another

$$S_{CC,CO_b[first]} \geq S_{CC,CO_{b'}[first]} + \beta_{b,b'} \cdot \left[\left(\sum_{h \in CO_{b'}} d_{CC,h} \right) + CC_{sut} \right] - (1 - \beta_{b,b'}) \cdot T \quad \forall b, b' \in B$$

$$S_{CC,CO_b[first]} \leq S_{CC,CO_{b'}[first]} - (1 - \beta_{b,b'}) \cdot \left[\left(\sum_{h \in CO_b} d_{CC,h} \right) + CC_{sut} \right] + \beta_{b,b'} \cdot T \quad \forall b, b' \in B$$

If binary variable $\beta_{b,b'}$ is equal to 1, then the first heat of batch b will start after the first heat of batch b' plus the total time span required for the casting of group b' (setup time included). The opposite in case the binary variable $\beta_{b,b'}$ is equal to 0

Delivery constraints:

$$F_{CC,CO_b[last]} - dt_b = +\delta_b^+ + \delta_b^- \quad \forall b \in B$$

$$\delta_b^+ \leq \Omega_b \cdot T \quad \forall b \in B$$

$$\delta_b^- \geq (\Omega_b - 1) \cdot T \quad \forall b \in B$$

In this case, the difference between the completion of the last heat of batch b and its delivery time must be equal to the sum of the positive slack variable δ_b^+ plus the negative one δ_b^- . The last two constraints force the solution to be either in delay or in advance

Energy price constraints:

$$\left(\frac{S_{EAF,h} + F_{EAF,h}}{2} \right) - pp = +dx_{h,pp} + sx_{h,pp} \quad \forall h \in H, \forall pp \in PP$$

$$dx_{h,pp} \leq \omega_{h,pp} \cdot T \quad \forall h \in H, \forall pp \in PP$$

$$sx_{h,pp} \geq (\omega_{h,pp} - 1) \cdot T \quad \forall h \in H, \forall pp \in PP$$

Similarly to previous constraints block, the time distance between the middle of a melting task and a **extreme price** must be equal to the sum of the positive slack variable $dx_{h,pp}$ plus the negative ones $sx_{h,pp}$. The last two constraints force the task to be either before or after a **extreme price**

$$dx_{h,pp} - sx_{h,pp} \geq z_{h,pp} \cdot \left[\left(\frac{30}{\delta} \right) + \left(\frac{d_{EAF,h}}{2} \right) + 1 \right] \quad \forall h \in H, \forall pp \in PP$$

$$dx_{h,pp} - sx_{h,pp} \leq (1 - z_{h,pp}) \cdot \left[\left(\frac{30}{\delta} \right) + \left(\frac{d_{EAF,h}}{2} \right) \right] + z_{h,pp} \cdot T \quad \forall h \in H, \forall pp \in PP$$

These two constraints rules the binary variable of escape/entrapment $z_{h,pp}$ of each element of **extreme price**. See Figure 17 for clarity. $dx_{h,pp} - sx_{h,pp}$ represents the positive time distance between a melting task and an element of **extreme price**. If this distance is higher than $\left[\left(\frac{30}{\delta} \right) + \left(\frac{d_{EAF,h}}{2} \right) + 1 \right]$, the task has completely escaped the whole extreme price hour and the binary variable $z_{h,pp}$ will be equal to 1. On the contrary, if the task (within its time length) touches a extreme price hour, the binary variable $z_{h,pp}$ will be equal to 0.

$$grade_h = \sum_{\forall pp \in PP} z_{h,pp} \cdot \Delta price^{pp} \cdot PW_{EAF} \cdot d_{EAF,h} \cdot \left(\frac{60}{\delta} \right) \quad \forall h \in H$$

Whit this constraint, every heat has a grade related to choice of the time location of its melting task. Every escape of a bad **extreme price** element leads to a positive point gain and every escape of a good **extreme price** element leads to a point loss. The model choice of consider the escapes and not the entrapments should sound strange, but after some runs it was clearly a better way to convergence

Objective function

$$\mathbf{maximize} \left\{ \sum_{\forall h \in H} grade_h + \left[\left(\frac{T - F_{CC,last_h} - CCsut}{btime} \right) \cdot brevenue \right] - \sum_{\forall b \in B} (\delta_b^+ \cdot df_b - \delta_b^- \cdot af_b) \right\}$$

This objective function is the general one (with all three cost components), but some component must be eliminated if it is not on the objective constant setting.

- For the energy cost we want to maximize all the grades of the heats in term of time location of their melting task. As mentioned before, this is not a real cost, but a MILP model trick based on severe simplifications of the problem (see preamble), that still leads to favourable results. Adding this component to a multi-objective function is delicate, because the other components are more realistic and quantifiable costs. Some runs and tuning should be performed, analysing the output of the solver
- For the makespan, we consider the ‘addable batches’ at the right end of the schedule, considering their average process time and revenue. As you can see from $F_{CC,last_h}$ this only works if the heats are ordered ex-ante.
- For the delivery time we consider each batch delay and advance, weighted by specific cost coefficients

Results

Similar to day-ahead optimization the weekly model is solved using Gurobi optimization through the Python API. In this section, we report the result of the scheduling optimization for various possible objectives:

Delivery-only optimization

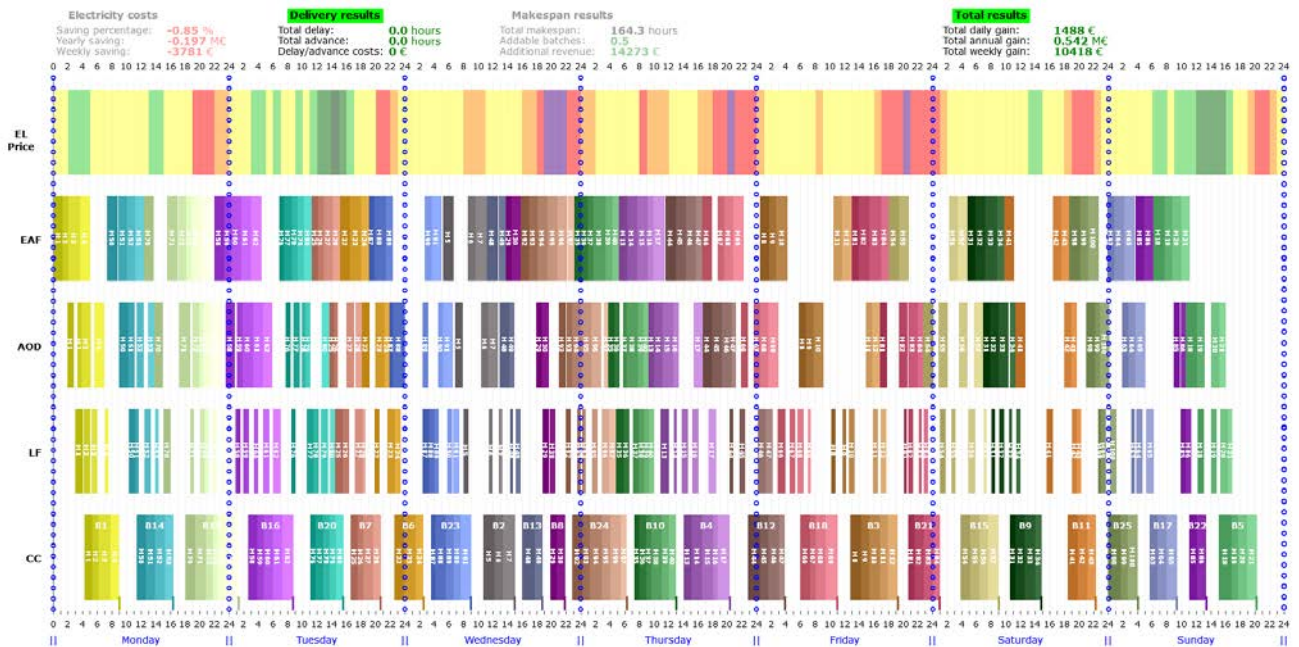


Figure 21 - Weekly results with the only objective of 'delivery time'

Figure 21 show the weekly scheduling where only when delivery is the main concern. As it is apparent from the CC part of the Gantt, every batch has been delivered in perfect time, but no emphasis has been put on avoiding bad extreme price hours and neither on production rate.

Makespan-only optimization

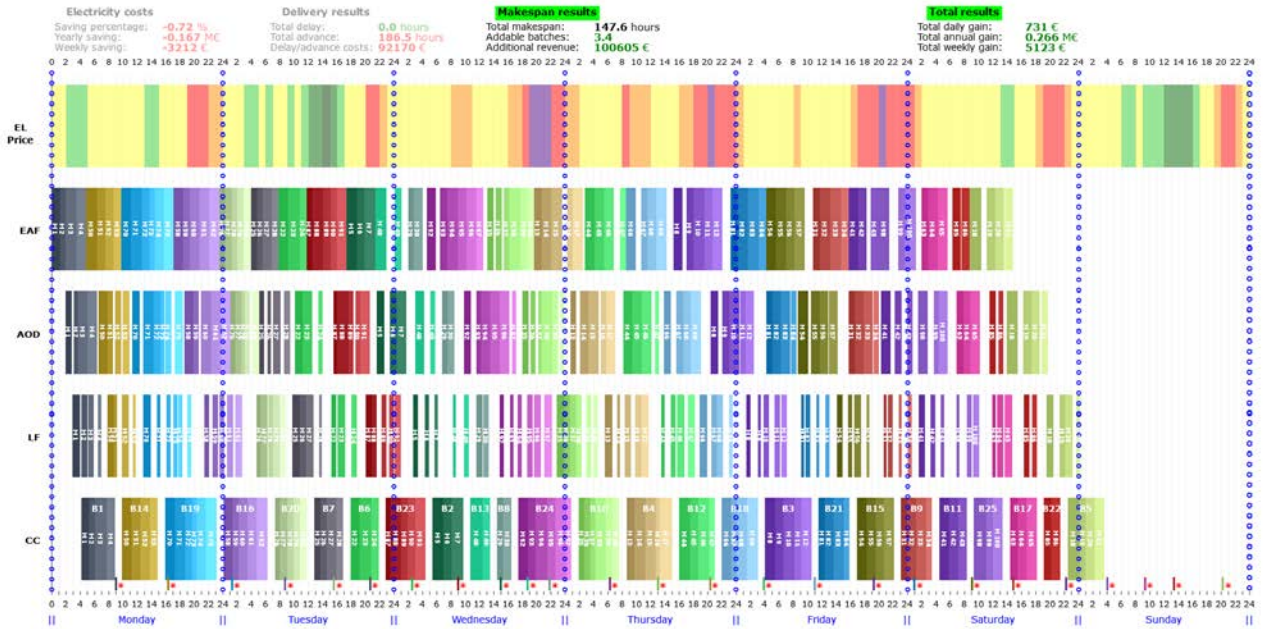


Figure 22 - Weekly results with the only objective of 'makespan'

On the other hand, Figure 22 illustrates the result for an optimization with the sole objective of makespan minimization where the highest possible production rate (up to 3 batches can be added to the schedule), but delivery timetables are not respected and bad peak price hours not avoided.

Energy-price only optimization

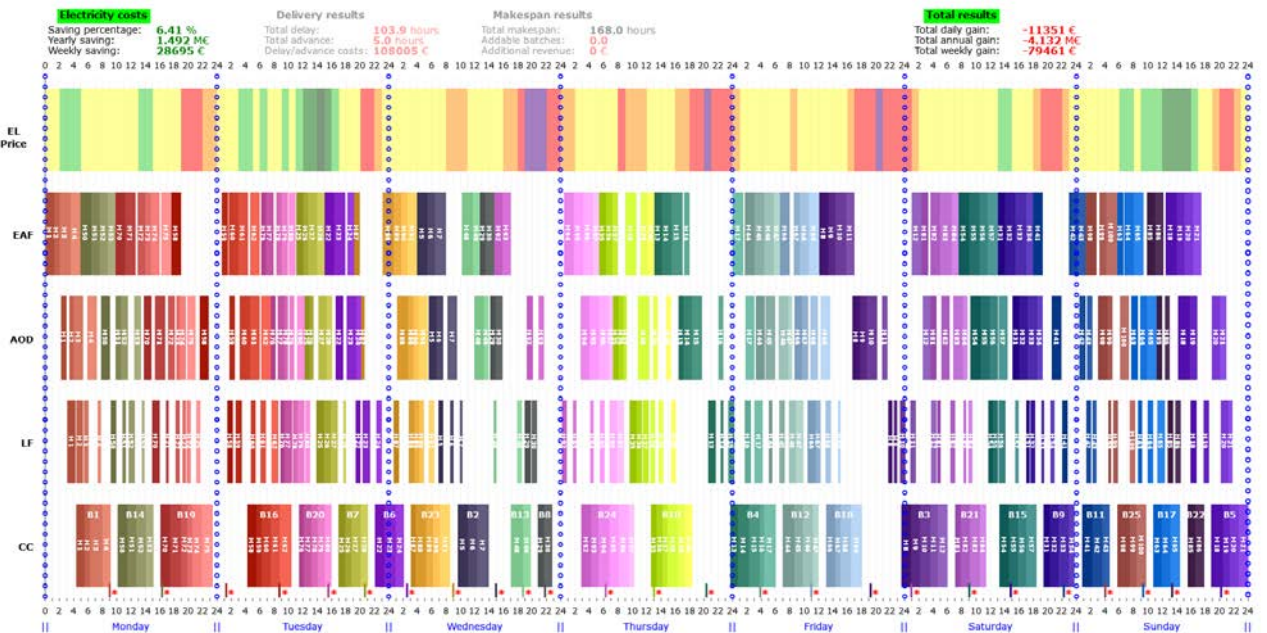


Figure 23 - Weekly results with the only objective of 'energy cost'

The third case of mono objective optimization is shown in Figure 23 where the focus is on avoiding bad peak price hours and stress production in good energy price zones.

Fully multi-objective

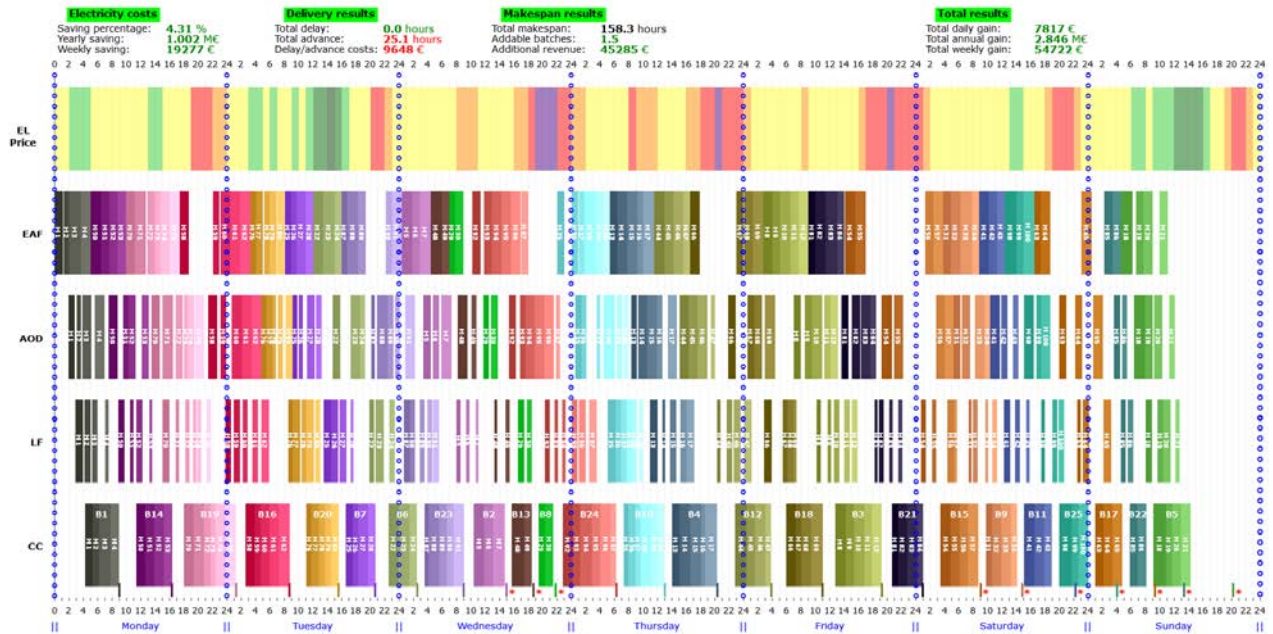


Figure 24 - Weekly results with full multi-objective optimization

Finally, the result of multi-objective optimization is shown in Figure 24 where a pareto-optimal solution is obtained as the best trade-off for all the above mentioned objectives. For a steelmaking plant with a production capacity of 1 million tonnes per year a total 2.846 Million euros increase in revenue can be achieved by a multi-objective optimization minimizing the energy costs and tardiness while maximizing productivity. It shows that by relaxing few delivery constraints it is possible gain a huge profit exploiting such flexibility in the minimization of energy and makespan, where in the latter case, the schedule can be extended to include more heats to increase the productivity.

Environmental applications

As the steel plant is a huge power consumer, it is indirectly responsible for the CO₂ emissions caused by the power generators involved in the energy supply. Thus, a change in the power consumption time curve of such a consumer would lead to a different time unit commitment of the generation mix, hence causing a reduction or a raise of the actual CO₂ emissions. For an optimization model standpoint, the very same approach used in the previous section could be integrated with an environmental optimization, minimizing the CO₂ emission in the power supply by means of time shifting of the energy consumption. To do so, instead of the hourly energy price curve, the hourly energy marginal emission curve is needed.

1.1 Metal Casting Process

In this section, we present the EAPO tool customized for the scheduling a foundry as one of the most energy-intensive sectors.

Figure 25: General layout of metal casting plant (in the rectangle: Finite State Machine representing operation each furnace)Figure 25 illustrates different production stages within a multi-product foundry. Depending on capacity, a generic plant configuration includes a number of parallel molding lines, equipped with pouring furnaces which receive batches of molten metal from melting furnaces. These furnaces are fed with different types of scrap based on the alloy composition of the final product.

This flow of material follows a production plan that is generated by ERP considering client orders. Based on the order characteristics such as material composition, number of products and their dimension at each stage different decision should be made regarding the unit assignment, lot sizing and sequencing of corresponding tasks. For melting furnaces, unit assignment applies only if their capacities vary.

Process description

From an operational point of view, a melt job is a sequence of different stages characterized by a peculiar pattern of the process variables (Power, Weight, Temperature) and representable in a finite-state machine (see Figure 25).

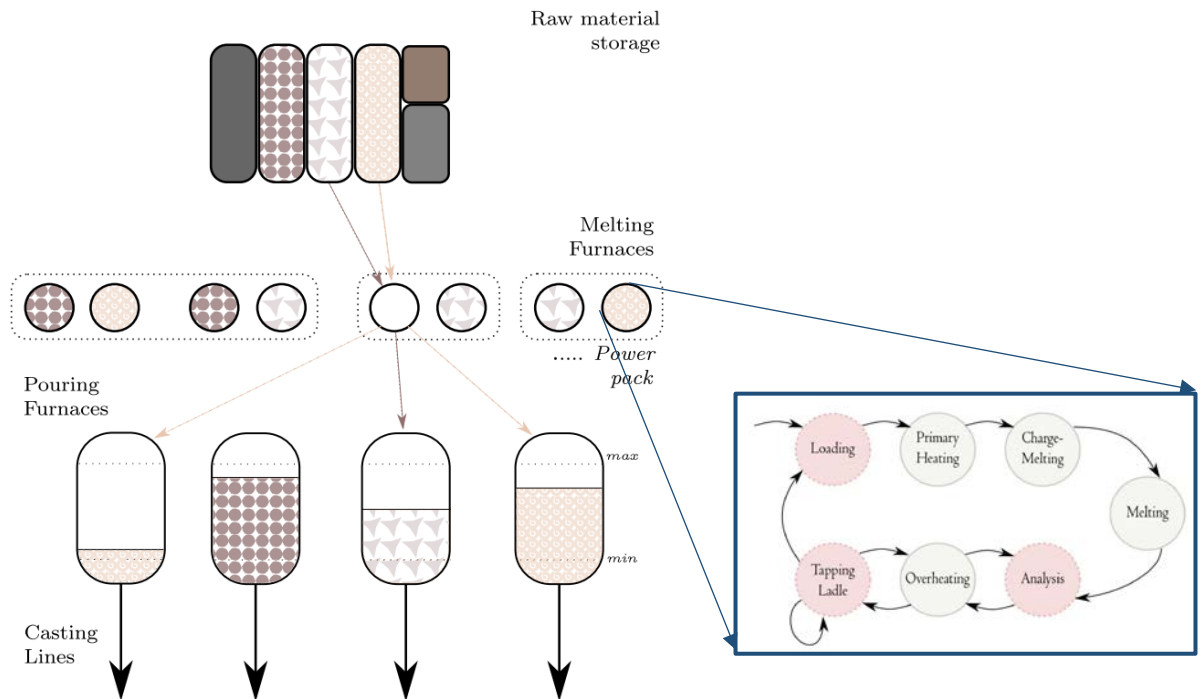


Figure 25: General layout of metal casting plant (in the rectangle: Finite State Machine representing operation each furnace)

These stages are:

1. Loading: scrap metal is fed into the crucible using feeding system, with the furnace off. Time required for this stage sets a minimum interval between two melting jobs.
2. Primary Heating: the initial load is heated to form the molten bath, without introducing new scrap. Depending on the furnace technology, power ramp up rate is limited in this stage.
3. Charge-Melting: while heating continues, feeding resumes until the furnace capacity is full. Melting increases the bulk density of the bath, allowing room for new charge. The main challenge is synchronizing charging and melting so that neither there is a risk of splash (by overheating) nor furnace overflow (by overcharging);
4. Melting: heating is continued until a target temperature is achieved;
5. Analysis: furnace is switched off for chemical analysis, composition correction and slag removal;
6. Overheating: heating is resumed to raise the temperature to poring point;
7. Tapping: molten metal is tapped into transportation ladles.

Phase transition is heterogeneously governed by exogenous and endogenous variables, such as temperature targets for stages 2, 4 and 6, weight for 1, 3 and 7 and analysis approval for stage 5. However, these transition variables can be effectively approximated by energy consumption and duration of each stage. Accordingly, the process stages can be classified into two subsets, based on their completion requirements:

\mathcal{J}^E	Energy-based stages that are completed after consuming a certain amount of energy
\mathcal{J}^T	Time-based stages that require no energy and whose completion is associated with a minimum duration

Optimization Model

The modeling processes is very similar to the previous case and follows the same line of reasoning to develop a Mixed Integer Linear Programming (MILP) model. Hence, here we do not cover all the modelling details and only report the mathematical constraint and objective according to the process dynamics.

Variables

The optimization variables of the EAPO are the power values $P_{f,m,j}^k$ defined at the grid nodes k for each furnace f , melt cycle m and stage j and the starting time of each stage $t_{f,m,j}$. The proposed modelling approach is based on the definition of boolean variable $x_{f,m,j}^k$ for each node on the time grid, which is True for the nodes occurring after the start of stage $j_{f,m}$ and False for those preceding it.

Parameters

r^{cast}	casting rate [m ³ /s]
r^{of}	overflow rate limit [kW]
r^{pwr}	power rate limit [kW/s]
r^{sp}	splash rate limit [kW]
v	pouring furnace volume [m ³]
\check{v}	tapped volume into pouring furnace [m ³]
\hat{v}	cast volume from pouring furnace [m ³]
$\bar{k}_{c,n}$	breakpoint n on casting rate for line c [s]
C	spot market objective function [€]
E, \hat{E}	stage energy (actual, min.) [kW h]
\hat{E}^{sp}	minimum energy causing splash in stage 2 [kW h]
N_q	market discretization to grid step ratio [-]
L_{max}	maximum number of ladles [-]
P^{max}	maximum power [kW]
P_l^{max}	maximum power of power pack l [kW]
$P_{f,m,j}^{\text{min/max}}$	min/max stage dependent power [kW]
γ_c	pouring furnace power coefficient [kW/m ³]
$\alpha_{f,j}$	energy correction parameter [-]
$\bar{\tau}$	maximum holding time without reheating [s]
$\hat{\Delta}$	stage time duration (minimal) [s]

$\Delta_{f,c}^{\leftrightarrow}$	ladle travel time [s]
$\widehat{\Delta}^{\text{of}}$	min. time with risk of overflow [s]
ΔT_m	time discretization step for market m [s]
ΔE_c	energy shifted in DAF mode for line c [s]
δt	time discretization step [s]

Constraints:

Melting operation

$$(1-x_{f,m,j}^k)(1+k) + K_{f,m,j}^{\min} \leq t_{f,m,j}/\delta t \leq x_{f,m,j}^k + (1-x_{f,m,j}^k)K_{f,m,j}^{\max} \quad \forall f,m,j,k$$

uses binary variable x to map the starting time of each stage onto the node at which corresponding stage starts

$$P_{f,m,j}^{\min}(x_{f,m,j}^k - x_{f,m,j+1}^k) \leq p_{f,m,j}^k \leq P_{f,m,j}^{\max}(x_{f,m,j}^k - x_{f,m,j+1}^k) \quad \forall f,m \in \mathcal{M}_f, j \in \mathcal{J} \setminus |\mathcal{J}|, k$$

renders the power consumed by task $j_{f,m}$ zero at any instance out of the stage interval

$$\sum_{f \in \mathcal{F}_l} \sum_{m \in \mathcal{M}_f} \sum_{j \in \mathcal{J}} p_{f,m,j}^k \leq P_l^{\max} \quad \forall l, k$$

Limits the maximum power available For each subset of furnaces connected to a single power line

$$\sum_{k \in \mathcal{K}} p_{f,m,j}^k \delta t = E_{f,m,j} \quad \forall f,m \in \mathcal{M}_f, j \in \mathcal{J}^E$$

$$t_{f,m,j+1} - t_{f,m,j} \geq \widehat{\Delta}_{f,m,j} \quad \forall f,m \in \mathcal{M}_f, j \in \mathcal{J}^T \setminus |\mathcal{J}|$$

$$t_{f,m+1,1} - t_{f,m,|\mathcal{J}|} \geq \widehat{\Delta}_{f,m+1,1} \quad \forall f,m \in \mathcal{M}_f \setminus |\mathcal{M}_f|$$

Imposes the stage completion conditions for both energy-based and time-based stages.

$$\sum_{j \in \mathcal{F}} \sum_{m \in \mathcal{M}_f} \sum_{j \in \mathcal{J}} p_{f,m,j}^k \leq P^{\max} \quad \forall k$$

Limits the overall power consumption

$$P_j^{\min} y_{f,m,j}^k \leq p_{f,m,j}^k \leq P_j^{\max} y_{f,m,j}^k \quad \forall f,m \in \mathcal{M}_f, k$$

make the power semi-continuous to avoid a particular low-power range without excluding the possibility for pre-emption (i.e. zero-power) where y is an auxiliary binary variable defined for each stage. Here

we assume that a linear model can be fitted to give an over-estimation of heat loss in each stage as the function of its duration:

$$E_{f,m,j} = \widehat{E}_{f,m,j} \left(1 + \sum_{j'' < j' \leq j} \alpha_{f,m,j'} \frac{t_{f,m,j'+1} - t_{f,m,j'}}{\widehat{\Delta}_{f,m,j'}} \right)$$

$$p_{f,m,2}^k \leq P^0 + r^{\text{pwr}} \sum_{k'=1}^k y_{f,m,2}^{k'} \delta t \quad \forall f,m \in \mathcal{M}_f, k$$

The same binary can be used to apply the power ramp limit for particular stages

$$r^{\text{of}} \left(\sum_{k'=1}^k x_{f,m,3}^{k'} \delta t - \widehat{\Delta}^{\text{of}} \right) \leq \sum_{k'=1}^k p_{f,m,3}^{k'} \delta t \leq \widehat{E}^{\text{SP}} + r^{\text{SP}} \sum_{k'=1}^k x_{f,m,3}^{k'} \delta t \quad \forall f, m \in \mathcal{M}_{f,k}$$

It keeps the power for the stage 2 within the feasible range which, in addition to the upper and lower power limits, is characterized by the overflow and splash limits

Moulding operation

$$v_c^{\text{min}} \leq v_c^0 + \sum_{f \in \mathcal{F}_c} \check{v}_f^{k-\Delta_{f,c}^{\vec{}}} - \widehat{v}_c^k \leq v_c^{\text{max}}$$

imposes buffer limits on the input-output balance of the molten iron from each pouring furnace where the input and output flow is respectively obtained by:

$$\widehat{v}_c^k = \sum_{n'=1}^{N_c-1} (\bar{k}_{c,n'} (r_{c,n'+1}^{\text{cast}} - r_{c,n'}^{\text{cast}}) - r_{c,n+1}^{\text{cast}} k) \delta t$$

$$\check{v}_{f,m}^k = v^{\text{tl}} \sum_{m \in \mathcal{M}_f} \sum_{j \in \mathcal{J}^{\text{tp}}} x_{f,m,j}^k \quad \forall f, m \in \mathcal{M}_{f,k}$$

respectively give the input and output flow

$$\sum_{k \in \mathcal{K}} p_{f,m,j}^k \delta t \geq \alpha_{f,m,j} ((t_{f,m,j+1} - t_j) / \bar{\tau}_{f,m,j}^{\text{tp}} - 1) \quad \forall f, m, j \in \mathcal{J}^{\text{tp}} \setminus \mathcal{J}$$

triggers reheating in case the holding time take longer than the minimum nominal value

$$\widetilde{p}_c^k = \gamma_c \left(v_c^0 + \sum_{f \in \mathcal{F}_c} \sum_{m \in \mathcal{M}_f} \check{v}_{f,m}^k - \widehat{v}_c^k \right)$$

approximates the power used by pouring furnaces to hold the temperature depends on their charged volume

Transposition ladle

$$\sum_{c \in \mathcal{C}} \sum_{f \in \mathcal{F}_c} \sum_{m \in \mathcal{M}_f} \sum_{j \in \mathcal{J}^{\text{tp}}} (x_{f,m,j}^k - x_{f,m,j}^{k-\Delta_{f,c}^{\vec{}}}) \leq L^{\text{max}} \quad \forall k$$

imposes an upper bound on the total number of ladles available on the shop floor

Load tracking

$$\left| \sum_{k \in \mathcal{K}_{q'}} \sum_{f \in \mathcal{F}_c} \sum_{m \in \mathcal{M}_f} \sum_{j \in \mathcal{J}} \frac{p_{f,m,j}^k}{N_q} - P_q^{\text{bl}} \right| \leq \delta^{\text{bl}}$$

Imposes the load tracking in the real-time optimization where load variations must be confined within $P_q^{\text{bl}} \pm \delta^{\text{bl}}$ in each interval q

Objective

Considering the whole shop floor, the day-ahead optimization problem can be decomposed into sub-problems for each subset of furnaces exclusively assigned to casting line c . It must be assumed that a maximum power can be imposed separately for each subset. The cost function for each casting line gives:

$$C_c = \sum_{f \in \mathcal{F}_c} \sum_{m \in \mathcal{M}_f} \sum_{j \in \mathcal{J}} \sum_{k \in \mathcal{K}} [p_{f,m,j}^k \lambda_k^{da} \delta t] + \sum_{k \in \mathcal{K}} \tilde{p}_c^k \lambda_k^{da} \delta t$$

where λ_k^{da} is the day-ahead market price.

Eventually the total cost of energy consumed by the whole plant is given by:

$$C = \sum_{c \in \mathcal{C}} C_c$$

It is worth mentioning that the additional fees regarding the maximum contracted power demand (MCD) have not been included in the cost function, as it is assumed to be negotiated for a much longer time

period and thus constant during the scheduling horizon. In addition, we assume that the total installed capacity of all power units is equal to the MCD.

In addition, by including the finish time of the last stage for each furnace it is possible to minimize the makespan in a similar way discussed in section 0 (page 22).

Real-time load tracker (MPC module)

On the day of operation, the baseline is passed on to the real-time load tracker where it supervises the production and modify the scheduling in the case of discrepancy with the day-ahead plan.

Different functionalities of this customized software are presented here. First, we describe the development of hardware-in-the-loop simulation of the process

Hardware-in-the-loop simulation

In this section we discuss the hardware-in-the-loop simulation process using Matlab. The simulation set-up has be illustrated in the Figure 26. In this case, the MILP model is solved using Gurobi, which together with the model builder are installed on an industrial PC. The model builder is in fact a Python API, which receives data including completion requirements for the tasks within the optimization horizon and send the MILP model for that specific time instance to the optimizer. For a more realistic simulation, the model builder is directly connected to the SCADA where operators command could be emulated for unforeseen events indicating a halt in process or premature completion of task or a melting cycle.

Gurobi, the optimizer, solves the model and sends the optimal power profile to the simulator, which is a simplified model of the furnace in Matlab environment.

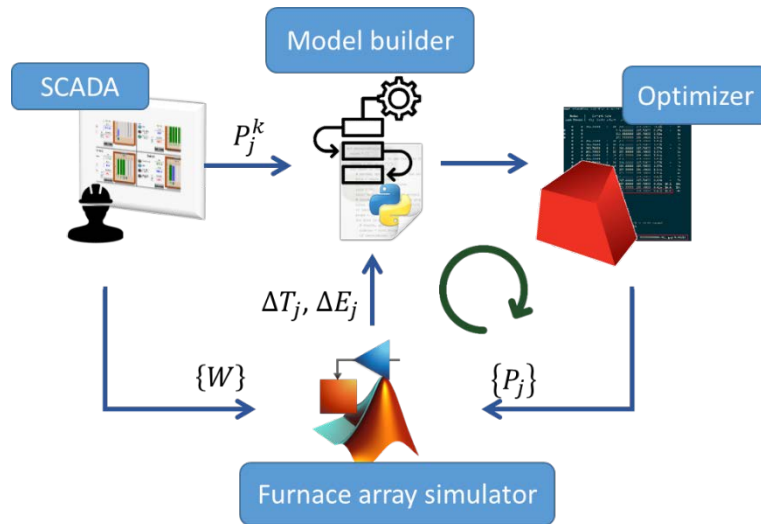


Figure 26 Hardware-in-the-loop simulation of EAPO real-time module

In the Matlab model, which is identified based on real data, the time and energy for the completion of tasks within optimization horizon is modified based on the optimized power profile and load weight given by the operator.

Shop-floor Installation

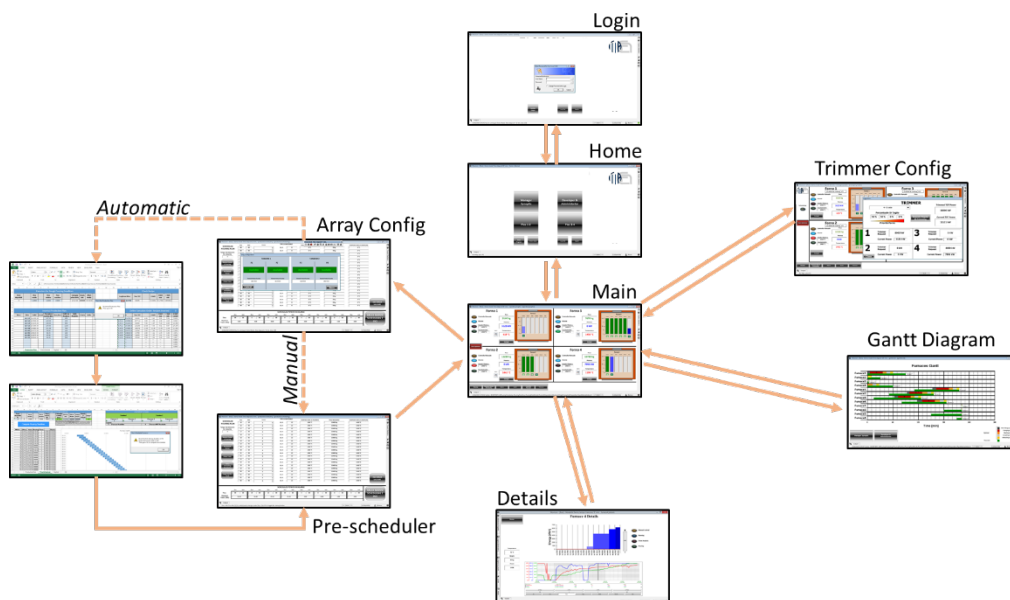


Figure 27 : Manager User Screen Map

Figure 27 shows a map of the screens navigable by the *Manager* User where each arrow shows a possible path. The optimizer is configured with a set of nominal parameters. The *Furnace Area Manager* must provide these data obtained from the day-ahead module at the beginning of a new scheduling session; he can modify these, as well as the production plan data, whenever is necessary. Variation of these

quantities will be accepted also online, when the optimizer is running, without requiring to stop and re-launch the system. Any modification of these data defines a new scheduling session. The Manager main screen shows the current status of the entire array of furnaces. For each Furnace are displayed the values of weight, power consumed, temperature.

Inside the orange box, a sketch of a furnace silhouette, each column represent a phase of the melting process; its completion level (from 0 to 100%) is shown by the filling bar. The read-only OK buttons, editable by the operators in their HMI, are shown to the manager.

To give the manager a feedback on the completion of the production plan, it is shown the code number that they are currently melting and how many melts are still required to finish it. (see Figure 28)

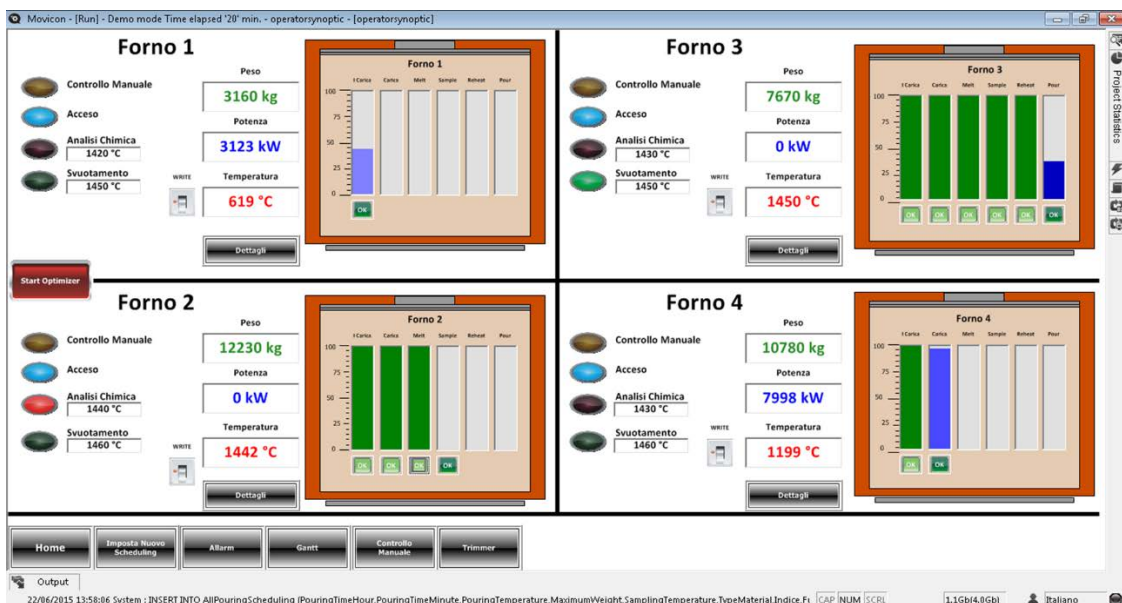


Figure 28 : Manager Main screen for a single furnace array

```

442 262 infeasible 53 - 3.8256e+07 - 488 55s
857 425 infeasible 56 - 3.8264e+07 - 339 60s
1237 574 3.8266e+07 15 653 - 3.8266e+07 - 337 65s
1614 691 infeasible 25 - 3.8266e+07 - 344 70s
2504 1070 3.8314e+07 18 599 - 3.8267e+07 - 300 76s
2988 1258 3.8725e+07 26 925 - 3.8267e+07 - 295 82s
2990 1259 3.9266e+07 34 525 - 3.8267e+07 - 295 85s
2998 1265 4.1169e+07 33 940 - 3.8267e+07 - 294 90s
3000 1269 3.8267e+07 13 755 - 3.8267e+07 - 11.8 97s
3006 1275 3.9551e+07 15 820 - 3.8267e+07 - 16.3 100s
3195 1347 4.0398e+07 24 406 - 3.8267e+07 - 38.1 105s
* 3732 1278 76 3.955820e+07 3.8267e+07 2.77% 48.9 108s
H 3799 1181 3.930672e+07 3.8278e+07 2.62% 49.1 109s
H 3810 1071 3.921247e+07 3.8278e+07 2.38% 50.1 109s
H 3811 1003 3.915515e+07 3.8278e+07 2.24% 50.4 109s
H 3817 942 3.914912e+07 3.8278e+07 2.23% 50.3 109s
H 3876 897 3.912592e+07 3.8278e+07 2.17% 51.1 109s
H 3878 845 3.911312e+07 3.8278e+07 2.14% 51.2 109s
H 3910 807 3.910207e+07 3.8278e+07 2.11% 51.5 109s
3937 816 3.8724e+07 22 211 3.9102e+07 3.8278e+07 2.11% 51.8 110s
H 3963 764 3.908767e+07 3.8278e+07 2.07% 53.3 110s
H 4019 732 3.906607e+07 3.8278e+07 2.02% 53.8 110s
H 4057 683 3.905974e+07 3.8318e+07 1.90% 55.4 111s
H 4382 575 3.897375e+07 3.8416e+07 1.43% 58.4 113s
4420 571 3.8716e+07 24 327 3.8974e+07 3.8416e+07 1.43% 59.6 115s
5356 627 3.8806e+07 37 105 3.8974e+07 3.8568e+07 1.04% 68.4 120s
7307 1039 3.8806e+07 30 148 3.8974e+07 3.8672e+07 0.77% 69.0 125s
9589 1218 infeasible 42 3.8974e+07 3.8796e+07 0.46% 66.7 130s
12851 733 3.8941e+07 44 83 3.8974e+07 3.8880e+07 0.24% 63.7 135s
*14370 437 66 3.895822e+07 3.8905e+07 0.14% 60.9 137s
*14376 436 67 3.895817e+07 3.8905e+07 0.14% 60.9 137s
*14789 306 67 3.895596e+07 3.8910e+07 0.12% 60.0 138s
*15209 194 63 3.894569e+07 3.8910e+07 0.09% 58.9 138s
*15860 126 59 3.894503e+07 3.8912e+07 0.09% 57.2 138s
*16312 40 60 3.894498e+07 3.8920e+07 0.07% 56.1 139s
16919 0 3.8920e+07 58 65 3.8945e+07 3.8920e+07 0.07% 54.7 140s

Cutting planes:
Learned: 16
Cover: 410
Implied bound: 202
MIR: 64
Flow cover: 8
GUB cover: 4
Inf proof: 2
Mod-K: 1

Explored 19030 nodes (1912955 simplex iterations) in 143.89 seconds
Thread count was 16 (of 16 available processors)

Solution count 10: 3.8945e+07 3.8945e+07 3.89457e+07 ... 3.90877e+07
Pool objective bound 3.8945e+07

Optimal solution found (tolerance 1.00e-04)
Best objective 3.894497696600e+07, best bound 3.894497696600e+07, gap 0.0000%

```

Figure 29 : log produced by the optimizer showing the progress of the optimization

The red button **Start Optimizer** launches the software's core executable. Every 30 seconds, SCADA triggers the execution of the optimization sending a socket command. The optimization procedure can be tracked from the log windows shown in the Figure 29.

From this time on, the Optimizer continuously updates the data and computes the remaining energies and launches again the optimization on the shifted control window. The plan for the operators is directly updated.

The furnace manager can monitor the job of its Operators from the dedicated Detail page, where indicators and graphical trends are shown.

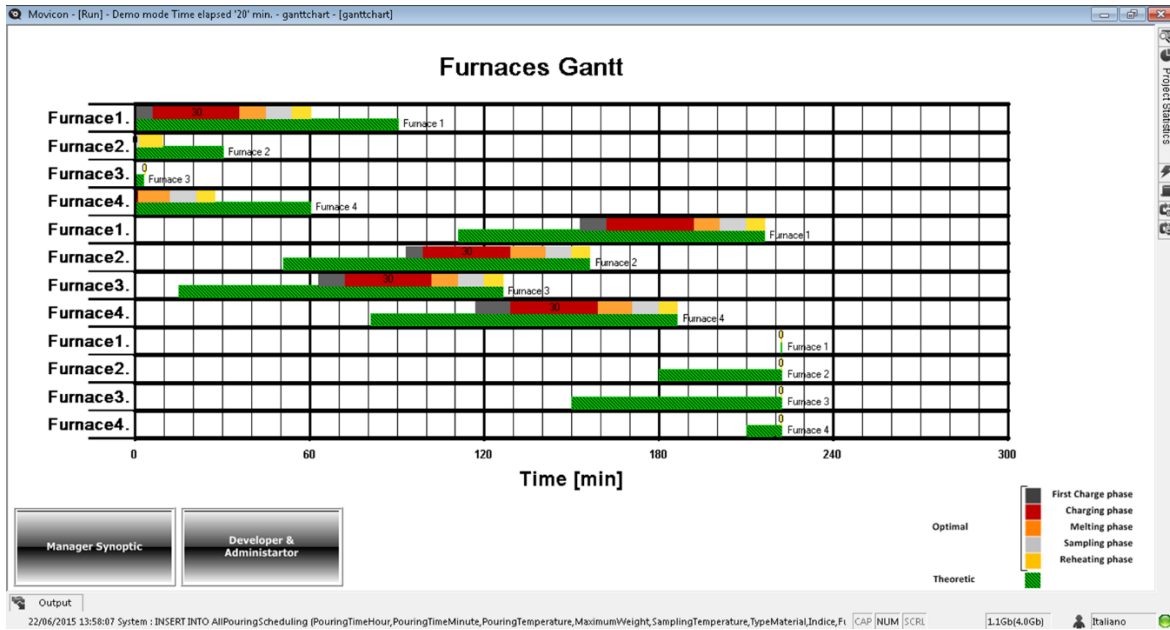


Figure 30 : Gantt Diagram (example from 8 furnace configuration)

A Gantt diagram (Figure 30) shows to the manager the schedule of the current and forthcoming melts. For each furnace, two bars present the pre-schedule (in green) representing the original scheduling strategy used in the foundry, and a multi-coloured bar which is the optimized melting schedule. Each colour is a phase of the melting process. Every cycle EAPO real-time module computes a new schedule using the updated information receiving from the plant.

Results

Here, for the case of spot market participation we have considered the hourly price from 2016, which has been shown in Figure 31. The same figure compares the sum of normalized power profile for four furnaces that deliver to single casting line. The yellow and blow curves respectively indicating the scheduled consumption for MCTS and DR program. The resultant committed load for the latter case have been shown with green dashed curve. From the figure, it is possible to see how consumption pattern has been modified according to price fluctuation as the load has been shifted away from time slot with higher energy cost. In the lower panel of the figure, we have also presented the normalized level of the buffer, using the same colours applied in the power profile panel. While the MCT solution maintains a level between 25% and 75%

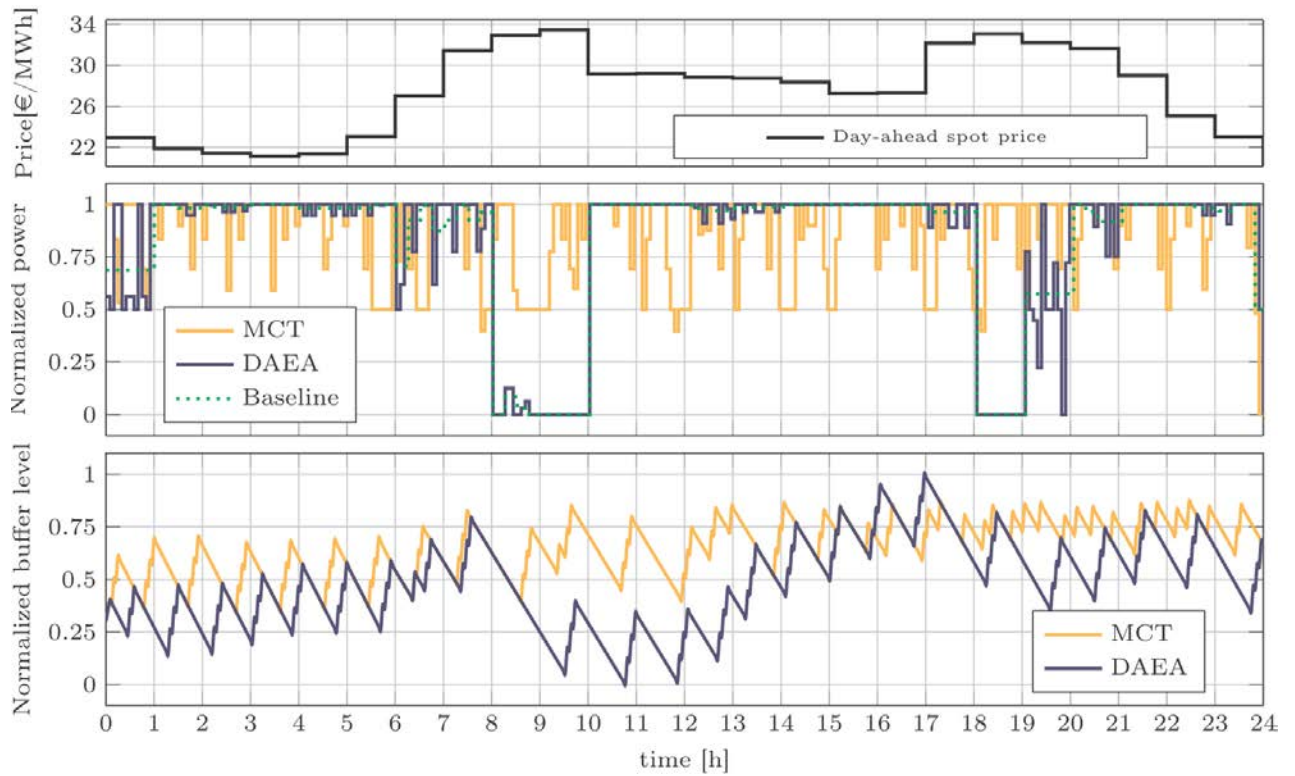


Figure 31 Up: Day-ahead price, Middle: Energy-away power optimization vs Minimum Cycle Time (MCT) profile, bottom: buffer level

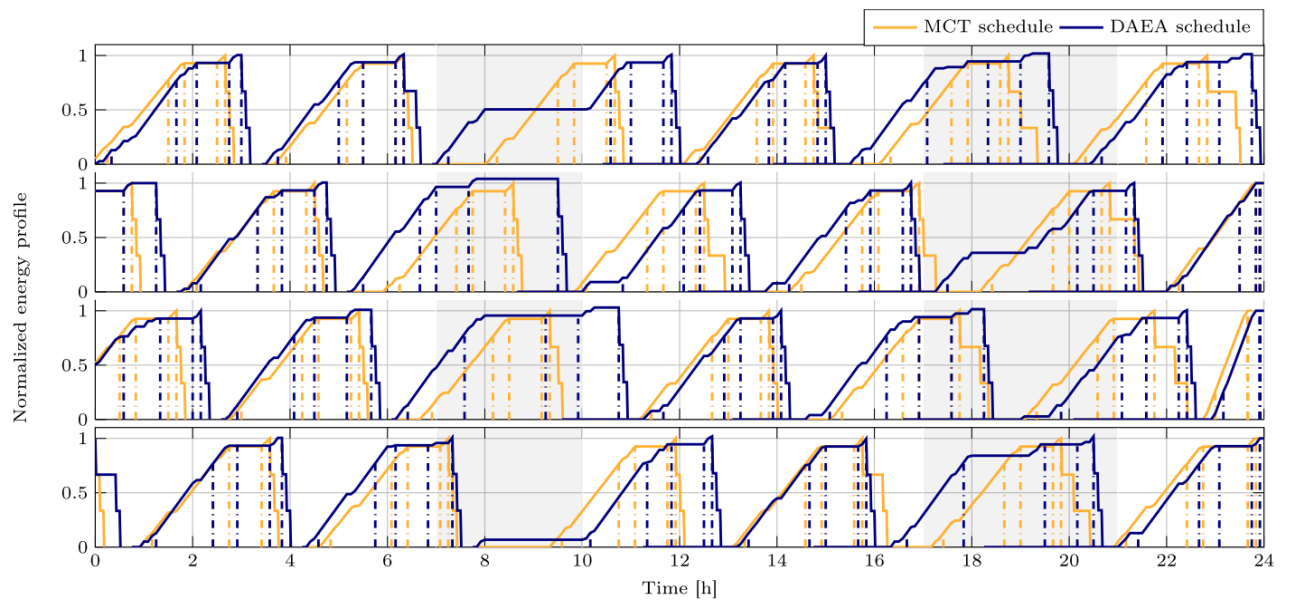


Figure 32 : Energy profile of induction furnace in the example for both minimum cycle time and Day-Ahead Energy Aware (DAEA) case

of the total capacity, DAEA optimization exploits the extremes of buffer capacity, in order to maintain the prescribed outflow even during low-power intervals. Accordingly, a rise in the buffer level before each price peak allows the postponement of cycle completion into cheaper periods, as it can be seen in Fig. 8, where the molten level rises from minimum to maximum in the period between two the peaks.

Figure 32 gives a more detailed account of flexibility provided by the underlying process. For each furnace the normalized energy profiles have been depicted for each scheduling case similarly with yellow and blue curves. Dotted lines have been used to indicate the stage changeover.

The grey area indicates intervals with the spot price over 30 Euro. One can see how DR programme affects the cycles falling within these high price time slots while maintaining a minimum cycle time for the ones under a relatively flat price.

For the sake of comparison, here we define as a measure the Equivalent Flat Rate (EFR), which is the price at which a long-term forward contract would cost the same as participation in the day ahead market. Table 3 reports the resulting EFR for a whole week.

Table 3 : Equivalent Flat Rate for optimal scheduling in day-ahead market (All the entries are expressed in €/MW h)

Spot price		Equivalent Flat Rate (EFR)							
Estimation	mean	Mo	Tu	We	Th	Fr	Sa	Su	Average
Exact	27.20	29.09	28.24	26.52	26.70	24.04	25.20	23.64	26.20
Last Week		30.29	28.29	26.75	26.78	24.28	25.35	23.67	26.49

Besides the fact that a major advantage of being able to purchase the electricity from spot market is its lower average cost, the resulting EFR is lower than the average daily price of spot market. According to this outcome, a foundry with a daily consumption of 300 MW h can approximately save up to 400 k€/year using the proposed DR approach and participating in Elspot instead of buying electricity from retailers via long-term contracts.

Moreover, with respect to a long-term TOU tariff, in which the EAS optimization resulted in an ERF of 27.8 €/MW h, participation in day-ahead energy market has proved to be more profitable. This is mainly due to a single peak hour tariff, which hinders the exploitation of process flexibility by the optimizer. While a down-to-zero reduction of consumption level consecutively for a long period may not be possible due to operational and capacity constraints, the same aggregated sum could be obtained if such reduction is broken down to multiple slots well apart from each other. Accordingly, the optimizer can take advantage of multiple peaks in price and minimize the costly energy consumption.

Conclusion and Future Work

In this document, we have given a detailed description of a prototype for a model-based control system for joint optimization of productivity and energy consumption of power-intensive processes. To this end, digitalization layer based on the concept of Cyber-Physical Systems (CPS) was developed to provide the required interconnection with the physical process and the management of the data flow from (and to) the field. Subsequently an optimization framework was introduced for the synthesis of an optimal scheduling in a generic production unit capable of incorporating various constraints and objectives including the ones required by various electricity markets. In this way, the proposed control system enables those industries to transform themselves into active nodes of the electricity smart grids and participate in various Demand-side management programmers.

Subsequently, prototypes have been developed to apply the proposed framework for two cases of energy-intensive industrial process: steelmaking and metal casting. In both cases various process accepts have been mathematically modelled using Mixed Integer Linear Programming technique. Then

we set up all the required connections with SCADA system to integrate the software to the shop floor and user interface. In addition using a Hardware-in-the-loop simulation environment, we verified the efficiency of the proposed framework.

Even though this work was primarily carried out for the optimal control of energy and production in a single production unit, the proposed control system can be implemented at the cluster level within a distributed framework (Figure 33). In such a concept, with the goal of minimizing the imbalance position of the cluster, maintaining congestion constraints and optimizing the costs of trading energy in the imbalance market, the central DR component starts a dialogue with the companies through shadow prices (λ_j). The companies respond to the prices and iterate in this manner with the central DR component. The iterations end either when a certain threshold for net deviations is achieved or when the time limit is hit, in which case the best solution hitherto is considered. This distributed framework can provide energy solution that is advantageous to the cluster as a whole, while keeping in mind the local constraints, and the costs and privacy of the individual companies.

WP1.1: TRL evolution:

TRL 4 → TRL 6

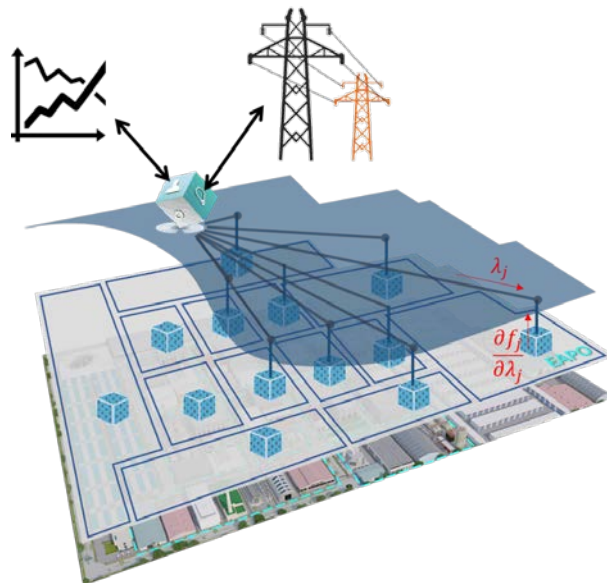


Figure 33 Distributed DR at cluster level

Quadro generale di riferimento, obiettivi e stato dell'arte

Introduzione

Le industrie manifatturiere si sono sempre focalizzate sul duplice asse produttività – qualità e, negli ultimi anni, anche la sostenibilità ha assunto un ruolo sempre più critico. Principalmente, sia l'industria che la ricerca, si concentrano sia sulla caratterizzazione energetica di risorse e componenti, sia su strategie di efficientamento energetico. Numerose strategie possono essere trovate in letteratura (e.g. Zhang (2013), Yoon et al. (2015b), Zhou et al. (2016)). A livello macchina, i componenti ausiliari possono facilmente richiedere un apporto di energia maggiore di quello strettamente necessario al processo poiché devono sia supportare l'esecuzione del processo stesso, sia mantenere la macchina nelle condizioni opportune che permettano l'inizio del processo successivo. Di conseguenza, le macchine utensili continuano a richiedere energia nonostante siano in stati non-operativi. Il controllo degli stati energetici delle macchine è una delle strategie più promettenti. Lo scopo di tale controllo è di ridurre il consumo energetico delle macchine utensili durante gli stati non-produttivi attraverso un appropriato spegnimento e una appropriata riaccensione di alcuni componenti della macchina. In letteratura, questa energia viene indicata come *"fixed energy"*, *"base load"*, *"consumo basale"*, o, in generale, *"non-processing energy"* (NPE). In diversi studi sulla caratterizzazione energetica delle macchine utensili, soprattutto per quelle dedicate all'asportazione di truciolo (e.g. Dahmus and Gutowski (2004), Yoon et al. (2015a)), il contributo NPE viene separato dal contributo PE (*processing energy*) che viene invece richiesto durante il processo. Vogliamo focalizzarci sulla riduzione della NPE ed in particolare sulle strategie di controllo energetico (energy efficient control = EEC). Ad un più alto livello della pianificazione aziendale è possibile eseguire una schedulazione opportuna della produzione al fine di migliorare l'efficienza energetica (energy efficient scheduling = EES). Una recente overview su EES è stata sviluppata da Gahm et al. (2016). EEC si posiziona a livello di controllo analizzando politiche di controllo implementate durante la produzione per lo più considerando stocasticità nell'arrivo delle parti.

La macchina utensile (riferendoci a macchine utensili per l'asportazione di truciolo) viene solitamente modellata attraverso un diagramma a stati come in Fig. 1. In aggiunta allo stato operativo *"busy"* (i.e., la macchina sta processando una parte) e lo stato *"idle"* dove la macchina è in attesa di materiale o bloccata, vengono aggiunti due stati: uno stato di *"standby"* a basso consumo energetico in cui la macchina è parzialmente disattivata e uno stato transitorio di *"startup"* in cui la macchina esegue una serie di procedure per rimettersi nelle condizioni opportune al processo. Un transitorio di *"shutdown"* può anche essere richiesto allo spegnimento della macchina. Le strategie di controllo proposte in letteratura decidono se le transizioni da e per lo stato di standby siano o meno vantaggiose.

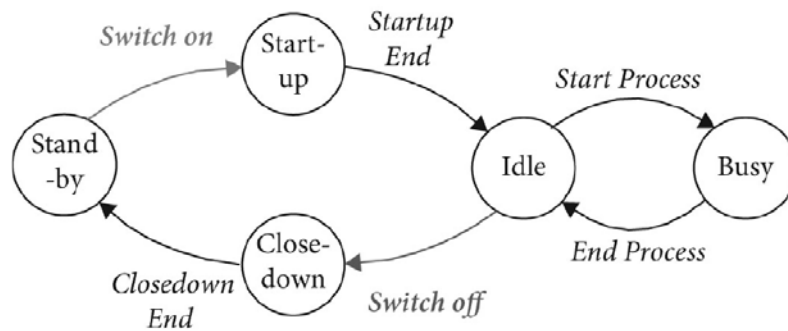


Fig. 1 Modello a stati di una macchina utensile controllata.

In letteratura, le transizioni off/on sono considerate immediate (Prabhu et al. (2012), Chen et al. (2011), Chang et al. (2013), Brundage et al. (2014)) o con una durata significativa. Mouzon et al. (2007), Frigerio e Matta (2015), Su et al. (2016), Frigerio et al. (2017a), e Jia et al. (2016) considerano una durata deterministica, mentre Nenes et al. (2012), Guo et al. (2013), Maccio and Down (2016), Frigerio e Matta (2016), e Frigerio et al. (2017b) studiano tempi di transizione stocastici. Come eccezione, Frigerio e Matta (2014) analizzano una durata dipendente dal tempo in cui la risorsa è stata nello stato standby, la diversa durata delle procedure di startu sono dovute ai fenomenici fisici e termici che influiscono sulla prontezza alla lavorazione della risorsa.

Due approcci modellistici sono utilizzati in letteratura per rappresentare la fase di processo: 1) il tempo ciclo è considerato deterministico ma le risorse sono affette da guasti (Chen et al. (2011); Chang et al. (2013); Brundage et al. (2014); Jia et al. (2016)), e 2) il tempo ciclo è una variabile stocastica su risorse perfettamente affidabili (i.e., i guasti sono modellati come variazioni sul tempo di processo nominale).

Le politiche di controllo energetico degli stati macchina possono essere basate sul tempo o sul livello dei buffer inter-operazionali. Una classificazione è proposta in seguito: 1) un primo gruppo di studi analizza il problema del controllo ove il servizio viene interrotto e ristabilito sulla base di informazioni temporali sugli arrivi (Mouzon et al. (2007); Prabhu et al. (2012); Frigerio e Matta (2014, 2015)); 2) un secondo gruppo di studi analizza politiche di controllo basate sul livello di parti nei buffer di sistema (Chang et al. (2013), Brundage et al. (2014), Jia et al. (2016), Maccio e Down (2016), Frigerio e Matta (2016), Su et al. (2016), Frigerio et al. (2017a,b)); 3) una combinazione di informazioni temporali e basate sull'occupazione dei buffer viene usata in un terzo gruppo di studi (Chen et al. (2011); Nenes et al. (2012); Guo et al. (2013)).

La letteratura su EEC studia applicazioni delle strategie di controllo a livello macchina considerando come applicazioni: stazioni single, flow shops, e linee di produzione sia con buffer a capacità finita che infinita. Quando la capacità del buffer è finita, la presenza dei transitori di startup e closedown influenza l'utilizzo della macchina utensile e di conseguenza, la sua produttività. Inoltre, per sistemi con multiple risorse controllate, il controllo di una risorsa può influenzare l'efficacia del controllo su un'altra risorsa. La propagazione degli effetti di starvation e blocking rendono non triviale l'effetto del controllo a livello macchina sulla produttività e sul consumo totale del sistema. Un'accurata analisi dei possibili deadlock deve essere condotta e condizioni di controllo appropriate devono essere introdotte.

Al fine di presentare alcuni esempi a livello di linea, Jia et al. (2016) studiano una linea di produzione seriale con machine Bernulliane dove alcune macchine possono essere controllate a seconda del livello

buffer. Su et al. (2016) discutono l'impatto di politiche di controllo macchina sulle performance di linea a seconda della politica utilizzata. Anche in questo caso il livello del buffer viene utilizzato come parametro di controllo e l'ottimo viene ricercato attraverso un software commerciale (OptQuest). Frigerio et al. (2017a) propongono un algoritmo basato su Nested Partitioning per ottimizzare una strategia che utilizza solo l'informazione derivante dal buffer a monte della macchina.

Bibliografia

- Brundage, M.P., Chang, Q., Li, Y., Xiao, G. and Arinez, J. (2014). Energy efficiency management of an integrated serial production line and HVAC system, *IEEE Transactions on Automation Science and Engineering*, 11(3), 789-797.
- Chang, Q., Xiao, G., Biller, S. and Li, L. (2013). Energy saving opportunity analysis of automotive serial production systems. *IEEE Transactions on Automation Science and Engineering*, 10(2), 334-342.
- Chen, G., Zhang, L., Arinez, J. and Biller, S. (2011). Feedback control of machine startup for energy-efficient manufacturing in Bernoulli serial lines. *Proceedings of IEEE International Conference on Automation Science and Engineering*, 666-671, Trieste, Italy.
- Dahmus, J.B. and Gutowski T.G. (2004). An Environmental Analysis of Machining. In *Manufacturing Engineering and Materials Handling Engineering ASME*, pages 643–652.
- Frigerio, N. and Matta, A. (2014). Energy efficient control strategy for machine tools with stochastic arrivals and time dependent warm-up. *Procedia CIRP*, 15, 56-61.
- Frigerio, N. and Matta, A. (2015). Energy-efficient control strategies for machine tools with stochastic arrivals. *IEEE Transactions on Automation Science and Engineering*, 12(1), 50-61.
- Frigerio, N. and Matta, A. (2016). Analysis on energy efficient switching of machine tool with stochastic arrivals and buffer information. *IEEE Transactions on Automation Science and Engineering*, 13(1), 238-246.
- Frigerio, N., Matta, A. and Lin, Z. (2017a). Nested partitioning algorithm for the optimization of control parameters in energy efficient production lines. *Proceedings of XIII Convegno - Associazione dell'Italiana di Tecnologia Meccanica*, Pisa, Italy.
- Frigerio, N., Matta, A., Ferrero, L., Rusina', F . (2013). Modeling Energy States in Machine Tools: An Automata Based Approach. *Re-Engineering Manufacturing for Sustainability - Proceedings of the 20th CIRP Int. Conf. on Life Cycle Eng.*, Springer, Singapore, pp. 203-208.
- Frigerio, N., Shanthikumar, J.G. and Matta, A. (2017b). Dynamic programming for energy state control of machine tools in manufacturing with part admission control. *Proceedings of 11th Conference on Stochastic Models of Manufacturing and Service Operations*, 85-92, Acaya, Italy.
- Gahm, C. Denz, F., Dirr, M. and Tuma, A. (2016). Energy-efficient scheduling in manufacturing companies: a review and research framework. *European Journal of Operational Research*, 248(3), 744-757.
- Ghadimi, P., Li, W., Kara, S. and Herrmann, C. (2014). Integrated material and energy flow analysis towards energy efficient manufacturing. *Procedia CIRP*, 15, 117-122.
- Guo, X., Zhou, S., Niu, Z. and Kumar, P.R. (2013). *Proceedings of International Teletraffic Congress*, 6662947, Shanghai, China.
- Jia, Z., Zhang, L., Arinez, J. and Xiao, G. (2016). Performance analysis for serial production lines with Bernoulli machines and real-time WIP-based machine switch-on/off control. *International Journal of Production Research*, 54(21), 6285-6301.
- Li, L., and Sun, Z. (2013). Dynamic energy control for energy efficiency improvement of sustainable manufacturing systems using Markov decision process. *IEEE Transactions on Systems, Man, and Cybernetics: Systems*, 45(5), 1195-1205.
- Lin, Z., A. Matta, and J. G. Shanthikumar. 2018. "Combining Simulation Experiments and Analytical Models with Different Area-Based Accuracy for Performance Evaluation of Manufacturing Systems". Accepted for publication in *IIE Transactions*, May 31st, 2018.
- Lin, Z., A. Matta, N. Li, and J. G. Shanthikumar. 2016. "Extended Kernel Regression: A multi-resolution method to combine simulation experiments with analytical methods". In *Proceedings of the 2016 Winter Simulation Conference*, edited by T. M. K. R. et al., 590–601. IEEE.
- Maccio, V.J. and Down, D.G. (2016). Exact analysis of energy-aware multi-server queueing systems with setup times. *Proceedings of 24th IEEE International Symposium on Modeling, Analysis and Simulation of Computer and Telecommunication Systems*, 11-20, London, UK.
- Matta, A., N. Li, Z. Lin, J. Shanthikumar et al. 2015. "Operational learning of approximate analytical methods for performance evaluation of manufacturing systems". In *10th Conference on Stochastic Models of Manufacturing and Service Operations SMMSO 2013*, 137–144. University of Thessaly Press.

- Mouzon, G., Yildirim, M.B. and Twomey, J. (2007). Operational methods for minimization of energy consumption of manufacturing equipment. *International Journal of Production Research*, 45(18-19), 4247-4271.
- Nenes, G., Panagiotidou, S. and Dekker, R. (2010). Inventory control policies for inspection and remanufacturing of returns: a case study. *International Journal of Production Economics*, 125(2), 300-312.
- Prabhu, V.V., Jeon, H.W. and Taisch, M. (2012). Modeling green factory physics - an analytical approach. *Proceedings of IEEE International Conference on Automation Science and Engineering*, 46-51, Seoul, Korea.
- Shi, L. and Olafsson, S. (2009) *Nested Partitions Method, Theory and Applications*, Springer.
- Su, H., Frigerio, N. and Matta, A. (2016). Energy saving opportunities and value of information: a trade-off in a production line. *Procedia CIRP*, 48, 301-306.
- Yoon, H.S., Kim, E.S., Kim, M.S., Lee, J.Y., Lee, G.B. and Ahn, S.H. (2015b). Towards greener machine tools – a review on energy saving strategies and technologies. *Renewable and Sustainable Energy Reviews*, 48, 870-891.
- Yoon, H.S., Lee, J.Y., Kim, H.S., Kim, M.S., Kim, E.S., Shin, Y.J., Chu, W.S. and Ahn, S.H. (2015a). A comparison of energy consumption in bulk forming, subtractive, and additive processes: review and case study. *International Journal of Precision Engineering and Manufacturing-Green Technology*, 1(3), 261-279.
- Zhang, Y. (2013). Energy efficiency techniques in machining process: a review. *International Journal of Advanced Manufacturing Technology*, 71(5), 1123-1132.
- Zhou, L., Li, J., Li, F., Meng, Q., Li, J., and Xu, X. (2016). Energy consumption model and energy efficiency of machine tools: a comprehensive literature review. *Journal of Cleaner Production*, 112, 3721-3734.

Obiettivi

L'obiettivo principale delle attività consiste in un'analisi di politiche di controllo per il miglioramento dell'efficienza energetica dei sistemi produttivi discreti e nell'identificazione di linee guida su tali strategie di controllo.

A valle di un'analisi della letteratura esistente, diverse politiche di controllo verranno identificate e discusse. L'analisi comparativa delle politiche di controllo porterà all'identificazione di quelli che sono i fattori determinanti per la scelta di una specifica politica. Inoltre, la ricerca di parametri di controllo in grado di migliorare il consumo energetico senza compromettere la produttività del sistema verrà perseguita attraverso opportuni problemi di ottimizzazione stocastica. L'ottimizzazione dei parametri di controllo presenta le seguenti criticità: (a) nell'alto numero di alternative da valutare, (b) la difficoltà tecnica nel valutare le alternative in un problema multi-obiettivo e (c) nella stocasticità del problema che rende la ricerca dell'ottimo ulteriormente critica. Software commerciali di ottimizzazione saranno utilizzati per la ricerca della combinazione ottima dei parametri di controllo. La migliore strategia applicabile a un dato sistema verrà analizzata supponendo che tale sistema sia in grado di operare in diverse modalità operazionali ottenute attraverso un target di produttività.

All'aumentare della complessità dei sistemi di produzione considerati, le performance di sistema devono essere accuratamente analizzate attraverso opportuni modelli. Una metodologia per la stima delle performance di sistemi controllati verrà proposta utilizzando una combinazione di simulazione ad eventi discreti e metodi analitici. Infatti, a causa della complessità dei sistemi di produzione in ambito manifatturiero e delle frequenti interazioni tra i parametri di controllo, le performance di un sistema controllato sono difficili da prevedere sia in termini di produttività che di consumo energetico. La simulazione ad eventi discreti viene spesso utilizzata in letteratura in quanto permette di ottenere previsioni accurate a fronte di un budget computazionale elevato. Inoltre, metodi analitici permettono di rappresentare il problema in modo rapido, ma sotto opportune limitazioni ed approssimazioni. In particolare, un approccio recentemente proposto in letteratura verrà utilizzato e modificato ad hoc per creare un meta-modello di stima di performance (Extended Kernel Regression or EKR proposto in

letteratura da Matta et al, 2015; Lin and Matta, 2017; Lin et al, 2018). Questo metodo permette di combinare modelli analitici approssimati (Low-Fidelity) con modelli accurati (High-Fidelity) per ottenere un meta-modello rappresentativo del sistema. In particolare, verrà analizzato un sistema di produzione in linea transfer composto da buffer a capacità finita e macchine controllate con una politica basata sull'occupazione dei buffer. I metodi analitici presenti in letteratura verranno analizzati e un meta-modello per la previsione di produttività e consumo energetico verrà costruito utilizzando il metodo EKR.

Risultati conseguiti

Le procedure di *startup* e di *closedown* delle machine utensili possono impattare negativamente sull'efficacia delle politiche di controllo applicate. Di conseguenza, all'aumentare della complessità dei sistemi di produzione considerati, le performance di sistema devono essere accuratamente analizzate attraverso opportuni modelli. Nuove soluzioni devono mantenere alta la produttività di sistema migliorandone simultaneamente la sostenibilità.

Modelli di simulazione e modelli analitici vengono comunemente utilizzati per prevedere le performance di sistemi controllati. Tuttavia, i primi richiedono un alto carico computazionale per ottenere stime accurate, mentre i secondi sono rapidi ma approssimati. Nuovi metodi per la stima delle performance di sistemi controllati e l'ottimizzazione dei parametri di controllo sono necessari ai fini dell'applicabilità di strategie di controllo a casi reali.

Il contributo principale delle attività A1.2 è duplice:

C1. Vengono definite guidelines per il controllo degli stati energetici di machine utensili in sistemi di produzione manifatturieri.

Le attività hanno permesso di stendere una serie di guidelines per il risparmio energetico nei sistemi produttivi. A valle di un'analisi della letteratura esistente, diverse politiche di controllo sono state identificate e descritte nelle loro peculiarità, potenzialità e limitazioni di applicazione. Una tabella riassuntiva delle politiche analizzate si trova in Tab.1. L'analisi comparativa delle politiche di controllo ha portato all'identificazione di diversi fattori determinanti per la scelta di una specifica politica di controllo (e.g. la saturazione delle macchine, il costo di accumulo delle parti in coda, il periodo di transizione per il riavvio della produzione). Vantaggi e svantaggi delle politiche sono raccolti in Tab.2. Un'analisi focalizzata su casi di studio realistici e basata su misurazioni sperimentali di profili di potenza e dati estratti dalla letteratura scientifica ha portato alla stesura di una serie di guidelines che permettono di guidare la scelta della politica di controllo in una serie di applicazioni quali: macchine senza evidenti transitori, linee bilanciate, linee non bilanciate, etc.

Tab. 1 Politiche di controllo analizzate e discusse. Le politiche UDS, US e DS sono politiche che utilizzano informazioni sull'occupazione dei buffer per controllare lo stato di una determinata macchina in un sistema (US utilizza informazioni sul buffer a monte, DS sul buffer a valle, e UDS informazioni da entrambi i buffer). Le politiche di tipo "Switching" utilizzano time-thresholds per il

controllo di una determinata macchina.

	UDS	US	DS	Switching	Switch off	Switch on
Policy Characteristics						
Time information				X	X	X
Upstream buffer	X	X				
Downstream buffer	X		X			
Machine control parameters	4	2	2	2	1	1
Possible Applications						
Stand alone				X	X	X
Transfer line	X	X	X	X	X	X
Assembly	X	X	X	X	X	X
Job shops		X		X	X	X

Tab. 2 Vantaggi e svantaggi delle più promettenti politiche di controllo degli stati energetici delle macchine utensili.

	UDS	DS	US	Switching	Switch on	Switch off
Pros						
Efficient for highly starved machine.	X		X	X	X	X
Efficient for highly blocked machine.	X	X				
Startup procedure starts in advance (reduce risk of production loss).				X	X	
More information used from system. Higher savings.	X					
Simple. Closed form available for some cases.				X	X	X
Cons						
Not applicable without buffer information.	X	X	X			
Parts wait for machine readiness.	X	X	X			X
Switch-on might not be necessary.				X	X	
Risk of frequent off/on procedures					X	
Deadlock analysis required	X	X	X			

C2. Viene proposta una nuova metodologia per la valutazione delle performance (e.g. energia consumata, produttività) di sistemi produttivi controllati con politiche di risparmio energetico.

La metodologia proposta permette di ottenere un meta-modello per la valutazione delle prestazioni di una linea di produzione seriale con capacità di buffer finita e tutte le macchine controllate con una politica di controllo basata sull'occupazione dei buffer che tenga conto della stocasticità dei processi. Una combinazione di metodi analitici già presenti in letteratura e modelli di simulazione ad eventi discreti viene utilizzata per la creazione del meta-modello integrando i vantaggi di entrambe le tecniche. Grazie alla flessibilità di tale metodologia, le potenziali applicazioni risultano essere molteplici nei confronti di applicazioni industriali reali. Le analisi numeriche sono concentrate su linee di produzione transfer bilanciate e non bilanciate.

Confronto con i risultati attesi ed eventuali scostamenti rilevati

Non si sono evidenziati scostamenti rilevanti rispetto ai risultati attesi.

Deliverables

Il principale deliverable di questa attività è il seguente:

- Report D_1.2: Definizione della metodologia di qualificazione energetica e definizione di guidelines sulle strategie di controllo di sistemi produttivi discreti al fine di migliorare performance produttive e consumo energetico. (POLIMI).

Descrizione report tecnico

Il Report D_1.2 riporta i risultati delle attività A1.2 in D3 - PROCESSI E MACCHINARI INDUSTRIALI: "Metodi di analisi e controllo per l'efficienza congiunta delle prestazioni produttive e dei consumi energetici di sistemi produttivi discreti". Il report è suddiviso in sezioni focalizzate sulle seguenti tematiche:

1. Introduzione;
2. La sezione 2 fornisce una revisione della letteratura sul controllo dell'efficienza energetica dei sistemi di produzione con particolare attenzione al controllo dello stato della macchina;
3. La formulazione del problema si trova nella sezione 3 con un'analisi delle politiche più promettenti in letteratura;
4. Una metodologia basata su una combinazione di metodi di simulazione e analisi è proposta e descritta nella sezione 4;
5. La sezione 5 raccoglie i risultati sperimentali. Gli esperimenti si basano su misurazioni reali di macchine utensili e dati provenienti dalla letteratura;
6. Un'analisi comparativa consente l'individuazione di linee guida (Sezione 6) per il controllo delle macchine in sistemi di produzione manifatturieri discreti al fine di aumentarne la sostenibilità.

Descrizione dell'approccio tecnico in "Descrizione report tecnico".

La metodologia Extended Kernel Regression (EKR), recentemente proposta in letteratura (Matta et al., 2015, Lin et al., 2016, Lin et al., 2018), consente la creazione di un modello surrogato globale che combina un modello capace di valutare accuratamente le performance di un sistema (i.e., tale modello viene detto ad alta fedeltà o HF) con uno o più modelli meno accurati (i.e., tali modelli vengono detti a bassa fedeltà o LF). Il modello HF è una rappresentazione estremamente accurata del sistema, ma è lento nell'esecuzione, mentre i modelli LF sono più veloci ma possono fornire stime distorte. Il metodo EKR identifica autonomamente quali modelli LF sono più utili al variare dei parametri del problema comparando la stima ottenuta da tali modelli LF e quella del modello HF. Occorre però una scelta accurata dei metodi analitici LF tale da non aggiungere rumore alle osservazioni HF, insieme ad un'ottimizzazione dei parametri di bandwidth delle funzioni di Kernel. Queste attività sono state svolte considerando il problema di sistemi con macchine controllate attraverso politiche di controllo per il risparmio energetico.

L'approccio usato è rappresentato in Fig. 2. Un piano sperimentale iniziale ($x_i^0 | i = 1, \dots, n$) permette di esplorare la funzione in relazione a variazioni dei parametri del problema, nel nostro caso si tratta

dei parametri di controllo delle macchine. L'effetto di ogni combinazione di parametri sulle performance del sistema (energia per parte prodotta, nel nostro caso) viene stimato utilizzando sia il modello HF ($y_h(x^0)$) che i modelli LF ($y_l(x^0) \forall l$). Data una combinazione x di parametri sconosciuta e da prevedere, il metodo EKR accetta le stime dei modelli LF in tale punto ($y_l(x) \forall l$), essendo di veloce esecuzione, ed applica una correzione basata sul piano sperimentale precedentemente acquisito senza ricorrere al modello HF e risparmiando quindi tempo computazionale. Tecniche di regressione polinomiale vengono utilizzate. Inoltre, un peso diverso (i.e., basato su un Kernel Gaussiano) viene assegnato ad ogni modello LF: la funzione *Gaussian Kernel* assegna pesi più elevati ai punti sperimentali che sono vicini al punto sconosciuto ed assegna pesi inferiori ai punti più lontani. Nella fase finale, le stime fornite dai modelli LF sono combinate per ottenere la stima finale del meta-modello $y(x)$.

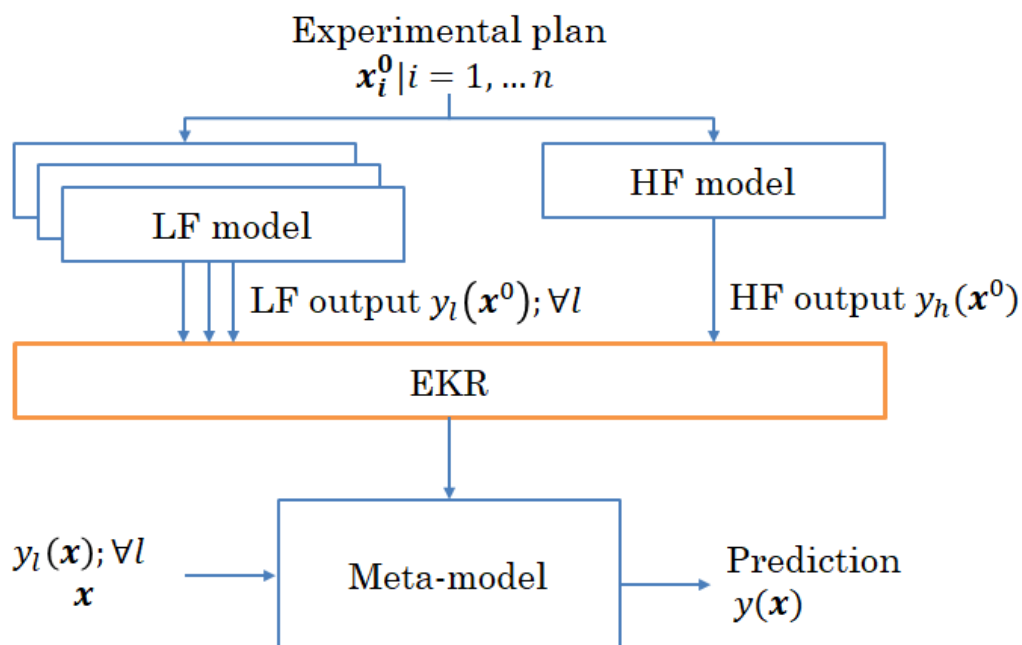


Fig. 2 Funzionamento del metodo EKR.

Un metodo analitico per rappresentare le performance di una linea di produzione composta da buffer a capacità finita e macchine controllate con politiche di spegnimento ed accensione è stato recentemente proposto in letteratura (Jia et al., 2016). Tale metodo analitico presenta tuttavia delle limitazioni in quanto limita il numero di macchine controllate (i.e., non è possibile controllare due

macchine adiacenti). A titolo esemplificativo, presentiamo il caso di una linea tandem a due macchine come in Fig. 3.

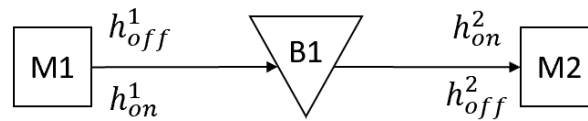


Fig. 3 Linea tandem a due macchine con buffer a capacità finita e macchine controllate con politiche di controllo energetico basate sul livello del buffer. I parametri di controllo sono evidenziali.

Consideriamo macchine Bernoulliane con probabilità $p_i | i = 1, 2$ di produrre una parte in un determinato time-slot Δt di riferimento. Le macchine richiedono un transitorio deterministico sia per l'accensione che per lo spegnimento. Le macchine vengono controllate come segue:

- M1 viene spenta quando il livello del buffer sale ad un livello di controllo h^1_{off} e riaccesa quando il livello del buffer scende ad un livello di controllo h^1_{on} ;
- M2 viene spenta quando il livello del buffer scende ad un livello di controllo h^2_{off} e riaccesa quando il livello del buffer sale ad un livello di controllo h^2_{on} .

Di conseguenza, M1 viene controllata quando il flusso di parti a valle è bloccato, mentre M2 viene controllata quando il flusso di parti viene interrotto a monte.

Il metodo analitico proposto da Jia et al. (2016) permette di controllare questa tipologia di sistema, con macchine aventi il modello a stati descritto e la politica di controllo, ma non permette di controllare entrambe le macchine. Consideriamo quindi 2 modelli LF basati sul metodo analitico di Jia et al. (2016) in cui: LF1 considera controllata solo M1 e LF2 considera controllata solo M2. Entrambi i modelli LF hanno una visione parziale del sistema e potrebbero ottenere stime non appropriate delle performance del sistema reale. Un modello ad eventi discreti rappresentativo del sistema nella sua interezza viene usato come modello HF. Gli errori di stima dei due modelli LF e del meta-modello creato con il metodo EKR sono confrontati in Fig.4 e Fig.5. Si può facilmente notare come l'errore di EKR sia significativamente inferiore a quello di entrambi i modelli LF. Viene anche riportato un confronto con il modello creato usando solo il modello HF e nessun modello LF: indichiamo quest'ultimo meta-modello con KR. Si nota come la combinazione di modelli LF e HF porti a benefici significativi soprattutto quando il budget di sperimentazione iniziale è limitato. In alcuni casi (e.g. Fig.4 per il ritmo produttivo), la differenza tra EKR e KR non è significativa.

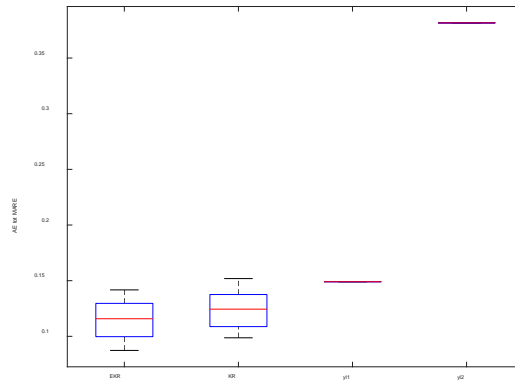


Fig.4: Errore di previsione (Mean Absolute Relative Error su 10 repliche) tra il modello HF e 4 modelli: LF1, LF2, il meta-modello creato con EKR e quello con KR. Scenario: $p_1 = 0.9$, $p_2 = 0.6$, $t_{cd} = 1$ e $t_{su} = 6$. Budget utilizzato: $n = 100$. Errori calcolati su 1000 checkpoints.

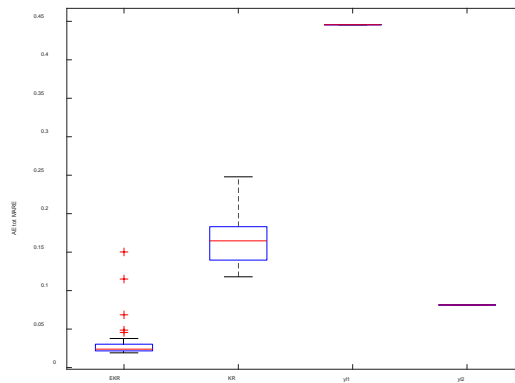


Fig.5: Errore di previsione (Mean Absolute Relative Error su 50 repliche) tra il modello HF e 4 modelli: LF1, LF2, il meta-modello creato con EKR e quello con KR. Scenario: $p_1 = 0.6$, $p_2 = 0.9$, $t_{cd} = 1$ e $t_{su} = 1$. Budget utilizzato: $n = 20$. Errori calcolati su 1000 checkpoints.

Il problema di ottimizzazione multi-obiettivo come compromesso tra un risparmio energetico senza ridurre eccessivamente il ritmo produttivo del sistema è stato formulato evidenziando tutti i vincoli di fattibilità del controllo stesso (e.g., evitando i deadlocks del sistema). In termini di risparmio energetico, le politiche analizzate si sono rivelate promettenti. Qualche risultato per linee non-bilanciate viene riportato in Tab. 3. Il confronto comprende 4 politiche:

- ✓ AON (Always On) dove nessuna macchina viene controllata;
- ✓ US (Upstream) dove le macchine sono controllate usando informazioni del buffer a monte e quindi durante i periodi di *starvation*;
- ✓ DS (Downstream) dove le macchine sono controllate usando informazioni del buffer a valle e quindi durante i periodi di *blocking*;
- ✓ UDS (Upstream and Downstream) dove le politiche US e DS sono combinate.

La politica US non ha prestazioni significative nello scenario M9 perché le macchine sono per lo più bloccate. Di conseguenza, il controllo non ha mai effettivamente luogo (vale a dire la funzione di

energia è piatta). Simmetricamente per il caso M9, le macchine hanno alti periodi di starvation in attesa dei pezzi e la politica di DS non è efficace (anche in questo caso la funzione è piatta). Il caso M5 rappresenta una situazione intermedia. Una buona soluzione è applicare DS alle macchine prima del collo di bottiglia e US dopo. Generalmente, in linee sbilanciate, i controlli hanno prestazioni migliori rispetto ai casi bilanciati, poiché le macchine senza collo di bottiglia sono meno saturate, quindi la quantità di energia consumata nel caso non controllato è più elevata. Per lo stesso motivo, la riduzione di ritmo produttivo è poco significativa in quanto la macchina collo di bottiglia non viene mai spenta.

Tab.3 Risultati ottenuti per linee di 9 macchine con buffer a capacità limitata (10 parti). La macchina bottleneck è, rispettivamente, la prima macchina (M1), la macchina centrale (M5), e l'ultima macchina (M9). La sigla "NH" indica che nessun costo è stato associato ai buffer. [Potenze richieste dalle macchine: standby 0.52 kW, idle and blocked 5.35 kW, startup 6 kW for 20s, closedown non presente].

M9/NH				
Machine	AON	US	DS	UDS
Energy M	231.92	-1.98%	-84.06%	-86.24%
Energy total	231.92	-1.98%	-84.06%	-86.24%
TH	33.02	-0.02%	-0.01%	-0.13%
M5/NH				
Machine	AON	US	DS	UDS
Energy M	231.93	-41.60%	-54.42%	-85.67%
Energy total	231.93	-41.60%	-54.42%	-85.67%
TH	33.02	-0.06%	-0.47%	-0.31%
M1/NH				
Machine	AON	US	DS	UDS
Energy M	231.68	-84.35%	-48.59%	-86.13%
Energy total	231.68	-84.35%	-48.59%	-86.13%
TH	33.02	-2.76%	-1.43%	-0.09%

Benefici per gli utenti finali

Il contributo per gli utenti finali delle attività A1.2 si può sintetizzare in tre punti:

R1. Sviluppo di linee guida per supportare l'utente nell'applicazione pratica di politiche di controllo dello stato-macchina al fine di perseguire un risparmio energetico. Diverse strategie di controllo sono state discusse e analizzate da un punto di vista pratico. Abbiamo inoltre fornito alcuni parametri di riferimento ottenuti attraverso simulazioni numeriche di casi applicativi ed abbiamo inoltre fornito le prestazioni ottenibili attraverso l'applicazione di diverse strategie di controllo in sistemi di produzione manifatturiera (linee di produzione bilanciate e sbilanciate).

R2. Sviluppo di conoscenze teoriche e modelli per facilitare la progettazione e il controllo di sistemi di produzione sostenibili. È stato proposto un metodo flessibile per rappresentare i sistemi con macchine controllate. Combinando i vantaggi dei metodi analitici selezionati dalla letteratura e della simulazione ad eventi discreti, il metodo EKR crea un meta-modello che rappresenta il sistema. Questo approccio può essere ampiamente utilizzato nelle applicazioni pratiche in cui i sistemi reali raramente corrispondono alle ipotesi del modello.

R3. Integrazione dei criteri di produttività e sostenibilità nel funzionamento dei sistemi di produzione. Sono stati forniti esempi numerici per mappare il controllo ottimale in base alle informazioni di controllo al fine di non compromettere la produttività dei sistemi.

Diffusione dei risultati

Si prevede la pubblicazione di un articolo conferenza (IEEE International Conference on Automation Science and Engineering): *A methodology for performance estimation of controlled production lines with off/on machine modes*. Si prevede inoltre la pubblicazione di un articolo su rivista (International Journal of Production Research): *“Optimization of energy-efficient controlled production lines using multi-fidelity models and simulation.”*

Apparecchiature disponibili e acquisite

Apparecchiature disponibili

Non sono state acquistate apparecchiature.

WP1.2: evoluzione del TRL:

iniziale: TRL3 - Alcuni dei metodi utilizzati sono presenti in letteratura. Le principali caratteristiche delle politiche di controllo energetico utilizzate sono state analizzate in letteratura per macchine singole.

finale: TRL4 - La metodologia proposta e' stata validata mediante casi numerici valutati in laboratorio. Le guideline sono basate su casi numerici rappresentativi di casi industriali realistici.

Quadro generale di riferimento, obiettivi e stato dell'arte

Energy efficiency measures have been promoted for years now and effects of these can already be seen in the reduction of ODEX ("Measuring energy efficiency progress in the EU: the energy efficiency index ODEX — ECEEE," n.d.), an index that measures sectorial demand for energy. Statistics show that an improvement of nearly 40% was reached in the years 1990 to 2009. It should be pointed out that quite a lot of attention was paid to the topic e.g. the European FP7 framework program, however the impact will be distributed over the period of many years ahead, due to the very long life-cycle of manufacturing plants. Nevertheless, a significant amount of effort has already been undertaken and applied, which, on the other hand, makes further energy reductions potentially more difficult, as many potential gaps have already been identified and technical solutions for them are available. In addition to that, the studies showed that the cost of energy with respect to the total operating cost of the metal cutting machine varies from around 1.8% in a small, non-automatized facilities to 7% in big manufacturing plants (Anderberg and Kara, 2009). This would indicate that improvements in energy efficiency will bring relatively limited impact on the total production cost and therefore they depend on affordability, which in this case means short return investment time, and on regulatory initiatives, devoted to a containment of the environmental impact.

Another study indicates that further potential in increasing energy efficiency of machine tools (in terms of bringing Best Available Technologies and Best Not Available Technologies components to machines) will range from 3% to 5% with respect to the state-of-the-art machine (Schischke et al., 2012), which, as a matter of fact, is not much.

The barriers listed above place a difficult challenge in front of the scientific community. One of the possible solutions is to focus attention on smarter utilization of machines during production planning and their use. This can be achieved by numerous measures, namely the organisation of energy awareness of manufacturing processes in the planning phase and during the life-cycle of the manufacturing plant. Cost savings are by far the main driver for adopting changes and bringing innovation to industry. Adopting smarter production schemes may fulfil the low-cost requirement as there is reduced or no need to invest in costly hardware solution for every machine produced or retro-fitted. Once an enterprise adopts relevant skills, know-how and software they can cheaply populate the benefits among multiple production plants.

Certainly a large group of industrial machinery, which demands a significant quantity of energy to run are machine tools. They are a wide group of machines which manufacture parts by shaping or removing material. The scope of the work presented in this work package are metal-cutting machine tools, namely numerically controlled (CNC) metal cutting machines: lathes, milling machines, transfer machines and manufacturing centres.

The theoretical efficiency of machine tool is rarely met as the machine would need to work continuously without stopping/any stops at its optimal working point. In real life, there are constraints that shift the working point far from the optimum to match produced part requirements. In addition to that, the production profile of a system will alter machine utilization, with respect to a machine working in isolation. Therefore, the seemingly optimal setup in nominal conditions may prove itself to be suboptimal if the machine would be e.g. facing prolonged periods of idleness, caused by low demand and supply of parts or low reliability due to random events.

In this work package this problem is addressed by delivering a model-based methodology which can propagate the "smart" approach to manufacturing. It is designed to analyse and optimize the

"performance-energy consumption" pair of a machine tool during production planning and configuration phases. Presented approach establishes a clear link between analysis of a single machine with the analysis of the system of machines through a flexible Pareto front interface.

Machine model for system level energy analysis ¹

1. Introduction and State of the art

The economic and environmental cost of energy consumption in industry puts the sustainability of production systems as one of the key issues in the global agenda. The manufacturing sector has a significant role to play due to its inherently large contribution to overall energy demand. In addition to improving efficiency at component level, the scientific community has, in recent years, centred its attention towards energy management in the configuration and use phases. A significant amount of effort was dedicated to modelling and optimization of manufacturing process in machine tools (MT) at various organizational levels: component, cutting process, machine and system. To properly evaluate the overall reduction of energy use produced by the selection of more efficient components, their actual use pattern, function of the part produced and the control strategy adopted, must be taken into account. Typically, energy-saving opportunities lying on the boundaries of neighbouring levels are overlooked.

Elementary empirical energy models, considering fundamental fixed and variable components: tip power and machine basal consumption can be used for a coarse estimation of overall demand of a MT. Dial et al. (Diaz et al., 2011, 2010a) used material removal rate (MRR) as a primary factor driving cutting energy expenditure, whereas Kara and Li (Kara and Li, 2011) have extended this concept to the total machine energy demand, including an empirically obtained lumped auxiliary component power demand. Mori et al. (Mori et al., 2011) provided an empirical model distinguishing axis positioning, spindle accelerating/stopping, machining and tool changing phases. This type of models does not provide information about energy loss sources in a MT, only a coarse estimation of energy consumption/efficiency as a function of processing rate.

Power requirement of a MT can be accurately evaluated by means of a tool-path simulation. A hardware in the loop simulation (HIL) can be used online for power demand estimation, including hydraulic system power demand (Abele et al., 2012). Borgia et al. (Borgia et al., 2017) used a detailed, offline simulation of general milling process to predict both energy demand and other KPI related to process dynamics. However, the usefulness of simulation methods in a multi-criterion optimization of production cycle at system level is limited, due to the computation power needed.

Operation oriented, physics-based models with controllable parameters are a more in-depth alternative to coarse empirical estimates, typically containing physical models of components from which energy losses information can be derived. Mativenga and Rajemi (Mativenga and Rajemi, 2011) introduced a model for the prediction of total energy of a single pass in a turning process, including a cutting parameters effect and spindle and tool limits. Kong et al. (Kong et al., 2011) proposed an overall structure for an energy model of a cutting process, including accurate timing required to consider feed acceleration and spindle run-up/run-down operations. Extending this concept, He et al. (2012) developed an operation-oriented energy model which includes simple spindle model, feed axes, variable time tool changes, cutting liquid and base power usage. Parsed G-code instructions and a workpiece documentation were used for the calculation of consumption using components models. The proposed model lacked load dependent losses in the drives, therefore underestimating the overall energy demand. The approach was consolidated by the work of Aramcharoen and Mativenga (Aramcharoen and Mativenga, 2014), who focused on the relationship between a toolpath and an overall power demand. Avram and Xirouchakis (Avram and Xirouchakis, 2011) utilized CAD/CAM

¹ large parts of this sections are taken from a published article (Wójcicki et al., 2018a), being the result of carried out research within this project

generated output containing information about tool position and actual process parameters to feed a similar model. The study suggested that the reduction of processing speed may be beneficial from the point of view of energy efficiency. In the search for the most efficient cutting conditions Calvanese et al. (Calvanese et al., 2013) developed an optimizable model, which considered part handling operations and a spindle loss dependent chiller consumption. In the minimization the part quality was expressed in form of cutting parameter ranges proposed by tool manufacturers, and confirmed that the reduction of processing speed may lead to energy savings. The model was later extended to fit different production phases: processing, part handling, tool changes (Albertelli et al., 2016), however assuming a constant electric motors efficiency for spindle unit, whereas Wójcicki et al. (Wójcicki et al., 2018b) demonstrated that there is a strong relationship between motor loading and optimal cutting conditions. A different approach was used by Peng and Xu (Peng and Xu, 2013), where, instead of using NC codes, states were defined to represent operations and associated grey-box energy models to machine subsystems. A process chain matrix described a deterministic sequence of states, an alternative to conventional part program. Similarly, Jia et al. (Jia et al., 2014) and Lv et al. (Lv et al., 2014) introduced a high-resolution Therblig-based modelling approach, conceptually inspired by workers motion studies in a factory. Every operation was split into elementary motions with their associated energy and time pairs, coming from energy models present in the literature. Further developments (Jia et al., 2017), using finite state machine model, included transient and high peak power state transitions.

Discussed literature positions concern energy modelling of a machining cycle for a single MT in isolation and do not include interactions with other machines in a manufacturing system. A common system level approach is to find a dispatching policy (Mouzon et al., 2007; Prabhu et al., 2012), putting MTs in a low energy stand-by mode when unutilized. These models typically use stochastic parts arrival times a fixed power per state assumption. Prabhu et al. (Prabhu et al., 2013) found an analytical solution for a single server M/M/1 model with a policy to switch to stand-by state when the MT idle time exceeds a settable threshold, whereas Chang et al. (2013) applied a similar technique for systems with finite interoperational buffers. Frigerio et al. (Frigerio et al., 2013) used a Markov-chain "automata"-based approach to predict optimum switch-off strategy, knowing only part-arrival distribution, but not knowing the state of remaining machines (Frigerio and Matta, 2014). Finally, a general-threshold model (Tolio and Ratti, 2018) can evaluate performance a two machine building block with buffer-level dependent policies and multiple up and down states. To prevent explosion of the problem for large buffer sizes, the discrete state, a continuous material flow assumption can be used.

The goal of manufacturing system optimization is to ensure most efficient operation, not only in terms of energy but also other cost factors and providing sufficient processing rate to satisfy the demand for parts. To find the optimal setup of a production line, a system-level Markov-chain models are commonly used for performance evaluation, which can indicate appropriate buffer allocation, part-loading strategies and, recently, energy management policies. Performing such an analysis requires basic machine level information: MT reliability record (MTTF and MTTR) and information on cycle time and energy per part/state. The latter come predictive machine-level models, typically with a number of controllable parameters. Optimizing these models for a given processing cycle in a single machine can be a complex task in itself. To produce a workpiece with several design features, each having a few settable parameters related to material removal (cutting speed, feed, depth of cut) and machine operation (rapid positioning speed and acceleration, spindle run-up/run-down rate), a complete cycle may involve as many as a few tens to over a hundred parameters (Zhou et al., 2016). Most state of the art optimization approaches focus on overall efficiency of the cutting process or, if considering e.g. tool path, they are rather limited to short manufacturing cycles. A complete approach to manage models for larger, multi-feature processing cycles is, as of now, missing. The optimization of machine level models, whether focused on lowest energy or highest performance, will eventually provide two numbers: cycle time and energy per part. Due to a strong dependence of a system performance on processing rates of individual machines, choices made at a machine level will strongly influence the

system wide performance, and can lead to suboptimalities. For example, if for a machine tool in isolation a less aggressive, slower processing rate brings energy savings, it does not explicitly imply the savings for the whole system. If this machine would be a bottleneck it could negatively influence performance of the system, possibly leading to upstream blocking or downstream starvation resulting in a higher consumption. Conversely, if the machine would be underutilized, from the system point of view, slowing it down would bring savings without putting the throughput at stake. Tackling the machine and system level problems separately inherently brings to two suboptimal solutions, whereas a globally optimal one is desired. It has been argued that a single level approach is insufficient to adequately model energy consumption and a cross level link is still missing (Avram et al., 2011; Peng and Xu, 2014). Verl et al. (Verl et al., 2011) proposed a multi-level architecture for online energy-aware state optimization, reaching as far as the factory level. His method assumes using local, real-time optimization loops to ensure most energy-saving state a given component/machine/line, based on self-learned model, respecting boundaries defining a production scenario that must be fulfilled. An intensive information exchange between various layers of the system must be provided real-time for reliable decision taking. The publication argues that it is very difficult to guarantee system set-up optimality upfront. While this statement is generally true, it is relevant to have a well-chosen a-priori system setup, which than can be fine-tuned e.g. by an online optimization.

A concept of a multi-level framework for energy consumption oriented optimization, was conceived by Wójcicki and Bianchi (2015) to connect machine and system level analyses. The machine level problem should consider controllable parameters and machine tool capabilities, whereas the system problem tackles optimal machine management policies in presence of demand variability and/or machine reliability. The machine level is analysed to identify a Pareto-optimal Minimal Energy-cycle Time function (MET) that answers the question: what is the minimum level of energy that this machine tool can consume, respecting a given, feasible cycle time for producing a given part? To answer this question we must identify the minimal energy requirement of the individual tasks performed by the machine, in function of possible execution times.

We propose a solution to the machine level problem, formulating a framework for systematic modelling and optimization of a manufacturing cycle, from the level of workpiece design features, up to the level of a complete machine, even composed by several processing units. The solution to the system level optimization problem, exploiting the proposed machine MET, is foreseen in a following publication.

The main outcome of this work is the novel, hierarchical approach to find optimal, in terms of energy demand and processing rate, a-priori setups of a machine tool in isolation. The complexity, coming from the large number of controllable process parameters and constraints, is tackled splitting the optimization problem into numerous sub-problems, easy to optimize locally. Local results can be verified, interpreted or manually fine-tuned at any level. A specific approach is proposed to propagate optimality through the hierarchical tree, to describe the global optimum at machine level. Lower levels tasks are merged into higher level ones considering their sequential or parallel execution scheme, preserving only Pareto-optimal solutions. Assumptions, under which optimality of the intermediate solutions is preserved, are formulated and discussed. The proposed framework allows the integration of many state-of-the-art, single-level energy models at a single task level.

2. Developments

2.1. Nomenclature

Note: indices i and j refer to the task number i of the level j

Parameter name	Symbol
Basal power consumption of subsystem X	$P_{base,X}$
Children task set for task i of level j	$C_{j,i}$
Cutting speed	v_c
Cutting torque	τ_{cut}
Depth of cut	a_p
Equality constraints for task i of level j	$f_{j,i}(\mathbf{p}_{j,i})$
Execution time of a task with constant duration	T_{fixed}
Feature depth, time spent cutting	z_{cut}, t_{cut}
Indices of the first and the last children of task i of level j	$n_{first}(j, i), n_{last}(j, i),$
Inequality constraints for task i of level j	$g_{j,i}(\mathbf{p}_{j,i})$
Level depth of the task tree	n_{lev}
Non-productive and productive spindle rotation time	t_{air}, t_{cut}
Operation dependent energy consumption of subsystem X	$E_{op,X}$
Operation dependent energy expenditure on a part	E_{part}
Pareto optimal set (Minimal Energy Time function: MET)	$E_{min,j,i}(t)$
Processing feed	f
Reference matrix containing task Nadir points	M_{ref}
Specific cutting force parameters	k_c, m_c
Spindle acceleration/deceleration time	t_a, t_d
Spindle electrical power as function of angular speed and load torque	$P_{sp}(\omega, \tau)$
Spindle electrical power in cutting operations	P_{cut}
Spindle speed	N
Task energy expenditure	$E_{j,i}$
Task execution time	$T_{j,i}$
Task execution time boundaries	$T_{lb,j,i}, T_{ub,j,i}$
Task objective function vector	$\psi_{j,i}$
Task parameter boundaries	$\mathbf{p}_{lb,j,i}, \mathbf{p}_{ub,j,i}$
Task parameter vector	$\mathbf{p}_{j,i}$
Tool distance from workpiece, time to approach the workpiece	z_{air}, t_{air}
Tool rake angle	γ
Tool sections dimensions (length, diameter)	z_{tool}, d_{tool}
Total energy used by the machine while manufacturing a part	$E_{machine}$

2.2. Hierarchical perspective on manufacturing cycle

The required energy and processing rate of a machine tool while working on a given workpiece is a result of a number of individual tasks performed. Typically, each of these tasks requires a certain amount of time and energy to complete. Let us assume that the most elementary task performed by a machine tool is machining a design feature of a workpiece. A feature could be defined as a few interconnected operations of MT subsystems that result in a basic, distinct geometrical shape of the work piece. This definition encapsulates typical features such as a hole, a pocket, a groove etc. Dependency between operations within one feature is due to shared operational parameters, e.g. spindle acceleration and tool passing operations (of the same feature) are bound by a common target spindle speed. Machining a production cycle of a part in a MT requires completing a group of task features. For some machines and part programs, these tasks may simply be organized in a series, but in more complex machines, such as flexible transfer machines or flexible machining centres, the cycle

might be more complicated. For example, tasks can be grouped into sub-sets and executed in parallel on multiple processing stations. Let us assume that the feature execution sequence and allocation on machine units is given and unchangeable.

The cycle can be divided into sub-cycles, an example of which is discussed in Sect. 2.5, and such a grouping can be considered a task on its own. The description of the whole cycle can be written in a form of a hierarchical tree (Fig. 1) in which lower level tasks add up to constitute a parent-task, and so on. Execution time and energy demand of the parent depends on the children tasks: energy is a mere sum whereas execution time will depend on how tasks are executed, in series or in parallel. Each parent can also become a child of a higher-level task: while theoretically the number of levels can be unlimited, in practice it ranges from 2 for simple machines (feature, machine) to 4 or more for complex machines (e.g. feature, processing station, sub-cycle, machine). The top level can be extended to include more than a MT, i.e. a production cell with auxiliary equipment, such as a robot.

Formally, we can write that execution of task i from level $j \in \{1, \dots, n_{lev}\}$, assuming certain controllable parameters vector $\mathbf{p}_{j,i}$, will yield an objective function vector ψ , containing information about the duration and the consumed energy:

$$\psi_{j,i} = [T_{j,i}(\mathbf{p}_{j,i}), E_{j,i}(\mathbf{p}_{j,i})] \quad (1)$$

A one-level-up task: $\psi_{j+1,k}$, has children which are a subset of all the j -level tasks, where n_{first} and n_{last} indicate their indexes:

$$C_{j+1,k} = \{\psi_{j,i}: i = n_{first}(j+1, k), \dots, n_{last}(j+1, k)\} \quad (2)$$

It is required that all children tasks are executed in the same manner, either in an ordered sequence or in parallel (simultaneously). If this would not be true, these functions can be recursively split into subsets of lower levels: $j-1, j-2, \dots$ until all the children of given parent meet the requirement. Energy demand of a parent is a sum of all the energy demands of the children, whereas the completion time will depend on the execution type. For sequential type, we have:

$$\psi_{j+1,k} = [T_{j+1,k}(\mathbf{p}_{j+1,k}), E_{j+1,k}(\mathbf{p}_{j+1,k})] = \left[\sum_{i=n_{first}(j+1,k)}^{n_{last}(j+1,k)} T_{j,i}(\mathbf{p}_{j,i}), \sum_{i=n_{first}(j+1,k)}^{n_{last}(j+1,k)} E_{j,i}(\mathbf{p}_{j,i}) \right] \quad (3)$$

In case of parallel tasks, the ones with shorter execution times will possibly remain idle, waiting for completion of the slowest task, without additional energy consumption (as the effect of basal energy use will be taken into account in a later stage). Therefore, we can formally write that the task execution time is going to be the equal to the duration of the longest of all its sub-tasks:

$$\psi_{j+1,k} = \left[\max\{T_{j,i}(\mathbf{p}_{j,i}): i = n_{first}(j+1, k), \dots, n_{last}(j+1, k)\}, \sum_{i=n_{first,j+1,k}}^{n_{last,j+1,k}} E_{j,i}(\mathbf{p}_{j,i}) \right] \quad (4)$$

The controllable parameter vector for task $(j+1, k)$ is obtained by joining the parameter vectors of its children:

$$\mathbf{p}_{j+1,k} = [\mathbf{p}_{j,i}: i = n_{first}(j+1, k), \dots, n_{last}(j+1, k)] \quad (5)$$

The highest level has only one task, denoted as $\psi_{n_{lev},1}$, which represents the total time and energy required to perform a manufacturing cycle of one part.

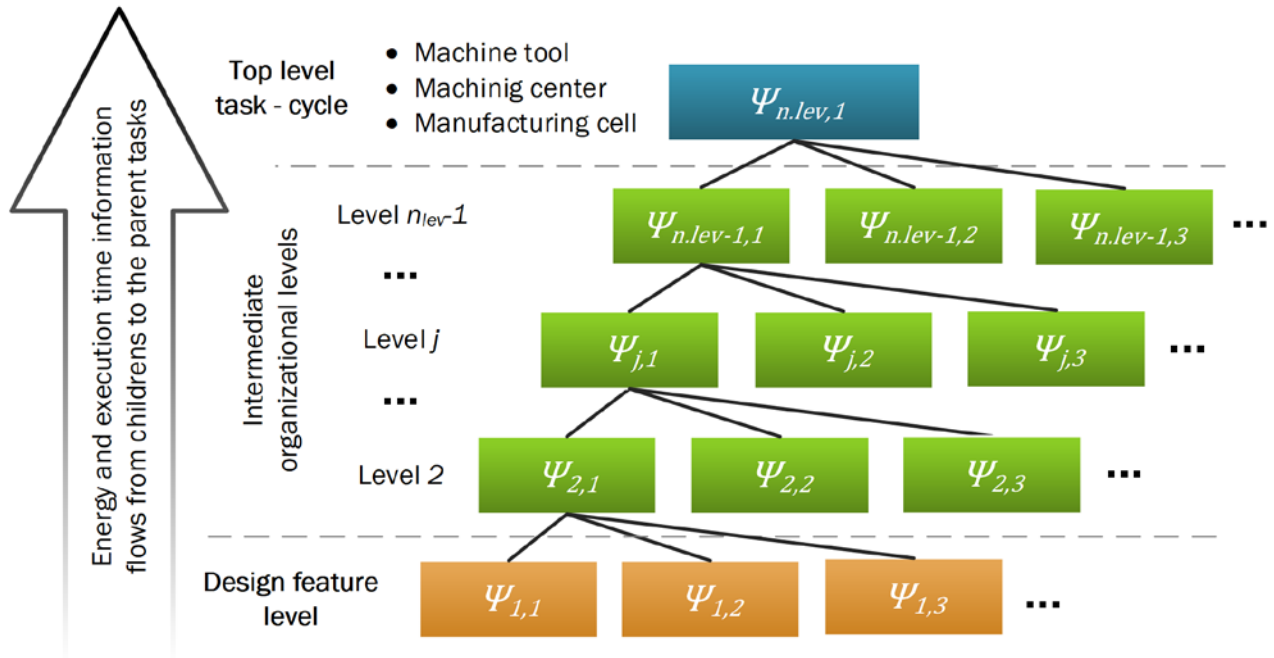


Fig. 1. Hierarchical tree of energy- and time-consuming tasks from the level of a design feature to the top-level representing a workpiece cycle in a MT, a machining center or a production cell

2.3. Hierarchical optimization of a manufacturing cycle

Considering a machine in a system context, cycle time and energy per part can be considered as key performance indicators (KPI). A system level management strategy will consider also other KPIs, such as tool wear or machine reliability, not tackled in the hierarchical framework, however their possible inclusion in the presented framework is discussed in Sect. 3.4. The pursued optimal solution is described by the vector of controlled parameters, which minimizes energy demand and maximizes productivity of the machine. In many cases these goals are contradictory, making it a multi-objective optimization problem. There are several aspects which make this problem difficult to solve. First, the machine-level vector $p_{n_{lev},1}$ can be long, containing several parameters per feature, which eventually yields tens to over a hundred design parameters. Moreover, parameters of each feature have constraints in form of upper and lower bounds (such as prescribed ranges for cutting parameters) but also functional constraints (power and torque limit, being functions of cutting parameters). During the start-up of a production it is common to introduce last moment modifications both in part design and in the process. Such changes could for example introduce another constraint (on processing parameter) or modify parameter of a feature, requiring recalculation of the optimization problem. Lastly, it may not be feasible to optimally choose the final ψ vector if the system level information (including buffer allocation, part-loading strategy etc.) is not yet known. For example, the effective cost behind changing the productivity and the energy demand may be different, depending on where the considered machine is in the system context: an underutilized machine can be potentially slowed down with little or no penalty to the throughput, potentially bringing energy savings, whereas for a bottlenecking machine this would be unacceptable. Moreover, the system level conditions may change over time due to high variability in demand for parts, typical of today's market, which could require dynamic adjustments of optimal ψ .

To mitigate the downsides of all-in-one optimization approach, authors propose to establish a hierarchical optimization scheme to solve the outlined problem and to postpone the final decision-making for machine level work point (which would also fixate all the underlying work points of individual tasks). Let us start at the optimization of the lowest level task: a feature, for example a milling operation. Depending on the adopted process parameters, e.g. cutting and feed velocities, assuming they respect machine and process-related constraints, different combinations of execution time and

used energy are obtained. The dimensions of the search space at feature level are given by the number of independent process parameters: the infinite set of feasible solutions (due to the fact that parameters are continuous variables) corresponds to an area in the ψ plane (Fig. 2). Typically, E and T are competing: to reduce cycle time it is necessary to increase energy use, but at the level of a single feature it is impossible to evaluate which is the best compromise between throughput and energy cost. To reduce the complexity of the information transferred to the above optimization level it is useful to introduce a Pareto frontier concept: no optimization strategy at machine or system level can get an advantage in choosing a dominated solution, e.g. one respecting a given process time but using more energy than another feasible solution with the same process time. The Pareto frontier of $\psi_{1,i}$ contains only dominant combinations of energy and time. Since for each value of possible execution time we can find an associated value of energy, we can describe the frontier as a function of time.

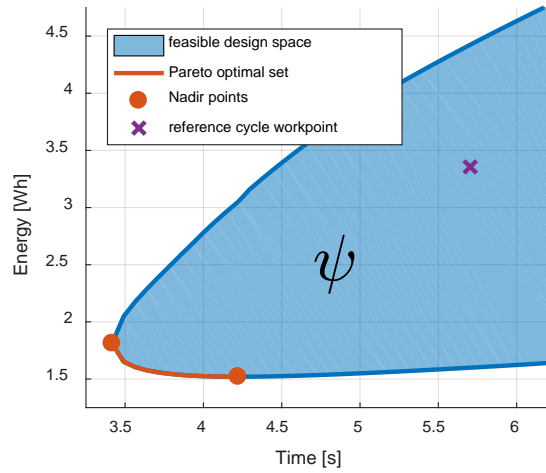


Fig. 2. An example of a Pareto frontier of a feature with energy and time objective functions, being a small subset of a large design space (example taken from the case study from Sect. 2.5). The reference cycle work point is non-dominant: a number of solutions exist that are better in at least one of the objectives.

This means a reduction from a $T_{j,i}(\mathbf{p}_{j,i}), E_{j,i}(\mathbf{p}_{j,i})$ representation, subject to constraints $g_{j,i}(\mathbf{p}_{j,i}) \leq 0, f_{j,i}(\mathbf{p}_{j,i}) = 0$ and $\mathbf{p}_{lb,j,i} \leq \mathbf{p}_{j,i} \leq \mathbf{p}_{ub,j,i}$ to a Pareto optimal set $E_{min,j,i}(t)$ and optimal solution set $\mathbf{p}_{min,j,i}(t)$, subject to a simple boundary $T_{lb,j,i} \leq t \leq T_{ub,j,i}$. The optimal parameters are confined to their level, whereas only task execution time is passed the higher level optimization, where it will be used as a parameter its task. The boundaries on the execution time are the points corresponding to time argument in the Nadir objective variable vector ψ (Fig. 3), which can be found in the second column of the reference matrix:

$$M_{ref} = \begin{bmatrix} E_{j,i}(\mathbf{p}_{j,i}|_{E_{min}}) & T(\mathbf{p}_{j,i}|_{E_{min}}) \equiv T_{ub,j,i} \\ E_{j,i}(\mathbf{p}_{j,i}|_{T_{min}}) & T(\mathbf{p}_{j,i}|_{T_{min}}) \equiv T_{lb,j,i} \end{bmatrix} \quad (6)$$

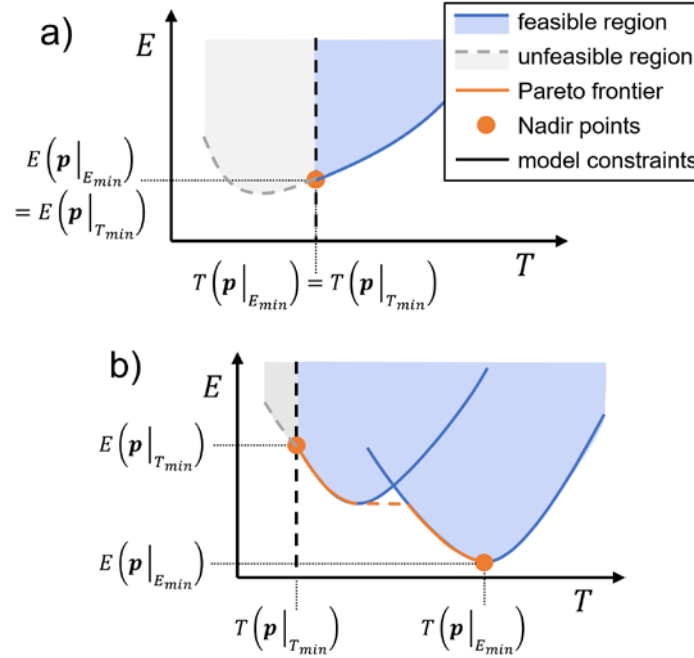


Fig. 3. Theoretical examples of Pareto frontiers in the energy and time plane. Nadir points define the boundaries of the optimization problem. Indexes were skipped for simplification. a) a feature for which there is a unique optimal value, due to a constraint: fastest processing strategy is always the best one b) a discontinuous Pareto frontier can occur e.g. if the feature model has a discrete parameter such as number of tool passes. In the discontinuity region the shorter task time is preferred (left bound of the region).

For convenience, let us call the found $E_{min,j,i}(t)$ Pareto functions *Minimal-Time-Energy (MET) functions* and $\mathbf{p}_{min,j,i}(t)$ *Minimizing-Parameter functions (MP)*. The focus of this section is on how to use the available information from feature-level MET to obtain MET higher-level tasks. Let us consider that we search for a MET of a parent task $j + 1, k$ (e.g. a processing unit), after having computed all METs of its children (features). We can find an optimal Pareto set by searching for dominant combinations of the children execution times which minimize energy. The parameter set of a parent task $\mathbf{p}_{j+1,k}$ is then constituted by its children execution times (Eq. (7)), which can be written as $\mathbf{p}_{j,l} = T_{j,l}$. The lowest tasks in hierarchy, the roots of each branch, have an underlying physical model, with specific parameters. For a design feature, this could be the cutting speed, feed or depth of cut. The process of finding MET from energy models of features is described in Sect. 2.4. The optimal parameters are confined to each level and only the execution time of the children is used at higher level. The bottom-level parameters can be queried by recursively going down the task tree.

$$\mathbf{p}_{j+1,k} = [\mathbf{p}_{j,l}: l = n_{first,j+1,k}, \dots, n_{last,j+1,k}] \quad (7)$$

Parents task parameters are subject to boundaries coming from children feasible execution time $[T_{lb,j,i} \leq T_{j,k} \leq T_{ub,j,i}]$, at the lowest level constraint by the physical-models. We can obtain the desired parent MET through minimization:

$$E_{min,j+1,k}(T_{j+1,k}) = \min_{\mathbf{p}_{j+1,k}} \sum_{l=n_{first,j+1,k}}^{n_{last,j+1,k}} E_{min,j,i}(T_{j,l}) \quad (8)$$

The parameter set in this case is not the feature parameters, as for the lowest level tasks, but the execution times of the children tasks. The $j + 1$ level MET execution time, being a constraint in this minimization, is considered differently for parallel and sequential groups of tasks:

$$\begin{aligned} T_{j+1,k} &= \sum T_{j+1,k} - \text{for sequential tasks} \\ T_{j+1,k} &= \max\{T_{j+1,k}\} - \text{for parallel tasks} \end{aligned} \quad (9)$$

Being able to recursively merge lower level MET functions into higher level MET functions means that any hierarchical tree of tasks can be optimized. The optimality of a task at level $j + 1$ with respect to all its children is preserved if the parameter sets of the children METs are independent, which can formally be written as:

$$\forall k, l \in \{1 \dots n\}: k \neq l \rightarrow \frac{\delta E_{j,k}}{\delta \mathbf{p}_{j,l}} = \frac{\delta E_{j,l}}{\delta \mathbf{p}_{j,k}} = 0 \quad (10)$$

This condition is practically only required for 1-st level functions: this already implies independent sets for the higher levels. If this condition is not met two tasks should be minimized together and their children task sets should be joined. The requirement for parameter independence is the reason why features were chosen to be the elementary representation of a manufacturing cycle, whereas lower organizational level, e.g. basic operations like cutting and spindle run-up and run-down, commonly share their parameters and are not appropriate candidates. Some auxiliary components may be shared e.g. a chiller may be removing heat load of several processing modules (motors) working in parallel. To avoid dependence between processing module level MET functions, the best course of action is to use linear models of power demand for the shared components in which the final consumption is a superposition of its inputs (Borgia et al., 2014a), what eliminates the dependence.

2.4. Practical consideration for finding Minimal-Energy-Time functions

There are many methods for finding Pareto front depending on the type of objective function, however, under certain assumptions, for functions describing physics-based models, the *epsilon constraint method* is reported to be very effective (Mastinu et al., 2006). It minimizes only one of the objective functions constraining all the others with an upper boundary ϵ , that is being gradually reduced in following steps.

$$\begin{aligned} \min_{\mathbf{p}_{j,i}} E_{j,i}(\mathbf{p}_{j,i}) \\ T_{j,i}(\mathbf{p}_{j,i}) \leq \epsilon \end{aligned} \quad (11)$$

The parameter ϵ must then be discretised, Eq. (12), and the choice of discretization parameter δ is arbitrary but a rule of thumb would suggest having around 50-100 levels of ϵ . It could potentially be beneficial to have a non-linear distribution of ϵ if e.g. $E_{min,j,i}(t)$ changes quicker for lower t (due to rapidly dropping resistive losses of the motor etc.), but this possibility is not discussed here.

$$\epsilon \in \{T_{lb,j,i}, T_{lb,j,i} + \delta, T_{lb,j,i} + 2\delta, \dots, T_{ub,j,i}\} \quad (12)$$

In deriving parent's MET function from its children, it is important to notice that the search space of children function is 1 dimensional, subject to simple boundary constraints. The underlying models behind original, lowest level feature model are physical, therefore multi-dimensional but generally well-behaved and convex that is: they have a minimum (sometimes on the boundary) and are at least C^0 class. Therefore, the process of finding a Pareto frontier of such an optimization problem is not computationally expensive.

The fundamental optimization problem that must be solved is to obtain the base, lowest level MET Pareto frontiers of the features, which are constituted by a number of operations performed by MT components on a workpiece (Fig. 4). In the literature, there are numerous models which can provide the execution time and energy vector Ψ . Due to the nature of components and process itself, there typically are several linear and non-linear constraints (speed, torque, power, acceleration limits) and boundaries (suggested ranges for the cutting parameters), as an expression of workpiece quality. The proposed framework could use any type of model: numerical, analytical or mixed. Providing that the functions describing these models are well behaved, typically gradient methods, such as the *active-set* (Murty, 1988), are preferred. An example of mixed model representation in boring/simple milling has been provided in the case study in Sect.

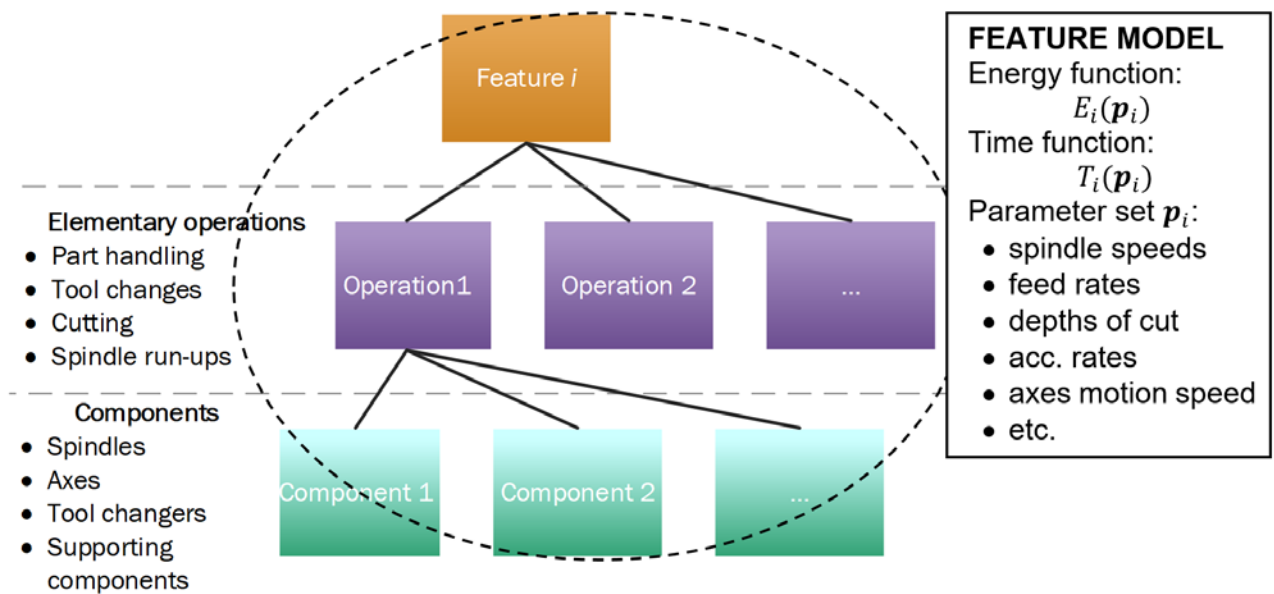


Fig. 4. Feature is a collection of operations performed by MT components resulting in a distinguished geometrical shape

Some operations in a machine might not be part of a feature, yet they do have a certain duration and energy demand – typically fixed. These include tool changes and part handling and, as far as they do influence overall energy consumption and cycle time of MT, they cannot be omitted. They can be represented by METs function that have only one execution time-energy point and do not need to undergo any optimization.

Machine tools, when on, consume a certain amount of power, no matter if producing or not. Base power is modelled as constant and is independent from activity of the MT. Base power P_{base} is a background process that does not have a defined duration by its own. Having a MET function describing the operation-dependent power of a part $E_{min,top,1}(t)$, we can obtain machine consumption per part in function of cycle time as:

$$E_{machine}(t) = E_{min,top,1}(t) + P_{base}t \quad (13)$$

2.5. Case study of flexible transfer machine

The introduced hierarchical framework has been employed to analyse a real production case. In this section, a model of machining process of a gas valve produced by a flexible transfer machine *Porta Solution MULTICENTER 3-Spindle* has been developed. Information on production was collected from a manufacturing plant dedicated to various fluid valves production. MT power consumption was characterized and main subsystems energy models were identified using methodology provided by Wójcicki (2017) on the same machine.

The goal is to verify the predictive capability of the feature models and perform optimization of processing cycle using the introduced energy framework. Study aims at exploring possible energy/cycle-time improvements and creating compact machine energy-cycle time representation that would be suitable for system level analysis, as discussed in the following chapter.

2.5.1. PRODUCTION CYCLE

The considered MT is a flexible rotary transfer machine, with three numerically controlled processing unit and a centrally placed rotary table with workpiece fixtures able to hold 4 parts (Fig. 5).

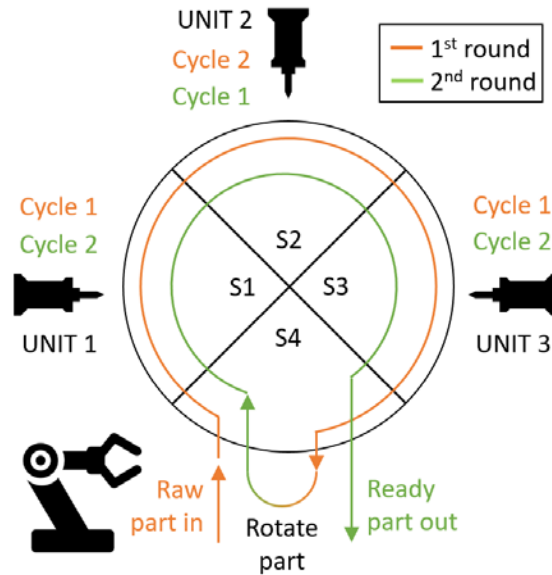


Fig. 5. Organization of processing within examined transfer machine from the workpiece point of view

Parts are inserted using a robotic arm to station $S4$, then the table is rotated, and machining process begins on station $S1$. Each unit will manufacture certain features and the part will continue to move to next unit ($S2$ and $S3$) until it finds itself again in the entry point $S4$. The robot will remove the half-completed part, reorient and reinsert it. Then, the second round of processing begins, and the part will again visit all three units one after another. In the end, the finished part will be removed by the robotic arm. In practice, there are 3 parts being machined simultaneously on stations $S1$ to $S3$. There are 2 production sub-cycles that units perform in turns. This means each unit will work alternately on workpieces from 1st and 2nd setup. After the second round, a completed part is removed and a raw one is inserted in-place. Finished part leaves MT approximately once per minute. Fig. 6 depicts organization of the same processing cycle from the point of view of the machine. Adopting the organizational scheme of the proposed energy framework: sequentially processed features and tool changes constitute the lowest level ($j = 0$); these sequences are performed by processing units in parallel ($j = 1$); sub-cycles and table rotations sequence constitute the level $j = 2$; the final, complete part manufacturing cycle is the root of the hierarchical task tree ($j = 3$).

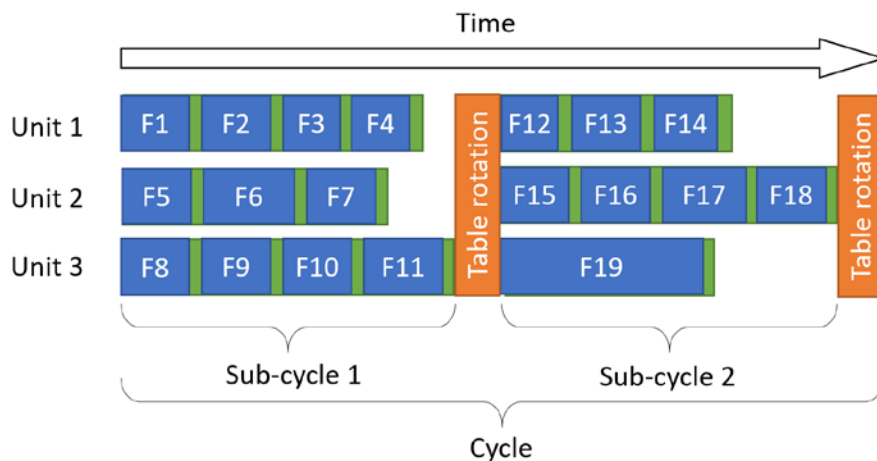


Fig. 6. Diagram present organization of processing with distinction of feature, unit, sub-cycle and cycle levels from a machine point of view. Tool changes are marked in green.

Measurement of spindle activity (via their active power), in Fig. 7, shows that there is a significant unbalance between units in both cycles reaching 9 to 10s over a 30s cycle. Such condition may be

considered typical for flexible transfer machines working on small batch productions, which, on the contrary to dedicated transfer machines, are reconfigured for different type of products for quite short production runs. It is therefore important to limit time and complexity of the setup phase. Usually it is the machine user who is setting up the machine and compose part program, therefore inefficiencies are more likely to occur, like it is showed in the example below. This leaves a certain degree of freedom that allows for energy oriented balancing of features and units execution using MET functions.

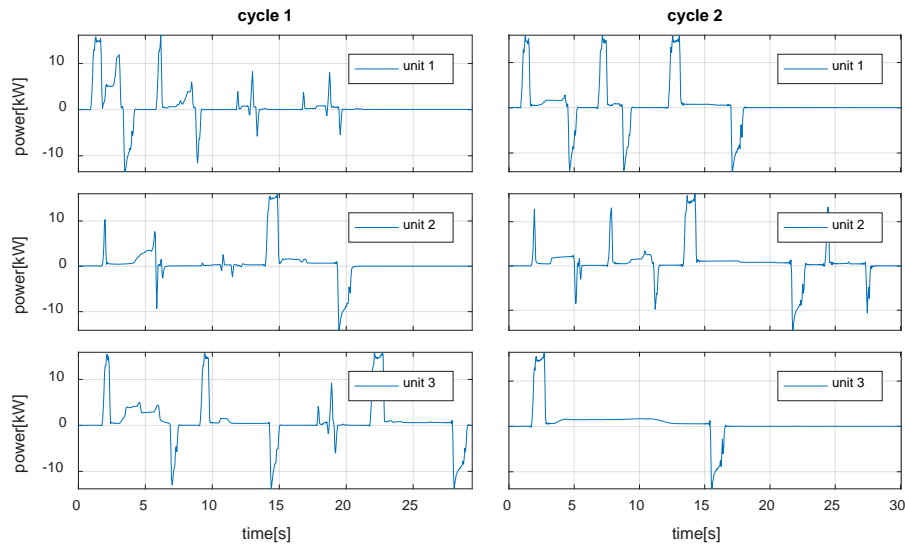


Fig. 7. Activity of spindles in during workpiece machining. In cycle 1 bottleneaking unit 3 takes 9s longer than remaining units. In cycle 2 this difference reaches 10s, for unit 2.

Table 4 reports the list of all features machined by units in both processing cycles. *Full models*, with variable process parameters, were used for features with heavy energy demand (like roughing). Other features (created through threading, or finishing with very low material removal) were modelled using either *acceleration only* or *single point* measured data variants (e.g. in threading), described in Sect. 2.5.2.

Table 4. List of workpiece features with nominal technological parameters by sub-cycle and unit. Last column contains type of model that has been used to represent each feature.

f. no.	depth [mm]	air-cut [mm]	pause [s]	tool	feed [mm/turn]	speed [rpm]	depth of cut [mm]	model variant	description
-	z_{cut}	z_{air}	t_{pause}	-	$f = [f_1 \cdot f_n]$	N	a_p	-	
sub-cycle 1 – unit 1									
1	33.0	7.0	0.15	T5	0.33	5500	$d_{tool}/2$	full	outlet drill.
2	-	-	-	-	-	3500	-	acc. only	outlet finish.
3	-	-	-	-	-	-	-	measured	int. thread.
4	-	-	-	-	-	-	-	measured	int. thread.
sub-cycle 1 – unit 2									
5	28.0	7.0	1.0	T2	0.26	2300	$d_{tool}/2$	full	ext. inlet mill.
6	-	-	-	-	-	-	-	acc. only	int. inlet thread
7	37.5	1.0	1.0	T4	0.19	6350	$d_{tool}/2$	full	channel drill.
sub-cycle 1 – unit 3									
8	21.0	13.0	0.8	T2	0.16; 0.07	4400	$d_{tool}/2$	full	ext. inlet mill.
9	10.0	11.0	3.0	T3	0.18	5000	$d_{tool}/2$	full	inlet drill
10	-	-	-	-	-	-	-	acc. only	thread mill.

11	-	-	-	-	-	6500	-	measured	inlet finish.
sub-cycle 2 – unit 1									
12	10.6	10.0	0.1	T2	0.09	5000	$d_{tool}/2$	full	inlet drill.
13	6.0	10.6	0.1	T3	0.2	5000	$d_{tool}/2$	full	inlet drill.
14	-	-	-	-	-	-	-	acc. only	int. inlet thread.
sub-cycle 2 – unit 2									
15	16	10.5	0.7	T5	0.24	2500	4.5	full	outlet drill.
16	8	10	0.45	T6	0.15; 0.08	3000	$d_{tool}/2$	full	channel drill.
17	-	-	-	-	-	3000	-	acc. only	int. thread mill.
18	-	-	-	-	-	-	-	measured	channel mill.
sub-cycle 2 – unit 3									
19	-	-	-	-	-	6500	-	acc. only	ext. inlet thread

Material of the workpiece is a copper alloy $CuZn40Pb2$ for which $k_c = 500 N/mm^2$, $m_c = 0.68$ and $\alpha = 30^\circ$ (*Recommended machining parameters for copper and copper alloys*, 2010). Feed limits are given as a function $f_{lim}(d)$ of tool diameter, presented in Fig. 8. Information on tool geometry used in machining of analysed workpiece is in Table 5.

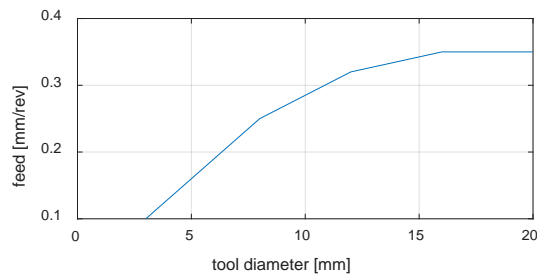


Fig. 8. Feed limit as function of tool diameter (*Recommended machining parameters for copper and copper alloys*, 2010)

Table 5. Tools dimensions

Unit	Tool number	Diameters [mm]	Working lengths [mm]
		d_{tool}	Z_{tool}
1	T2	11.0	10.6
1	T3	5.1	50.0
1	T5	14.0; 21.0	20; 14.0
2	T2	17.0; 25.0	11.5; 4.0
2	T4	5.5	76.0
2	T5	22.0	16.0
2	T6	12.7; 20.0	6.0; 2.0
3	T2	18.0	34.7
3	T3	16.0; 17.0	15.0; 7.0

2.5.2. A FEATURE MODEL: DRILLING/BORING A HOLE

A typical feature realized in valve production is a drilled or bored hole. Manufacturing of this kind of feature is composed by several operations, starting after tool change or workpiece handling. To represent the time and energy consumed in hole machining, three model variants were considered. For operation with significant material removal a *full model* variant was used, in which all elementary operations were represented by either numerical (spindle run-up/run-down) or analytical

representation (the rest). For features with geometrical or operational complexities, but with small energy demand, simplified representation were used: a physics-based model for spindle acceleration and measured values for the cutting process. In this case, spindle speed N_{nom} must be preserved, as the measured cutting process is fixed, but acceleration rates during spindle run-up and run-down can be modified, as they do not interfere with the material removal process. In threading, in which a particular spindle motion sequence must be performed, with limited energy and time contribution only a single point, directly measured ψ was used. The following sub-sections present elementary models of the operations, omitting for clarity, feature indexes (i, j, k etc.). The hole feature model is composed of the following operations:

1. Spindle run-up
2. Approaching workpiece (with cutting feed rate)
3. Cutting (sequence of tool diameters)
4. Pause
5. Rapid tool retraction
6. Spindle run-down

Energy function for the described set of operations is:

$$E(\mathbf{p}) = E_a(N, t_a) + E_d(N, t_d) + E_{air}(N, \mathbf{f}) + E_{cut}(N, \mathbf{f}) \quad (14)$$

This model implements a complete machining process description including spindle speed (or cutting speed), multiple feeds, multiple tool diameters and variable spindle acceleration rates. Time function is a sum of spindle run-up and run-down, air cutting (while tool approaches workpiece), cutting time and pause for tool retraction and workpiece rotation:

$$\mathbf{p} = \{t_a, t_d, N, \mathbf{f}\} \\ T(\mathbf{p}) = t_a + t_{air} + \text{sum}\{\mathbf{t}_{cut}\} + t_d \quad (15)$$

2.5.3. SPINDLE ACCELERATION

To represent spindle acceleration/deceleration operations (op. 1 and 6) a pre-optimized numerical model was used (Wójcicki and Bianchi, 2017). It considers moderation of acceleration rate through controllable run-up/run-down time parameters t_a and t_d , by imposing optimal values of motor acceleration (torque) limit and power limits. The energy in the of the operations is given by $E_a(N, t_a)$ and $E_d(N, t_d)$, where N is a target speed required for cutting.

2.5.4. MATERIAL REMOVAL

Often, for high volume production, custom combined tools with complex geometry (typically several diameter sections) are employed, example of which is shown in Fig. 9. Air cutting and removal process time depends on spindle speed N , tool segments length vector \mathbf{z}_{tool} and feed per turn vector \mathbf{f} , corresponding to each segment:

$$t_{air}(\mathbf{f}, N) = 60 \frac{z_{air}}{f_1 \cdot N} \quad (16) \\ \mathbf{t}_{cut}(\mathbf{f}, N) = \left[60 \frac{z_{tool,1}}{f_1 \cdot N}, \dots, 60 \frac{z_{tool,n-1}}{f_{n-1} \cdot N}, 60 \frac{\sum_i^n z_{tool,i} - z_{cut}}{f_n \cdot N} \right]$$

For cutting power demand, a spindle power model (Wójcicki and Bianchi, 2017), which relates spindle speed and load torque with power demand, is used. For cutting, the total energy is the sum of time and power products:

$$E_{cut}(N, \mathbf{f}) = \mathbf{P}_{cut} \mathbf{t}_{cut}^T \\ \mathbf{P}_{cut}(N, \mathbf{f}) = [P_{cut,1}, \dots, P_{cut,n}] \quad (17) \\ P_{cut,i} = P_{sp} \left(\frac{2\pi N}{60}, \tau_{cut}(N, f_i, d_{tool,i}) \right)$$

Cutting torque is estimated from a standard constant specific power model and takes a following form (Borgia et al., 2014b):

$$\tau_{cut}(f, d, a_p) = \left(\frac{k_c d a_p}{4} \left(\frac{f}{2} \right)^{1-m_c} + \frac{\gamma d}{2} \right) \cdot 10^{-3} \quad (18)$$

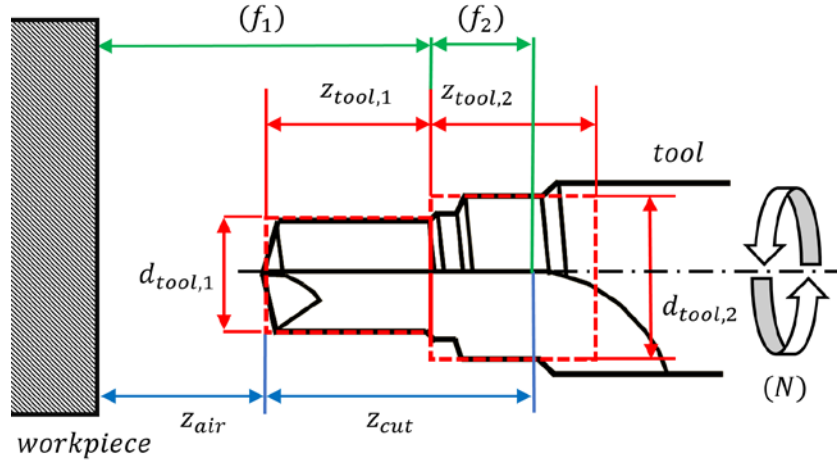


Fig. 9. Sample geometry of a combined tool. Tool shape were approximated by using cylinders of height $z_{tool,i}$ and diameter $d_{tool,i}$

2.5.5. NON-PRODUCTIVE TIME

Operations 2, 4, 5, are non-productive and include approaching the workpiece, pausing the cutting to eliminate any roughness at the drill tip and retracting the tool. Then energy consumed in those “air-cutting” operations can be written as:

$$E_{air}(N, f) = t_{air} \cdot P_{sp} \left(\frac{2\pi N}{60}, 0 \right) \quad (19)$$

, where spindle external load is equal to zero. Coefficient t_{air} is the total measured non-productive time.

2.5.6. CONSTRAINTS

There are certain limiting factors to material removal process coming from tool limits and spindle capabilities. These include spindle acceleration time bounds (in function of cutting speed), spindle speed, torque and power limits, feed limit (in function of tool diameter) and allowed cutting speed range:

$$\begin{aligned} t_a &\in \langle T_{amin}(N), T_{amax}(N) \rangle \\ t_d &\in \langle T_{dmin}(N), T_{dmax}(N) \rangle \\ N &< N_{max} \\ \tau_{fric} \left(\frac{2\pi N}{60} \right) + \tau_{cut}(f, d, a_p) &\leq \tau_{max} \\ \frac{2\pi N}{60} \left(\tau_{fric} \left(\frac{2\pi N}{60} \right) + \tau_{cut}(f, d, a_p) \right) &\leq P_{max} \\ f &< f_{lim}(d) \\ N\pi \cdot \max(\mathbf{d}_{tool}) &\leq v_{c,max} \\ N\pi \cdot \min(\mathbf{d}_{tool}) &\geq v_{c,min} \end{aligned} \quad (20)$$

2.5.7. TOOL CHANGES, TABLE ROTATIONS AND BASAL CONSUMPTION.

To complete the machine model, time and energy offsets must be considered. These include part handling times and energy demand of auxiliary subsystems (operation and time depended).

MT performs tool changes, independently for each unit, after processing of every single feature. Time required by this operation is denoted as t_{tool} , equal to 1.65[s] for the examined machine. Table rotation is performed after cycle completion and lasts for $t_{rot} = 1.2$ [s].

A simple model of axes, pumps and remaining auxiliary subsystems was used, differentiating between base (constant average power) and operation-dependent energy use:

$$\begin{aligned} E_{axis}(t) &= P_{base,axis}t + E_{op,axis} \\ E_{pump}(t) &= P_{base,pump}t + E_{op,pump} \end{aligned} \quad (21)$$

Values of components model coefficients listed in Table. 6 were obtained by the experimental energy characterization of the considered transfer MT via the procedure described by Wójcicki (2017). These components can be added at the very end of process optimization. Here are computed lumped values of energy offset and basal consumption for the whole machine:

$$\begin{aligned} E_{base} &= E_{op,axis} + E_{op,pump} = 84e3[J] \\ P_{base} &= P_{base,axis} + P_{base,pump} + P_{base,aux} = 6.5kW \end{aligned} \quad (22)$$

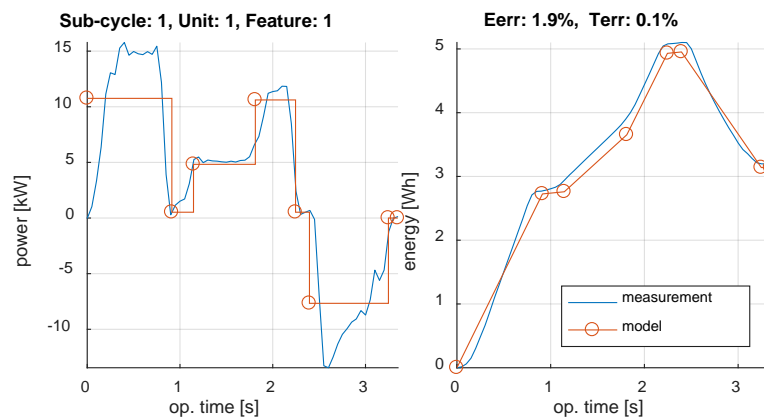
Table. 6. Auxiliary subsystems energy coefficients

coeff.	value	unit
$E_{op,axis}$	48e3	J
$E_{op,pump}$	36e3	J
$P_{base,axis}$	0.4	kW
$P_{base,pump}$	3.1	kW
$P_{base,aux}$	2.0	kW

3. Results and discussion

3.1. Feature energy model validation

In this subsection, a comparison of the power predicted by the modelled features, using the reference (or *nominal*) processing parameters, with the measured power consumption is presented. Nominal parameters include cutting parameters from Table 4 and spindle acceleration/deceleration rates set at the maximum value, as normally used by the machine. Fig. 10 shows goodness of *full* model fitting for two example features. Mean relative error of fitting reaches a value of 2.5% with maximum error equal to 5.8%. Model predicts the average power use in each operation, therefore there are some considerable differences in the power transient phases (e.g. spindle acceleration. However, comparison of cumulative energy plots show only minor deviations, which do not disturb the final accuracy.



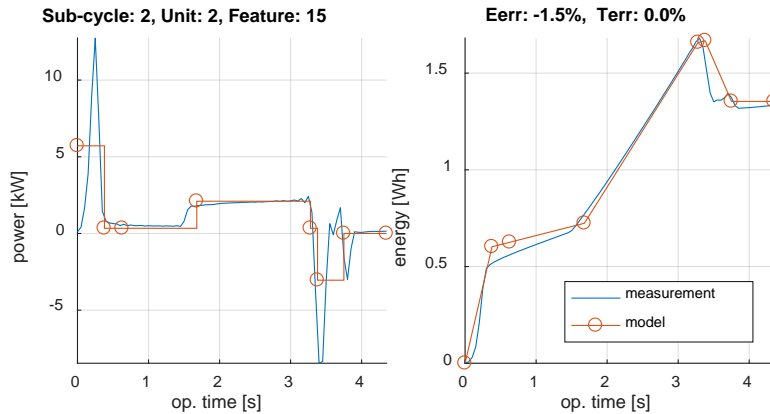


Fig. 10. Goodness of fitting for two full feature models: feature 1 and 15. Errors on total time and energy are presented above each plot.

3.2. Feature level optimization results

Model derived above were minimized as proposed in section 2.3 for a possible range of time spans under constraints from Eq. (11). There are two examples for optimization results of *full model* and one of *acceleration only*.

In case of the MET function for the first feature (Fig. 11), nominal cutting parameters were violating adopted torque constraints which force spindle to stay in the S1 region, allowing continuous operation. In the reference cycle spindle operates in the S6 intermittent regime (which is allowed for spindle low duty cycle). Modifying the control parameters, the optimization algorithm lowered down the cutting speed and increase feed in proportion which preserved the minimal execution time, respecting S1 torque limit. Feature energy was reduced by 18% for the fastest processing rate and by around 26% for the lower energy.

The optimal choice of parameters was to maximize the feed up to the limit and lower down the spindle speed and, therefore, the cutting speed. This means that it is more efficient to reduce friction-related losses in the spindle/cutting process, accepting higher copper losses due to higher load torque. A lower spindle speed also reduces energy lost in acceleration and deceleration phases. When extending the execution time, it is preferred to first lower down spindle speed until the lower cutting speed limit is reached and then start increasing spindle run-up/down time. Minimum of energy is found when feature is processed at speed around 26-28% slower than the maximum. The second feature (Fig. 12) exhibits a similar behaviour. We can observe that setting low feed is the least wanted strategy and causes a rapid increase in consumed energy per feature.

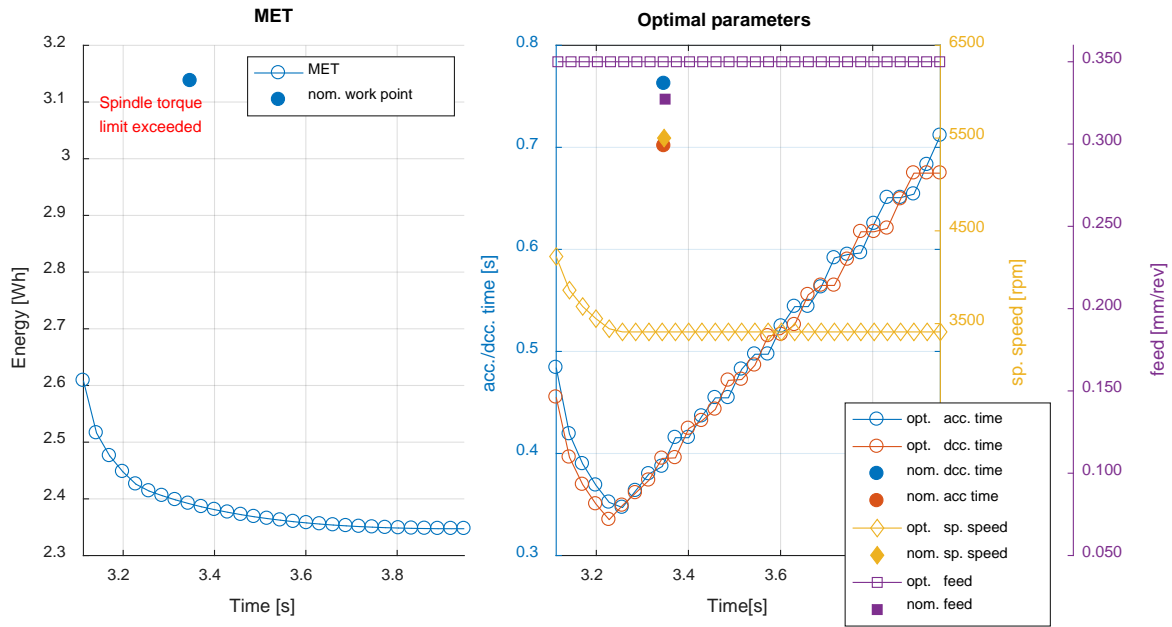


Fig. 11. ET function for a feature 1 of unit 1, cycle 1, full model. Optimization detected that in nominal conditions spindle torque constraint has been violated (continuous torque, S1). Found solution is both less energy demanding and does not exceed torque limit.

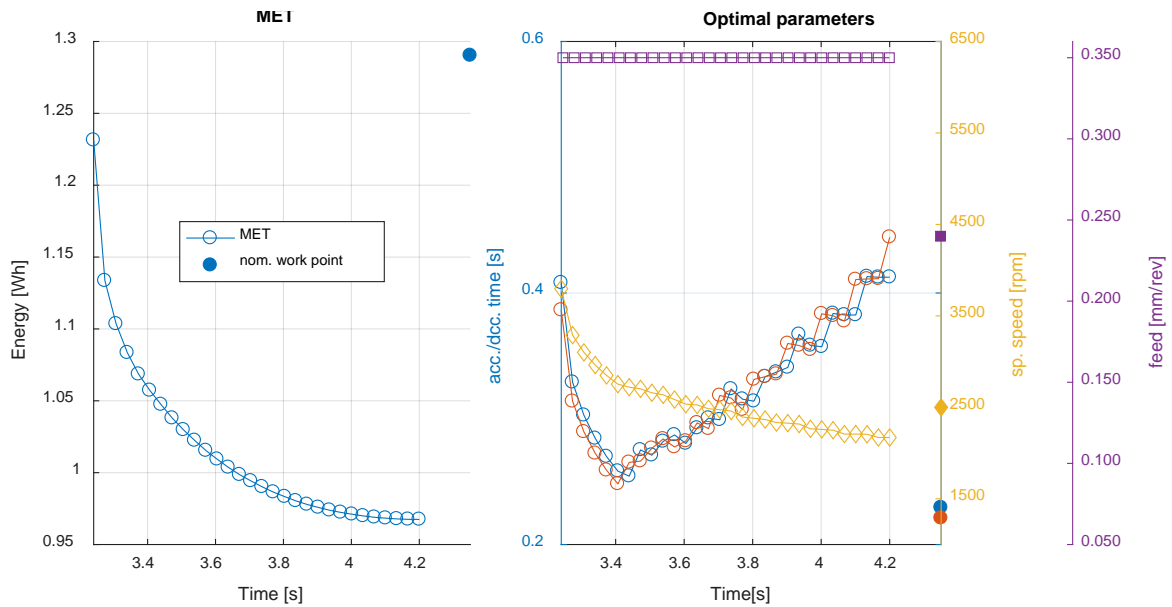


Fig. 12. ET function for feature 1 of unit 2, cycle 2, full model

In case of *acceleration only* model variants (i.e. with fixed cutting speed), modest power savings are possible by reducing acceleration rates of the spindles (Fig. 13). Assuming optimal acceleration times brought savings of around 9.9% with respect to the feature total demand.

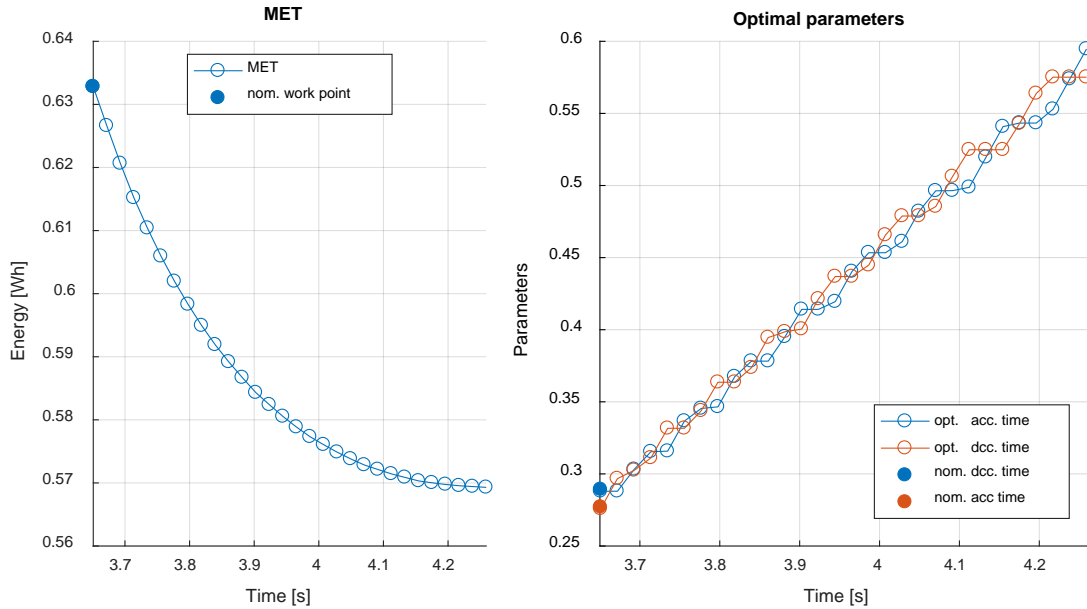


Fig. 13. MET function for feature 4 of unit 2, cycle 2, acceleration only model

3.3. Unit and machine level results

In Fig. 14 we can see how ET functions of a set of 4 features were merged into a new function representing time-energy Pareto frontier of a unit. Energy of feature 3 is a single point, therefore its execution time does not change. Instead, in the remaining functions, one can observe a gradual increase of execution time with respect to demanded unit processing time. Rate at which optimal execution time increases reflects energy saving potential of a feature, e.g. feature 1 execution time increases rapidly at the beginning (around 27s) as its MET is steeper than the others, whereas for longer execution times, it's more efficient to slow down the features 2 and 4 at faster rate than the feature 1. The energy minimum of the unit MET is at around 30s duration, close to the nominal process timing. As a result, a relative energy consumption reduction of 31% can be achieved.

Results of the units METs parallel merging are shown in Fig. 15. Unit 3 was bottlenecking the process, therefore the other units can stay always at their energy minimum work point, as they always finish unit 3. Total improvement of energy comparing to reference cycle is 21.5%.

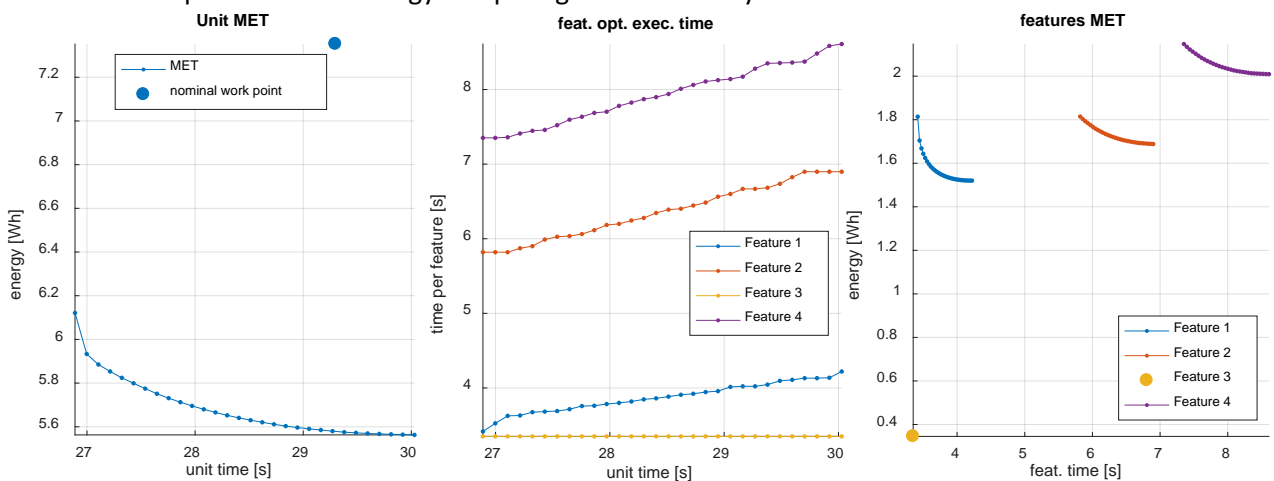


Fig. 14. MET function for unit 3 (left) in sub-cycle 1, resulting from sequential merge of 4 feature functions. Optimal execution time of each feature are given as a function of unit total execution time (centre).

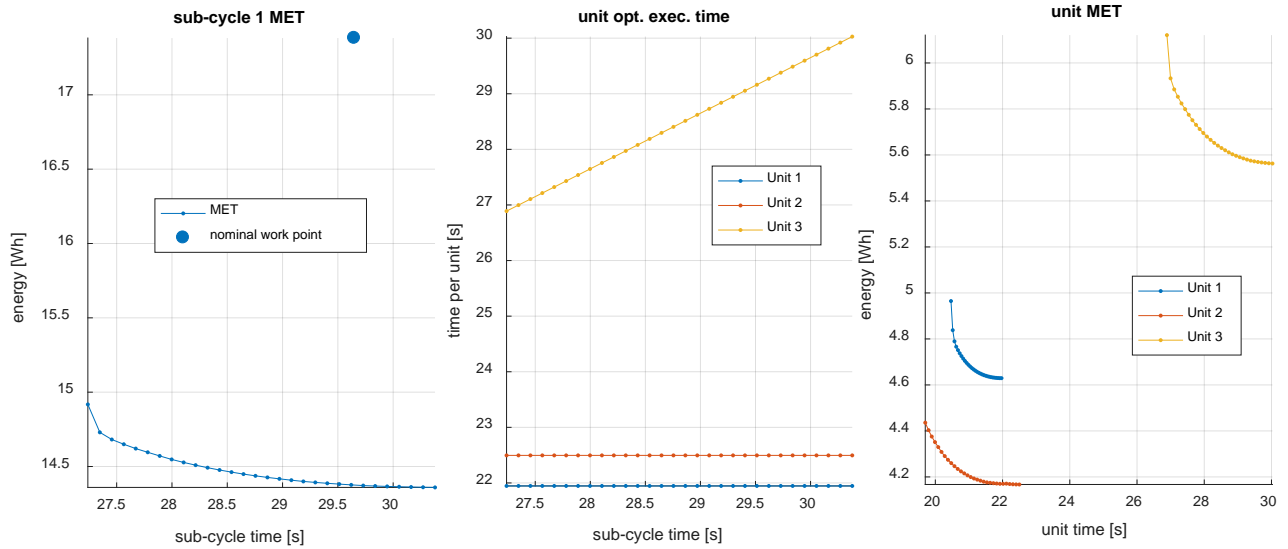


Fig. 15. Minimal ET function for cycle 1 (left) obtained by parallel merging of unit (1-3) functions (right). Optimal execution times for units are located in the central plot.

Finally, a sequential merge of both sub-cycles shows that one can obtain higher saving by prolonging execution time of sub-cycle 1 more than execution time of sub-cycle 2 (Fig. 16). MET function of operation-dependent consumption (including offset from axes and pump models) has a visible minimum achieved close to the nominal cycle time. Overall reduction of 8.5% is achieved by using parameters of optimized processing cycle.

The fastest cycle point indicates projected energy consumption if all features would execute at maximum speed. By comparing this value of energy to the equivalent execution time from the cycle MET, energy saving due to inter-cycle balancing can be estimated. Thanks to balancing at unit level, non-bottlenecking units are slowed down to their optimal work-points without deterioration to overall cycle time and bringing reduction in energy demand of 4.5%. To obtain the total energy consumption, the machine base power component has been added to the operation-dependent MET function. Considered machine's high ratio of base to mean consumption (71%) results in domination of base consumption over the operation-dependent cycle MET, which shifts the minimum energy point nearly to the minimum processing time. Choosing reference cycle time a 3.5% energy reduction is achievable, whereas highest processing rate (4.9s or 8.3% faster) an overall 8% reduction is possible.

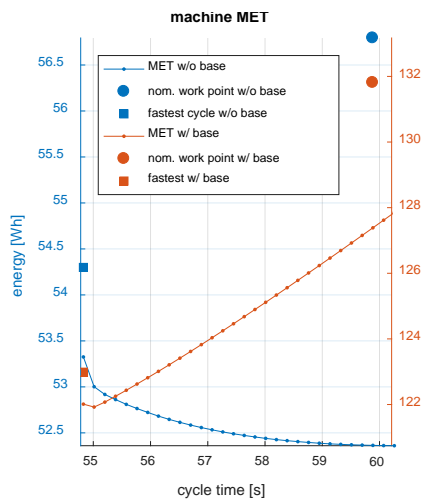


Fig. 16. Minimal ET function of the entire process (left) without base consumption (in blue) and with basal consumption (in red).. Optimal cycle execution times are in the central plot.

3.4. Discussion

3.4.1. FRAMEWORK CONSIDERATIONS

By design in the framework the information between levels is communicated via Pareto frontiers, therefore the knowledge coming from detailed models of low level processes (components, operations and eventually features) is preserved and used in the high-level analysis of the machine. At the same time, these details do not increase complexity higher level optimizations, as only the optimal subset of the information is implicitly carried by the MET functions. In comparison to an all-in-one optimization of the whole cycle (e.g. using heuristic methods like genetic algorithms), the optimization process is decomposed in a number of smaller problems which are easier to compute and converge. The intermediate results can be useful by themselves, to investigate machine efficiency, and can be manually adjusted, if required, e.g. fine tuning of the process after some experimental runs. Optimality is guaranteed, if the feature independence assumption is valid, which is not the case when all-in-one heuristic optimization is applied. If, due to a new technological constraint, model of one feature changes, only the MET of that feature has to be re-computed, followed by an automatic update of only the higher level METs that directly depend on it (one branch of the hierarchy tree). On the contrary, in all-in-one analysis, the whole optimization has to be fully repeated.

The ability to speed up or slow down particular tasks (with associated varying costs) may be considered an additional degree of freedom in pursuing system-wide optimality, also during throughput optimization. On the downsides, as the Pareto functions, after each minimization, are kept in numerical form, some data degradation may occur, especially for structures with large number of levels. In addition to time and energy objective functions used in the proposed framework, other KPIs, e.g. tool wear, can considerably influence overall running costs. Tackling this issue could involve adding additional dimensions (each representing the considered KPI) to the optimization problem: the presented framework could be easily extended to fulfil this requirement, as the concept would not change. It could ensure optimality of the final solution at the highest level, with an additional computational cost.

Some challenges can arise if physical models (like features) have both continuous and discrete parameters. However, this is mainly a matter of choosing a suitable optimization solver, like *mixed integer programming* or *heuristic methods*, while the framework structure is preserved.

3.4.2. CASE STUDY ANALYSIS

In the industrial case study on a rotary transfer machine tool, different types of energy models for feature processing have been adopted, mixing analytical and numerical formulations. The models have been validated on measured power profiles. Analysis and optimization of features revealed that there is a potential for improvement with respect to the reference process (used by the part manufacturer) and that the highest processing speed is not necessarily the most efficient for individual features or processing units. Lowering cutting speed while maximizing feed proves to be the best direction for efficiency, however the degree to which it can be done can be determined only by solving several constraints. Lowering speed also reduces spindle energy expense on run-up and run-down. Fig. 17 presents relative difference in energy demand between the reference process and Nadir Points (i.e. minimum energy or minimum time) of the cycle MET. The most savings can be observed in the improvement of efficiency of the material removal process, namely reduced friction and resistive losses due to slower processing rate. Friction and acceleration losses during non-productive acceleration phases were considered as a lumped value (Wójcicki and Bianchi, 2018) .

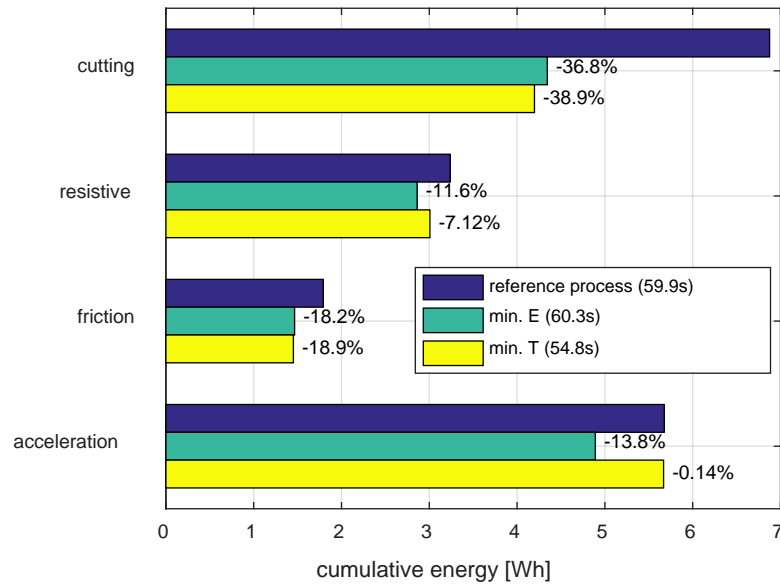


Fig. 17. Breakdown of energy savings from perspective of all spindles. 9 features with full model were used to compute these values.

Table 7 shows relative changes in energy, mean processing time and energy per feature. In the shortest cycle case, even though the overall cycle time has been decreased by around 5s, the mean time per feature has barely changed, which can be explained by better distribution of time per cycle: faster execution of bottlenecking units and slower of the rest. In the most energy efficient configuration, whose cycle time is almost the same as of the reference cycle, we can observe a considerable extension of per-feature-time and significant energy savings: 9% of the operation-dependent power component.

Table 7. Performance per feature for MET Nadir points with respect to the reference cycle.

Case	Cycle time [s]	Mean time per feature [s]	Δ_E [%]	Mean energy per feature [Wh]	Δ_T [%]
Reference	59.9	5.40	-	1.76	-
Minimum cycle time	54.8	5.39	0.82	1.58	-5.87
Minimum energy	60.3	5.68	6.36	1.53	-9.03

In the optimization, the spindle torque was limited by a conservative continuous duty (S1) thermal constraint, whereas, in the reference cycle, the S6, intermittent duty, limit has been utilized for feature 1. In S6 motor can be loaded periodically with higher torque than in S1, but such operation must be intermittent, to allow intermediate motor cooling. Such condition is problematic to implement in the presented framework, because this would break the independence of parameters between tasks, which is required by the hierarchical optimization approach: the torque limit in one task would depend on the motor load in the previous tasks. A possible mitigation could be to identify bottlenecking tasks/features in the first optimization cycle and then apply to those few the S6 limit, repeating then the optimization process.

4. Conclusions and potential exploitation

The developed novel framework for systematic modelling and optimization of manufacturing cycle in machine tools focuses on two primary objective functions: energy consumption and cycle time. Hierarchical description of the cycle allows decoupling the problem into simple tasks. Each of them is optimized, in Pareto sense, decreasing complexity and providing intermediate results which are interpretable and adjustable, if necessary. Modular structure of the problem makes it possible to use

various state-of-the-art models of operations and MT components. The framework, therefore, can be easily applied to a variety of machines and processes in the discrete manufacturing sector. The positive aspects and foreseeable limitations were thoroughly discussed, supported by an analysis of an industrial case. The study demonstrated that applying the developed energy framework helps to identify and eliminate inefficiencies at each analysis level and to reach an optimal balancing of processing units, bringing savings in terms of both cycle time and energy efficiency. The final decision on the work point on the final, machine-level, MET can be postponed until a system wide analysis brings enough information to choose the optimal cycle time and related energy consumption. These considerations were addressed in section XXX of the report, expanding analysis to a manufacturing system, taking into account stochastic behaviours.

Exploitation in industry can be achieved by adopting developed model for machining cycle optimization and an a-priori as well as real-time manufacturing systems optimization, thanks to the possibility of a variable processing rate. These type of optimization models can be ported to a cloud based platform and be used in a pay-per-optimize sales model.

Further developments will consider automatization of the generation of features energy models, e.g. by a CAM software, to speed up model preparation. The possibility to alter the sequence of tasks and their distribution to different units of the machine as demonstrated by (Hu et al., 2017) can further improve the overall performance of the machine and could possibly be integrated into the proposed framework. Moreover, usage of MET functions is aligned with the *network part program* concept (Borgia et al., 2014c) so it could be adopted to consider also energy use during optimal jobs allocation on various machines, in a flexible manufacturing systems.

Integrated energy optimization of a machine tool and its material removal process

Note: large parts of this sections are taken from a published article (Wójcicki et al., 2018b) and PhD thesis (Wójcicki, 2017). While activities carried out in years 2014-2016 have been supported by the EMVeM Project ², activities in 2017 have been funded by this project.

1. Introduction and State of the art

Correct selection of cutting parameters in machining is very important to achieve the prescribed quality with an economical, productive process. The choice is driven by various criteria, to assure the required accuracy of the workpiece and surface integrity, with an optimal balance between production rate and production cost. In (Leonesio et al., 2012) a multi-objective optimization of process planning is presented that tackles vibration and tool life issues. In (Bort et al., 2016) productivity and chatter avoidance criteria are used to control spindle speed and feed rate for a generic milling process. In (Yang and Tarn, 1998) statistical methods are used to choose the best cutting parameters of turning operations aiming at surface roughness and tool life improvements.

Additionally, in recent years, a wide attention has been devoted to machine tools (MTs) environmental impact, which is usually dominated by energy consumption in the use phase. In (Diaz et al., 2010b) - furtherly extended in (Diaz et al., 2011) - the machining process efficiency, in terms of overall energy consumption with respect to productivity is analyzed. In (Xiong et al., 2016) the machining energy efficiency of heavy-duty CNC machine tools is optimized together with other performance factors like costs and chattering. A pioneering attempt to outline a systematic approach for including energy efficiency objectives in manufacturing systems and processes is provided by (Duflou et al., 2012), while a recent and comprehensive review can be found in (Zhou et al., 2016). Tools and methodologies are

² 26) EMVeM Project: Energy efficiency Management for Vehicles and Machines (prog No. 315967; Marie Curie Initial Training Networks (ITN) Call: FP7-PEOPLE-2012-ITN), 01/2013 - 12/2016.

therefore investigated to predict MT energy consumption, evaluated for its main subsystems, during machining of generic mechanical work pieces (Borgia et al., 2016). One major issue concerns the link between specific consumed energy in machining, i.e. the ratio between consumed energy and volume of removed material, and the parameters that could have an influence on it. In fact, these parameters modify both the power used by the MT, where in this sense the main spindle usually represents an important unit, and the amount of material removed (Borgia et al., 2014b). In (Draganescu et al., 2003) a study was performed about the influence of main cutting parameters (feed rate, axial depth of cut, radial depth of cut, cutting speed, and number of teeth) on both MT efficiency and on specific energy consumption. A similar analysis was performed by Mori et al. (Mori et al., 2011), that presented a study on the effects of cutting parameters on total energy consumption in face-milling operations. Both works state that, during machining, the most relevant energy usage is due to the spindle unit, which performs the material removal.

Following the track outlined by (Draganescu et al., 2003), the present work tackles an integrated analysis of the efficiency of material removal process and spindle-chiller subsystem (herein denoted as *Processing Unit* (PU)) for turning operations. Framing a joint machine - process design approach, the proposed analysis is aimed at the selection of the optimal combination of cutting parameters (feed rate, depth of cut and spindle speed) for a given PU, able to minimize the energy consumption during machining.

Additionally, the analysis provides useful data to machine designers, about losses and efficiency of spindle and chiller during reference machining operations. Coherently with the industrial practice, spindle and chiller are considered as an holistic elementary unit. In a “what if” analysis with respect to different possible PU combinations, e.g. based on induction or synchronous motors, an efficiency comparison must consider also the different requirements in terms of motor cooling.

Conversely to the works presented in (Draganescu et al., 2003) and (Mori et al., 2011), where the efficiency analysis is fully empirical basing on extended cutting test campaigns, here a model-based approach is adopted and validated by experiments. Analytical relationships are identified, expressing the efficiency maps as a function of the various process parameters. Models are based on systems physics, taking into account electrical and mechanical energy dissipation, which occurs both in PU and in the material removal process. Models parameters identification can be carried out exploiting a reduced set of experimental data (spindle ramp-up and cutting tests); then, once validated, models can be used to get a general insight about process efficiency.

Even though the work is focused on PU efficiency, the possibility to carry out a global MT energy optimization is anyway guaranteed by expressing the optimal PU efficiency as a function of the Material Removal Rate (*MRR*), in turn related to the machining time. This choice allows weighting also the contribution of the basal consumption of other MT peripherals (which can be considered independent from the activity of PU and only dependent on overall processing time) in the computation of the overall cutting specific energy (according to the approach presented, for instance, in (Diaz et al., 2010b) and (Diaz et al., 2011)). The work presented in (Avram and Xirouchakis, 2011) suggests that decreasing *MRR* can lead to reduction of specific energy, therefore this possibility was further explored.

2. Developments

Nomenclature

Parameter name	Symbol
average cut diameter [mm]	d
basal energy consumption [J]	E_0
chiller basal consumption [W]	P_b
chiller heat load function [W]	P_h
chiller effectiveness coefficient [-]	θ
chiller unit electrical power demand [W]	$P_{chiller}$
cutting coefficient associated to the edge component of tangential cutting force [N/mm]	k_{te}

cutting coefficient associated to material shear [N/mm ²]	k_{tc}
cutting torque [Nm]	τ_{cutt}
cutting power [W]	P_c
cutting speed [m/min]	v_c
depth of cut [mm]	a_p
direct current component [A]	i_d
efficiency of cutting process [-]	η_{cut}
efficiency of spindle and chiller assembly [-]	η_{PU}
efficiency (maximized through optimization) [-]	η_{max}
efficiency (overall) [-]	η
feed rate (per turn) [mm]	f
field weakening coefficient [A·rad/s]	α
field weakening coefficient [-]	β
field weakening starting speed [rad/s]	ω_0
machine basal power loss [W]	P_0
material removal rate [mm ³ /min]	MRR
material removal mechanical energy [J]	E_{mech}
mechanical specific energy $k_c = \frac{P_c}{MRR}$ [N/mm ²]	k_c
overall specific energy [N/mm ²]	e_c
processing unit energy consumption [J]	E_{PU}
quadrature current component [A]	i_q
resistive losses in the motor [W]	$P_{mot\ loss}$
spindle motor load torque [Nm]	τ_{load}
spindle external load torque (process and inertia)	τ
spindle motor electrical power demand [W]	P_{el}
spindle speed [rad/s]	ω
spindle speed limit [rad/s]	ω_{max}
spindle power limit [W]	P_{max}
spindle torque limit [Nm]	τ_{max}
static friction coefficient [Nm]	μ_s
tangential component of the cutting force [N]	F_c
torque constant [Nm/A]	K_T
total spindle moment of inertia [kg·m ²]	J
total energy consumption [J]	E_c
viscous friction coefficient [Nm·s/rad]	μ_v
winding resistance [Ω]	R

2.1. Maximization of cutting process energy efficiency

PU efficiency depends on its thermo-electromechanical characteristics and on spindle velocity and torque, required to machine the work piece material with given process parameters. Thus, an effective PU energy optimization must include the cutting process. The objective is to establish, for given PU, workpiece material, tool and MRR , the optimal cutting parameters that minimize the process energy consumption. The goal is achieved by coupling a mechanistic model of material removal with the thermo-electro-mechanical model of the PU. Since the efficiency is expressed as a function of MRR , the resulting relationship can be exploited to carry out the overall machining energy optimization at MT level, once all the other energy consumers in the machine are known. In formula, for a turning process and parametrizing the result with respect to bar diameter, the problem can be stated as follows:

$$\eta_{max}(MRR|d) = \begin{cases} \max_{a_p, f, \omega} \eta(a_p, f, \omega, d) \\ \text{s. t. } a_p \cdot f \cdot \omega \cdot \frac{d}{2} = MRR \end{cases} \quad (23)$$

Following the proposed approach, a PU unit of a CNC lathe is identified and analyzed. The obtained results allow, on one side, to optimize the cutting parameters and, on the other side, to asses a PU

design for a given set of reference operations. The proposed approach can be applied to all spindle equipped with brushless motors, that are more and more common: to obtain quantitative results, the identification and analysis procedures must be executed on spindle-chiller assembly of interest.

2.2. Energy models of the processing unit and the material removal process

2.2.1. ENERGY MODEL ARCHITECTURE

System under consideration is a PU (a spindle-brushless motor-chiller assembly), which performs a material removal operation (Fig. 18). In this section state of the art models of electric motor, spindle and chiller losses are used to assemble a complete model of the PU. PU efficiency η_{PU} is the ratio of useful mechanical output, used for cutting, and electrical power demand of both spindle and chiller. Whereas spindle efficiency is a function of cutting torque and speed, chiller demand depends on its basal power and heat load delivered by the spindle, because of its internal resistive and friction losses.

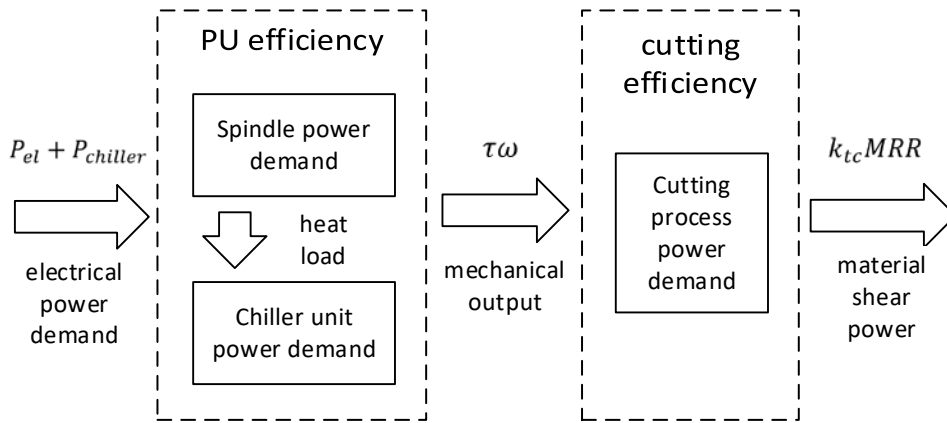


Fig. 18. Architecture of efficiency models of PU and cutting process.

Cutting process efficiency η_{cut} is expressed as ratio of material shear power and mechanical input power used in that process. For a given tool, shear power corresponds to the product of the material specific energy (k_{tc}) and the adopted MRR and is theoretically the minimum value of energy needed to remove a certain volume of material. Overall efficiency is therefore a product of cutting process efficiency and processing unit efficiency, which incorporates both spindle and chiller subsystems:

$$\eta(a_p, f, \omega, d) = \eta_{PU} \cdot \eta_{cut} \quad (24)$$

2.2.2. EFFICIENCY OF SPINDLE AND CHILLER ASSEMBLY

Note: Spindle and chiller models used for this experiment can be found in (Wójcicki et al., 2018b). Spindle efficiency is a ratio of the useful mechanical output power to the electrical power demand. Torque loading due to spindle inertia is only significant in the model identification phase, to properly characterize effective output power. Typically, during material removal, spindle speed is constant, therefore for efficiency analysis of the cutting process the inertial torque term $J\dot{\omega}$ can be omitted.

$$\eta_{spindle}(\tau, \omega) = \frac{\tau\omega + J\dot{\omega} \stackrel{\omega \neq 0}{\rightarrow} \tau\omega}{P_{el}(\tau, \omega)} \rightarrow \frac{\tau\omega}{P_{el}(\tau, \omega)} \quad (25)$$

Spindle motors require appropriately scaled cooling systems. For direct drive electro-spindles, an external chiller is a common solution, whereas in case of mechanical spindles with external motor, often air cooling is sufficient. Because these two subsystems are tightly bonded together, a machine designer that considers efficiency of different spindle alternatives should include energy demand of cooling system in the overall efficiency calculation. For that reason, we extend the definition of spindle

efficiency to include cooling system as well, as formalized in Eq. (26). As the cooling system does not provide usable output for removal process, it will only affect the denominator of the efficiency function:

$$\eta_{PU}(\tau, \omega) = \frac{\tau\omega}{P_{el}(\tau, \omega) + P_{chiller}(\tau, \omega)} \quad (26)$$

Such a formulation allows direct comparison of efficiency between several types of spindle systems, which seem to be more practical for day-to-day choices in energy aware design and configuration.

2.2.3. CUTTING PROCESS MODEL

The mechanical specific energy is also known as “cutting coefficient” and it is the key parameter for computing cutting power and torque: it depends on the tool and the work piece material properties and it is often provided by tool suppliers to verify machine cutting capability constraints during process planning. Let a longitudinal turning operation be considered, where a_p denotes the depth of cut, f the feed per turn, v_c the cutting speed, ω the spindle speed and d the average cut diameter. The MRR expression becomes:

$$MRR = a_p f v_c = a_p f \frac{d}{2} |\omega| \quad (27)$$

Then, the mechanical specific energy k_c can be expressed as the ratio between cutting power and MRR , the former being equal the tangential cutting force component multiplied by the cutting velocity. Namely:

$$k_c = \frac{P_c}{MRR} = \frac{F_c v_c}{MRR} = \frac{F_c \omega d}{2MRR} \quad (28)$$

A great amount of past scientific works dealt with cutting force modelling (e.g. (Ehmann et al., 1997) and (Arrazola et al., 2013)) and with turning process in particular (Dong et al., 2009). All of them consider both the force originated by material shear (cutting component, proportional to chip section) and friction in the contact area between the tool flank face and the workpiece surface (edge force component, proportional to the depth of cut). In the simple and very widespread model proposed in (Altintas, 2012), the tangential cutting force component assumes the following expression:

$$F_c = (k_{te} a_p + k_{tc} a_p f) \quad (29)$$

The process coefficients appearing in Eq. (13) depend on tool properties (characteristic angles, coating, etc.), workpiece material and lubrication condition, thus, they must be identified and/or estimated for each tool-workpiece combination. Moreover, cutting force is often influenced by cutting velocity, which is herein neglected. More comprehensive models would give a more accurate force prediction, but the corresponding increased complexity would not be compensated by significant enhancements in the results. By substituting Eq. (27) and Eq. (28) into Eq.(29), a formula for mechanical specific energy can be obtained. This expression suggests, to reduce the energy use, increasing as much as possible the feed per turn:

$$k_c = \left(\frac{k_{te}}{f} + k_{tc} \right) \quad (30)$$

Efficiency of the cutting process can be written as a ratio of useful power spent on the effective material shear to the mechanical output power of the spindle:

$$\eta_{cut}(a_p, f, \omega) = \frac{k_{tc} MRR}{\omega \tau} \quad (31)$$

2.2.4. OVERALL ENERGY EFFICIENCY

The overall energy consumption can be decomposed into the energy used by the spindle and the associated chiller unit (E_{PU}), the "basal" energy consumed by the machine peripherals (E_0) and the energy used by machine axes to counteract cutting forces and friction. The latter component is usually

negligible in roughing (Calvanese et al., 2013). Then, the overall energy consumption can be approximated as follows:

$$E_c = E_{PU} + E_0 \quad (32)$$

Spindle and chiller energy demand depends on the mechanical energy required by the tool for material removal and on the efficiency of spindle and chiller themselves:

$$E_{mech} = \eta_{PU} E_{PU} \quad (33)$$

Differentiating overall energy consumption E_c with respect to time and dividing both by MRR , an overall specific energy for cutting process (including efficiency of both spindle and chiller) is derived:

$$e_c = \frac{k_c(f)}{\eta_{PU}(a_p, f, v_c, d)} + \frac{P_0}{MRR(a_p, f, v_c)} \quad (34)$$

It may intuitively seem that increasing MRR through modifying process parameters a_p, f, v_c can minimize energy consumption (the right term) by reducing the contribution of machine basal power. However, it is not that obvious, considering the variable PU efficiency, which is function of the same parameters. Also, specific cutting energy depends on the feed, and behavior of these two terms influences the optimal choice of MRR . Workpiece diameter d is not to be considered a decision variable, as it is upfront defined by workpiece size. However, in the energy analysis of PU we consider a range of possible diameters, as they do influence efficiency functions and therefore may change optimal values for cutting parameters and resulting MRR .

2.2.5. CUTTING MODEL IDENTIFICATION

Cutting tests were performed with 8 combinations of feed and depth of cut (Table 8), using *DNMG 15-06-04-PM-4325* chip breaker by Sandvik Coromant™. Material was removed from cylindrical test samples of 65mm in diameter, made of medium-carbon steel C45, and cutting force model identified. Motor quadrature current was saved by the machine control system as a proxy for torque measurement. Depending on the depth of cut, different number of tool passes were performed, from 3 to 10, for a total of 42 passes. It has to be noted that the proposed cutting tests are just aimed at identifying model parameters for the specific combination of tool and workpiece material, while the validation of the model itself, together with the limits in cutting parameters extension, can be found in (Altintas, 2012). Relying on literature claims, in section 5 and 6 model predictions will be extrapolated to broader ranges of feed per revolution and depth of cut.

Table 8. Performed cutting tests configuration

	Feed per revolution [mm]	Depth of cut [mm]	Chip section area [mm ²]	Average torque [Nm]
1	0.20	4.0	0.800	40.10
2	0.30	3.0	0.900	43.86
3	0.20	3.0	0.600	30.43
4	0.30	2.0	0.600	35.25
5	0.15	2.5	0.375	23.95
6	0.25	1.5	0.375	21.72
7	0.10	2.0	0.200	13.93
8	0.20	1.0	0.200	11.07

Cutting torque was computed as a product of measured quadrature current and identified motor torque constant. To fit the linear model of cutting forces from section 2.3.3, a least square method was used. Estimated coefficients and fitting errors are presented in Table 9. Adjusted coefficient of determination R^2 is 0.9687 and the condition number of the observation matrix is 16.8. Based on the

statistical analysis of the goodness of fitting, cutting forces coefficients have been identified with high level of confidence and precision.

Table 9. Cutting parameter estimation and statistical goodness of fitting

parameter	estimate	squared error	t-statistic	p-value
k_{te} [N/mm]	63.82	20.39	3.13	0.00325
k_{tc} [N/mm ²]	1705.1	91.14	18.7	2.19e-21

2.3. Optimal cutting condition in function of Material Removal Rate and workpiece diameter

To explore most efficient strategies for material removal with the considered PU, the problem described by Eq. (23) has been set up: it maximizes the overall efficiency of PU and cutting process. Maximization procedure was repeated for a range of possible *MRR* and cutting diameters, which allows to explore energy performance under various production conditions. Varying diameter serves the purpose of representing different workpiece sizing and is important to understand how well the given PU is suited for a certain type of production mission. Varying *MRR* is used to explore possibility of reducing overall performance in terms of material removal for the sake of energy saving. Spindle continuous operating region (also known as S1 duty cycle (Drury, 2001)) has been imposed in form of a set of constraints limiting spindle mechanical output power, torque and speed:

$$\begin{cases} \omega \tau_{load}(a_p, f, \omega) \leq P_{max} \\ \tau_{load}(a_p, f, \omega) \leq \tau_{max} \\ \omega \leq \omega_{max} \end{cases} \quad (35)$$

Limits related to tool impose certain minimum and maximum values of cutting speed, feed rate and depth of cut, for the given workpiece material:

$$\begin{cases} v_{c\ min} < v_c(\omega) \leq v_{c\ max} \\ f_{min} \leq f \leq f_{max} \\ a_{p\ min} \leq a_p \leq a_{p\ max} \end{cases} \quad (36)$$

Each workpiece diameter defines a certain maximum *MRR* which can be achieved by PU (due to PU and tool constraints). These values are found by solving an optimization problem in Eq. (37) for every diameter of interest and will formulate a starting point for efficiency maximization.

$$MRR_{max}(d) = \max_{a_p, f, \omega} MRR(a_p, f, \omega | d) \quad (37)$$

To perform numerically a multidimensional constrained nonlinear minimization for problems formulated in Eq. (23) and Eq. (37), an *active-set* (Hazewinkel, 1988) method has been used. This numerical method is capable of handling bounded parameters and multiple constraints presented above.

3. Results and discussion

3.1. Efficiency of the cutting process with a spindle-chiller pair

Overall efficiency surfaces as a function of cutting parameters were drawn, based on the identified PU and cutting process model, from Eq. (24). Three values of cutting diameter were considered – small (20mm), medium (100mm) and large (300mm), corresponding to different sizes of workpieces that could be produced on the examined machine. To visualize efficiency for a wide range of parameter values, several working points were chosen to define 2D intersections in the 3D efficiency space (Table 10). Working points which are marked on the plots have been arbitrarily chosen for each considered cutting diameter to show representative features of the efficiency surfaces. Table 11 collects limits of the parameter that were used in efficiency surfaces generation. *Iso-MRR* lines were drawn to underline how moving along certain dimension may affect productivity of the material removal process.

Table 10. Arbitrary working points for 3D efficiency surfaces intersections

Diameter [mm]	Depth of cut [mm]	Feed [mm/rev]	Spindle speed [rpm]
20	5	0.2	2600
100	6	0.2	800
300	4	0.15	250

Table 11. Parameter ranges used in efficiency optimization corresponding to spindle/chip breaker limits

Parameter	Lower limit	Upper limit
Spindle speed ω [rad/s]	1	6000
Cutting speed v_c [m/min]	-	255
Feed rate f [mm/rev]	0.005	0.3
Depth of cut a_p [mm]	0.1	10
Spindle torque τ_{load} [Nm]	-	350
Spindle power P_{el} [kW]	-	40

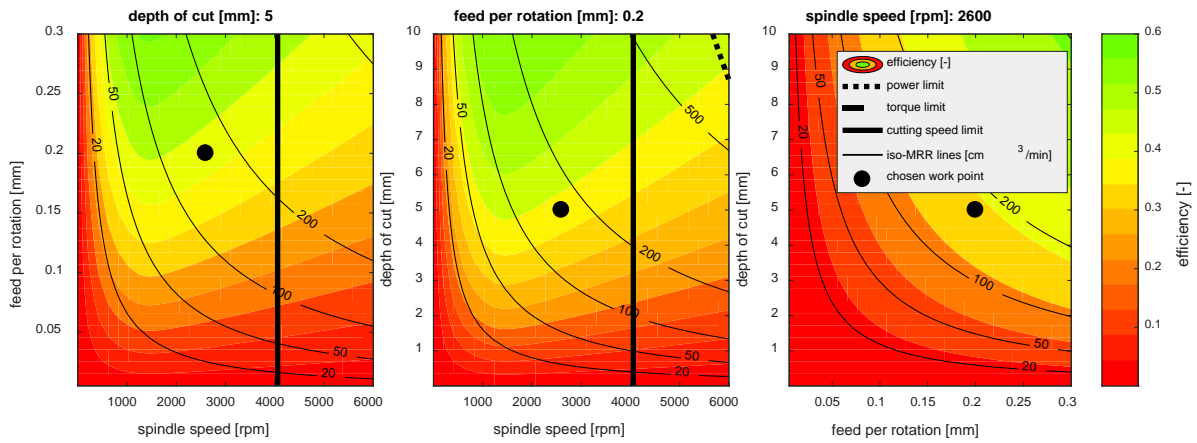


Fig. 19. Overall PU efficiency for working diameter of 20mm.

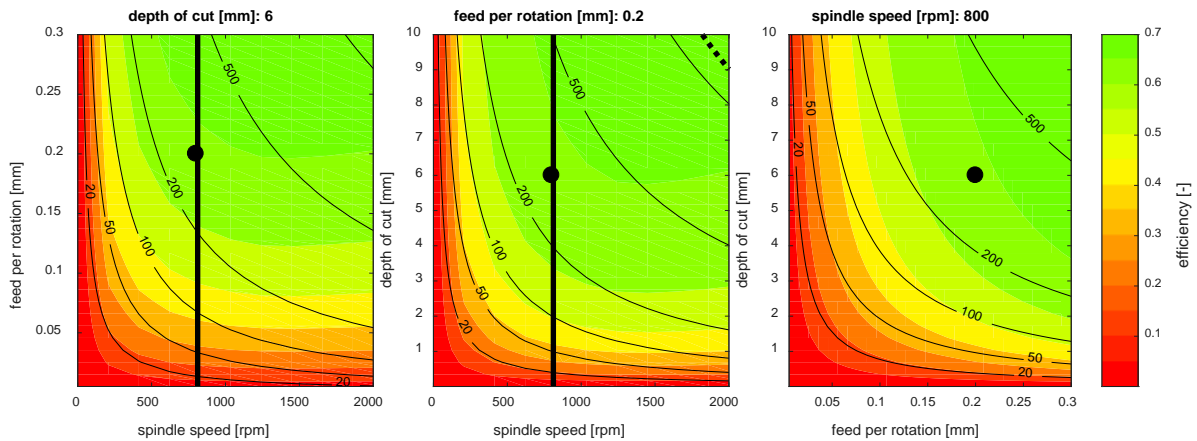


Fig. 20. Overall PU efficiency for working diameter of 100mm.

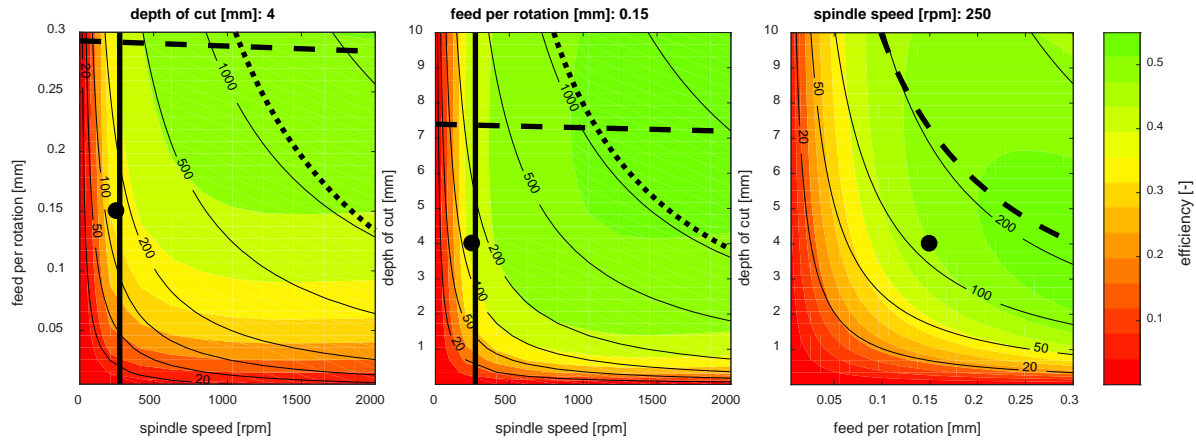


Fig. 21. Overall PU efficiency for working diameter of 300mm.

The efficiency surfaces related to low and medium diameter cutting (Fig. 19 and Fig. 20) reveal that an increase of depth of cut and feed result in a general improvement of process efficiency: both these parameters cause a proportional increment in spindle torque, which produces a strong positive effect on PU efficiency for a wide range of spindle speed. In high diameter region (Fig. 21) maximizing a_p and f has limited impact on efficiency, as for its highest values efficiency stays constant or even decreases by few percent. Similar behavior was spotted in experimental study of (Draganescu et al., 2003) in Fig. 3, where for face milling operation was performed using a tool with high diameter (250mm). Achieving highest values of both feed and depth of cut at the same time is not possible because of spindle torque limit, and overall it is better to maximize feed rather than depth of cut, as it this way impact of edge component losses can be reduced (see Eq. (30)).

Whereas for diameters of 100mm and 300mm increasing MRR by maximizing cutting parameters increases efficiency, for low diameter turning the effect is no longer that simple: Fig. 19 shows that there is an optimal cutting speed above which efficiency starts to drop. This can be attributed to rapid growth of friction losses and resistive losses (field control related) with speed. Similar phenomenon can be observed in experimental study (Draganescu et al., 2003).

3.2. Optimal cutting parameters in function of MRR

Efficiency optimization was performed by searching for cutting parameters which maximize overall efficiency from Eq. (24) but do not violate spindle and tool limits (Eq. (35) and Eq. (36)), for a range of predefined diameters and material removal rates (Table 12). Authors propose to consider two strategies to apply, in an industrial context, the proposed efficiency formulation: with and without considering the basal power component.

Table 12. Optimization ranges

Parameter	Lower limit	Upper limit	No. of values
workpiece diameter (d') [mm]	5	200	80
material removal rate (MRR') [mm^3/min]	$0.1MRR_{max}(d)$	$MRR_{max}(d)$	25

Strategy one (Fig. 22): Completion time on the cutting operation determines turn-on time of the machine. In this case, basal power of the PU and the whole machine affects the energy performance of the material removal process as discussed in section 2.6. This is a typical case for a standalone machine with a single spindle, where the machine is turned off, or put into energy saving mode while not in use.

Strategy two (Fig. 23): Machine is always on during shift but is not fully utilized (e.g. often waiting for part arrival from upstream machines). In such a scenario the machine consumes the same amount of basal power independently on the actual MRR . Similarly, in a multi-spindle machine with cycle unbalance between the various spindles, the non-bottlenecking spindles may not work at highest MRR

if it produces energy saving. In this scenario, machine basal consumption P_0 and chillers basal power P_b are not considered, been a constant factor during optimization.

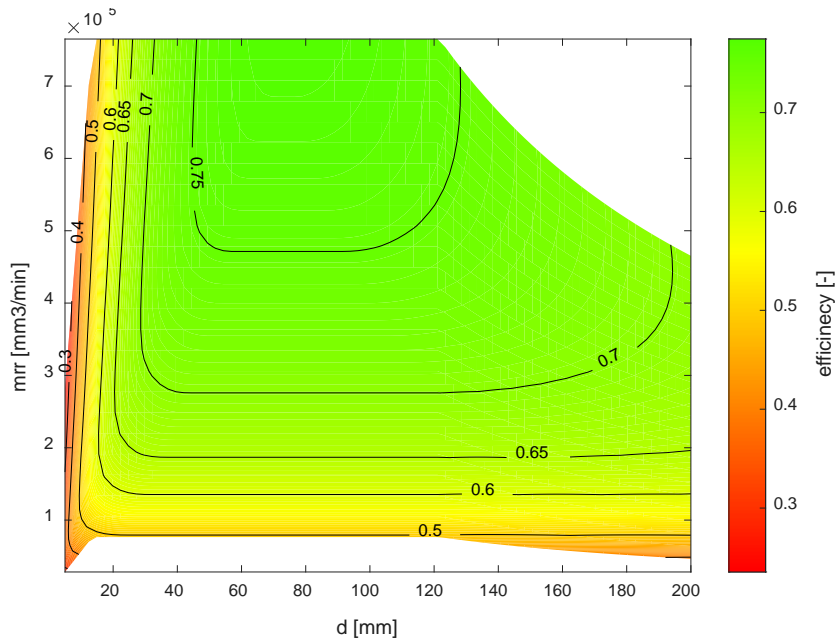


Fig. 22. Maximized PU efficiency of material removal for a given forced MRR and cutting diameter d including chiller basal power term (Strategy 1)

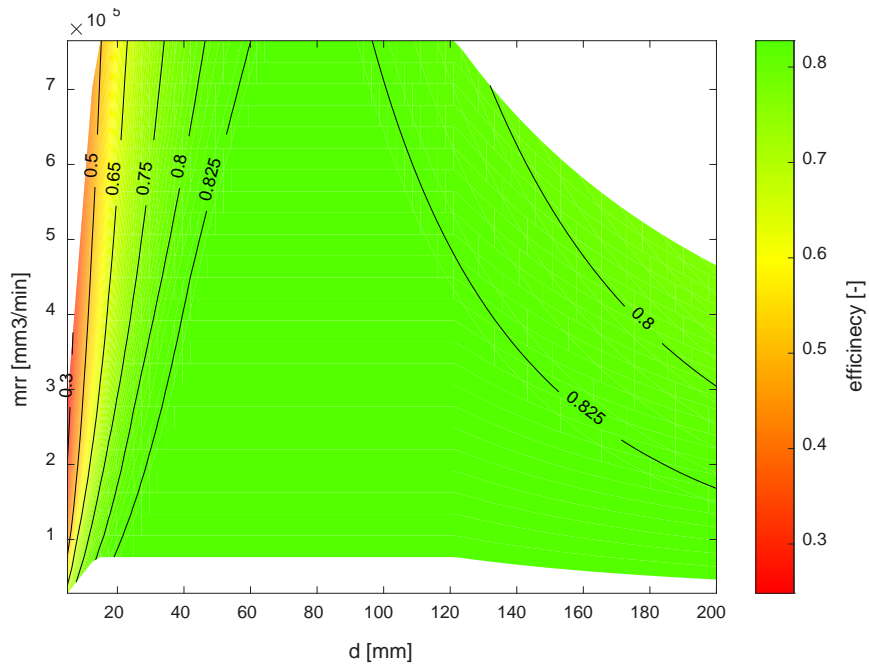


Fig. 23. Maximized PU efficiency of material removal for a given forced MRR and cutting diameter d . excluding chiller basal power term (Strategy 2).

For clarity, each strategy will be discussed separately, distinguishing three workpiece diameter regions: small (up to 40mm), medium (40-120mm) and large diameter (more than 120mm).

Scenario one – small diameter: efficiency is lowest in this region (25-60%), and is decreasing with decreasing diameter. Maximum productivity is also low, limited by spindles top speed (6500rpm). Highest efficiency for a given diameter is not achieved for maximum MRR value but there is a visible optimum. For smallest considered diameter (5mm), reducing MRR from highest $28.4 \cdot 10^4 \text{ mm}^3/\text{min}$ to

optimal $8.1 \cdot 10^4 \text{ mm}^3/\text{min}$ results in efficiency improvement (from 23.5% to 35.9%). Efficiency loss is dominated by friction.

Scenario one – medium diameter: this region is of highest efficiency and productivity, which reach 78% and $76.5 \cdot 10^4 \text{ mm}^3/\text{min}$, respectively. Productivity is limited only by material cutting speed limit. Reducing *MRR* progressively reduces efficiency.

Scenario one – large diameter: maximum productivity is limited due to maximum spindle torque. Efficiency deteriorates with increasing diameter, from 75% at 120mm to 46% at 200mm. Similar to medium diameter region, decreasing *MRR* deteriorates efficiency. Main contribution of losses are copper losses, due to high quadrature current component.

Scenario two – small diameter: similar to *Scenario one*; efficiency is low with respect to other regions, but it increases progressively with reduction of *MRR*. For 5mm diameter, efficiency boost from 24.8% to 69.8% is possible solely due to less aggressive material removal strategy. High friction losses, due to high speed operation.

Scenario two – medium diameter: highest efficiency region. Without basal power component, efficiency remains invariant to changing *MRR*, settling at the level of around 83%.

Scenario two – large diameter: efficiency drops slightly with increasing diameter but less intensively with respect to *Scenario one* (from 83% to 76.7%). Slight improvement of up to 6.5% can be achieved by reducing *MRR*. Less intensive production requires less torque, therefore copper losses can be reduced at smaller *MRR*.

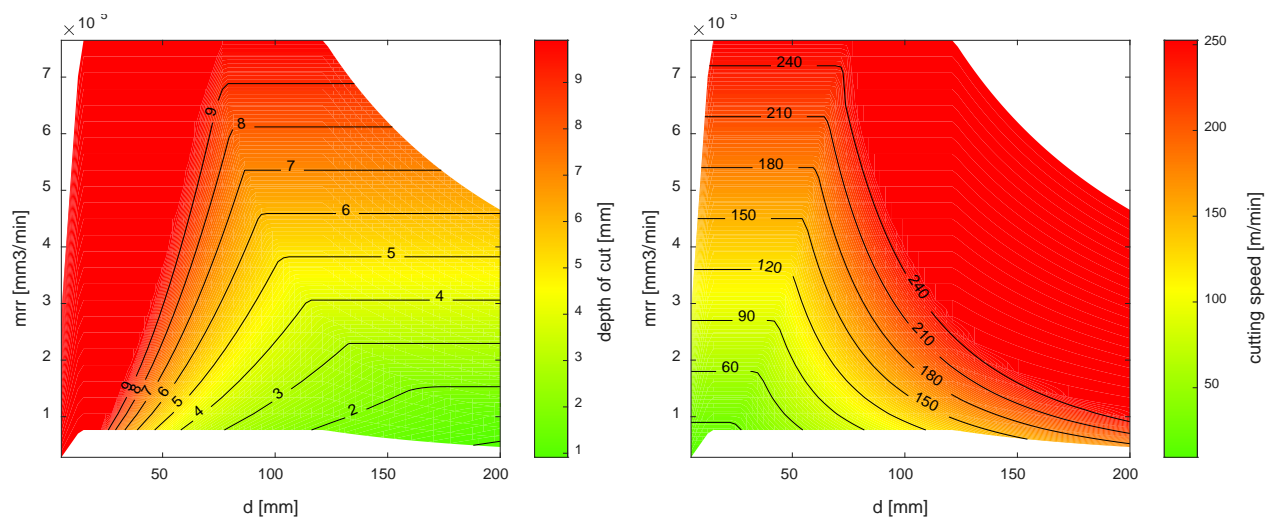


Fig. 24. Cutting parameters maximizing efficiency of material removal process by the considered PU: depth of cut and cutting speed. Feed plot is not shown, as its value assumes always maximum reachable value of 0.35mm/rev.

As far as basal power consumption is neutral from the point of view of minimization (as the basal energy required to remove a given amount of material is fixed, if the *MRR* is given), both scenarios share the same optimal cutting parameter sets, Fig. 24. The third parameter: feed per turn, is always at its maximum value (0.35mm/rev), therefore it has not been plotted: for any diameter and production rate, maximizing feed results in efficiency improvement. Depth of cut and cutting speed are however less trivial. For low diameter range, efficiency can be maximized ensuring highest depth of cut, whereas for large diameter workpieces it is suggested to maximize cutting speed instead. Mid-range workpieces can be manufactured with a certain optimal combination of both parameters. Appendix B contains spindle, chiller and cutting losses breakdown as well as spindle operating conditions for considered ranges of processing rate and workpiece diameter.

The overall optimization strategy is synthesized in Fig. 25 for different workpiece diameters and productivity (i.e. *MRR*). The reachable region is limited by both process and machine specification: at

low diameters by the maximum spindle speed and tool depth of cut, at high diameters by the maximum spindle torque and tool cutting speed, at high MRR, by the maximum tool feed per turn, cutting speed and depth of cut. The power limit, for the considered spindle, is never reached in the adopted optimization. From Eq.(27), a given MRR can be realized by ∞^2 combinations of parameters $a_p f v_c$. The developed optimization shows that energy per part is minimized always adopting the maximum feed per turn. Additionally, for smaller diameters, the cutting depth should be maximized, while, at higher diameters, the maximum cutting speed should be adopted.

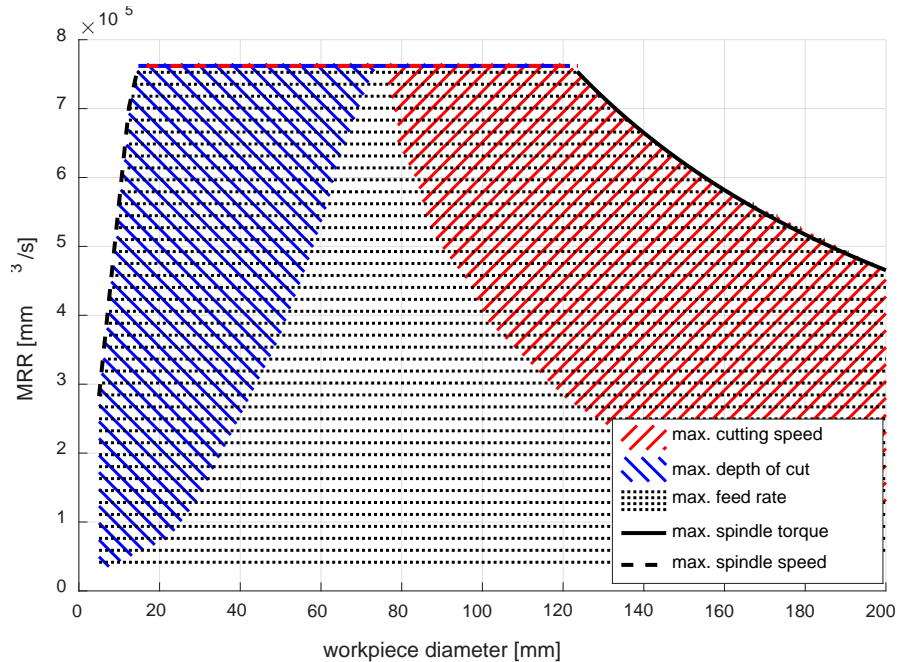


Fig. 25. Constrains that are active in efficiency maximization as function of MRR and workpiece diameter. The highest possible feed must be always selected. Additionally, in the low diameter region, maximization of depth of cut brings the highest efficiency, whereas, for large diameters, highest cutting speed is the optimal choice. Maximum productivity (i.e. maximum MRR) is limited by spindle speed (for low diameters), by both cutting speed and depth of cut (for intermediate diameters) and by spindle torque (for high diameters).

4. Discussion

4.1. Overall efficiency in cutting process

When combining PU and cutting process efficiencies, the proposed methodology can provide counter-intuitive suggestions for energy optimization of the turning process. It has been pointed out that, in some cases, a MRR increase impairs the overall process efficiency. In general, the overall process efficiency is dominated by PU efficiency, therefore, when MRR is increased by increasing spindle speed, the overall process efficiency decreases, according to PU efficiency behavior. Nevertheless, cutting efficiency plays a significant role when spindle speeds are low (for example when turning on large diameters, or hard-to-cut materials like titanium alloys). In this case, an increase in the depth of cut causes an increase in the edge components of cutting force, producing an impairment of efficiency that is not compensated by the slight PU efficiency improvement implied by the torque increase.

4.2. Optimal cutting conditions in function of MRR and d

Efficiency maps clearly indicate that efficiency of PU cannot be treated simply as a fixed value and strongly depends on several factors. One driving factor is workpiece size, which was modelled through parameter d . Optimal cutting parameters change significantly as d varies, with exception of feed rate which, when maximized, always leads to efficiency improvements. For depth of cut and spindle speed

the choice is less trivial, however the general rule could be increasing depth of cut for small diameter ranges and increasing cutting speed for large diameters.

Another dimension to be considered in efficiency analysis of cutting process is *MRR*. Here also choice is not evident and depends also on machine working condition. In *scenario 1*, overall consumption strongly depends on basal power of both chiller and remaining machine peripherals. Potential energy saving through reduction of *MRR* was only possible for small diameter workpieces, but chosen strategy must be individually weighed against basal consumption of the whole machine. As an obvious consequence, for machines with significant basal consumption, it might be best to always maximize *MRR*. The general tendency in machine tools is to reduce basal consumption through better selection of machine components (chiller, hydraulic units etc.), avoiding oversizing, and using intelligent stand-by modes. Therefore, it's most likely that future generations of machines will exhibit reduced basal consumption and will be able to utilize shown opportunity for energy use reduction via lowering *MRR*. *Scenario 2* showed that, if in a considered production scenario, the basal power consumption is fixed, no matter the activity of the machine, the opportunities to increase processing efficiency arise. Staying at highest productivity in low cutting diameter region indicates high losses due to friction as well as increased resistive losses due to PM motor field weakening at high speed. Similarly, in the highest diameter region, cutting is performed at the maximum torque, which contributes to i_q -related resistive losses. In both cases, applying a less aggressive processing strategy brings considerable overall energy savings. Charts as the one represented in Fig. 25 are easily computed, for a given turning machine, considering different workpiece materials and tool geometries (i.e. for different sets of cutting parameters), giving useful overall indications to optimize energy efficiency in process planning.

The analysis demonstrated that the efficiency of a spindle subsystem varies significantly with the operating conditions: between low speed heavy operations and high speed light machining the absolute difference in efficiency can reach 50-60%. This fact invalidates, for production scenarios with a wide range of operating parameters, the constant spindle efficiency hypothesis adopted in (Albertelli et al., 2016, Xiong et al., 2016) during cutting parameters optimization.

5. Conclusions and potential exploitation

A novel integrated approach for energy efficiency optimization in turning operations has been presented, taking into account the strong interrelations between cutting process, spindle with permanent magnet motor and its chiller. The model-based approach, after a reduced set of experiments for model identification, provides general results and additional insight, indicating where and why, in the system, energy dissipations occur.

Tests on a turning machine show the quality of the identified models and provide general guidelines for energy optimization, considering workpieces of different diameters and various production scenarios. On the contrary to the experimental study of (Mori et al., 2011) which showed that efficiency increase can only be achieved by maximization of the processing rate, it has been demonstrated that, in some cases, increasing *MRR* impairs the overall process efficiency. This misalignment can be explained by the fact, that typically experimental studies cover a limited number of operational conditions, whereas the proposed model-based approach to efficiency analysis covers a complete range of operating conditions, including varying workpiece size. As much as 34.5% of saving of the PU energy can be achieved by reducing processing speed in small diameter cutting. Given that the examined permanent magnets spindle + chiller assembly is often used in different machine tool types, the same approach can possibly be extended to similar processes, like drilling and boring. The extension to milling is also achievable, where the d parameter would represent the tool diameter, but it implies the introduction of further parameters concerned with tool engagement and milling path; thus, a consistent energy analysis and optimization would become more complicated.

The provided pre-optimized function, relating efficiency/energy to processing rate (*MRR*) and workpiece characteristic (namely, diameter d), constitutes a building block which can be used at

machine level to support energy use prediction in production optimization. For example, it can be used to optimize process planning for different machine tool configurations, based on the same PU but characterized by diverse peripheral equipment: for each possible processing rate, processing time is easily calculated and then used to compute the corresponding energy consumption of the peripheral units, due to the basal power consumption. The proposed approach will be used, in future developments, to represent the relationship between cycle time and energy use while optimizing a machining cycle on a given machining center.

These results can be easily used in industrial context e.g. by implementation of a model hosted by machine tool controller that could in real time evaluate efficiency of the process and propose to the operator more optimal cutting parameters. The cutting process and PU model can also be applied to predict energy consumption on the design phase of a workpiece and early optimization of the cycle. Developed model can be utilized as a part of a larger model of the whole machine tool and manufacturing system.

Proposal for a standard energy assessment of metal cutting machine tools, by a “Machine-based” approach

Introduction

Europe, after having expressed its commitment towards contrasting climate change, addressed the energy efficiency targets through specific Directives. In July 2005, the European Commission and the European Parliament adopted the EuP 2005/32 / EC "Ecodesign Directive for Energy-using Products" (EC Directive, 2005), which deals with the development of eco-design specifications for products that use, generate and transfer energy, such as computers, televisions, fans, including machine tools. In September 2009, the ErP directive 2009/125 / EC "Eco-design Directive for Energy-related Products" (EC Directive, 2009) was adopted, widening the scope to products that do not consume energy by themselves but which have a potential impact on it, including passive assets as window frames. Under the stimulus of the EuP Directive, CECIMO - the European association of machine tool industries - has launched a Self-Regulation Initiative (CECIMO, 2018) to develop new legislation on energy efficiency, with the aim of improving "green" performance " in Machine Tools while avoiding the introduction of hard regulatory limitations to their development and innovation. The European Commission, as foreseen by the Directives, commissioned a Preliminary Study, assigned to Fraunhofer IZM and IPK (Fraunhofer IZM IPK, 2012), aimed at assessing the installed machine base, the forecasted evolutions and identifying suitable ways to increase the environmental performance of machine tools during their life cycle. Generally the analysis is focused on the energy used during the use phase. Following a modular approach, machines are seen as assembled components and subsystems, each of which is powered by energy sources (electrical, hydraulic, pneumatic elements). Given this modular vision, the industrial machinery integrating components and modules similar to those used in machine tools are also covered by the analysis: machinery for welding, plastic injection, processing of wood, glass, plastics.

The ISO 14955 Environmental evaluation of machine tools

In 2010, the ISO / TC 39 Technical Committee initiated an ISO working group (WG 12) on the Environmental Assessment of Machine Tools, in order to define a standard, intended for both manufacturers and users, that can guide and standardize the energy assessment of a machine. At the Italian level, UNI has therefore created the corresponding GL 2 workgroup "Environmental Assessment

of Machine Tools", made up of sector operators who, by providing their own point of view and experiences, develop proposals for the regulatory content. The Italian GL2 is coordinated by a researcher from ITIA-CNR (now named STIIMA-CNR).

The standard analyses the energy consumption of machine tools (in terms of electricity, compressed air, pressurized oil, gas, etc.), considering that the use of a machine during its long operational life typically produces a greater environmental impact than that one related to its construction and disposal. The ISO 14955 "Environmental evaluation of machine tools" (ISO/TC 39 Machine tools WG12, 2017), is currently structured in 5 parts, two of which are general (parts 1 and 2) and three specific for different machine tools families (parts 3, 4 and 5).

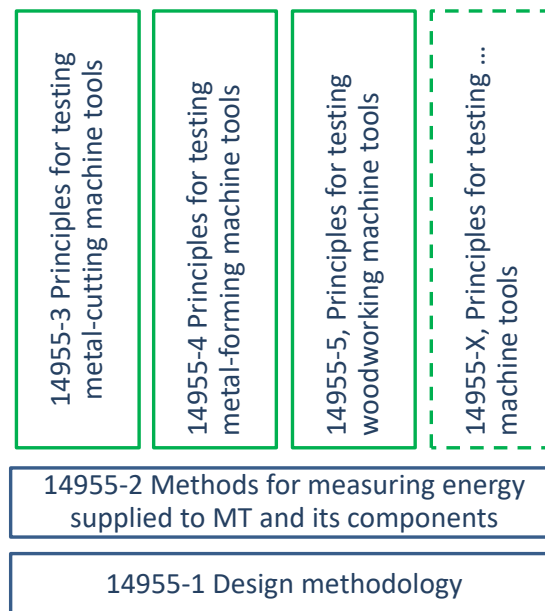


Fig. 26. Architecture of the ISO 14955 standard Environmental evaluation of machine tools.

- ISO 14955-1 "Design methodology for energy-efficient machine tools" (last edition in 2017): intends to provide a method to integrate energy assessments in the design of a new machine tool, considering all energy flows that cross the "boundaries" of the machine. The measured energy flows are associated with the useful outputs of the machine components, defining the useful functions performed by the various components. A list of possible technical improvements (the so-called "Best Available Technologies") is included, which can be used as a useful check-list while designing a new machine. Particular attention is given to auxiliary devices such as hydraulic power unit, chillers, pumps and cutting fluid circulation, that often produce a significant energy use.
- ISO 14955-2 "Methods for measuring the supply of machine tools and machine tool components" (published in 2018): provides indications for carrying out energy measurements on a machine and related elements (for example, how to make measurements on electric motors and hydraulic components, how to evaluate the energy absorbed by the compressor used to supply pressurized air to the machine) and how to document the results. However, the test cycle is not specified, i.e. what the machine must do during the measurements: it will be defined, for the different machine families, in the later parts of the standard.

- ISO 14955-3 "Principles for testing metal-cutting machine tools with respect to energy efficiency": provides indications and specifications on how to perform tests during energy measurements on metal cutting machines. A first version has been approved as Committee Draft.
- ISO 14955-4 "Principles for testing metal-forming machine tools with respect to energy efficiency": provides indications and specifications on how to perform tests during energy measurements on plastic deformation machines. The developed Draft International Standard has been recently approved for as Final Draft International Standard.
- ISO 14955-5 "Principles for testing woodworking machines with respect to energy efficiency": provides indications and specifications on how to perform tests during energy measurements on woodworking machines. A first version has been approved as Committee Draft. This subgroup sees the direct participation of the main manufacturers worldwide and of machinery users.

To discuss the different approaches adopted in ISO 14955, two general use cases can be considered:

- A) a machine tool user is setting up a production plant to produce a new part, in large volumes. He/she intends to buy a dedicated and already configured production system, a so-called "turnkey system", and wants to know how much energy it will consume. In some cases, e.g. in the automotive sector, it may be required to declare the energy consumption associated with the production of parts, in other cases, a reduction in consumption of more than 20% allows subsidized loans (e.g. KfW Energy Efficiency Programme - Production Facilities and Processes³). The standard must prescribe how to perform and document energy measurements, starting from the electric and pneumatic ones. This scenario is described, in 14955-2, as "task-based testing scenario": the measurements are linked to a specific, user-defined, production mission. This is the main approach covered in 14955 part 3.
- B) a machine tool builder wants to develop a new family of machines that, hopefully, will be sold to numerous customers, each of which, in turn, will produce different types of parts over time. In this scenario, it is impossible to optimize the machine design for a single production case: the designer must refer to a generic "average energy efficiency" of the machine, considering a typical production mix for a given market sector (e.g. production of molds or aerospace or general mechanics). This situation is described, in 14955-2, as "machine-based testing scenario", aimed at evaluating a machine "by itself".

In the two cases, the scope of the analysis is different. To give a simple example, let us suppose, in a task-based scenario, to analyze the production of a part by milling operations. If a tool with a more positive rake angle is selected (i.e. a "sharper tool"), the cutting forces and therefore the electrical consumption of the spindle are reduced, usually to the detriment of a shorter tool life. The task-based analysis will report this improvement, while it would make no sense, in a machine-based analysis, to assume that the machine itself is more efficient thanks to the different tool used. This difference is illustrated in the following figure: in the task-based analysis the technologist must optimize the machining cycle, for the specific machine used, while, in the machine-based analysis, the working cycle

³ <https://www.kfw.de/inlandsfoerderung/Unternehmen/Energie-Umwelt/index-2.html>

is considered fixed or, better, the load applied to the machine must be fixed (e.g. torque and spindle speed, lubrication-refrigeration requirements, ...).

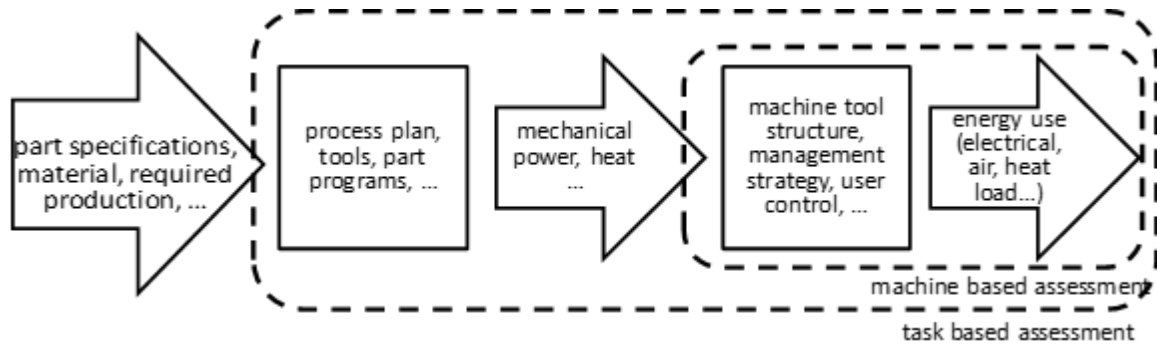


Fig. 27. energy assessment focused on a specific production case (Task based) or on a machine-tool model (Machine based).

For a "task-based" evaluation the standard does not specify what the machine should do, but rather how to make measurements (what to measure and how). On these aspects the reference standard is ISO 14955 part 2, which in turn is substantially compatible (even if, unfortunately, not exactly) with the German standard VDMA 34179 (March 2015): "Instructions for measuring machine tool consumption of electricity and other energy sources, for mass production", produced by an agreement between German machine tool and automobile manufacturers. The VDMA standard, focused on mass production, obviously follows a task-based approach, indicating what energy flows must be measured (electricity, compressed air, lubricant-refrigerant, suction, cooling water) and how (instruments, timing, ...). Non-electric power flows are generally converted into corresponding electrical energy (for example, compressor efficiency must be taken into account for compressed air). Simplifying, we can think that the result of the assessment is simply the amount of energy spent for each piece produced, obtained by measuring the energy absorbed during the production of a significant number of pieces, enough to get the plant up and running. However, given the continuous reduction in the volume of produced batches, it is increasingly important to take into account, even for energy analysis, non-productive times, linked to setup at the change of production or waiting for semi-finished products, etc. For these reasons, the standard requires to measure also the average power absorbed in the non-productive states (defined as off, standby, operational, ...) and also in the energetically relevant transitions (such as the warm up), as illustrated in the following figure.

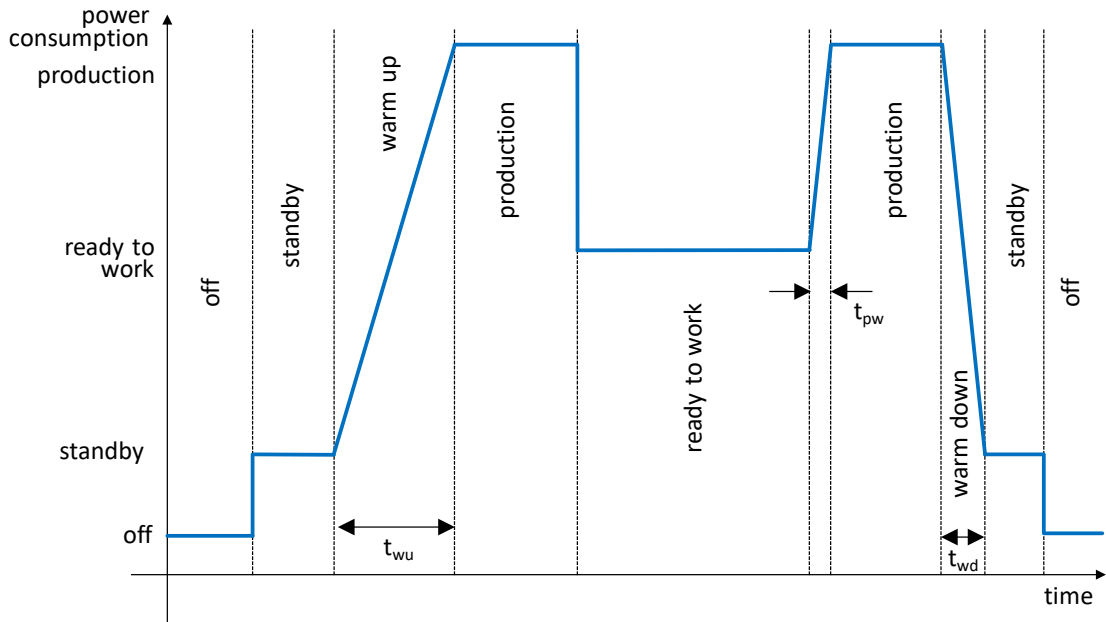


Fig. 28. sample power measurement in the various operating phases [VDMA 34179].

Going back to the ISO 14955, in order to define a “machine-based” approach that gives useful indications for machine design, a reference process must be defined, to represent the average machine use, for the considered machine tool typology and a selected industrial application sector.

For example, in ISO DIS 19544-4, which deals with machines for plastic deformation and laser cutting, the test work cycles for a press are defined without requiring the presence of a mold (usually not available during the preliminary evaluation of alternative presses). The prescribed machine activity is defined referring to the declared machine performance. The following figure shows the test cycle proposed for hydraulic presses, defined to emulate a deep drawing operation.

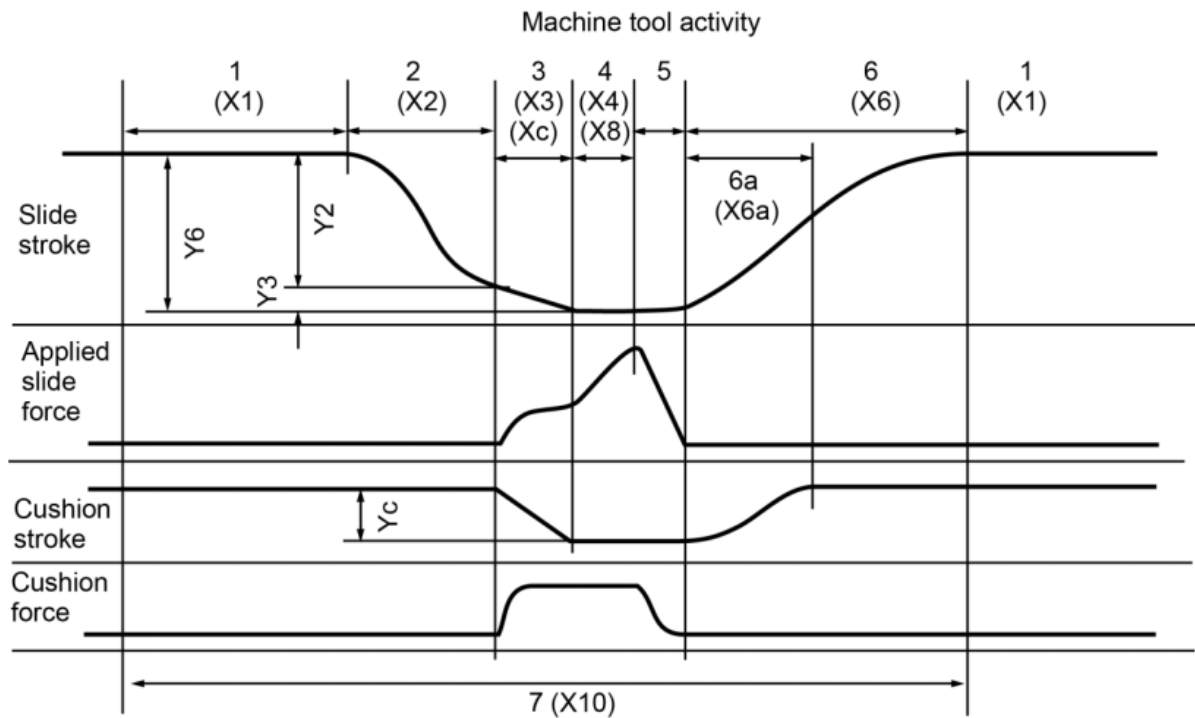


Fig. 29 definition of a machine-based test cycle for a hydraulic press [DIS 14955-4].

Key

- 1 machine tool activity 1: slide Waiting in TDC: Slide is waiting for start signal while workpiece is loaded into die.
The waiting time is X1.
- 2 machine tool activity 2: slide close: Slide is closing the die with velocity X2 and distance Y2.
- 3 machine tool activity 3: forming: Slide is forming the workpiece with velocity X3 and distance Y3.
The distance the cushion is displaced is Yc and the cushion force during displacement is Xc.
- 4 machine tool activity 4: embossing: Slide applies set-force X8 in BDC and start of BDC dwell time X4.
- 5 machine tool activity 5: decompression: Decompression of press frame, die cushion and slide cylinder (hydraulic press) / gear and drive mechanism (mechanical press). Decompression is not adjustable by the user.
- 6 machine tool activity 6: slide return: Slide moves back to TDC travelling the distance Y6.
- 6a machine tool activity 6a: workpiece ejection: Die cushion lifts workpiece for unloading, the distance is Yc.
- 7 X10: complete cycle (cycle time)

The numerical parameters of the cycle are defined according to the nominal specifications of the analyzed machine, as described in the following Table.

Table 13 cycle parameters for an hydraulic press [ISO DIS 14955-4]

Machine tool component	Machine tool activity	Set-value for distance	Set-value for speed, time, force	
Slide	Closing and return speed (X2, X6)	Y2, Y6	100%	
	Working speed (X3)	Y3 or Yc	70%	
	Force (X8)		70%	
	BDC dwell time (X4)	Presses with a nominal cycle time of less than 5 s		0,3 s
		Presses with a nominal cycle time of equal or more than 5 s but less than 30 s		1 s
		Presses with a nominal cycle time of equal or more than 30 s		20 s
	TDC dwell time (X1)	Manual fed presses with a nominal cycle time of less than 5 s		1 s
Manual fed presses with a nominal cycle time of equal or more than 5 s but less than 30 s			4 s	
Manual fed presses with a nominal cycle time of equal or more than 30 s			8 s	
Die cushion(s)	Die cushion force (Xc, % of nominal cushion force)		80%	
	Die cushion stroke (Yc, % of nominal cushion stroke)		80%	
Automation system	Moving speed of all axis		80%	

ISO 14955-4 also indicates how to calculate, as performance factor, the efficiency of the various subgroups to identify relevant and inefficient components, on which to concentrate the efforts for the optimization of the project.

Defining machine activities during a machine-based test is the most complex part of standard development. Within the ISO working group, there are frequent discussions: some experts believe it is not possible to define meaningful and sufficiently general tests, especially for metal cutting machine tools, characterized by very varied and complex types of workpieces and work cycles.

For this reason, at the actual development of ISO 14955 part 3, devoted to metal cutting machine tools, the machine-based approach is not developed, on the contrary of parts 4 and 5: no machine activities are proposed for specific machine types (e.g. milling machines, turning machines, etc.).

The Italian delegation considers this approach interesting for its simplicity but too limited to guide machinery builders toward the development of energy efficient machines and to support machinery users, especially in SME and sub-contractors, in choosing the best compromise between productivity, cost and energy efficiency. Given that Italian machine tool manufacturers are specialists in the field of flexible and small-batch production, often by large machine tools, ITIA-CNR decided to invest, in collaboration with Politecnico di Milano and interested Italian machine tools companies, in conceiving

a Machine-based approach for metal cutting machine tools. The proposed methodology is described in the following chapter.

1 Rationale of the proposed machine-based assessment for metal cutting machine tools

The proposed approach is similar to what has been illustrated for the metal forming machine tools: the efficiency of the main sub-groups must be evaluated against a given effort required by the process, isolating the influence of a particular tool and workpiece.

In a milling machine, for example, a significant percentage of energy goes into the spindle, and it depends on the torque and rotational speed required by the process. If an electro-spindle is used, it is also necessary to consider the consumption of the chiller that cools the motor windings: the pump circulating the refrigerant fluid makes an important contribution to the "base" consumption, i.e. the consumption independent from machine's activities. The efficiency of the spindle + refrigerator sub-assembly, defined as the ratio between the mechanical power emitted by the spindle, towards the process, versus the total electrical power absorbed by spindle and refrigerator, depends on the load, constituted by the cutting process. It can be evaluated by submitting the spindle to different combinations of torques and speeds: the following figure shows the energy efficiency map identified by ITIA-CNR for a turning electro-spindle. The blue "circles" on the graph correspond to speeds and torques used during a test cycle. The various operations can be distinguished: longitudinal turning (at constant speed), facing and slotting (at increasing speed, because of the decreasing radius) and acceleration and deceleration at the maximum power, corresponding to spindle start and stop. The brushless motor used would, by itself, achieve 95% efficiency, in the high torque region, with speeds lower than that of the field weakening speed (when the required voltage reaches the drive limit value). The refrigerator consumption penalizes the areas with low torque: most of the considered test cycle takes place in regions with efficiency between 20 and 70%, producing an overall efficiency much lower than the theoretical maximum.

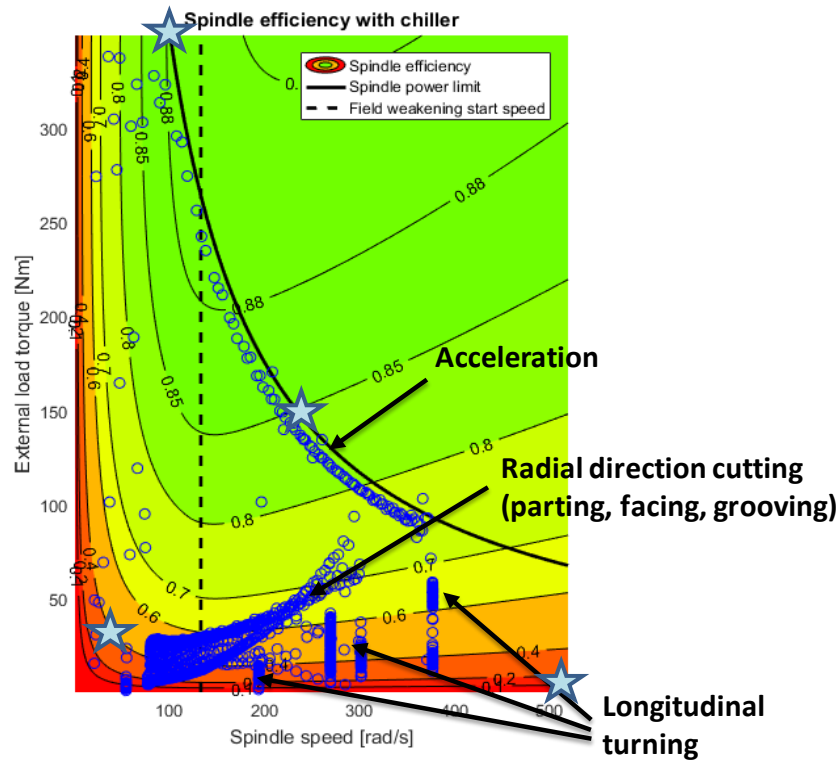


Fig. 30 efficiency map of an electro spindle in a turning machine and trace (blue circles) of the test cycle. The solid line indicates the torque limit, the dashed line the defluxing speed. The stars indicate possible measuring points for the energetic characterization.

It is therefore important, when designing or choosing a machine tool, to evaluate the efficiency of the spindle system (plus chiller, if present), with respect to the needs of its machining cycles, in terms of torque and speed. The map shown in the previous figure is produced by a model identified on experimental measurements. Such approach, while informative and effective, is not appropriate for an industrial assessment standard, like the ISO 14955: it would be necessary to evaluate the accuracy of the proposed model and the adopted algorithms to identify the model parameters. It is preferable, for the standard, to characterize the efficiency map by prescribing measures that sample the map in some significant points, such as those indicated by the "stars" symbols in the previous figure.

The proposed approach is based on the following points:

- 1) following the functional methodology proposed in ISO 14955-1 (clause 7), a machine tool is evaluated assessing its **generalized functions** (part 1, clause 6.3): machine tool **operation** (machining process, motion and control), **process conditioning**, **workpiece handling**, **tool handling or die change**, **recyclables and waste handling**, **machine tool cooling/heating**.
- 2) all generalized functions that entail a significant energy use are assessed, measuring the energy required to perform the required functional unit or activity (e.g. material removal, tool or workpiece change, etc.).
- 3) if the same functional unit is used on different machine models (e.g. a spindle & chiller set adopted in different machine models), in the same configuration and size, a single energy assessment can be performed and then associated to the various machine tool models. In a future perspective, some peripheral equipment could be qualified by the corresponding

component manufacturer (e.g. by the supplier of the cutting fluid management system) [this approach is discussed in Work Package 1.4, for spindle characterization]. If a single machine peripheral unit is modified, all non-related units don't have to be requalified.

- 4) in addition to the measured quantities, **performance indicators** must be provided to guide in comparing alternative design solutions. The key indicator is the “**energy efficiency**”. When a function delivers an output power (e.g. a spindle), the efficiency is defined as (average output power)/(average input power). When a function is continuously delivered without a measured output power (e.g. a waste removal system), the performance indicator is the average used power. When the delivered function is discrete (e.g. tool change operation), the performance indicator is the energy used per function (i.e. average energy per tool change) plus base used power (when the equipment is active but not operating)
- 5) testing conditions for the experimental energy assessment are defined **referring to declared machine tool performance** (e.g. % of the maximum spindle power and torque), as done in part 4 to define test cycles for metal-forming machine tools
- 6) for a given machine tool type, the reference process (shift regime) can be defined, if desirable, considering different application scenarios (e.g., for a milling machine: mould and dies production, automotive parts, etc). The reference shift regime specifies the time-share for each operating state (e.g. OFF, STANDBY, WARM UP, READY FOR PROCESSING, PROCESSING). For each operating state, if relevant, activities at the level of generalized functions shall be defined, e.g. spindle speed and torque, number of tool changes per hour, etc.
- 7) machine tool builders have expressed their preference for testing procedures that do not require actual machining of test parts, especially on medium-large machines: the machine-based standard must propose a way to load the motor at the prescribed speed & torque level without real cutting.

Proposed machine-based assessment for metal cutting machine tools

NOTE: the proposed assessment approach is described in the following referring to milling machine tools⁴.

1.1 Functional description

The testing procedures must quantify, for each generalized function, its base consumption (in the ready to operate state) and the energy used to deliver the required “functional units” or to perform the requested activity. It is therefore necessary to define all requested outputs involved in the machine-based assessment. For a milling machine, sample proposed outputs are:

- 1) **machine tool operation (machining process, motion and control)**. **Spindle**: mechanical power delivered to the process, at different speed/torque combinations. **Axes**: covering a given distance at different speeds, accelerating, pushing with a given force (it happens during machining, to balance the cutting force).
- 2) **process conditioning**: providing coolant at a prescribed pressure and flow.
- 3) **workpiece handling, tool handling**: executing a tool or workpiece change operation.
- 4) **recyclables and waste handling**: removing waste (chip transport, dust suction,...).
- 5) **machine tool cooling/heating**: realizing the prescribed machine temperature control.

⁴ The following description is focused on three axes milling machines: further indications could be added for five axes machine tools.

1.2 Shift regimes

A shift regime defines the time-share of the various operating states and, when relevant, the performed activities. To support a machine-based assessment, each activity is mapped onto the corresponding functions and components, as exemplified in Table 1.

Default shift regimes are proposed by the present standard for different kind of metal cutting machine tools. Different shift regimes can be defined, for the same machine tool type, referring to various application scenarios, e.g., for a milling machine: general mechanics, mould and die, aerospace. Machine tool builders can also propose additional shift regimes, for a given machine type and/or for a specific application scenario. Additional cases could be defined in agreement with the customer.

NOTE: the goal is to define an “average use” of the machine tool. Machine tool designers typically adopt a similar approach, defining “average duty profiles”, for selecting and dimensioning machine tool components (e.g. thermal sizing of motors, life expectancy of ball screws,..).

Table 14 Shift regime for milling machine tools: mould and dies scenario

functions	operating states	OFF	STANDBY	READY FOR OPERATION	WARM UP	PROCESSING roughing	PROCESSING finishing	PROCESSING rapid motion
	hours	8	1	3	0.25	4	7	0.75
MT operation	control	ON	ON	ON	ON	ON	ON	ON
	spindle	OFF	OFF	OFF	$S = S_{max}, M = 0$	$S = 50\% S_{nom}$ $M = 75\% M_{nom}$	$S = (S_{nom} + S_{max})/2$ $M = 10\% M_{nom}$	$S = S_{nom}$ $M = 0$
	axis	OFF	OFF	ON ⁵	$Vel = 50\% V_{max}$ $Ks = 100\%$	$Vel = 25\% V_{max}$ $For = 50\% F_{max}$ $Ks = 50\%$	$Vel = 50\% V_{max}$ $For = 10\% F_{max}$ ⁶ $Ks = 100\%$	$Vel = 50\% V_{max}$ 30 %time @ Vel_{max} $Acc = Acc_{max}$ $Ks = 75\%$
process conditioning	coolant fluid	OFF	OFF	OFF	OFF	high pressure	low pressure	OFF
workpiece handling	(manual wp change)	-	-	-	-	-	-	-
tool handling	tool changer	OFF	OFF	OFF	OFF	10 changes/h	5 changes/h	ON
waste handling	chip conveyor	OFF	OFF	OFF	OFF	ON	ON	ON
MT cooling / heating	axis & structure	ON	ON	ON	ON	ON	ON	ON
	spindle	OFF	OFF	OFF ⁷	ON	ON	ON	ON

Note: a component in “ON” state uses its base power consumption

Legend:

S, M: spindle speed (S) and torque (M) prescribed for the test

S_{nom}, S_{max} : respectively nominal and maximum spindle speed

⁵ standing still axes, with active position control (e.g. master-slave coupling active and preloaded, if present)

⁶ the requested force includes also the effort requested for acceleration

⁷ even if spindle cooling is sometime kept active for few minutes in this state, after a machining operation, this energy use is neglected. If specified by the spindle manufacturer, chiller could be considered ON also in the READY FOR OPERATION state

M_{nom} :	nominal spindle torque
Acc, Vel:	axis acceleration and velocity prescribed for the test
For:	prescribed external force applied to the axis
F_{max} :	maximum external force (S1, continuous duty) applicable on the axis (note: this value is lower than the force corresponding to the axis motor S1 torque, because of axis friction)
V_{max}, ACC_{max} :	maximum axis velocity and acceleration
Ks:	simultaneity factor for warmup, roughing, finishing and rapid motion activities (respectively called in the following: $K_{S_{warm}}$, $K_{S_{rough}}$, $K_{S_{finish}}$, $K_{S_{rapid}}$). They express the percentage of time (duty cycle) in which each axis is operating, for the analysed activity

1.3 Testing procedures

According to 14955 part 2, before assessing the key components, as described in the following, a warmup cycle shall be performed to reach a stable thermal condition, and then the average consumption of significant functions is measured, for all non-productive states of interest (e.g. standby, ready for operation). Outcome: base power consumptions of all functions with a significant energy use.

General notes:

- the measurement and reporting methodologies, described in 14955 part 2, shall be adopted
- when the energy consumption depends on the thermal equilibrium of the machine tool (e.g. when chillers are involved), measurements must be executed in a stable thermal state
- all forms of energy supplied to the examined function shall be measured: electric, compressed air, other fluids. The machine tool shall be setup as during normal operations, including the foreseen energy-saving features.

The prescribed measurements shall provide the data (e.g. the average power) required to estimate the energy consumption in all foreseen shift regimes, for the given machine tool type, i.e. measurements do not have to be repeated if a different shift regime is considered.

1.3.1 Function: machine tool operation (with its sub-functions: machining process, motion and control).

Tests are designed to allow estimating energy used by the significant machine functions in different shift regimes. To avoid complexity and cost of actual machining operations, the corresponding loads are emulated applying external forces (on the axes) and exploiting inertial forces and torque during axes or spindle acceleration.

Required measures: spindle torque and speed (typically exploiting the measurements delivered by the numerical control and drives), used energy (via a power meter on the drive supply or via the drive itself, if available). Power measurement on the chiller supply. Compressed air and other fluid power, when relevant.

Spindle: measure of input (electrical) and output power (velocity x torque) at the following speed/torque combinations:

- 1) **free run** (null output torque) at 50% of S_{nom} , S_{nom} , $(S_{nom}+S_{max})/2$ [similar to the “Load operation mode” in (JIS, 2010)]. To be reported: average motor input power and average chiller or ventilation power⁸, base power consumption. Performance indicator: average input power, for each velocity.
- 2) **sawtooth velocity profile:** the cycle shall be defined to obtain a +/- 5% velocity oscillation around the requested average speed, with a negligible time spent at constant speed (the goal is to maintain the spindle under a constant torque). The acceleration value is set to produce the prescribed level of torque, indicated in the following table.

Table 15 speed and torque set points for spindle characterization

	1	2	3
speed	50% S_{nom}	100 % S_{nom}	$(S_{nom}+S_{max})/2$
torque	75% M_{nom}	50% M_{nom}	10% M_{nom}

To be reported: average motor power and average chiller or ventilation power (separated from the corresponding base consumptions). Performance indicator: average power for the prescribed test conditions.

Axes (repeated for each axis, number “i”):

- 1) back and forth motion along the available axis travel at 25% 50% 100% of the maximum speed (Vel_{max}) [similar to the “Load operation mode” in (JIS, 2010)]. To be reported: total energy, time, distance for the prescribed test conditions and the corresponding average power $\left(P_{axis_{vel_i}} \right)$. Performance indicator: covered distance/used energy. Referred in the following as “velocity test”.
- 2) back and forth motion from zero to maximum velocity and down to zero, using the maximum acceleration. To be reported: distance covered in one cycle, maximum speed, cycle time, energy per cycle (axis motor and chiller, if present) and corresponding average power $\left(P_{axis_{acc_i}} \right)$. Performance indicator: number of cycles/used energy. Referred in the following as “acceleration test”.
- 3) a load cell is connected between spindle head and the workpiece table (as specified in the ASME B5.54-2005 standard for machine stiffness measurement). The axis is pushed against the load cell in order to reach 25%, 50% and 75% of the maximum declared axis force (in S1: continuous duty). To be reported: force value, average input power $\left(P_{axis_{for_i}} \right)$ (axis motor and chiller, if present). Performance indicator: force “For” divided by the average power for the prescribed test conditions. Referred in the following as “force test”.

⁸ if the motor mechanically drives its fan, the related power is accounted measuring the motor power

1.3.2 Process conditioning

In case of water or oil process conditioning, measure the pressure at the pump⁹, the coolant flow rate (e.g. by a simple graduated bucket) and the energy used (at steady state): 20% and 100% of the nominal flow rate. Repeat for the different pressure levels available (e.g. low / high pressure). Outcome: average process conditioning power $P_{proc\ cond}$ (pressure, flow rate) for the prescribed test conditions.

1.3.3 Workpiece handling, tool handling

Execute repeated operations (i.e. workpiece / tool change), in a random sequence covering all available tool / workpiece positions. Measure the power used by the employed electrical motor or hydraulic or pneumatic systems. Remove from the measured power the average base power, that have been quantified in the ready to process state. Computes the additional energy associated to a single operation. Performance indicators: additional energy per operation, average base power. Outcome: energy per tool change E_{tool} and energy per operation that involves workpiece handling: E_{workp} , base powers P_{tool} , P_{workp} .

1.3.4 Recyclables and waste handling

Measure the average power of the involved components (electric motors for chip removal, circulation pumps, compressed air,...) during operation (chip removal). Outcome: average recyclables and/or waste handling power P_{recyc} .

1.3.5 Machine tool cooling/heating

Measure the chiller average power at steady state. If possible, repeat the measurement with different ambient temperatures. Outcome: average machine tool cooling (or heating) power $P_{MachCond}$.

1.4 Shift regime assessment

Exploiting the experimental data collected on the relevant machine functions, the average power consumption for a given shift regime can be estimated, together with the corresponding share of energy used by the different functions.

NOTE: faster machines could require a higher power but, thanks to a shorter cycle time, could deliver a lower energy per produced part. A complete energy assessment requires therefore also the evaluation of the reachable cycle time, for the examined machine tool. Evaluation of the dynamic performance of a machine tool involves considering the accuracy of the machined part: only machining cycles producing acceptable parts shall be considered. This complex topic is not covered by the present standard: to complete the machine-based assessment, appropriate ISO standards can be applied to evaluate the machine dynamic performance (e.g. ISO 10791-7¹⁰). If those additional tests are performed, the overall energy used to produce the test part shall also be measured and reported.

The energy used in machine states without processing are computed from the base consumption of the modules & components active in that state. For example, for the standby state:

$$E_{stand\ by}[J] = P_{stand\ by}^{base} [W] \cdot 3600 \cdot T_{standby}[h]$$

⁹ pressure measurement near the tool would be more appropriate, but usually not available

¹⁰ ISO 10791-7:2014 Test conditions for machining centres -- Part 7: Accuracy of finished test pieces

where:

$P_{standby}^{base}$ is the base power consumption of all modules active in standby

$T_{standby}$ is the duration of the standby state [hours]

For the “PROCESSING - roughing” activity:

- the average spindle power is taken from the corresponding spindle test:

$$P_{rough}^{spindle} = P_{spindle}(S_{rough}, M_{rough})$$

- the average axes power is approximated as the sum of the losses of the corresponding “velocity test” and “force test”, plus the nominal output power due to cutting, for each axis “i”. The calculation takes into account the prescribed simultaneity factor:

$$P_{rough}^{axes} = P_{base}^{axes} + K_{S_{rough}} \cdot \sum_{i=1}^3 \left[P_{vel_i}^{axis}(Vel_{rough_i}) + P_{for_i}^{axis}(For_{rough_i}) + Vel_{rough_i} \cdot For_{rough_i} \right]$$

where:

P_{base}^{base} is the base power consumption of all axes

The energy used for the “PROCESSING - roughing” activity is then computed:

$$E_{rough} = \left[\left(P_{rough}^{base} + P_{rough}^{spindle} + P_{rough}^{axes} + P_{proc\ cond}(\text{press}) + P_{recyc} + P_{mach\ cond} \right) \cdot 3600 + N_{ToolCh_{rough}} \cdot E_{tool} \right] \cdot T_{rough}$$

where:

P_{rough}^{base} is the sum of base power consumptions for the functions active in the roughing activity which are described by a constant power use and are not explicitly treated in the formula. It includes the base power consumption of tool / workpiece handling.

T_{rough} is the duration of the roughing activity [hours]

$N_{ToolCh_{rough}}$ is the number of tool change operations per hour in the roughing activity [number/hour]

For the “PROCESSING – finishing” activity:

- the average spindle power is taken from the corresponding spindle test:

$$P_{finish}^{spindle} = P_{spindle}(S_{finish}, M_{finish})$$

- the average axes power is approximated as the sum of the losses of the corresponding “velocity test” and “force test”, plus the nominal output power due to cutting, for each axis “i”. The calculation takes into account the prescribed simultaneity factor:

$$P_{finish}^{axes} = P_{base}^{axes} + K_{S_{finish}} \cdot \sum_{i=1}^3 \left[P_{vel_i}^{axis}(Vel_{finish_i}) + P_{for_i}^{axis}(For_{finish_i}) + Vel_{finish_i} \cdot For_{finish_i} \right]$$

The energy used for the finishing activity is then computed:

$$E_{finish} = \left[\left(P_{finish}^{base} + P_{finish}^{spindle} + P_{finish}^{axes} + P_{proc\ cond}(\text{press}) + P_{recyc} + P_{mach\ cond} \right) \cdot 3600 + N_{ToolCh_{finish}} \cdot E_{tool} \right] \cdot T_{finish}$$

where:

- P_{finish}^{base} is the base power consumption for the modules active in the finishing activity which are described by a constant power use and are not explicitly mentioned in the formula. It includes the base power consumption of tool / workpiece handling.
- T_{finish} is the duration of the finishing activity [hours]
- $N_{ToolCh_{finish}}$ is the number of tool change operations per hour in the finishing activity [number/hour]

For the “PROCESSING - rapid motion” activity, with an “ R_{vel} ” percentage of time spent at the maximum speed (30% of the cycle time, in Table 1), the average axes power is estimated as:

$$P_{rapid}^{axes} = P_{base}^{axes} + K_{S_{rapid}} \cdot \sum_{i=1}^3 \left[R_{vel} \cdot P_{vel_i}^{axis}(Vel_{max}) + (1 - R_{vel}) \cdot P_{acc_i}^{axis} \right]$$

The energy used for the “PROCESSING - rapid motion” activity is then computed:

$$E_{rapid} = \left[\left(P_{rapid}^{base} + P_{rapid}^{spindle} + P_{rapid}^{axes} + P_{proc\ cond}(\text{press}) + P_{recyc} + P_{mach\ cond} \right) \cdot 3600 \right] \cdot T_{rapid}$$

where:

- P_{rapid}^{base} is the base power consumption for the modules active in the rapid motion activity which are described by a constant power use and are not explicitly mentioned in the formula
- $P_{rapid}^{spindle}$ is the power consumption of the spindle during rapid motion. A typical value is the power consumption at no load, for the typical machining speed
- T_{rapid} is the duration of the rapid motion activity [hours]

The total energy consumption associated to the given shift regime is then computed, as sum of all the planned machine states and activities.¹¹

The shift regime assessment shall report the total estimated energy per day and its subdivision per machine state and activities (i.e. columns of table 1) and by machine function/components (i.e. rows of the same table).

Machine designers can therefore evaluate the significance of the different functions and components for a given production scenario. If alternative solutions for the same function are energetically characterized (e.g. alternative solutions for the hydraulic system), the corresponding effect on the average overall power consumption can be estimated, to support optimal design.

Experimental tests

In order to verify the feasibility of the proposed assessment methods, tests have been performed on a milling machine, in cooperation with Jobs spa manufacturer, member of the FFG group.

The examined machine is a Jobs-Sachman Thora T, a medium-power and medium-size milling centre with “T” architecture, non-rotating table sliding along the X axis and a universal, indexed head, moving in the Y and Z directions.



Fig. 31 Jobs Sachman Thora T Moving column milling centre (T configuration) for the energetic characterization.

¹¹ If the shift regime involves component activities not directly assessed experimentally (e.g. different values of speed and output torque for the spindle), the corresponding energy use can be interpolated from the assessed operating points [to be further detailed].

Table 16 Thora T technical data

AXES STROKE		THORA T			THORA RT	
X axis (longitudinal)	mm inch	2500 / 3000 98 / 118			2000 78	
Y axis (transversal)	mm inch	1200 47				
Z axis (vertical)	mm inch	1200 47				
Worktable width	mm inch	2700, 3200 x 800 106, 126 x 31			1000 x 1000, 1000 x 1250, 1250 x 1250 39 x 39, 39 x 49, 49 x 49	
Worktable loading capacity	kg lb	5000 11023			up to 5000 up to 11023	
AXES SPEED						
X - Y - Z axes	m/min ipm	«Basic» configuration 24 - 945 (with Universale head)				
	m/min ipm	«Speed» configuration 45 - 1771 (with T3T head)				
MILLING HEADS	C axis	A axis	Power	Torque	Spindle speed	Tool taper
	°	°	kW - S6 [S1] hp - S6 [S1]	Nm - S6 [S1] lb'ft - S6 [S1]	rpm	
UNIVERSAL HEADS						
Universale	indexed 2,5	indexed 2,5	33 [25] 44 [33]	637 [482] 470 [355]	5000	HSK-A-100 ISO 50

Additional machine performance, used as a reference to define the energy assessment:

- Max axis speed: 24 m/min,
- nominal axis acceleration: 1 m/s²,
- nominal jerk: 3 m/s³,
- strokes: 3000 x 1200 x 1200 mm
- X axis: 8000N max thrust,. X axis preload: approx. 15% of the static torque, motor Siemens FK7083 5AF
- Y,Z axes FK7063 Siemens. Stall torque M₀=11Nm, Nominal torque M_N= 3Nm. Z axis transmission 1/5 gear reducer, lead: 25mm: total transmission ratio: 1turn /5mm -> 13800 N theoretical thrust.

The measurements focused on the characterization of the linear axes, as described by the proposed methodology. Explorative measurements have been performed on the spindle, while a complete spindle+ refrigerator characterization is covered in WP1.4, that focus on machine tool components.

Experimental setup

During the tests, measurements have been performed with:

The machine numerical control (Heidenhain 640)

For each tested axis:

Time (sampling time 3ms), actual feed [mm/min], Nominal Current [A], displacement [mm], acceleration [m/s²], jerk [m/s³], Mechanical Output power [kW], Electrical Input power [kW].

ITIA CNR high speed power meter

Three phase active and reactive power measurements: Spindle (drive 1 & drive 2). X axis: motors 1 and 2. Z axis motor.

Before performing the various tests, the feasibility of measuring the used power via the machine tool drives has been assessed, comparing the results with the power measured by an external high speed power meter developed specifically by ITIA-CNR in previous projects. The following figure illustrates the results, showing an good correspondence: therefore, during the tests, power has been measured, interchangeably, with drives, through the Numerical Control, and by the ITIA-CNR power meter.

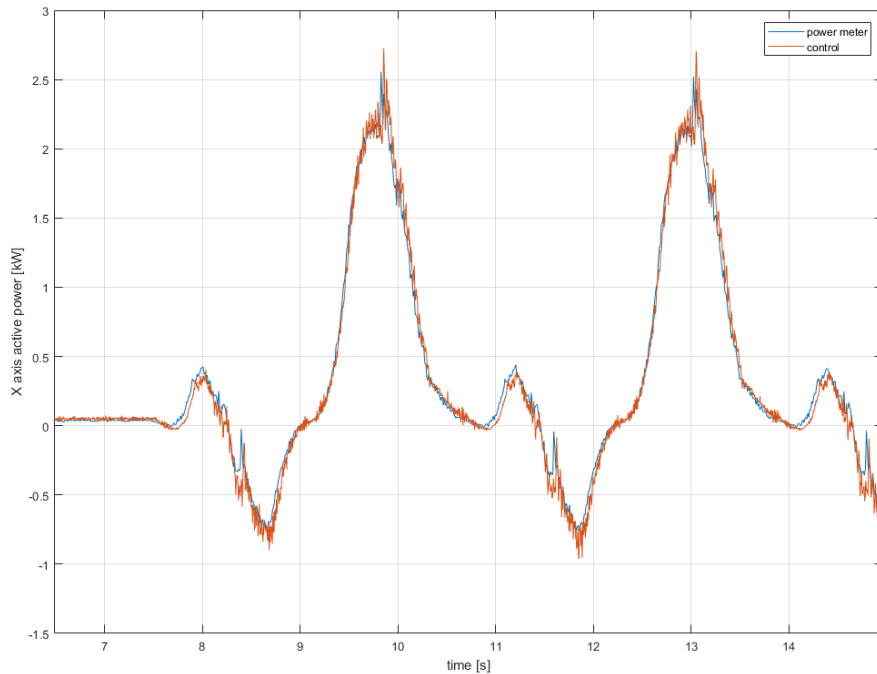


Fig. 32 Test on Jobs Thora: comparison of power measured by the drive and ITIA-CNR power meter.

As described in the previous chapter, the following tests have been performed to characterize the X, Y and Z axes:

- constant velocity, at different speeds
- continuous acceleration, at the nominal axis acceleration and jerk
- constant external force, at various force levels

For the sake of brevity, only representative results are reported and commented in the following. The full experimental results are available at ITIA-CNR.

In the tests at constant speed, one axis at the time was moved at different speeds, covering 90% of the available stroke, to minimize the effect of acceleration at axis inversion.

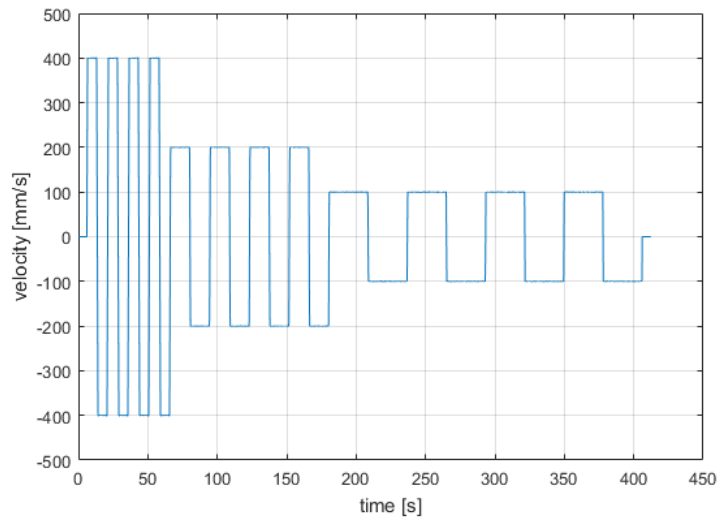


Fig. 33 Test on Jobs Thora: X axis testing at various constant speeds.

The X axis is equipped by a rack and pinion transmission, preloaded by two independent motors (herein called motors X1 and X2), each one with a gear reducer and pinion, controlled in order to get the prescribed internal preload and net moving force. The power delivered by motor X1 is depicted in the figure here below: it will be used to compute the performance indicators, described in the following. Most of the instantaneous power is transferred between the drive and the axis inertia and, for this axis with two counteracting motors, between the two drives.

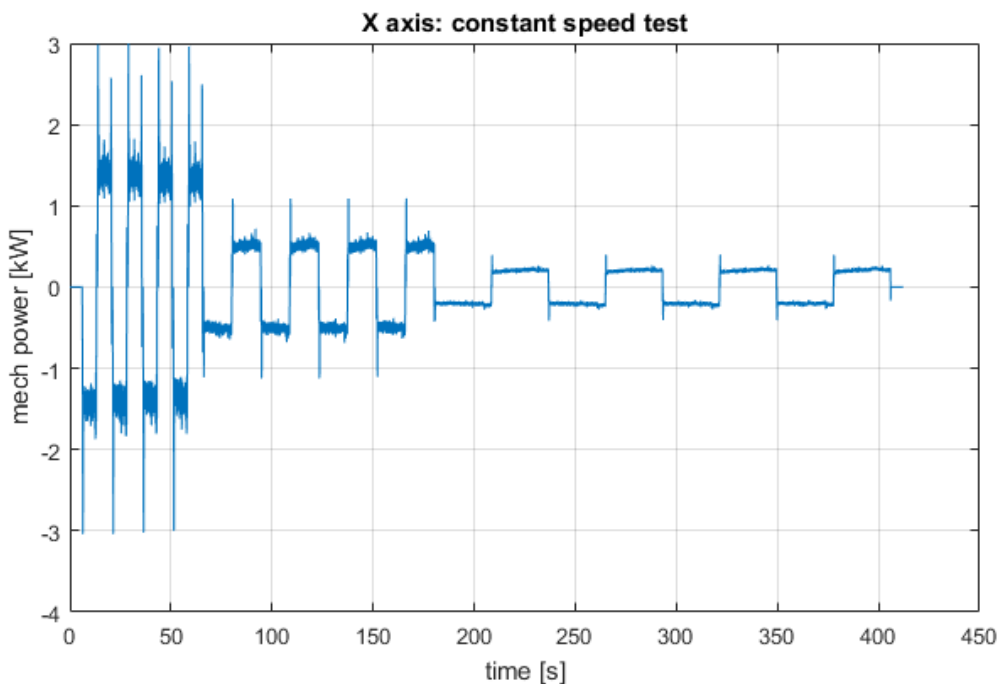


Fig. 34 Test on Jobs Thora: X axis testing at various constant speeds. Total mechanical power.

For the energy assessment, we are more interested into the energy transferred into heat (“lost”): given that a periodic motion is performed, losses can be easily computed from the average power during the test, as depicted in the next figure. The machine assessment has been designed not only to quantify

the total losses, but also to provide useful information to support machine optimization, both during design (of a future upgrade of the machine) and during normal machine use. The lost power strongly depends on the speed: the linear trend highlighted in the plot suggests that losses are mainly due to friction forces in the axis's transmission, guideways and protections. Friction forces are almost constant at low speed but increase with speeds, as it can be seen from the value measured at 385 mm/s.

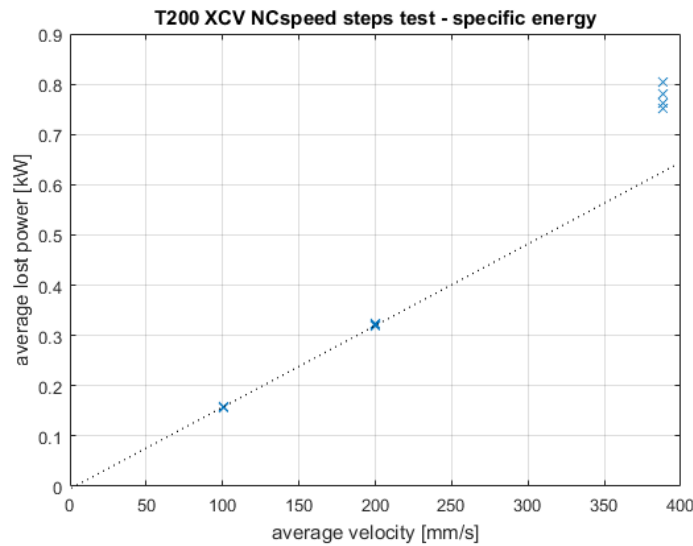


Fig. 35 Test on Jobs Thora: X axis testing at various constant speeds. Average lost power.

As discussed in the previous chapter, lost power is not a significant Key Performance Indicator (KPI): environmental impact and operational cost are indeed linked to the dissipated energy. To produce a part, the machine tool, while executing the corresponding part program, must cover a fixed distance, during machining and rapid motions. A better KPI is therefore defined as the energy spent per covered distance (as done to quantify consumption for cars...). The results, for the X, Y and Z axes, are reported in the next figure. The three machine axes move different inertias but have similar friction forces, giving therefore similar KPIs. The X axis, because of the preloading system, exhibits higher losses at low speeds (even at standing still), that became negligible at higher speeds.

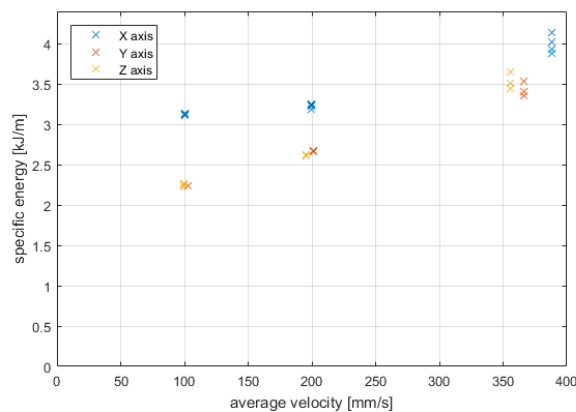


Fig. 36 Test on Jobs Thora: specific energy lost KPI for the constant speed tests.

The continuous acceleration tests are performed at the nominal acceleration and jerk. The stroke is adjusted in order to start deceleration just after the maximum speed is reached, in order to keep the axis in continuous acceleration/deceleration.

It can be expected that the different inertias moved by each axis play a more significant role but instead this effect is quite limited, for examined axes, because losses, as already discussed, occur mainly in the mechanical structure and, therefore, depends on displacement and speed. The following figure shows the energy used by the three axes.

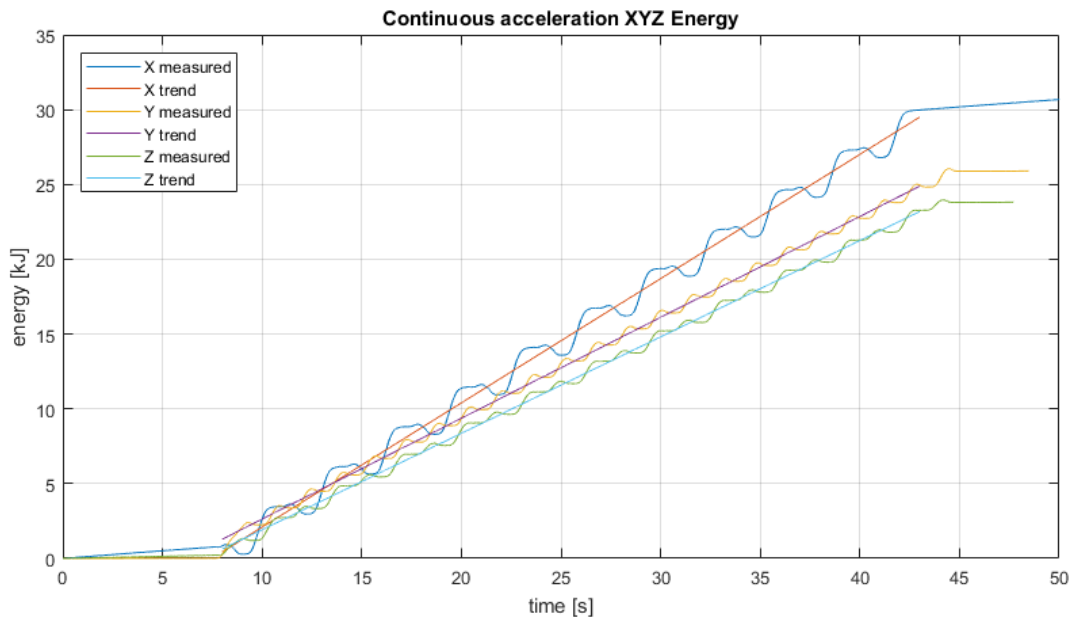


Fig. 37 Test on Jobs Thora: energy used by the three axes during continuous acceleration tests.

The corresponding specific energy, referred to the covered distances, are reported in the following table. It can be noticed that those values are quite near to the values obtained at high speed, during the constant speed tests.

continuous acceleration tests		
axis	mean power [kW]	specific energy [kJ/m]
X	0.83	4.40
Y	0.67	3.38
Z	0.64	3.17

Finally, a set of tests have been executed applying an external force on the machine head by an hydraulic piston, in the X, Y and Z directions, one direction at the time, as illustrated in the following picture (for the Z direction).

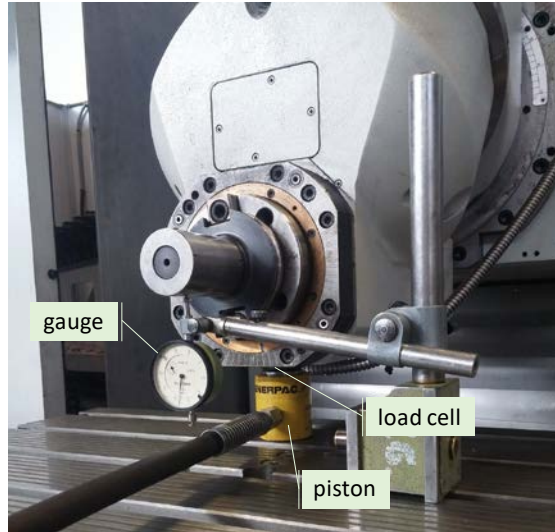


Fig. 38 Test on Jobs Thora: power used when an external force is applied along the X axis.

The applied load was increased until the nominal motor current, for each axis, was reached. The powers measured during the tests were quite limited, confirming that the rotary brushless motors are very efficient. The following figure shows the power used by X axis motors to balance the external force along X: the parabolic trend can be related to Joule losses in the motor windings. The non-null power at zero force is due to the internal preload realized by the two motors, in the X axis transmission: the following figure shows the Y axis case, where the power is almost null when the external force is zero (note: even when the external force is null, the motor could exert a torque, because of the friction in the transmission).

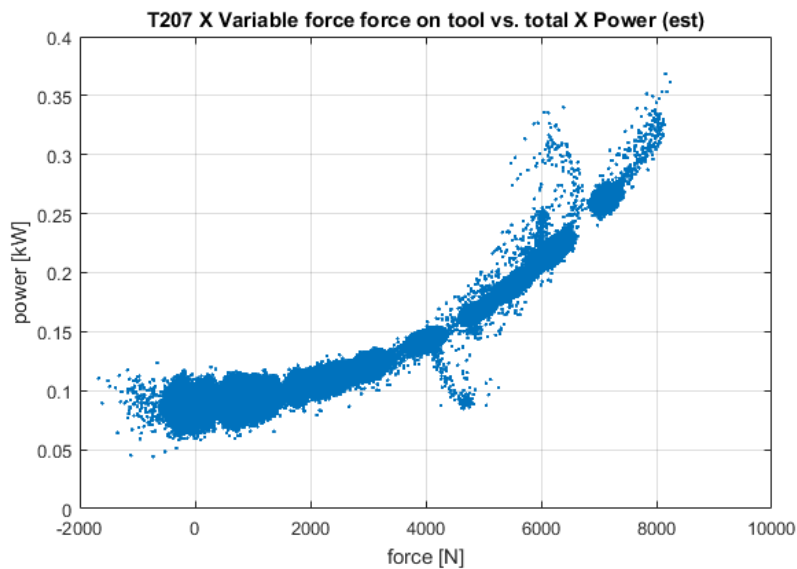


Fig. 39 Test on Jobs Thora: power used when an external force is applied along the X axis.

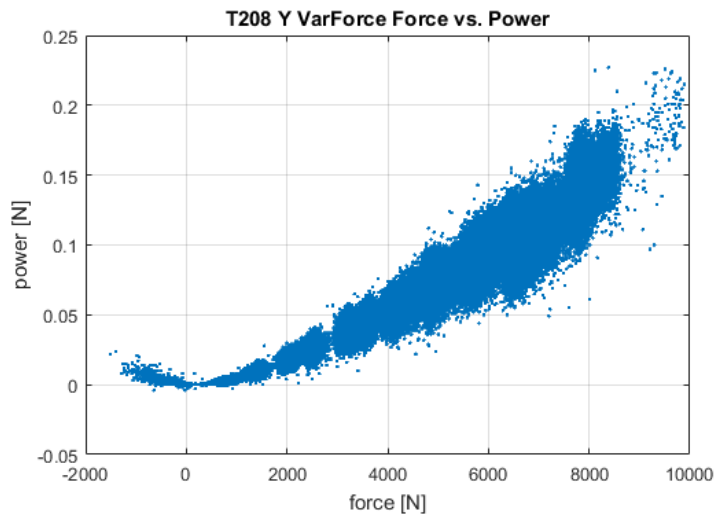


Fig. 40 Test on Jobs Thora: external constant force on the Y axis (single motor).

Spindle tests

In the first spindle test, a sequence of run up and run down at different constant speeds has been performed, as depicted in the following figure.

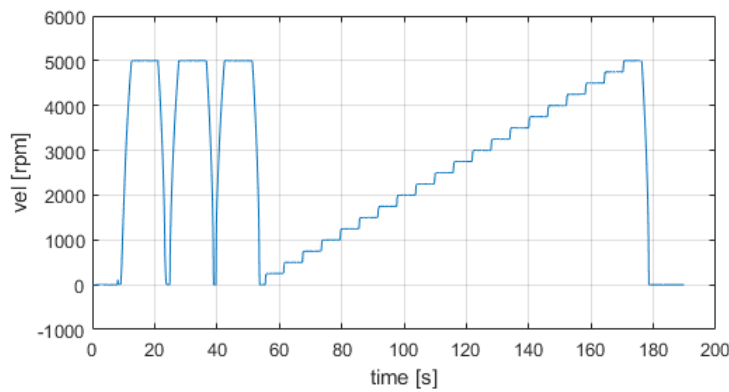


Fig. 41 Test on Jobs Thora: power used when an external force is applied along the Y axis. The used power goes to zero when the force is null.

Power measurements have been performed by the spindle drive, that records the input electrical power and the output mechanical power, plotted in the following figure.

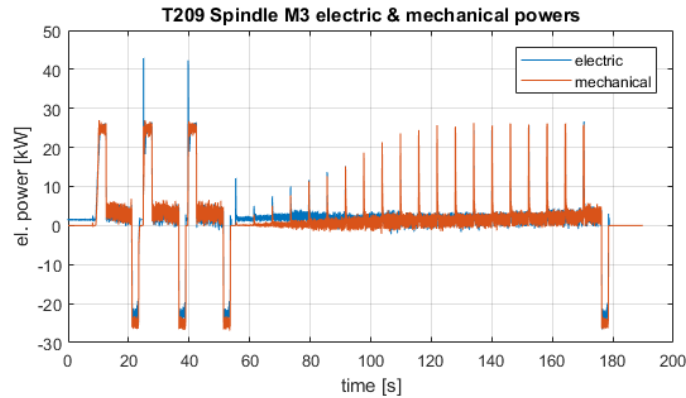


Fig. 42 Test on Jobs Thora: speed profile during the first spindle test (T209).

Differently from the axes cases, where brushless motors are applied, here an induction motor is used: in normal operation, the motor is kept in magnetized state, injecting a proper direct current. This generate a constant power consumption also when, as at the beginning of the test, the spindle is standing still, unloaded.

Spindle losses can be analysed examining the electrical energy entering the spindle and the mechanical energy delivered to the rotating axis by the spindle motor, plotted here below. The mechanical energy goes into kinetic energy during acceleration phases (“KE” arrows in the plot) and into friction dissipation (“FL” arrows in the plot), proportionally to the spindle speed. Its final value, when the spindle stops, summarizes the mechanical energy lost by friction during the test. Torque plots showed that friction variation with speed, for the examined spindle, is quite limited. The input electrical energy is mainly transformed into mechanical energy and, partially, dissipated by the motor itself. Motor losses strongly depend on the magnetizing current i_d . To avoid incurring into drive voltage saturation, the drive automatically reduces the magnetizing current at high speeds, when the defluxing threshold speed is exceeded, accepting a corresponding reduction of the maximum available torque. This explains why motor losses are lower at higher speeds.

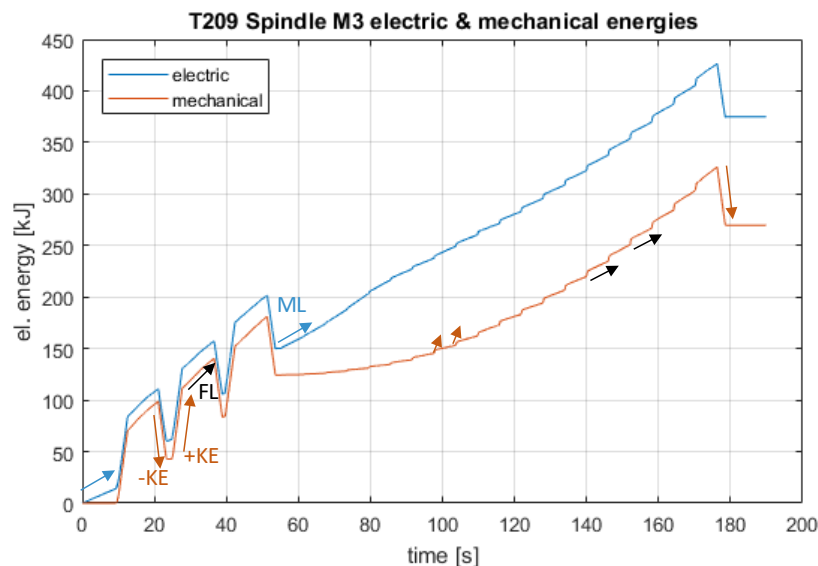


Fig. 43 Test on Jobs Thora: electric and mechanical powers during the first spindle test (T209).

In this test, with no external torque applied, a significant torque occurs only during the acceleration phases, which are quite brief. To allow a simple characterization of the motor, avoiding model fittings that are not adequate for an industrial standard like the ISO 14955, the proposed assessment procedure prescribes to perform spindle tests under continuous accelerations, e.g. requiring a sinusoidal spindle speed variation around a given mean speed value.

In the examined Thora machine the spindle has a gear transmission. Given that, in this kind of transmission, a minimal backlash is always present, it has been decided to suppress spindle tests with continuous speed variation, because the frequent torque inversions could damage the gear coupling. This choice is further discussed in the conclusions.

Conclusions

The performed tests have allowed an evaluation of the industrial feasibility of the proposed assessment methodology.

The execution of the axes tests was simple, requiring a very limited instrumentation, especially if the machine tool is equipped with a drive able to deliver an adequate measurement of the input electric power (as it is the case in all modern drives).

No practical problems occurred also during the test with an external force applied on the head: the instrumentation required is often available in the shop floor, because it is used to assess the static stiffness of the machine. Indeed, the described energy tests and the static stiffness tests could be combined to minimize setup time. This test delivered interesting results, that quantify the “energy cost” of generating significant thrust forces, at low speeds. It has to be noted that, as usually happens with axes equipped with rotary motors, their overall energy consumption is quite limited, compared to other machine tool functions: it is planned to repeat the test on a machine equipped by linear motors, where the corresponding energy cost is expected to be significantly higher.

The proposed KPIs are easy to compute and give a useful indication on the energy cost for the basic axes functionalities: moving, accelerating and “pushing”. Losses are distinguished in motor and mechanical losses, due to friction.

For the spindle, only the test at constant speed have been executed. This test provides a clear indication of motor and friction losses at the various speeds.

In order to avoid damaging spindles equipped with mechanical transmissions, it has been decided to avoid tests with continuous acceleration, planned to characterize the spindle when stressed by a significant (inertial) torque. This decision is an important limitation for the proposed approach: even if direct drive spindles (or “electro-spindles”) are quite common, spindles with a mechanical transmission are anyhow relevant. While this topic will be further discussed with spindle manufacturers, it has been decided, for the project, to characterize those units using specific test benches where a brake is used to load the motor, as demonstrated by Politecnico di Milano in WP1.4.

It must be anyhow noted that, for an accurate and fast machine tool energetic assessment, a modular approach is desirable: the most significant sub systems, like chillers, hydraulic power units, must be characterized by the respective suppliers. The spindle would follow the same approach: in this scenario, a test performed on a dedicated test bench, at the spindle manufacturer premises, is easily acceptable.

The next step, for the evaluation of the proposed assessment methodology, is to repeat the test on different machine tools, in order to assess its ability to “catch” their different energy profiles.

Benefits for the users

The developed methodology represents a contribution, by the Italian delegation, to the works of ISO 14955 Working Group. The goal is to define a “machine-based” approach to evaluate the average energy efficiency of a metal cutting machine tool. The impact of such a methodology would be quite broad, being applied at world level, in supporting, on one side, machine tool manufacturers in optimizing their machines and, on the other side, the users in selecting more efficient machines, for the planned production mission.

The proposed approach is to be integrated with the method presented in WP1.4, to qualify spindles for machine tools.

FORMAL DATA MODEL FOR SUSTAINABLE MANUFACTURING

1. Introduction

Although there is no universally accepted definition for the term “sustainable manufacturing”, numerous efforts have been made in the recent past, with much more concurrent efforts underway. The U.S. Department of commerce defines sustainable manufacturing as: “The creation of manufactured products that use processes that minimize negative environmental impacts, conserve energy and natural resources, are safe for employees, communities, and consumers and are economically sound.” Furthermore, according to the National Council for Advanced Manufacturing (NACFAM, 2009), sustainable manufacturing includes the manufacturing of sustainable products and the sustainable manufacturing of all products. The former includes manufacturing of renewable energy, energy efficiency, green building, while the latter emphasizes the sustainable manufacturing of all products taking into account the full – sustainability/total life–cycle issues related to the manufactured products. Sustainable manufacturing systems design and management means taking into account both economic and ecological constraints. The environmental and climate impacts of energy use are rapidly becoming a major issue. Carbon dioxide (CO₂), a major greenhouse gas, is emitted into the atmosphere directly when fuels are combusted on – site and indirectly when electricity is consumed (particularly when fossil fuels are used to generate electricity). The rising cost of energy is also a factor that must be understood during the factory design throughout the factory lifecycle. More energy–efficient solutions can create huge savings during the lifetime of equipment.

The concept of sustainable and energy-efficient factory entails the analysis of several areas, such as building, product, process and production resource. Each of these aspects is complex by itself and even more challenging when sustainability is considered because of the interrelations between these areas. Product characteristics like material, geometry, accuracy and series volume significantly affect the manufacturing technologies and therewith the energy needs in production. A concurrent development of product and production process is generally desirable. At the process level, there is a need of optimized technological and process planning improvements for reducing energy and resource consumptions, toxic wastes occupational hazards, etc. Based on product specifications, the necessary processes have to be defined and alternative solutions can be assessed in terms of energy and resource consumptions.

At the machine tool level, a lot of research has been carried out for the reduction of machine tool energy consumption throughout the machine tool life cycle: manufacturing, transportation, use and end-of–life. Recent research also includes power consumption analysis of machine tool use.

However, the energetic analysis of machining processes and machine tools cannot be treated independently from the behavior of production systems. Indeed, the analysis of single manufacturing processes and machine tools is fundamental to optimize the energy-related performance of factories and production systems during both the design and management phases. For instance, the design of a production system and the selection of machine tools can benefit from information related to the energy states; machining operations can be assigned to different machine tools based on their estimated energy consumption; manufacturing execution can be dynamically optimized while considering the trade-off between machining operation time and energy consumption; management policies can be updated based on the actual energy consumptions derived from monitoring data. Therefore, there is the need of a common framework to deal with the key areas related to energy consumption in the manufacturing industry. The integration of process, machine and system data will lead to a deeper understanding of the factory behavior and will foster the interoperability among the ever increasing number of software tools and platforms employed in industry to support various business processes. Herein, a **formal data model** is proposed to support the interoperability across the technological platforms of a wide range of factories and manufacturing systems.

2. State of the art

The existing literature and technical standards have been evaluated, selected and extended. A knowledge-based platform based on the Semantic Web technologies was adopted and further developed to enable the exploitation of the data model to structure information adequately to the requirements of representing and enhancing the energy efficiency of machine tools. The resulting data model provides (1) explicit semantic characterization of the manufacturing system and its components, (2) enablers for ontology driven collection of data that characterize the system, (3) the integrated modeling of heterogeneous information about machines and processes within the system, and (4) semantically coherent information flow across the diverse representational domains of the system regarding its design, reconfiguration, monitoring, evaluation and management.

The interoperability between the software tools supporting the activities involved in the design and management of energy efficient machine tools and processes is enabled by the adoption of a common data model. Such data model is formalized as an OWL ontology T-box (W3C, 2004a) to exploit Semantic Web potentiality in terms of formal semantic characterization, flexibility, extendibility and support for re-use and integration of different knowledge sources. Indeed, ontologies (Guarino, et al., 2009) have been developed and investigated in the field of information modeling, artificial intelligence and natural language processing to facilitate knowledge representation, sharing and reuse as well as automated reasoning (Kulvatunyou et al., 2005).

Differently from diagrammatic data modelling languages, like the Unified Modeling Language (UML), or Entity-Relationship (ER), formalized ontologies provide logic-based methodologies and technologies for the integration of different data models into a unique system while preserving the semantic content of each (Hepp et al., 2007; Moser et al., 2011). In addition, ontologies formalized in first order logic (FOL), or more tractable languages like Description Logic (DL), or Web Ontology Language (OWL) ensure data consistency on a semantic level and automated reasoning can be performed. Ontologies are also well suited to model relationships between different modelling elements, as well as axiomatic constraints between them, which can then be used to derive assertions based on available data (e.g. data coming from the shop floor).

The importance of having a comprehensive data model for the manufacturing domain has already been addressed in the literature concerning standard data models and reference frameworks for knowledge representation based on ontologies (Gunendran et al., 2007; Terkaj, Urigo, 2012).

The next sub-sections will address the following steps regarding the development of the data model:

1. Available modelling languages are considered and the Web Ontology Language (OWL) is adopted to formalize relevant information.
2. Analysis relevant technical standards and information models that can be employed to formalize the target domain.
3. Analysis of relevant data models and ontologies.

A standard-based data model requires several adjustments of the selected reference standards to the specific modelling task resulting in the requirements for (a) *standards conversion* and (b) *model extension*.

- a) *Standard conversion*. Capturing knowledge of manufacturing systems on various levels of granularity requires additional extrapolation of the relevant information by means of *conversion* of certain standards. The epistemic content of standards is expressed by means of concepts, classes, and relations that are represented in a natural and/or artificial language often different from the selected modelling language (see e.g. Borgo et al., 2014, 2015). Accordingly, the content presented within the reference standards needs to be converted and/or translated into the selected modelling language (i.e. OWL).
- b) *Model extension*. Regarding the modelling goal, the data model also asks for an extension of the selected reference standards and models with the additional information acquired from the domain experts.

2.1 Web Ontology Language

The proposed data model supports the interoperability and data integration based on the computational ontologies and Semantic Web technologies. The main reason for adopting an ontology based framework to model data originates from the need to provide models fulfilling the role of integration enablers. Knowledge captured with an ontology model can be easily re-used and shared across diverse computational system, processed, and analysed by both machines and humans (Guarino, et al., 2009). Ontology development requires the specification of a formal language that will, at the application level, be serialised in a particular syntax. The proposed model is formalised in OWL 2 (W3C, 2004b). More specifically, the model is formalised in RDF/XML exchange syntax, according to the recommendations of the World Wide Web Consortium (W3C, 2012). The following sections present the main features of OWL and relevant editing tools that are compatible with OWL.

Web Ontology Language (OWL) is a Semantic Web modelling language explicitly designed to support the development of Semantic Web-based ontologies (W3C, 2009b). Knowledge represented in OWL makes information content explicit in a declarative form, which is understandable to both humans and machines. Explicitly represented knowledge can be also processed automatically. In particular, OWL is based on a decidable fragment of description logic, namely SROIQ (Horrocks et al., 2006), that enables automatic reasoning over the represented classes, relationships, and instances. The reasoning with OWL can be performed by computational reasoners (Sirin et al., 2007; Shearer et al., 2008; Tsarkov, Horrocks, 2006), which support verification of the knowledge consistency and explication of implicitly represented information. Thus, OWL can be used to support new inference, knowledge enrichment and discovery.

Figure 34 depicts the basic structure of OWL. In particular its latest version OWL 2, in the relation to the set of recommended semantic and syntax specifications that is documented in (W3C, 2012b).

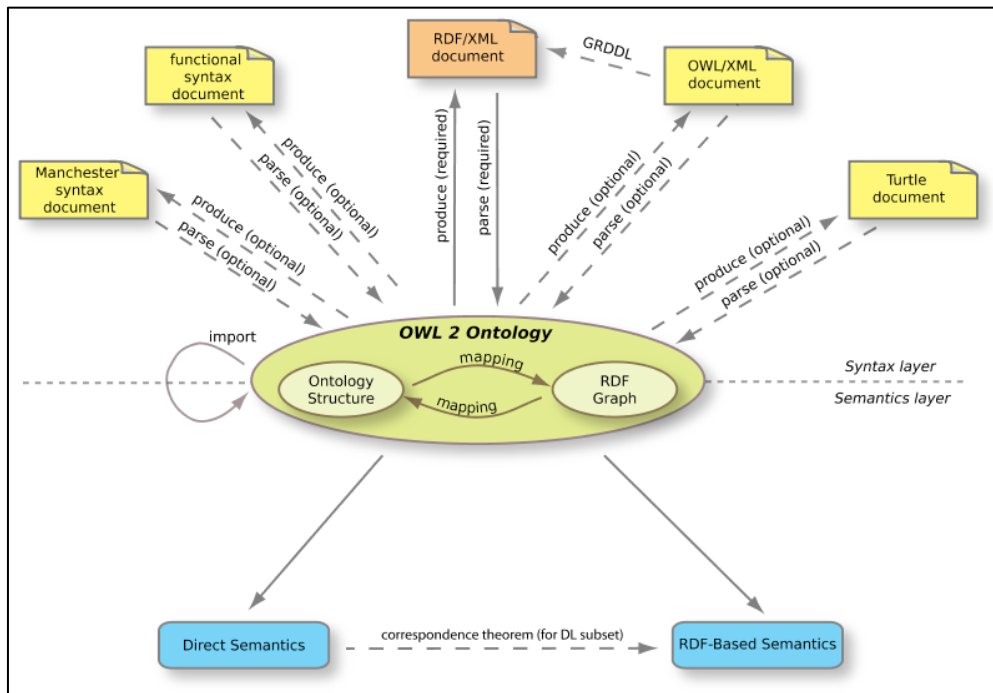


Figure 34: An outline of OWL2 semantic and syntax specifications (W3C 2012b)

The ontology files (Figure 34) can be published in the World Wide Web (WWW) and may contain references to other ontologies and reference terminologies. This is a useful feature for knowledge integration and re-use across various representational domains.

OWL has been adopted to define explicitly the classes, properties and restrictions that are relevant to describe machine tools and processes from an energy efficiency perspective.

2.2 Reference Standards

The standardization efforts relevant for the information management within the manufacturing domain have resulted in several international standards that are taken into account as the most relevant for the project activities.

The Automation systems and integration - Product data representation and exchange (ISO 10303) standard, informally known as STEP - Standard for the Exchange of Product Model Data (ISO,1994), supports the exchange of information by creating a common framework to support the representation and exchange of manufacturing product data.

The Process Specification Language (PSL) (ISO 18629, 2004) standard provides a generic ontological representation of process knowledge and supports the exchange of information and knowledge about processes. In particular, PSL is recognized as a standard based on robust logical theory that can support integration of multiple process-related applications throughout the manufacturing life cycle.

The standard ISO 14955-2 is particularly relevant for the environmental evaluation of machine tools (see Section X).

The ISO 14649 "Data model for computerized Numerical Controllers" (ISO 14649-10, 2004) machining model and the STEP standard ISO 10303 concerning product geometry, geometric dimensioning,

tolerancing and product data management information have been combined to form STEP-NC. The result is the enhanced STEP “Standard for the Exchange of Product model data” standard ISO 10303-238. It specifies the STEP-NC standardized application protocol 238 published by the International Organization for Standardization in 2007. The object and feature-oriented STEP-NC standard is designed to describe the machining operations executed on a work-piece. Thus, STEP-NC machining model includes geometric dimension and tolerance data for inspection. The product description of the machined part is connected to the computer numerical controlled machining operation data using the object-oriented concept of working steps. These working steps correspond to associated process parameters as well as high-level machining features.

The Industry Foundation Classes (IFC) (BuildingSmart, 2013) is a standard providing an open vendor-independent file format and data model for data interoperability and exchange for Architecture, Engineering, Construction and Facility Management (AEC/FM). It is released by buildingSMART International (formerly the International Alliance for Interoperability, IAI) and the current release IFC 4 is registered as ISO 16739. IFC supports interoperability across different applications used to design, construct and operate construction facilities by capturing information about all aspects of a building throughout its lifecycle. The development of IFC was motivated at its early stages by the slow and unresponsive evolution of standards for product lifecycle modeling, like STEP, to match the modelling needs of the AEC/FM industry (Laakso, Kiviniemi, 2012). Although part of the team that developed STEP participated in the definition of the IFC data model (Laakso, Kiviniemi, 2012), as of today there is no precise analysis on the relationship between the two standards.

STEP, STEP-NC and IFC are all formalized in EXPRESS modelling language. Therefore, based on the work by Pauwels and Terkaj (2016) and Pauwels et al. (2017) these standards can be automatically converted into OWL ontologies, thus facilitating their integration with other ontologies, as discussed in the following sections.

2.3 Reference Data Models and Ontologies

Various ontologies have been developed to support industrial and manufacturing applications. Lin et al. (2004) designed a Manufacturing System Engineering (MSE) ontology to provide a common understanding of manufacturing-related terms and to enhance the semantic and reuse of knowledge resources within globally extended manufacturing teams. The MSE ontology is based on seven key classes that the authors determined based on Manufacturing System (MS) information models. Lemaignan et al. (2006) presented a Manufacturing's Semantics Ontology (MASON) that is built upon three main concepts: entities, operations and resources. Similarly, Martin and D'Acunto (2003) developed an ontology decomposed into product, process and resource areas. ADACOR (A Collaborative Production Automation and Control Architecture) could be classified as general-purpose manufacturing ontology (Leitão, Restivo, 2006). More recently, Badra et al. (2011) proposed a Semantic Web compliant representation of the objects, concepts and services related to Renault Product Range Specification (PRS) that is used to specify the set of all possible car configurations. Baqar-Raza and Harrison (2011) developed an ontology aimed at the formalization of product data throughout its lifecycle, in particular for the automotive sector. The research focused on the integration of product, process and resource information from multiple sources and making the information available via web services. Moser et al. (Moser et al., 2011) presented a tool to support real time decision making, by providing an integrated view on relevant engineering knowledge in typical design time and runtime models, which were not originally designed for machine-understandable integration.

Terkaj et al. (2012) proposed a semantic data model named Virtual Factory Data Model (VFDM) to formalize and integrate concepts of building, product, process and production resource handled by the

digital tools supporting the factory life-cycle phases. The development of the VFDM aimed at exploiting as much as possible the already existing technical standards for manufacturing, thus trying to favour the interoperability between software tools. Therefore, the work focused on the integration (managing redundancies and inconsistencies) of various knowledge domains represented by different technical standards. This approach requires both the translation of the existing standards into a common language and the development of the required extensions to represent needed concepts that were not included within the reference standard..

The modeling of knowledge related to energy management in industrial systems has been addressed by the modular ontology Smart Energy Aware Systems (SEAS) (Lefrancois 2017). This includes ontology modules related to automation and control, such as modules *DeviceOntology*, *OptimizationOntolog*, and *FailableSystemOntology*.

Several works focused on the energy management of facilities (Kaiser, 2015), such as airports (Tomasevic, 2015). An approach for domotics intelligent devices (DogOnt) was proposed by Bonino et al. (2008). The integration of buildings with grid and energy market information is tackled in the ThinkHome ontology (Reinisch et al., 2011).

Among the various ontologies related to automation&control and smart appliances, the Smart Appliances REference (SAREF) ontology (Daniele et al., 2015) unifies common accepted conceptualisations into one reference ontology.

A well established ontology for the formal specification of sensor data is the W3C Semantic Sensor Network (SSN) ontology (Compton et al., 2012). The SSN ontology has been recently updated (Haller et al., 2017) by including also the more general module SOSA (Sensor, Observation, Sample, and Actuator) making it possible to model key concepts also for the automation and control systems domain, including sensor, actuator, observations, observable properties and results.

Within the reported approaches it may be observed that typically taxonomies are used to describe the actual control behaviour of a certain control logic in a automation and control systems. A modelling effort to specify UML state machines, a well-known modeling approach for state-based control logic, as an OWL ontology was presented by Dolog (2004).

3. Data Model

The data model is a key element to support interoperability between different digital tools, providing the capability to retrieve, store and share information. Therefore, a suitable data model must be able to cover and integrate heterogeneous knowledge domains, while guaranteeing extensibility. Semantic Web technologies and in particular ontologies can be employed to meet these requirements (Blackburn and Denno, 2015; Ekaputra et al., 2017). Herein, a modular ontology-based Factory Data Model is proposed to formalize the information that is in particular relevant to the design and management of modular reconfigurable pallets. As anticipated, the OWL 2 ontology language is adopted. The earlier works by Pellegrinelli et al. (2016) and Terkaj et al. (2017) have been taken as the basis of the proposed Factory Data Model that aims at representing machine tools and machining operations from an energy consumption perspective.

The ontology reuse, even if often applied in a limited fashion, represents a key best practice that was followed in this work. Indeed, already existing ontologies have been reused, integrated, and extended.

The key requirements of the data model can be summarized as follows:

- Integration of concepts related to building, product, process and production resources

- Modeling of object states and control logics.
- Modeling of sensors and actuators.
- Modeling of performance and evolution of the factory objects along time.
- Modeling of energy behavior of machine tools
- Modeling of machining operations and their relations with production resources, including operation time and energy consumption.

The proposed modular data model architecture is shown in **Figure 35** and consists of the following ontology modules:

- *list*, an ontology defining the set of entities used to describe the OWL list pattern (Pauwels and Terkaj, 2016).
- *express*, ontology mapping the concepts of EXPRESS language (International Organization for Standardization, 2004) to OWL (Pauwels and Terkaj, 2016).
- *IFC4_ADD1*, the ifcOWL ontology that is converted from the IFC standard defined in EXPRESS language (Pauwels et al., 2017).
- *IFC4_ADD1_rules*, an enhancement of the ifcOWL ontology with axioms derived from WHERE rules in the original IFC EXPRESS schema (Terkaj and Sojic, 2015).
- *fsm*, an ontology defining the concepts required for modelling finite state machines (Dolog, 2004).
- *sosa*, the Sensor, Observation, Sample, and Actuator (SOSA) Core Ontology (Haller et al., 2017).
- *ssn*, the Semantic Sensor Network Ontology (Haller et al., 2017).
- *statistics*, an ontology that defines probability distributions and descriptive statistics concepts (Terkaj et al., 2017).
- *expression*, an ontology modelling algebraic and logical expressions (Terkaj et al., 2017).
- *osph*, an ontology modelling Object States and Performance History, while integrating the ontology modules *fsm*, *statistics*, *ssn*, *sosa*, *expression* (Terkaj et al., 2017)
- *IFC4_ADD1_extension*, an ontology module integrating *osph* and *IFC_ADD1_rules* modules, while adding general purpose extensions to *IFC_ADD1*.
- *ISO14649-10*, based on the STEP-NC standard (International Organization for Standardization, 2003) converted from EXPRESS schema into OWL ontology according to the pattern defined in (Pauwels et al., 2017).
- *factory*, a specialization of *IFC_ADD1* with definitions related to production processes, part types, manufacturing systems and machine tools.
- *FO1.3*: a fragment of the *FixOnt* ontology presented in Gemeir and Shea (2013).
- *dmanufacturing*, ontology module integrating four modules (*ISO14649-10*, *factory*, *inspection*, *FO1.3*), while adding specializations for the discrete manufacturing domain.

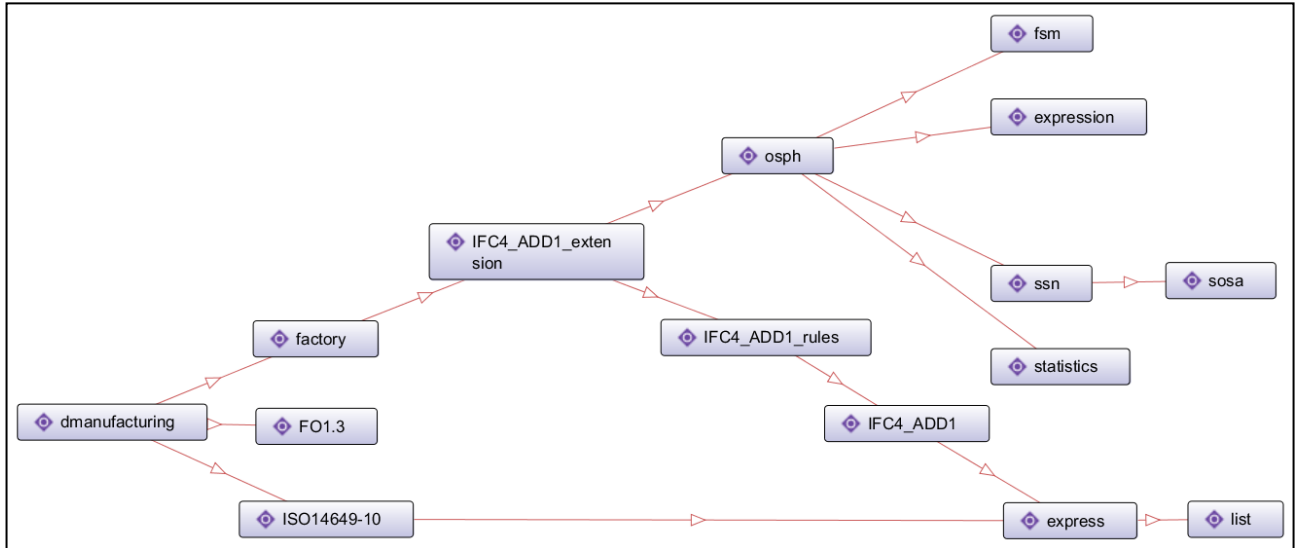


Figure 35: Ontology modules of the Factory Data Model linked by import relations as shown by Protégé software tool (Musen, 2015)

The prefixes reported in Table 17 have been defined with reference to vocabularies and ontology modules.

Prefix	Value
xsd	http://www.w3.org/2001/XMLSchema#
rdf	http://www.w3.org/1999/02/22-rdf-syntax-ns#
rdfs	http://www.w3.org/2000/01/rdf-schema#
owl	http://www.w3.org/2002/07/owl#
expr	https://w3id.org/express#
list	https://w3id.org/list#
fsm	http://www.learninglab.de/~dolog/fsm/fsm.owl#
stat	http://www.ontoeng.com/statistics#
ex	http://www.ontoeng.com/expression#
sosa	http://www.w3.org/ns/sosa/
ssn	http://www.w3.org/ns/ssn/
osph	http://www.ontoeng.com/osph#
ifc	http://ifcowl.openbimstandards.org/IFC4_ADD1#
ifcext	http://www.ontoeng.com/IFC4_ADD1_extension#
factory	http://www.ontoeng.com/factory#
dm	http://www.ontoeng.com/dmanufacturing#

Table 17: Prefixes

The Factory Data Model can be instantiated to generate libraries of objects such as machine tools, part types, operations, and fixtures, that can be later exploited to define specific factories and system configurations.

The following sub-sections present the content of the ontology modules. The ontology modules deriving from background research are only briefly introduced for sake of completeness: **list**, **express**, **IFC4_ADD1** (Pauwels and Terkaj, 2016), **IFC4_ADD1_rules** (Terkaj and Sojic, 2015), **fsm** (Dolog, 2004), **sosa** and **ssn** (Haller et al., 2017), **ISO14649-10**, **FO1.3** and **dmanufacturing** (Pellegrinelli et al., 2016).

More attention is dedicated to the ontology modules that were newly developed or significantly extended in the scope of this project:

- **statistics**, **expressions** and **osph** presented in Terkaj et al. (2017) with acknowledgment to the project. These modules enable the characterization of static and dynamic properties of generic objects in industrial systems.
- **IFC4_ADD1_extension** enables the integration of the IFC standard with the newly developed **osph** module
- **factory** where energy-related characterizations of machining processes and machine tools have been added by extending previous works addressing the modeling of the factory environment.

3.1 Expression module

The **expression** ontology (Terkaj et al., 2017) aims at formalizing algebraic and logical expressions. A generic expression can be decomposed into atomic, unary, and binary expressions. An atomic expression can be a constant or a variable. This ontology was developed to provide a simple formal definition of expressions that can be used also as conditions to be met before a transition is triggered. The classes and properties of the expression ontology are sketched in **Figure 36**.

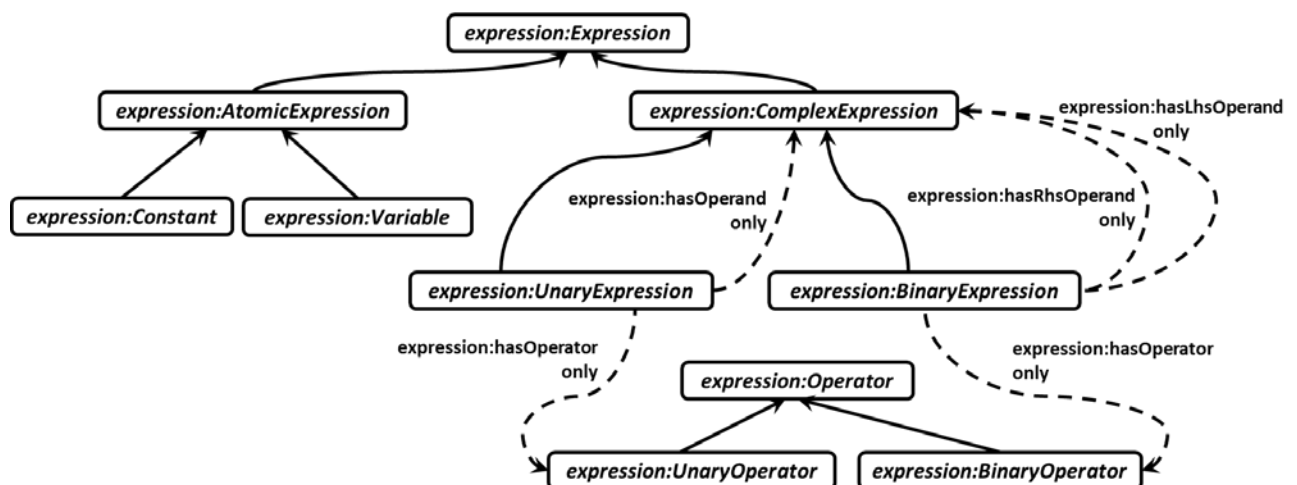


Figure 36: Classes and relations in the expression ontology. Dashed lines represent OWL restrictions, whereas solid lines represent subsumption relations.

3.2 FSM module

The **FSM** ontology (Dolog, 2004) formalizes the UML statechart (defined in OMG Unified Modeling Language, Superstructure, Version 2.2) as an ontology. Figure 37 shows the main classes.

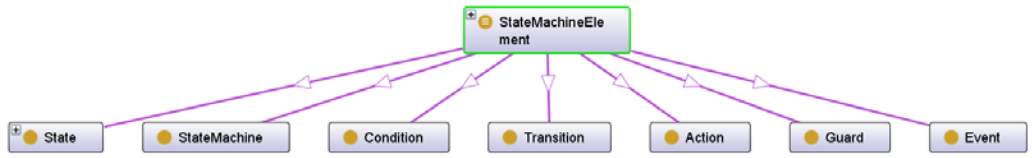


Figure 37: FSM module main classes

3.3 Statistics modules

The **Statistics** ontology (Terkaj et al., 2017) is a lightweight ontology without commitments to upper ontologies. This ontology represents descriptive statistics and basic probability distributions via semantic characterization of key parameters. Figure 38 shows the main classes.

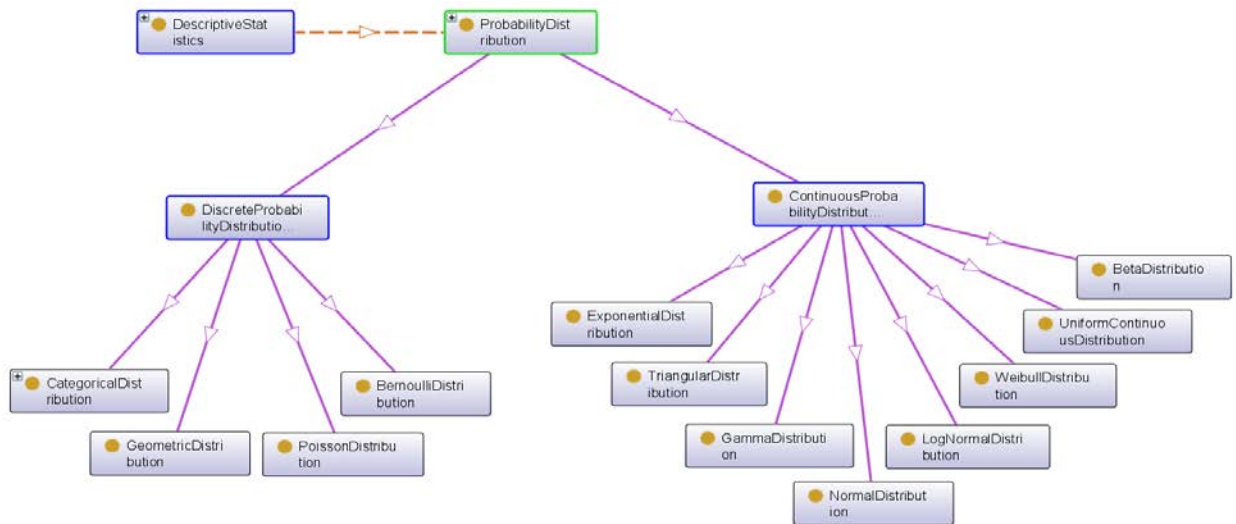


Figure 38: Statistics module main classes

3.4 SOSA and SSN modules

The **SOSA** and **SSN** are taken as published in the W3C standard (Haller et al., 2017). Figure 39 shows the main classes and relations.

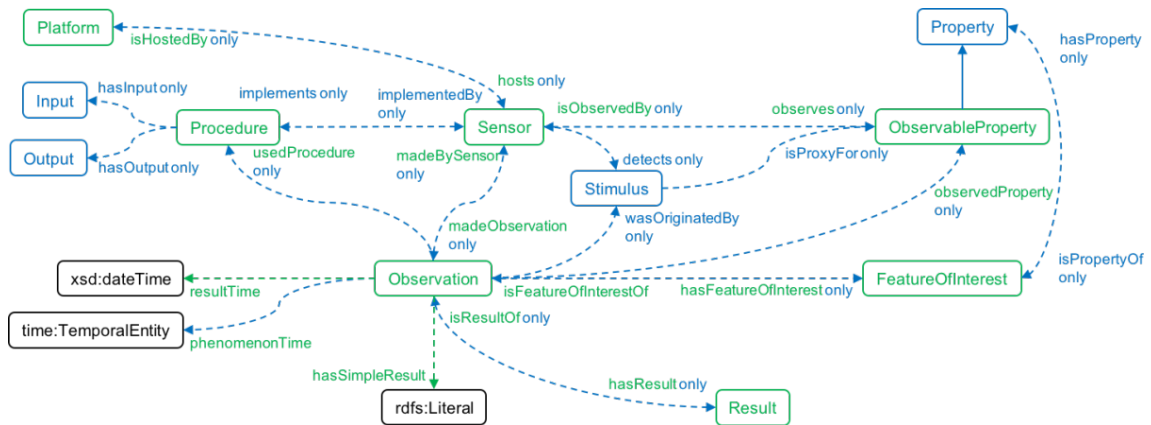


Figure 39: SOSA and SSN modules main classes and relations

3.5 OSPH module

The **osph** ontology (Terkaj et al., 2017) is the evolution and generalization of an early proposal that was based on the ifcOWL ontology (Terkaj and Uργο, 2014). This ontology plays a key role because it models Object States and Performance History (OSPH). The following classes are defined in the osph ontology:

- *osph:ObjectDefinition* is an abstract class whose definition resembles that of IfcObjectDefinition in the IFC standard.
- *osph:ObjectHistory* defines a history interval in the lifecycle of a generic object that is assigned via the object property *osph:isHistoryOf*. An interval can be decomposed into other intervals via the property *osph:isDecomposedByHistory*. A history interval can be characterized by a start and end time as *xsd:dateTime* via the properties *osph:hasIntervalStartTime* and *osph:hasIntervalEndTime*, respectively. A history interval can be related to individuals of *osph:StateFrequency* via the property *osph:hasStateFrequency*.
- *osph:StateFrequency* describes the stay of an object in a specific state during a history interval.
- *osph:UnitOfMeasurement* is a class defining a generic unit of measurement.
- *osph:StaticProperty* is a subclass of *ssn:Property* and defines the static property of a generic object. The value of the property can be set with the object property *osph:hasPropertyValue* or with the datatype property *osph:hasPropertySimpleValue*

The relations between these classes are shown in Figure 40.

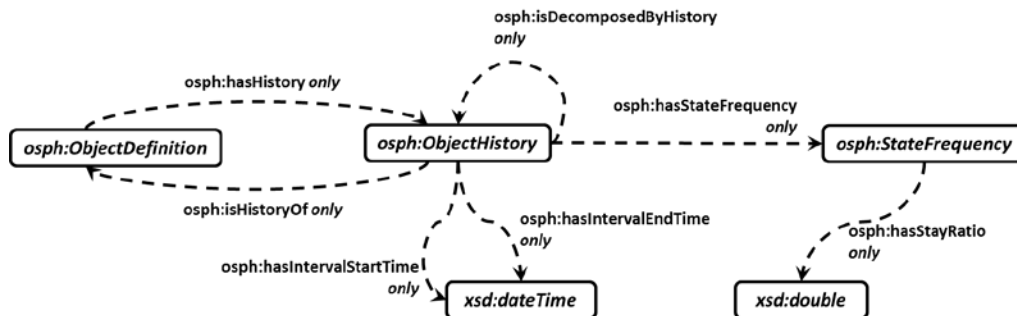


Figure 40: Classes and relations in the osph ontology, where dashed lines represent OWL restrictions

Moreover, the OSPH module integrates the fsm, statistics, ssn, and expression modules. Indeed, the module osph mainly play the role of ontology mediator creating links between different domains, as it can be noticed in the diagram of Figure 41. Some of the key alignments between the various ontology modules are reported in Table 18 by specifying which are the aligned modules, which are the involved classes and properties, and finally providing a description. A generic object (*osph:ObjectDefinition*) can be characterized by a state machine (*fsm:StateMachine*) and also by one or more histories (*osph:ObjectHistory*) that are able to capture the evolution of the object in terms of observations and state. An expression (*expression:Expression*) can be composed by constant values (*ifcmr:IfcValue*) and variables (*expression:Variable*) that are related to measurable properties (*ssn:Property*). The result of an observation (*sosa:Observation*) can be a descriptive statistics (*statistics:DescriptiveStatistics*) or a quantity value (*ifcmr:IfcValue*). The relevant alignments are also graphically represented in Figure 41.

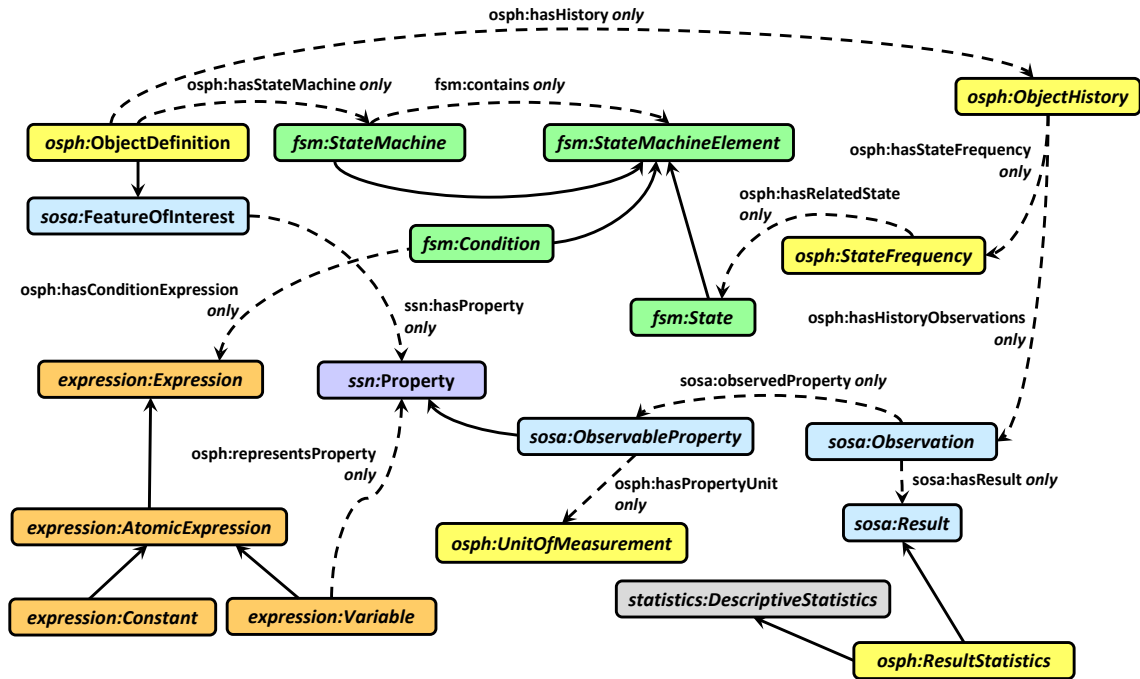


Figure 41: Excerpt of classes and relations in the OSPH Ontology showing the key alignments. Dashed lines represent OWL restrictions, whereas solid lines represent subsumption relations.

Aligned modules	Involved classes	Description
sosa, osph	osph:ObjectDefinition, sosa:FeatureOfInterest	osph:ObjectDefinition is defined as a subClassOf sosa:FeatureOfInterest.
fsm, osph	osph:ObjectDefinition, fsm:StateMachine	An individual of osph:ObjectDefinition can be with an individual of fsm:StateMachine via the property osph:hasStateMachine, and with individuals of osph:ObjectHistory via property osph:hasHistory.
fsm, osph	osph:StateFrequency, fsm:State	An individual of osph:StateFrequency is related with an individual of fsm:State via the property osph:hasRelatedState.
sosa, osph	osph:ObjectHistory, sosa:Observation	A history interval can be related to individuals of sosa:Observation via the property osph:hasHistoryObservations.
statistics, sosa	statistics:DescriptiveStatistics, sosa:Result	statistics:DescriptiveStatistics is a subClassOf sosa:Result, thus the result of an observation can be defined in terms of a descriptive statistics.
expression, fsm	fsm:Condition, ex:Expression	An individual of class fsm:Condition can be related to an individual of ex:Expression via the object property osph:hasConditionExpression.
expression, ssn	ex:AtomicExpression, ssn:Property	ssn:Property is a subClassOf ex:AtomicExpression, thus it can be used to define expressions (e.g. a sosa:ObservableProperty can be used to define an expression employed by an fsm:Condition)

Table 18: Alignments between the modules in the OSPH ontology

3.6 IFC4_ADD1 module

The IFC4_ADD1 module is automatically generated from the IFC standard thanks to the converter by Pauwels et al. (2017). Figure 42 shows the top level hierarchy classes.

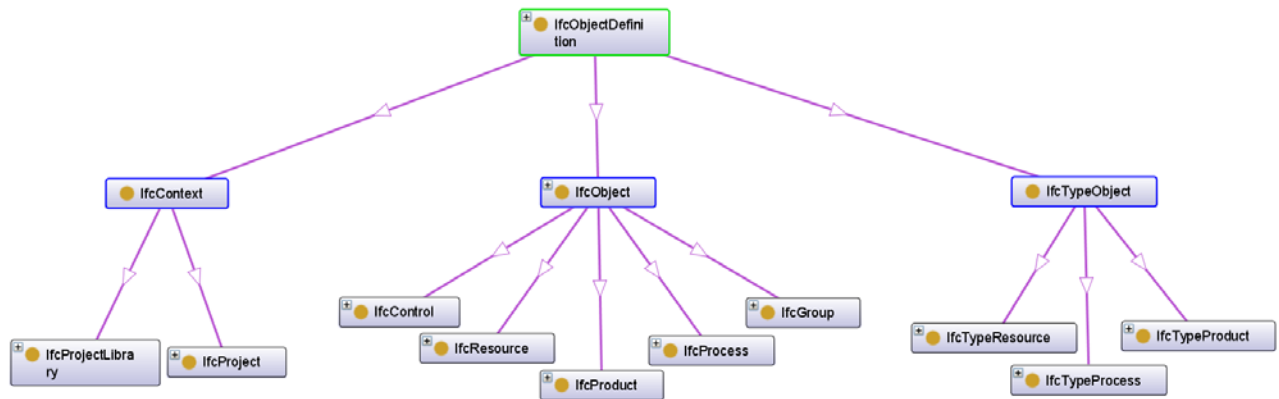


Figure 42: Top level classes in the IFC4_ADD1 module

3.7 IFC4_ADD1_rules module

The IFC4_ADD1_rules module is an extension IFC4_ADD1 that is automatically generated by converting some EXPRESS WHERE rules into OWL Class Expressions to support direct instantiation of ifcOWL and CWA/OVA validation/consistency check. The following patterns are taken in consideration

- Typing relationship between subclasses of IfcObject and IfcTypeObject
- Relationship between pre-defined property sets and subclasses of IfcObject/IfcTypeObject

3.8 IFC4_ADD1_extension module

The IFC4_ADD1_extension module act as the mediator of **OSPH** and **IFC4_ADD1_rules** modules, thus creating a link between them. In particular, the following links have been defined:

- ifc:IfcObjectDefinition is a subclass of osph:ObjectDefinition
- ifc:IfcActuator is a subclass of sosa:Actuator
- ifc:IfcSensor is a subclass of sosa:Sensor
- ifc:IfcValue is a subclass of ex:Constant
- ifcext:ProductSimpleState is a subclass of fsm:Simple to model the states of a generic product
- ifcext:ProductHistory is a subclass of osph:ObjectHistory to model the history of a generic product
- ifc:IfcUnit is a subclass of osph:UnitOfMeasurement

3.9 factory module

The factory module extends the IFC4_ADD1_extension module for the factory domain defining the concepts of:

- factory:Artifact, factory:BufferElement, factory:MachineTool, factory:Pallet as subclasses of ifc:IfcElement
- factory:ProductionResource as subclass of ifc:Resource
- factory:TransformationSystem as subclass of ifc:System

- factory:AssemblyTask, factory:MaintenanceTask, factory:ManufacturingTask, factory:TransportTask as subclasses of ifc:IfcTask
- factory:ProductionPlan as subclass of ifc:IfcWorkPlan
- factory:ProductionSchedule as subclass of ifc:IfcWorkSchedule
- factory:BufferElementHistory, factory:MachineToolHistory as subclasses of ifcext:ProductHistory
- factory:ProductionPlanHistory, factory:ProductionScheduleHistory as subclasses of osp:ObjectHistory
- factory:MachineToolSimpleState as subclass of ifcext:ProductSimpleState to model the states of a machine tool.

The definition of classes listed above exploit the modelling patterns of the IFC, SOSA, and OSPH ontology modules to represent their static and dynamic characteristics of factory-related concepts. Herein these concepts have been further extended to model energy properties of machine tools (see Sect.3.9.1) and machining operations (Sect.3.9.2).

3.9.1 factory module – Machine Tool and Energy Consumption

The behavior of a machine tool can be defined as the total of events or actions that a system can perform, the order in which they can be executed and maybe other aspects of this execution such as timing, event and transition probabilities, or continuous aspects (Baeten, et al., 2007). As an example, a machine can be idle waiting for a part to process and then be working as soon as a raw part is provided. In addition, it can be in a failed status if a failure occurs and, hence, it needs a maintenance action to be able to operate again. Moreover, some machines can be operative only if some conditions are guaranteed, e.g. a given temperature is reached. If the actions are discrete, then the process is also called a discrete event system. Several approaches to model the behavior of a discrete event system have been proposed in the literature, such as State Charts, Petri Nets, Finite State Automata, Queuing Networks, etc.

Herein, it has been decided to follow an approach based on Finite State Machine (FSM) (Kohavi, 1978), thus explicitly modeling the possible states of an object and the events that may cause the transition from one state to another. Moreover, the extensions included in the UML state machine (statecharts, see (Harel, 1987) have been considered. The characterization of the machine tool energy states has been defined according to the standard ISO 14955-2 (see WP1.3 section: Proposal for a standard energy assessment of metal cutting machine tools, by a “Machine-based” approach) by introducing the class factory:MachineToolEnergyState as a subclass of factory:MachineToolSimpleState. In turn, factory:MachineToolEnergyState is specialized by the following classes:

- factory:MachineToolExtendedStandbyState
- factory:MachineToolOffState
- factory:MachineToolProcessingState
- factory:MachineToolReadyForProcessingState
- factory:MachineToolStandbyState
- factory:MachineToolWarmupState

The duration of stay in a specific state can be modeled thanks to the generic feature of a UML statechart. For instance, the warm up of a machine tool is modeled as a task with deterministic duration (see ifc:IfcTask and ifc:IfcTaskTime) that plays the role of action (fsm:Action) that is started whenever

the machine tool enters (fsm:Entry) the state factory:MachineToolWarmupState. At the end of the warm up an event is generated (fsm:Event) that triggers the transition (fsm:Transition) from an instance of factory:MachineToolWarmupState (fsm:Source) to an instance of factory:MachineToolReadyForProcessingState (fsm:Target).

The expected power consumption associated with each energy state of a machine tools can be specified thanks to the static property factory:MachineNominalPowerConsumption that is a subclass of ospi:StaticProperty. An instance of factory:MachineNominalPowerConsumption can be linked with:

- its machine tool as an instance of factory:MachineTool via ssn:hasProperty
- the corresponding energy state as an instance of a subclass of factory:MachineToolEnergyState via factory:hasMachineEnergyState
- the nominal power consumption as an instance of ifc:IfcPowerMeasure via ospi:hasPropertyValue

The actual energy consumption during operation can be modeled with the observable property factory:MachineEnergyConsumption that is a subclass of sosa:ObservableProperty, whereas the energy consumption observations are modeled with the class factory:MachineEnergyConsumptionObs (measured with ifc:IfcEnergyMeasure) that is a subclass of sosa:Observation.

The overall monitoring of a machine tool is modeled with the class factory:MachineToolHistory that is representing a time interval of machine history and can be characterized by observations (e.g. actual energy consumption).

3.9.2 factory module – Machining Operations

The IFC class ifc:IfcResource helps to define the relation between a generic task (ifc:IfcTask) and the objects (ifc:IfcObject) needed to perform the process. This modelling pattern has been exploited by defining the class factory:ProductionEquipmentResource (as a subclass of ifc:IfcResource and factory:ProductionResource) to model the relation between a manufacturing task (factory:ManufacturingTask as subclass of ifc:IfcTask) and the machine tool that can execute the task itself.

The same pair of manufacturing task and machine tool can be linked via more than one instance of factory:ProductionEquipmentResource to represent different operating mode. Indeed, one machine tool can execute the same operation according to different part programs, thus leading to different processing time and energy consumption. Therefore, an instance of factory:ProductionEquipmentResource can be linked with:

- processing time defined as ifc:IfcResourceTime via object property factory:usage_ProductionResource
- energy consumption as ifc:IfcEnergyMeasure via object property factory:hasResourceEnergyConsumption.

This modeling pattern can be exploited to represent in a discrete way diagrams plotting total processing time vs total energy in case of machining operations (see WP1.3 section: Proposal for a standard energy assessment of metal cutting machine tools, by a “Machine-based” approach).

3.10 ISO14649-10 module

The standard *STEP-NC part 10* (ISO 14649-10,2003), available as an EXPRESS schema, was chosen to represent the workpiece and its operation. The EXPRESS schema has been automatically converted to an OWL ontology by exploiting the work by Pauwels et al. (2016).

Errore. L'origine riferimento non è stata trovata. Figure 43 shows the complexity of the relations between some of the key classes in the ISO14649-10 module.

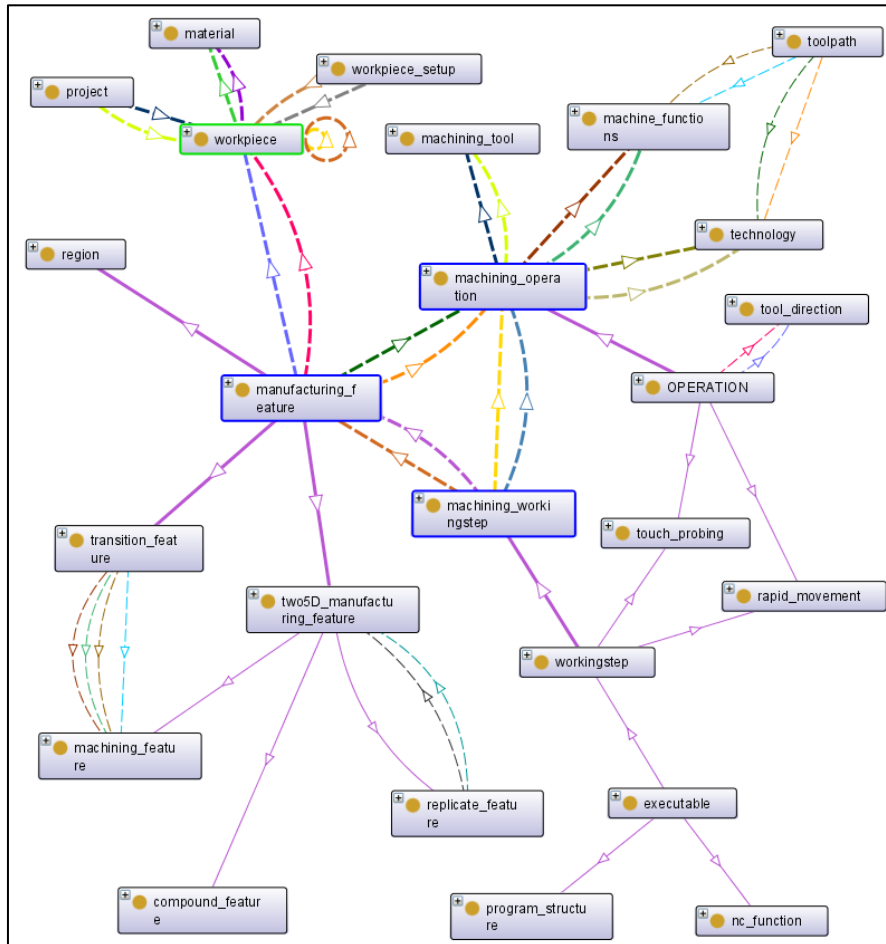


Figure 43: Capturing the key connections between classes in the STEP-NC ontology

3.11 FO1.3 module

The ontology module FO1.3 defines components to build modular fixtures as proposed in the FixOnt ontology by Gmeiner and Shea (2013). Only a fragment of FixOnt was included, in particular the class FixtureComponent and its subclasses (see Figure 44).

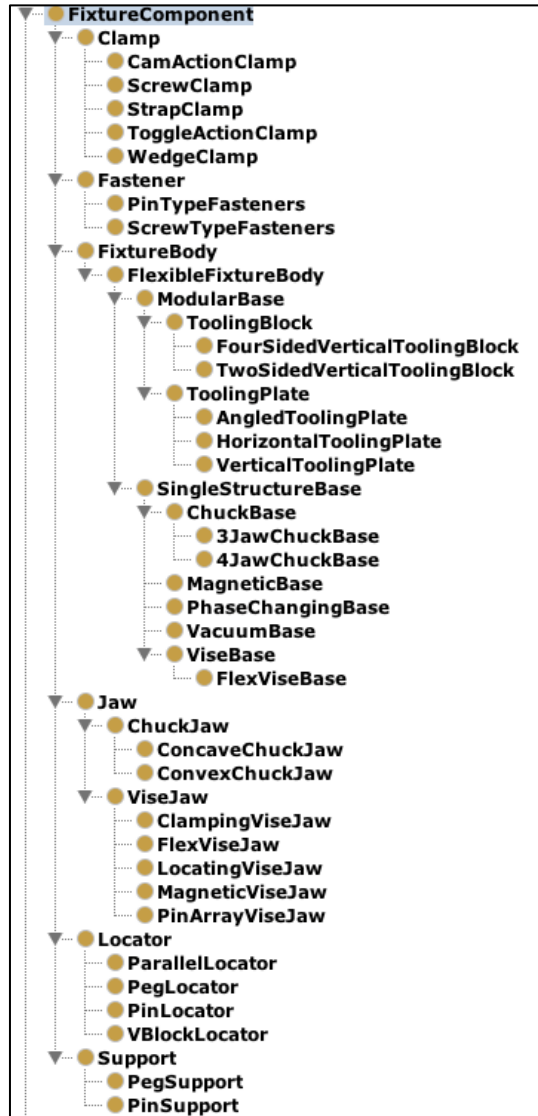


Figure 44: Subclasses of FixtureComponent

3.12 dmanufacturing module

The dmanufacturing ontology defines concepts for discrete manufacturing while integrating the modules *factory*, *FixOnt*, *ISO14649-10* thanks to the following links and extensions:

- **FixtureComponent** is defined as a subclass of **ifc:IfcElement**.
- **WorkpieceOccurrence** is a subclass of **Artifact** from IFC.
- **WorkpieceType** is a subclass of **workpiece** from STEP-NC and **ArtifactType**.
- **machining_workingstep** from STEP-NC is a subclass of **MachiningTask**.

4. Implementation

4.1 Software tools

The data model (see Figure 45 for *factory* module) has been developed using the Protégé software tool (Musen, 2015) that is a free, open-source platform that provides a growing user community with a suite of tools to develop Semantic Web ontologies. It implements a rich set of knowledge modelling structures and actions that support the creation, visualization and manipulation of ontologies in various representation formats. It can be customized to provide domain-friendly support for creating knowledge models and entering data. Also, it can be extended by a plug-in architecture and Java-based application programming interface (API) for building knowledge-base tools and applications. Protégé allows the definition of classes, class hierarchy's variables, variable-value restrictions, and the relationships between classes and the properties of these relationships.

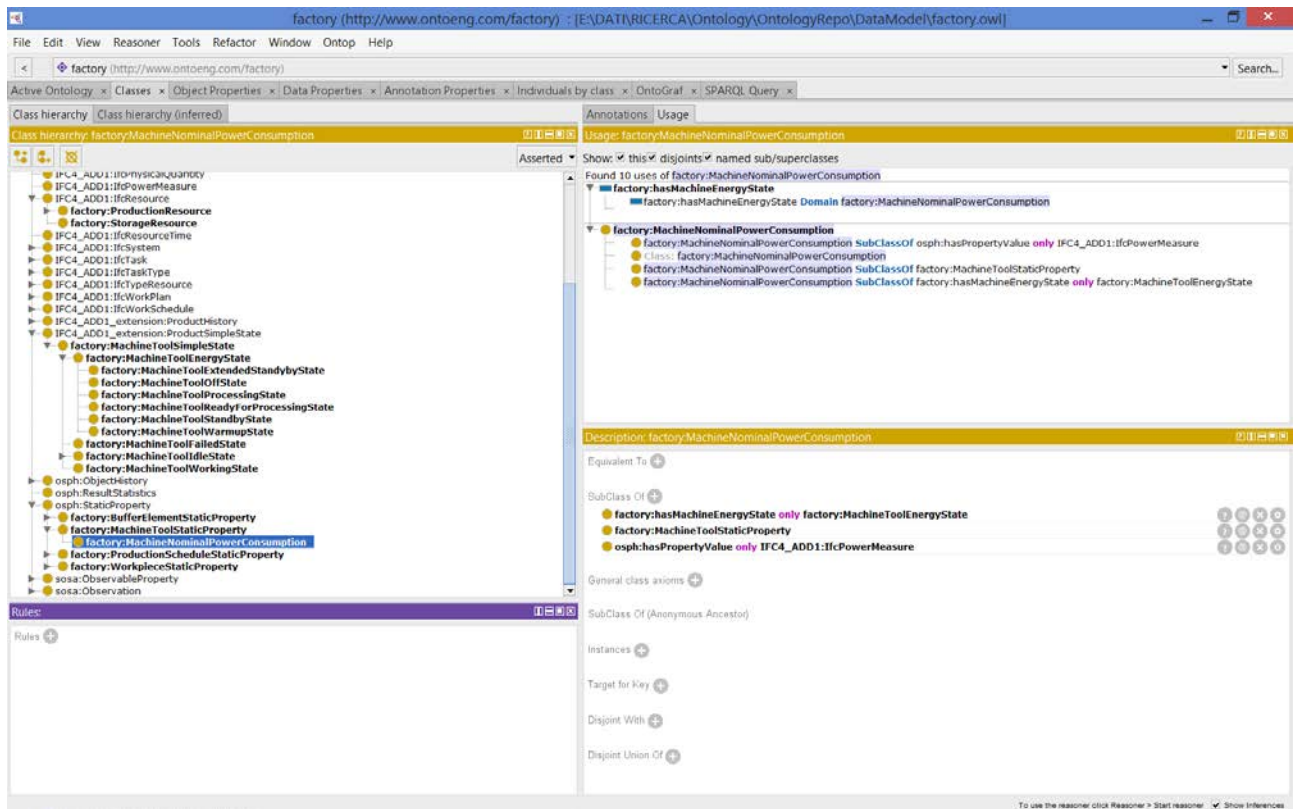


Figure 45: Snapshot of Protégé related to the factory module

The testing and instantiation of the data model has been carried out using the prototype software tool *OntoGui* (Terkaj, 2017). This tool consists of a control panel that allows creating and loading ontologies and a set of other applications for the exploration and generation of OWL individuals. In particular, the application called *OWL Individuals Manager* (Figure 46) is able to extract information related to axioms characterising any OWL class according to the definitions in the T-box. The characterization of the classes with their restrictions is exploited by the Individuals Manager tool both for exploring and generating relations between individuals and also for checking the consistency of the individuals. After loading an ontology populated with individuals, i.e. a T-box and an associated A-box, Individuals Manager allows to select any OWL class defined in the T-box and to perform the following operations with respect to this class:

- **Generation** of a new individual belonging to the selected class;
- **Listing** of the individuals belonging to the selected class (and its subclasses if this option is flagged) and selection of one of them;
- **Navigation** through all the possible relations involving the selected individual according to the restrictions defined in the T-box for the class(es) it belongs to. For each restriction it is possible to visualise the target individuals or literals that can be found at the end of the property chain defined by the restriction itself;
- **Creation of new relations** between the selected individual and already existing individuals or individuals/literal generated on demand;

Finally, it must be stressed that no hard-coding customized for a specific T-box has been implemented in the OntoGui Individuals Manager and in principle this tool can work with any T-box ontology the user decide to load.

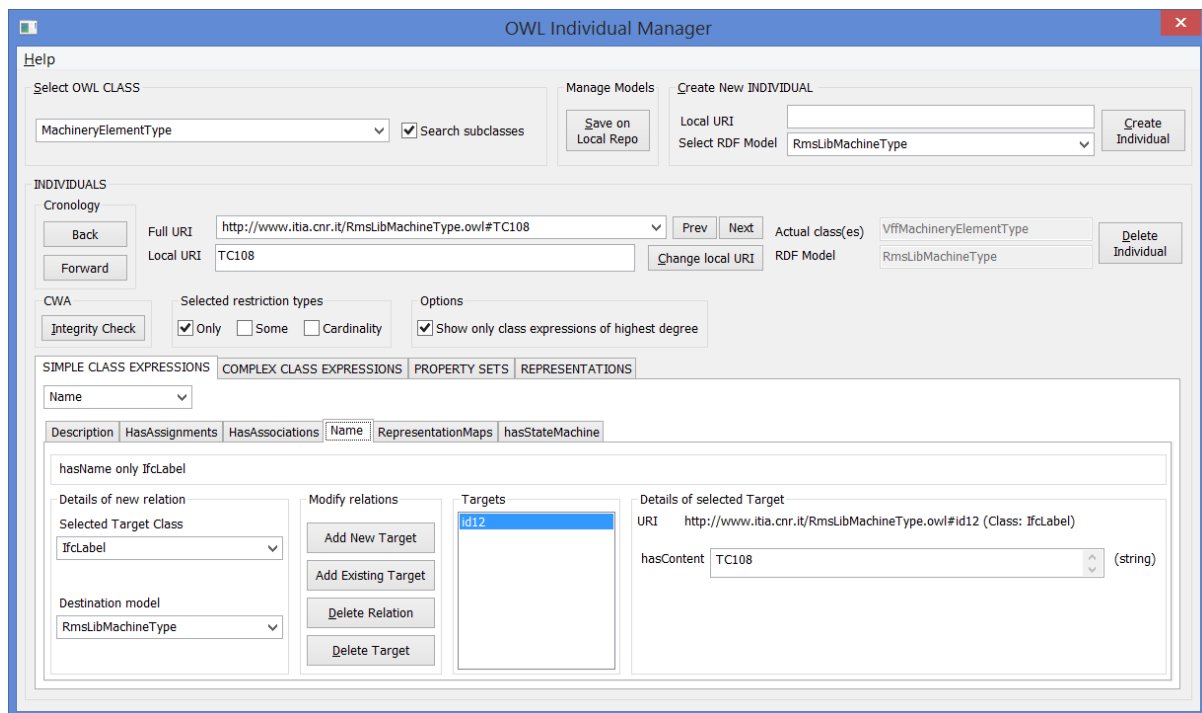


Figure 46: OntoGui OWL Individuals Manager tool

4.2 SPARQL Queries

The following examples show how SPARQL queries (W3C, 2013) can be used to generate new data and to parse the content of the database related to machine tools and machining operations in the scope of the project.

The following definitions of prefixes are needed to run the queries:

```

PREFIX xsd:      <http://www.w3.org/2001/XMLSchema#>
PREFIX rdf:      <http://www.w3.org/1999/02/22-rdf-syntax-ns#>
PREFIX rdfs:     <http://www.w3.org/2000/01/rdf-schema#>
PREFIX owl:    <http://www.w3.org/2002/07/owl#>

```

```

PREFIX fsm:      <http://www.learninglab.de/~dolog/fsm/fsm.owl#>
PREFIX stat:    <http://www.ontoeng.com/statistics#>
PREFIX ex:      <http://www.ontoeng.com/expression#>
PREFIX sosa:    <http://www.w3.org/ns/sosa/>
PREFIX ssn:     <http://www.w3.org/ns/ssn/>
PREFIX osph:    <http://www.ontoeng.com/osph#>
PREFIX list:    <https://w3id.org/list#>
PREFIX expr:    <https://w3id.org/express#>
PREFIX ifc:    <http://ifcowl.openbimstandards.org/IFC4_ADD1#>
PREFIX ifcext:  <http://www.ontoeng.com/IFC4_ADD1_extension#>
PREFIX factory: <http://www.ontoeng.com/factory#>
PREFIX dm:      <http://www.ontoeng.com/dmanufacturing#>
PREFIX stepnc:  <http://www.ontoeng.com/ISO14649-10#>

```

4.2.1 SET Machine Tool Energy States

SPARQL UPDATE to generate the information about the energy states of a machine tool, including the expected power consumption measured in Watt.

```

INSERT {
  GRAPH ?graphuri {
    ?urimachine a owl:NamedIndividual , factory:MachineTool ;
      rdfs:label ?label;
      osph:hasStateMachine ?stM ;
      ssn:hasProperty ?uriprop .

    ?stM a owl:NamedIndividual , fsm:StateMachine ;
      fsm:contains ?uristate .

    ?uristate a owl:NamedIndividual , ?uristateclass .

    ?uriprop a owl:NamedIndividual , factory:MachineNominalPowerConsumption ;
      osph:hasPropertyValue ?uripower ;
      factory:hasMachineEnergyState ?uristate .
    ?uripower a owl:NamedIndividual , ifc:IfcPowerMeasure ;
      expr:hasDouble ?powerdt .
  }
}
where{
VALUES (?id ?label) { ("MachineTool1" "Machine Tool n.1") } .
VALUES (?state ?stateclass ?powercons) { ("stateExtSB" "MachineToolExtendedStandbyState" "10") ("stateOff" "MachineToolOffState" "11") ("stateProc" "MachineToolProcessingState" "12") ("stateReady" "MachineToolReadyForProcessingState" "13") ("stateSB" "MachineToolStandbyState" "14") ("stateWU" "MachineToolWarmupState" "15") } .

VALUES ?graph {"http://www.ontoeng.com/Par2015"} .
VALUES ?factorygraph {"http://www.ontoeng.com/factory"} .

BIND(URI(CONCAT(?graph,"#",?id)) AS ?urimachine) .
BIND(URI(?graph) AS ?graphuri) .
BIND(URI(CONCAT(?graph,"#",?id,"_stM")) AS ?stM) .
BIND(URI(CONCAT(?graph,"#",?state)) AS ?uristate) .
BIND(URI(CONCAT(?graph,"#",?state,"_prop")) AS ?uriprop) .
BIND(URI(CONCAT(?graph,"#",?state,"_cons")) AS ?uripower) .

BIND(URI(CONCAT(?factorygraph,"#",?stateclass)) AS ?uristateclass) .

BIND(STRDT(?powercons, xsd:double) AS ?powerdt) .
}

```

4.2.2 GET Machine Tool Energy States

SPARQL Query to retrieve the information about the energy states of a machine tool, including the expected power consumption.

```
select ?machine ?label ?statemach ?state ?powercons

FROM <http://ifcowl.openbimstandards.org/IFC4_ADD1>
FROM <http://www.ontoeng.com/IFC4_ADD1_extension>
FROM <http://www.ontoeng.com/factory>
FROM <http://www.ontoeng.com/dmanufacturing>
FROM <http://www.ontoeng.com/Par2015>

WHERE{
  ?machine rdf:type owl:NamedIndividual .
  ?machine rdf:type/rdfs:subClassOf* factory:MachineTool .

  ?machine rdfs:label ?label.
  ?machine osph:hasStateMachine ?statemach .
  ?statemach fsm:contains ?state .
  ?state rdf:type/rdfs:subClassOf* factory:MachineToolSimpleState .

  OPTIONAL{
    ?state rdf:type/rdfs:subClassOf* factory:MachineToolEnergyState .
  }

  OPTIONAL{
    ?machine ssn:hasProperty ?prop .
    ?prop osph:hasPropertyValue/expr:hasDouble ?powercons ;
      factory:hasMachineEnergyState ?state .
  }

}
```

4.2.3 SET Duration of Machine Tool Warm up

SPARQL UPDATE to set the transition between the warm up and the ready to process state, while specifying the duration of the warm up (measured in seconds).

```
INSERT {
  GRAPH ?graphuri {

    ?transition a owl:NamedIndividual , fsm:Transition ;
      fsm:TransitionGuard ?trGuard ;
      fsm:Source ?stateWU ;
      fsm:Target ?stateReady .

    ?trGuard a owl:NamedIndividual , fsm:Guard ;
      fsm:GuardEvent ?wuprocessend .

    ?stM fsm:contains ?transition .

    ?stateWU fsm:Entry ?wuprocess .

    ?wuprocess a owl:NamedIndividual , ifc:IfcTask ;
      ifc:taskTime_IfcTask ?wuprocesstime .
    ?wuprocesstime a owl:NamedIndividual , ifc:IfcTaskTime ;
      ifc:scheduleDuration_IfcTaskTime ?wuprocessduration .
    ?wuprocessduration a owl:NamedIndividual , ifc:IfcDuration ;
      expr:hasString ?duration .
    ?wuprocessend a owl:NamedIndividual , factory:MachineToolEvent .
    ?wuprocessRel a owl:NamedIndividual , ifc:IfcRelSequence ;
      ifc:relatingProcess_IfcRelSequence ?wuprocess ;
```

```

        ifc:relatedProcess_ifcRelSequence ?wuprocessend .
    }
}
USING <http://www.ontoeng.com/Par2015>
where{

VALUES ?graph {"http://www.ontoeng.com/Par2015"}
VALUES ?machine {"http://www.ontoeng.com/Par2015#MachineTool1" }
VALUES ?duration {"PT20S"}

BIND(URI(?machine) AS ?urimachine) .
BIND(URI(?graph) AS ?graphuri) .
BIND(URI(CONCAT(?machine,"_trWuReady")) AS ?transition) .
BIND(URI(CONCAT(?machine,"_trWuReady")) AS ?trGuard) .
BIND(URI(CONCAT(?machine,"_Warmup")) AS ?wuprocess) .
BIND(URI(CONCAT(?machine,"_WarmupEnd")) AS ?wuprocessend) .
BIND(URI(CONCAT(?machine,"_WarmupEndSeq")) AS ?wuprocessRel) .
BIND(URI(CONCAT(?machine,"_WarmupTime")) AS ?wuprocesstime) .
BIND(URI(CONCAT(?machine,"_WarmupDuration")) AS ?wuprocessduration) .

?urimachine rdf:type/rdfs:subClassOf* factory:MachineTool .

?urimachine ospm:hasStateMachine ?stM .

?stM fsm:contains ?stateWU , ?stateReady .
?stateReady a factory:MachineToolReadyForProcessingState .
?stateWU a factory:MachineToolWarmupState .

}

```

4.2.4 GET Duration of Machine Tool Warm up

SPARQL Query to get the duration of the machine warm up.

```

select ?machine ?stateWU ?warmupduration

FROM <http://ifcowl.openbimstandards.org/IFC4_ADD1>
FROM <http://www.ontoeng.com/IFC4_ADD1_extension>
FROM <http://www.ontoeng.com/factory>
FROM <http://www.ontoeng.com/dmanufacturing>
FROM <http://www.ontoeng.com/Par2015>

WHERE{

    ?machine rdf:type owl:NamedIndividual .
    ?machine rdf:type/rdfs:subClassOf* factory:MachineTool .

    ?stM fsm:contains ?stateWU .
    ?stateWU a factory:MachineToolWarmupState .

    ?stateWU fsm:Entry ?wuprocess .

    ?wuprocess ifc:taskTime_ifcTask ?wuprocesstime .

    ?wuprocesstime ifc:scheduleDuration_ifcTaskTime/expr:hasString ?warmupduration .

}

```

4.2.5 SET Duration and energy consumption of machining operations

SPARQL UPDATE to set how a machine tool can process a machining operations in different ways characterized by specific processing time (measured in seconds) and energy consumption (measured in Joule).

```

INSERT {
  GRAPH ?graphuri {

    ?urioperation a owl:NamedIndividual , stepnc:machining_workingstep .

    ?restype rdf:type owl:NamedIndividual , factory:ProductionEquipmentResourceType .

    ?reassigntaskrestype rdf:type owl:NamedIndividual , ifc:IfcRelAssignsToProcess ;
      ifc:relatingProcess_IfcRelAssignsToProcess ?urioperation ;
      ifc:relatedObjects_IfcRelAssigns ?restype .

    ?resource a owl:NamedIndividual , factory:ProductionEquipmentResource ;
      factory:usage_ProductionResource ?resourcetime ;
      factory:hasResourceEnergyConsumption ?ifcenergy .

    ?reltypingrestyperes a owl:NamedIndividual , ifc:IfcRelDefinesByType ;
      ifc:relatingType_IfcRelDefinesByType ?restype ;
      ifc:relatedObjects_IfcRelDefinesByType ?resource .

    ?resourcetime a owl:NamedIndividual , ifc:IfcResourceTime ;
      ifc:scheduleWork_IfcResourceTime ?ifcduration .

    ?ifcduration a owl:NamedIndividual , ifc:IfcDuration ;
      expr:hasString ?durationdt .

    ?ifcenergy a owl:NamedIndividual , ifc:IfcEnergyMeasure ;
      expr:hasDouble ?energydt .

    ?reassign a owl:NamedIndividual , ifc:IfcRelAssignsToResource ;
      ifc:relatingResource_IfcRelAssignsToResource ?resource ;
      ifc:relatedObjects_IfcRelAssigns ?urimachine .
  }
}
USING <http://www.h2020-proregio.eu/ComauProcessLib>
where{

VALUES ?operation {"MachOperation1" }
VALUES ?machine {"MachineTool1" }
VALUES ?graph {"http://www.ontoeng.com/Par2015"}
VALUES (?duration ?energycons) { ("40" "10") ("50" "8")}

BIND(URI(?graph) AS ?graphuri) .
BIND(URI(CONCAT(?graph,"#",?operation)) AS ?urioperation) .
BIND(URI(CONCAT(?graph,"#",?machine)) AS ?urimachine) .
BIND(URI(CONCAT(?graph,"#",?operation,"_restype")) AS ?restype) .
BIND(URI(CONCAT(?graph,"#",?operation,"_reassign_restype")) AS ?reassigntaskrestype)
BIND(URI(CONCAT(?graph,"#",?operation,"_res_",?machine,"_",?duration,"_",?energycons)) AS ?resource) .
BIND(URI(CONCAT(?graph,"#",?operation,"_restype_retyping_res")) AS ?reltypingrestyperes)
BIND(URI(CONCAT(?graph,"#",?operation,"_",?machine,"_",?duration,"_",?energycons)) AS ?resourcetime) .
BIND(URI(CONCAT(?graph,"#",?operation,"_",?machine,"_",?duration,"_",?energycons)) AS ?ifcduration) .
BIND(URI(CONCAT(?graph,"#",?operation,"_",?machine,"_",?duration,"_",?energycons)) AS ?ifcenergy) .
BIND(URI(CONCAT(?graph,"#",?operation,"_",?machine,"_",?duration,"_",?energycons)) AS ?reassign) .

BIND(STRDT(CONCAT("PT",?duration,"S"), xsd:string) AS ?durationdt) .
BIND(STRDT(?energycons, xsd:double) AS ?energydt) .
}

```

4.2.6 GET Duration and energy consumption of machining operations

SPARQL Query to get how a machine tool can process a machining operations in different ways characterized by specific processing time and energy consumption.


```

select ?operation ?machine ?duration ?energycons

FROM <http://ifcowl.openbimstandards.org/IFC4_ADD1>
FROM <http://www.ontoeng.com/IFC4_ADD1_extension>
FROM <http://www.ontoeng.com/factory>
FROM <http://www.ontoeng.com/dmanufacturing>
FROM <http://www.ontoeng.com/Par2015>

WHERE{

?operation a stepnc:machining_workingstep .

?reassigntaskrestype a ifc:IfcRelAssignsToProcess ;
    ifc:relatingProcess_IfcRelAssignsToProcess ?operation;
    ifc:relatedObjects_IfcRelAssigns ?restype .

?reltypingrestyperes a ifc:IfcRelDefinesByType ;
    ifc:relatingType_IfcRelDefinesByType ?restype ;
    ifc:relatedObjects_IfcRelDefinesByType ?resource .

?resource factory:usage_ProductionResource ?resourcetime ;
    factory:hasResourceEnergyConsumption ?ifcenergy .

?resourcetime ifc:scheduleWork_IfcResourceTime/expr:hasString ?duration .

?ifcenergy expr:hasDouble ?energycons.

?reassign a owl:NamedIndividual , ifc:IfcRelAssignsToResource ;
    ifc:relatingResource_IfcRelAssignsToResource ?resource ;
    ifc:relatedObjects_IfcRelAssigns ?machine.

}

```

5. WP1.3 Dissemination:

- Jeremi Wójcicki, Giacomo Bianchi, Tullio Tolio, 2018. Hierarchical modelling framework for machine tool energy optimization, Journal of Cleaner Production, Volume 204, Pages 1044-1059, ISSN 0959-6526, <https://doi.org/10.1016/j.jclepro.2018.09.030>.
- Terkaj W (2017) OntoGui: a Graphical User Interface for Rapid Instantiation of OWL Ontologies. Proceedings of the Workshop Data Meets Applied Ontologies, Joint Ontology Workshops 2017, CEUR Workshop Proceedings, vol. 2050
- Italian contribution to WG12 ISO 14955 “Environmental Evaluation of Machine Tools”

6. WP 1.3: TRL evolution

- **Energetic modelling and optimization of machine tools:** TRL: 4 →5 The proposed methodologies have been applied to production machinery applied to a real industrial case. Industrial exploitation require an integration into existing CAM and CAPP softwares.
- **Methods for Standard Energy Assessment of Metal Cutting Machin Tools:** TRL: 5 →6 The proposed methodology has been applied to an industrial machine. Some aspects deserve further development.
- **Ontologies for formal Data Models in Sustainable Manufacturing:** TRL: 4 → 5. New ontologies have been defined, integrated with widespread ontologies used for data modeling in the manufacturing sector.

7. References for WP1.3

- Abele, E., Eisele, C., Schrems, S., 2012. Simulation of the Energy Consumption of Machine Tools for a Specific Production Task, in: *Leveraging Technology for a Sustainable World*. Springer Berlin Heidelberg, Berlin, Heidelberg, pp. 233–237. https://doi.org/10.1007/978-3-642-29069-5_40
- Albertelli, P., Keshari, A., Matta, A., 2016. Energy oriented multi cutting parameter optimization in face milling. *J. Clean. Prod.* 137, 1602–1618. <https://doi.org/10.1016/J.JCLEPRO.2016.04.012>
- Altintas, Y., 2012. *Manufacturing automation: metal cutting mechanics, machine tool vibrations, and CNC design*, 2nd ed. ed. Cambridge University Press, Cambridge ; New York.
- Anderberg, S., Kara, S., 2009. Energy and cost efficiency in CNC machining.
- Aramcharoen, A., Mativenga, P.T., 2014. Critical factors in energy demand modelling for CNC milling and impact of toolpath strategy. *J. Clean. Prod.* 78, 63–74. <https://doi.org/10.1016/J.JCLEPRO.2014.04.065>
- Arrazola, P.J., Özel, T., Umbrello, D., Davies, M., Jawahir, I.S., 2013. Recent advances in modelling of metal machining processes. *CIRP Ann. - Manuf. Technol.* 62, 695–718. <https://doi.org/10.1016/j.cirp.2013.05.006>
- Avram, O., Stroud, I., Xirouchakis, P., 2011. A multi-criteria decision method for sustainability assessment of the use phase of machine tool systems. *Int. J. Adv. Manuf. Technol.* 53, 811–828. <https://doi.org/10.1007/s00170-010-2873-2>
- Avram, O.I., Xirouchakis, P., 2011. Evaluating the use phase energy requirements of a machine tool system. *J. Clean. Prod.* 19, 699–711. <https://doi.org/10.1016/J.JCLEPRO.2010.10.010>
- Badra F., Servant F.-P., Passant A., “A Semantic Web Representation of a Product Range Specification based on Constraint Satisfaction Problem in the Automotive Industry,” in *1st International Workshop on Ontology and Semantic Web for Manufacturing*, Heraklion, 2011.
- Baeten J.C.M., van Beek D.A, Rooda J.E., “Process Algebra,” in P.A. Fishwick (ed) *Handbook of Dynamic System Modeling*, Chapman and Hall, 2007.
- Baqar-Raza M., Harrison R., “Ontological Knowledge Based System for Product, Process and Resource Relationships in Automotive Industry,” in *1st International Workshop on Ontology and Semantic Web for Manufacturing*, Heraklion, 2011.
- Bianchi, G., Tolio, T., 2018. Hierarchical modelling framework for machine tool energy optimization. *J. Clean. Prod.* <https://doi.org/10.1016/j.jclepro.2018.09.030>
- Blackburn MR, Denno PO (2015) *Using Semantic Web Technologies for Integrating Domain Specific Modeling and Analytical Tools*, *Procedia Computer Science.* 61:141-146.
- Bonino D. and F. Corno. *DogOnt - Ontology Modeling for Intelligent Domotic Environments*. *Lecture Notes in Computational Science*, 5318:790–803, 2008.
- Borgia, S., Albertelli, P., Bianchi, G., 2016. A simulation approach for predicting energy use during general milling operations. *Int. J. Adv. Manuf. Technol.* 1–15. <https://doi.org/10.1007/s00170-016-9654-5>
- Borgia, S., Albertelli, P., Bianchi, G., 2017. A simulation approach for predicting energy use during general milling operations. *Int. J. Adv. Manuf. Technol.* 90, 3187–3201. <https://doi.org/10.1007/s00170-016-9654-5>
- Borgia, S., Leonesio, M., Bianchi, G., Albertelli, P., 2014a. Machine Tool Energetic Simulation during General Milling Operations, in: Neugebauer, R. (Reimund), Drossel, W.-G. (Eds.), *Innovations of Sustainable Production for Green Mobility: Energy-Efficient Technologies in Production*. Verlag Wissenschaftliche Scripten, Chemnitz, pp. 583–599. <https://doi.org/ISBN: 9783957350046>
- Borgia, S., Pellegrinelli, S., Bianchi, G., Leonesio, M., 2014b. A Reduced Model for Energy Consumption Analysis in Milling. *Procedia CIRP* 17, 529–534. <https://doi.org/10.1016/J.PROCIR.2014.01.105>

- Borgia, S., Pellegrinelli, S., Petrò, S., Tolio, T., 2014c. Network part program approach based on the STEP-NC data structure for the machining of multiple fixture pallets. *Int. J. Comput. Integr. Manuf.* 27, 281–300. <https://doi.org/10.1080/0951192X.2013.814158>
- Bort, G., Carlos, M., Leonesio, M., Bosetti, P., 2016. A model-based adaptive controller for chatter mitigation and productivity enhancement in CNC milling machines. *Robot. Comput. Integr. Manuf.* 40, 34–43. <https://doi.org/10.1016/j.rcim.2016.01.006>
- Calvanese, M.L., Albertelli, P., Matta, A., Taisch, M., 2013. Analysis of Energy Consumption in CNC Machining Centers and Determination of Optimal Cutting Conditions, in: *Re-Engineering Manufacturing for Sustainability*. Springer Singapore, Singapore, pp. 227–232. https://doi.org/10.1007/978-981-4451-48-2_37
- CECIMO, 2018. Self Regulatory Initiative [WWW Document]. URL <http://www.cecimo.eu/site/publications/magazine/cecimo-self-regulatory-initiative/>
- Chang, Q., Xiao, G., Biller, S., Li, L., 2013. Energy Saving Opportunity Analysis of Automotive Serial Production Systems (March 2012). *IEEE Trans. Autom. Sci. Eng.* 10, 334–342. <https://doi.org/10.1109/TASE.2012.2210874>
- Compton M., P. Barnaghi, L. Bermudez, and et al. The SSN ontology of the W3C semantic sensor network incubator group. *Journal on Web Semantics*, 17:25 – 32, 2012.
- Daniele L., F. den Hartog, and J. Roes. Created in Close Interaction with the Industry: The Smart Appliances REFERENCE (SAREF) Ontology. In R. Cuel and R. Young, editors, *Formal Ontologies Meet Industry*, volume 225, pages 100–112. Springer International Publishing, Cham, Switzerland, 2015.
- Diaz, N., Choi, S., Helu, M., Chen, Y., Jayanathan, S., Yasui, Y., Kong, D., Pavanaskar, S., Dornfeld, D., 2010a. Machine Tool Design and Operation Strategies for Green Manufacturing.
- Diaz, N., Helu, M., Dornfeld, D., 2010b. Design and Operation Strategies for Green Machine Tool Development. *Lab. Manuf. Sustain.*
- Diaz, N., Redelsheimer, E., Dornfeld, D., 2011. Energy Consumption Characterization and Reduction Strategies for Milling Machine Tool Use, in: *Globalized Solutions for Sustainability in Manufacturing*. Springer Berlin Heidelberg, Berlin, Heidelberg, pp. 263–267. https://doi.org/10.1007/978-3-642-19692-8_46
- Dolog P (2004) Model-Driven Navigation Design for Semantic Web Applications with the UML-Guide. In *Proc. ICWE*, pages 75–86, 2004.
- Dong, Y.H., Xu, H.T., Lin, H., 2009. Simulation of Cutting Force in Turning Machining Process on CK7815 NC Lathe. *Key Eng. Mater.* 392–394, 64–68. <https://doi.org/10.4028/www.scientific.net/KEM.392-394.64>
- Draganescu, F., Gheorghe, M., Doicin, C.V., 2003. Models of machine tool efficiency and specific consumed energy. *J. Mater. Process. Technol.* 141, 9–15. [https://doi.org/10.1016/S0924-0136\(02\)00930-5](https://doi.org/10.1016/S0924-0136(02)00930-5)
- Drury, B., 2001. *Control Techniques Drives and Controls Handbook*. IET.
- Duflou, J.R., Sutherland, J.W., Dornfeld, D., Herrmann, C., Jeswiet, J., Kara, S., Hauschild, M., Kellens, K., 2012. Towards Energy and Resource Efficient Manufacturing: A Processes and Systems Approach. *CIRP Ann. - Manuf. Technol.* 61.
- EC Directive, 2005. EuP 2005/32/EC Ecodesign Directive for Energy-using Products [WWW Document]. URL <http://eur-lex.europa.eu/LexUriServ/LexUriServ.do?uri=OJ:L:2005:191:0029:0058:en:PDF>
- EC Directive, 2009. ErP 2009/125 EC Eco-design Directive for Energy-related Products [WWW Document]. URL <https://eur-lex.europa.eu/legal-content/EN/TXT/?qid=1541159519339&uri=CELEX:32009L0125>

- Ehmann, K.F., Kapoor, S.G., DeVor, R.E., Lazoglu, I., 1997. Machining Process Modeling: A Review. *J. Manuf. Sci. Eng.* 119, 655. <https://doi.org/10.1115/1.2836805>
- Ekaputra FJ, Sabou M, Serral E, Kiesling E, Biffi S (2017) Ontology-Based Data Integration in Multi-Disciplinary Engineering Environments: A Review. *Open Journal of Information Systems (OJIS)*, 4(1):1-26.
- Fraunhofer IZM IPK, 2012. Preliminary Study Eco Machine Tools [WWW Document]. URL <http://www.ecomachinetools.eu>
- Frigerio, N., Matta, A., 2014. Energy Efficient Control Strategy for Machine Tools with Stochastic Arrivals and Time Dependent Warm-up. *Procedia CIRP* 15, 56–61. <https://doi.org/10.1016/J.PROCIR.2014.06.040>
- Frigerio, N., Matta, A., Ferrero, L., Rusinà, F., 2013. Modeling Energy States in Machine Tools: An Automata Based Approach, in: *Re-Engineering Manufacturing for Sustainability*. Springer Singapore, Singapore, pp. 203–208. https://doi.org/10.1007/978-981-4451-48-2_33
- Gmeiner T, Shea K (2013) An Ontology for the Autonomous Reconfiguration of a Flexible Fixture Device. *Journal of Computing Information Science in Engineering* 13(2), 021003.
- Guarino, N., Oberle, D., Staab, S. (2009). "What is an Ontology?" In *Handbook on ontologies* (pp. 1-17). Springer Berlin Heidelberg.
- Gunendran, A. G., Young, R. I., Cutting-Decelle, A. F., & Bourey, J. P. (2007) "Organising manufacturing information for engineering interoperability", In *Enterprise Interoperability II* (pp. 587-598). Springer London.
- Haller A, Janowicz K, Cox S, Phuoc DL, Taylor K, Lefrançois M (2017) Semantic Sensor Network Ontology. <https://www.w3.org/TR/vocab-ssn/>. Accessed 20 April 2018.
- Harel D., "Statecharts: A visual formalism for complex systems," *Sci. Comput. Program.*, 8:231-274, 1987.
- Hazewinkel, M. (Ed.), 1988. *Encyclopaedia of mathematics: an updated and annotated translation of the Soviet "Mathematical encyclopaedia."* Reidel ; Sold and distributed in the U.S.A. and Canada by Kluwer Academic Publishers, Dordrecht ; Boston : Norwell, MA, U.S.A.
- He, Y., Liu, F., Wu, T., Zhong, F.-P., Peng, B., 2012. Analysis and estimation of energy consumption for numerical control machining. *Proc. Inst. Mech. Eng. Part B J. Eng. Manuf.* 226, 255–266. <https://doi.org/10.1177/0954405411417673>
- Hepp M., De Leenheer D., De Moor A., Sure Y., *Ontology Management: Semantic Web, Semantic Web Services, and Business Applications*, Springer-Verlag, 2007.
- Horrocks, I., Kutz, O., Sattler, U. (2006). The Even More Irresistible SROIQ. *KR*, 6, 57-67.
- Hu, L., Liu, Y., Lohse, N., Tang, R., Lv, J., Peng, C., Evans, S., 2017. Sequencing the features to minimise the non-cutting energy consumption in machining considering the change of spindle rotation speed. *Energy* 139, 935–946. <https://doi.org/10.1016/J.ENERGY.2017.08.032>
- International Organization for Standardization (2004) ISO 10303-11 Industrial automation systems and integration — product data representation and exchange — part 11: description methods: the EXPRESS language reference manual. http://www.iso.org/iso/iso_catalogue/catalogue_tc/catalogue_detail.htm?csnumber=38047. Accessed 20 April 2018.
- International Organization for Standardization (ISO), "Industrial Automation Systems and Integration - Product Data Representation and Exchange. Part 1: Overview and Fundamental Principles", ISO 10303-1:1994(e) Ed., 1994.
- International Standards Organization, ISO 18629 - Process Specification Language, ISO, 2004.
- ISO 14649-10 (2004) - Industrial automation systems and integration — Physical device control — Data model for computerized numerical controllers — Part 10: General process data, ISO 14649-10:2004

- ISO/TC 39 Machine tools WG12, 2017. ISO 14955-1:2017 Machine tools -- Environmental evaluation of machine tools -- Part 1: Design methodology for energy-efficient machine tools [WWW Document]. URL <https://www.iso.org/standard/70035.html?browse=tc>
- Jia, S., Tang, R., Lv, J., 2014. Therblig-based energy demand modeling methodology of machining process to support intelligent manufacturing. *J. Intell. Manuf.* 25, 913–931. <https://doi.org/10.1007/s10845-012-0723-9>
- Jia, S., Tang, R., Lv, J., Yuan, Q., Peng, T., 2017. Energy consumption modeling of machining transient states based on finite state machine. *Int. J. Adv. Manuf. Technol.* 88, 2305–2320. <https://doi.org/10.1007/s00170-016-8952-2>
- JIS, 2010. JIS TS B 0024-1 Machine tools - Test methods for electric power consumption - Part 1 : Machining centres [WWW Document].
- Kaiser J. and P. Stenzel. eeEmbedded D4.2: Energy System Information Model - ESIM. Technical report, eeEmbedded Consortium, Brussels, Belgium, 2015.
- Kara, S., Li, W., 2011. Unit process energy consumption models for material removal processes. *CIRP Ann.* 60, 37–40. <https://doi.org/10.1016/J.CIRP.2011.03.018>
- Kohavi Z., “Switching and Finite automata theory,” 2nd ed. McGraw-Hill, 1978.
- Kong, D., Choi, S., Yasui, Y., Pavanaskar, S., Dornfeld, D., Wright, P., 2011. Software-based tool path evaluation for environmental sustainability. *J. Manuf. Syst.* 30, 241–247. <https://doi.org/10.1016/J.JMSY.2011.08.005>
- Kulvatunyou B., Cho H., Son Y., "A semantic web service framework to support intelligent distributed manufacturing," *International Journal Knowledge-Based Intelligent Engineering Systems*, pp. 107-127, 2005.
- Laakso M., Kiviniemi A., “The IFC Standard - A Review of History, Development, and Standardization” in *Journal of Information Technology in Construction (ITcon)*, 17:134- 161, 2012
- Lefrancois M., J. Kalaoja, T. Ghariani, and A. Zimmermann. D2.2: The SEAS Knowledge Model. Technical report, ITEA2 12004 Smart Energy Aware Systems, Brussels, Belgium, 2017.
- Leitão P., Restivo F., "ADACOR: A holonic architecture for agile and adaptive manufacturing control," *Computers in Industry* , pp. 121-130, 2006.
- Lemaignan, S.; Siadat, A.; Dantan, J.-Y.; Semenenko, A., "MASON: A Proposal For An Ontology Of Manufacturing Domain," *Distributed Intelligent Systems: Collective Intelligence and Its Applications*, 2006. DIS 2006. IEEE Workshop on , vol., no., pp.195,200, 15-16 June 2006
- Leonesio, M., Tosatti, L.M., Pellegrinelli, S., Valente, A., 2012. An Integrated Approach for Joint Process Planning and Machine Tool Dynamic Behavioral Assessment. *Procedia CIRP*, 1st CIRP Global Web Conference: Interdisciplinary Research in Production Engineering (CIRPE2012) 2, 38–43. <https://doi.org/10.1016/j.procir.2012.05.036>
- Lin H., Harding J., Shahbaz M., "Manufacturing system engineering ontology for semantic interoperability across extended project teams," *International Journal of Production Research*, vol. 42, no. 24, pp. 5099-5118.
- Lv, J., Tang, R., Jia, S., 2014. Therblig-based energy supply modeling of computer numerical control machine tools. *J. Clean. Prod.* 65, 168–177. <https://doi.org/10.1016/J.JCLEPRO.2013.09.055>
- Martin D’Acunto A., “Design of a production system: an application of integration product process”, *Int. J. Computer Integrated Manufacturing*, vol. 16, no. 7, pp. 509-516.
- Mastinu, G., Gobbi, M., Miano, C., 2006. Multi-objective Optimisation, in: *Optimal Design of Complex Mechanical Systems*. Springer Berlin Heidelberg, Berlin, Heidelberg, pp. 47–98. https://doi.org/10.1007/978-3-540-34355-4_3
- Mativenga, P.T., Rajemi, M.F., 2011. Calculation of optimum cutting parameters based on minimum energy footprint. *CIRP Ann.* 60, 149–152. <https://doi.org/10.1016/J.CIRP.2011.03.088>

- Measuring energy efficiency progress in the EU: the energy efficiency index ODEX — ECEEE [WWW Document], n.d.
- Mori, M., Fujishima, M., Inamasu, Y., Oda, Y., 2011. A study on energy efficiency improvement for machine tools. *CIRP Ann.* 60, 145–148. <https://doi.org/10.1016/J.CIRP.2011.03.099>
- Moser T., Sunindyo W., Merdan M., Biffi S., “Supporting Runtime Decision Making in the Production Automation Domain Using Design Time Engineering Knowledge,” in *Ontology and Semantic Web for Manufacturing*, Heraklion, Crete, Greece, 2011.
- Mouzon, G., Yildirim, M.B., Twomey, J., 2007. Operational methods for minimization of energy consumption of manufacturing equipment. *Int. J. Prod. Res.* 45, 4247–4271. <https://doi.org/10.1080/00207540701450013>
- Murty, K.G., 1988. Linear complementarity, linear and nonlinear programming. Heldermann.
- Musen MA (2015) The protégé project: A look back and a look forward. *AI Matters*, 1(4):4–12.
- NACFAM - National Council for Advanced Manufacturing, "Sustainable Manufacturing," 2009.
- Pauwels P, Krijnen T, Terkaj W, Beetz J (2017) Enhancing the ifcOWL ontology with an alternative representation for geometric data. *Automation in Construction*, 80:77–94.
- Pauwels P, Terkaj W (2016) EXPRESS to OWL for construction industry: Towards a recommendable and usable ifcOWL ontology. *Automation in Construction*, 63:100–133.
- Pellegrinelli S, Terkaj W, Urgo M (2016) A Concept for a Pallet Configuration Approach Using Zero-point Clamping Systems. *Procedia CIRP* 41:123–128.
- Peng, T., Xu, X., 2013. A Universal Hybrid Energy Consumption Model for CNC Machining Systems, in: *Re-Engineering Manufacturing for Sustainability*. Springer Singapore, Singapore, pp. 251–256. https://doi.org/10.1007/978-981-4451-48-2_41
- Peng, T., Xu, X., 2014. Energy-efficient machining systems: a critical review. *Int. J. Adv. Manuf. Technol.* 72, 1389–1406. <https://doi.org/10.1007/s00170-014-5756-0>
- Prabhu, V. V., Jeon, H.W., Taisch, M., 2012. Modeling green factory physics — An analytical approach, in: *2012 IEEE International Conference on Automation Science and Engineering (CASE)*. IEEE, pp. 46–51. <https://doi.org/10.1109/CoASE.2012.6386361>
- Prabhu, V. V., Jeon, H.W., Taisch, M., 2013. *Simulation Modelling of Energy Dynamics in Discrete Manufacturing Systems*. Springer, Berlin, Heidelberg, pp. 293–311. https://doi.org/10.1007/978-3-642-35852-4_19
- Recommended machining parameters for copper and copper alloys, 2010. . Düsseldorf.
- Reinisch C., M. J. Kofler, F. Iglesias, and W. Kastner. ThinkHome Energy Efficiency in Future Smart Homes. *EURASIP Journal on Embedded Systems*, (104617):1–18, 2011.
- Schischke, K., Hohwieler, E., Feitscher, R., Kreuzschner, S., Wilpert, P., Nissen, N.F., 2012. Machine tools and related machinery: Task 6 report improvement potential. Fraunhofer Institute for Reliability and Microintegration, Berlin, Germany.
- Shearer, R., Motik, B., Horrocks, I. (2008, October). Hermit: A Highly-Efficient OWL Reasoner. In *OWLED (Vol. 432)*.
- Sirin, E., Parsia, B., Grau, B. C., Kalyanpur, A., Katz, Y. (2007). Pellet: A practical owl-dl reasoner. *Web Semantics: science, services and agents on the World Wide Web*, 5(2), 51–53.
- Terkaj W (2017) OntoGui: a Graphical User Interface for Rapid Instantiation of OWL Ontologies. *Proceedings of the Workshop Data Meets Applied Ontologies, Joint Ontology Workshops 2017, CEUR Workshop Proceedings*, vol. 2050
- Terkaj W, Pedrielli G, Sacco M (2012) Virtual Factory Data Model. *Workshop on Ontology and Semantic Web for Manufacturing OSEMA 2012, CEUR Workshop Proceedings*, vol. 886, pp 29–43.

- Terkaj W, Schneider GF, Pauwels P (2017) Reusing Domain Ontologies in Linked Building Data: the Case of Building Automation and Control. Proceedings of the 8th Workshop Formal Ontologies Meet Industry, Joint Ontology Workshops 2017, CEUR Workshop Proceedings, vol. 2050.
- Terkaj W, Sojic A (2015) Ontology-based Representation of IFC EXPRESS rules: an enhancement of the ifcOWL ontology. *Automation in Construction*, 57:188-201
- Terkaj W., Urgo M. (2014) Ontology-based modeling of production systems for design and performance evaluation. Proceedings of 12th IEEE International Conference on Industrial Informatics (INDIN), pp 748-753
- Terkaj W., Urgo M., "Virtual Factory Data Model to Support Performance Evaluation of Production Systems," in Proceedings of the Workshop on Ontology and Semantic Web for Manufacturing, Graz, Austria, 24-27 July, 2012, pp. 44–58, 2012.
- Tolio, T.A.M., Ratti, A., 2018. Performance evaluation of two-machine lines with generalized thresholds. *Int. J. Prod. Res.* 56, 926–949. <https://doi.org/10.1080/00207543.2017.1420922>
- Tomasevic N.M., M. C. Batic, L. M. Blanes, M. M. Keane, and S. Vranes. Ontology-based facility data model for energy management. *Advanced Engineering Informatics*, 29(4):971–984, 2015.
- Tsarkov, D., Horrocks, I. (2006). FaCT++ description logic reasoner: System description. In *Automated reasoning* (pp. 292-297). Springer Berlin Heidelberg.
- Verl, A., Westkämper, E., Abele, E., Dietmair, A., Schlechtendahl, J., Friedrich, J., Haag, H., Schrems, S., 2011. Architecture for Multilevel Monitoring and Control of Energy Consumption, in: *Glocalized Solutions for Sustainability in Manufacturing*. Springer Berlin Heidelberg, Berlin, Heidelberg, pp. 347–352. https://doi.org/10.1007/978-3-642-19692-8_60
- W3C, OWL Web Ontology Language - RDF/XML Syntax Specification (Revised). [Online]. <http://www.w3.org/TR/REC-rdf-syntax/> (W3C, 2004b)
- W3C, OWL Web Ontology Language – OWL 2 Overview, <http://www.w3.org/TR/2012/REC-owl2-overview-20121211/> (W3C, 2012b)
- W3C, OWL Web Ontology Language – OWL Guide, <http://www.w3.org/TR/owl-guide/> (W3C, 2009b)
- W3C, OWL Web Ontology Language - Use Cases and Requirements. <http://www.w3.org/TR/webont-req/> [Online]. (W3C, 2004a)
- W3C, OWL Web Ontology Language OWL, <http://www.w3.org/TR/2012/REC-owl2-overview-20121211/> (W3C, 2012)
- W3C, SPARQL 1.1 Overview, <https://www.w3.org/TR/2013/REC-sparql11-overview-20130321/>
- Wójcicki, J., 2017. Energy efficiency of machine tools. Politecnico di Milano. <https://doi.org/10.13140/RG.2.2.30523.11047>
- Wójcicki, J., Bianchi, G., 2015. MINIMIZATION OF ENERGY CONSUMPTION OF A MACHINE TOOL : A MULTI-LEVEL APPROACH, in: *23rd ABCM International Congress of Mechanical Engineering*. <https://doi.org/10.20906/CPS/COB-2015-2719>
- Wójcicki, J., Bianchi, G., 2017. Electric load management in spindle run-up and run-down for multi-spindle machine tools via optimal power-torque trajectories and peak load synchronization. *Int. J. Adv. Manuf. Technol.* <https://doi.org/10.1007/s00170-017-1341-7>
- Wójcicki, J., Bianchi, G., 2018. Electric load management in spindle run-up and run-down for multi-spindle machine tools via optimal power-torque trajectories and peak load synchronization. *Int. J. Adv. Manuf. Technol.* 95, 1819–1835. <https://doi.org/10.1007/s00170-017-1341-7>
- Wójcicki, J., Leonesio, M., Bianchi, G., 2018. Integrated energy analysis of cutting process and spindle subsystem in a turning machine. *J. Clean. Prod.* 170, 1459–1472. <https://doi.org/10.1016/j.jclepro.2017.09.234>

- Xiong, Y., Wu, J., Deng, C., Wang, Y., 2016. Machining process parameters optimization for heavy-duty CNC machine tools in sustainable manufacturing. *Int. J. Adv. Manuf. Technol.* 87, 1237–1246. <https://doi.org/10.1007/s00170-013-4881-5>
- Yang, W.H., Targ, Y.S., 1998. Design optimization of cutting parameters for turning operations based on the Taguchi method. *J. Mater. Process. Technol.* 84, 122–129. [https://doi.org/10.1016/S0924-0136\(98\)00079-X](https://doi.org/10.1016/S0924-0136(98)00079-X)
- Zhou, L., Li, J., Li, F., Meng, Q., Li, J., Xu, X., 2016. Energy consumption model and energy efficiency of machine tools: a comprehensive literature review. *J. Clean. Prod.* 112, 3721–3734. <https://doi.org/10.1016/J.JCLEPRO.2015.05.093>

Attività 1.4 Metodologia per l'analisi dell'efficienza energetica dei moduli principali dei beni strumentali

Quadro generale di riferimento, obiettivi e stato dell'arte

In this WP, a methodology for assessing the energy efficiency of machine tool components was conceived. The procedure adequately combines experimental and modelling approaches. Basically, the experimental data are used for identifying a regression model of a specified machine tool component (group or subsystem) that can be exploited both for assessing its energy efficiency and for analysing its role on the overall machine efficiency. Such a model can be even used for estimating the impact of energy-oriented improvements or alternative design solutions.

Although the procedure is generic, in this project, in order to better show its potentialities, it was exploited for carrying out a comprehensive assessment of the energy saving opportunities linked to the introduction of direct drives solutions in machine tool spindle systems.

Motivations and research summary

Although there is a clear industrial trend towards the replacement of the traditional motor-transmission based spindle solutions, there is a lack of scientific studies focused on the associated energy-related aspects. For this purpose, two spindle units characterized by similar performances were analyzed from the energy consumption, losses and efficiency perspective. Empirical spindle system energy models were developed exploiting experimental tests performed on a motor test bench used for reproducing different machining conditions. The identified models were used to estimate the energy savings that can be achieved substituting the traditional gearbox-based solution with the novel direct-drive spindle. The analysis was carried out considering a realistic production scenario for the machine equipped with the analyzed spindle. It was demonstrated that about 7% of the energy absorbed by the overall machine can be saved and that this improvement accounts for the 147% of the requested cutting energy. For sake of generality, the analysis was repeated considering different production scenarios and ways of using the machine. It can be concluded that the achievable energy savings are even robust to the change of the executed machining operations.

State of Art Analysis

Since manufacturing is one of the most energy demanding industrial sectors, institutions, universities, industrial organizations and companies, each one at different levels and with different roles, started tackling the challenging issues of using energy in a more efficient way. The European Commission, in order to fulfil the Worldwide greenhouse gas emission reduction target, delivered a directive for the eco-design of energy-related products ErP (EU (2009)) that establishes a common framework for the promotion of energy efficiency policies.

This framework is useful also for machine tools and production systems. CECIMO, the European Association of Machine Tool Industries, launched a self-regulation initiative (CECIMO (2009)) that supported machine tool builders for the first implementation of eco-oriented actions. Fraunhofer-IZM (2011) issued a preparatory study that identifies a set of best available/not yet available technologies (BAT/BNAT) that could be successfully used for reducing the consumed energy by machinery. Moreover, it was stated that the machine use phase is much more relevant, for what concerns the absorbed energy, than other phases (i.e. machine production, transportation and post-use), Jayal et al. (2010)). In this scenario, the International Organization for Standardization ISO released the first part of a more structured standard (ISO/DIS 14955-1) that is focused on methodologies for the energy efficient machine tools design, ISO (2014). Other parts of the standard (testing procedures) are under development.

In the last few years a great research effort has been done to make manufacturing more efficient. As observed in Yingjie (2014), energy savings in machine tools can be accomplished by a proper energy-oriented machine tool components design or by promoting a better machine usage, both in terms of machining strategy or process parameter selection. Neugebauer et al. (2011) tried to outline general principles for enhancing the efficiency in machine centres.

The awareness of the most power-demanding machine tool components is without doubts the starting point for conceiving further energy saving strategies. For this purpose, an energy assessment approach based on experimental measurements was generally preferred. A standardized methodology for the energy assessment of machine tool (under development in ISO (2016)) is now close to be released. Analyzing the experimental measurements reported in several papers (i.e. Li et al. (2011)), it was found that almost every machine uses relevant amount of energy just for being ready to operate. This is mainly due to the auxiliary equipment typically installed on modern machines.

Although the experimental approach is helpful for a first rough energy analysis, the availability of energy models would be very useful for investigating potential energy savings. This opportunity stimulated the scientific community that conceived various modeling approaches, described by Zhou et al. (2016) in their review paper.

Gutowski et al. (2006) applied the Exergy analysis to manufacturing. A theoretical reverse trend between specific energy consumption (SEC energy per unit of processed material) and the material removal rate MRR was found. The SEC was also used for comparing different machining processes. Gtze et al. (2012) proposed a methodology for modeling the energy flows and devising energy savings in machine tools. Yang et al. (2016) proposed a learning-based modeling approach that allows analyzing the effect of cutting parameters on energy consumption. He et al. (2012) developed a technique for estimating the machine energy consumption directly analyzing the NC code. It was observed that the presented methodologies, due to the introduced approximations, are not useful in many interesting cases. For this reason, empirical approaches or approaches that combine empirical and analytical methodologies are preferable. For instance, Diaz et al. (2009) developed a simple model for estimating the consumed energy: a power contribution linked to the machine, measured when it is performing air cutting, and a term connected to the process were considered. Kara and Li (2011) proposed an empirical energy modeling that describes the relationships between the SEC and the main cutting parameters in turning.

Draganescu et al. (2003) extended the study to milling machines. Balogun and Mativenga (2013) developed an empirical machine power model that consider the MRR as the main process-related quantity. Despite the spindle system is one of the most important machine tool components, in many researches it was modelled in a very simple way: for instance, Mativenga and Rajemi (2011) proposed a model that considers exclusively the friction losses at different spindle speeds. Only few works that deal with machine tool energy consumption proposed more complex models for this component (i.e. (Borgia et al., 2016)).

Since it was demonstrated that energy can be saved through a proper cutting parameters selection (Diaz et al. (2009)), machine energy models have been used for the optimization of the machining

conditions. The first research works were focused on turning. For instance, Velchev et al. (2014) proposed a methodology for modelling and minimizing the SEC. Rajemi et al. (2010) dealt with the energy footprint minimization. For that purpose, they developed an energy model that considers the wear of the tool and the energy required for producing the inserts. Yi et al. (2015) worked on a multi-objective parameter optimization in turning where the absorbed energy and the surface finishing were simultaneously considered. Campatelli et al. (2014) adopted the response surface methodology for minimizing the power consumption in milling. Kant and Sangwan (2014) exploited a similar approach for optimizing both the absorbed energy and the surface quality. Albertelli et al. (2016) proposed a generalized multi-parameter energy optimization approach based on a combined empirical-analytical model suitable for milling applications. Li et al. (2014) experimentally demonstrated that both low energy consumption and high production rates can be simultaneously achieved by selecting the right cutting parameters. Yan and Li (2013) presented a multi-objective optimization methodology that opportunely weights energy consumption, process-rate and the quality of the machined parts. Wang et al. (2014) used a genetic algorithm for the above described optimization while Hanafi et al. (2012) adopted the grey relationship theory and the Taguchi approach.

Much research effort was also dedicated to the definition of specific energy-oriented machining strategies, Aramcharoen and Mativenga (2014). For instance, Newman et al. (2012) showed that energy consumption can be considered an additional criterion in process planning. Pavanaskar et al. (2015) demonstrated that a proper tool-path definition policy can be used for minimizing the energy consumption. Huang and Ameta (2014) developed a first rough tool for estimating the energy linked to the part production. Borgia et al. (2016) developed a simulation approach for predicting and minimizing the energy consumption during general milling operations. Altintas et al. (2016) used the response surface methodology for finding the machining strategy that assures the minimization of the consumed energy. Guo et al. (2015) developed an 1operation-mode simulation approach that can be used to simultaneously optimize, from the energy perspective, the tool path and the cutting parameters in turning.

Although the results of these researches demonstrated that appreciable energy savings can be achieved, the efficiency enhancement of machine tool components remains one of the most profitable ways for promoting sustainability in manufacturing. Several studies (i.e. Li et al. (2013)) focused on the reduction of the electric power absorbed when the machine is ready-to-operate were carried out. A relevant share of the energy is typically associated to cooling systems and hydraulic units. Some research projects dealt with the efficiency improvement of such systems. For instance, Brecher et al. (2012) analyzed two cooling systems from the energy consumption perspective: one that is based on state-of-art technology and another one equipped with an optimized solution. (Brecher et al., 2017) carried out a similar analysis on hydraulic units. In this study, the eco-efficient hydraulic units (i.e. equipped with a pressure booster or with an inverter coupled to an axial piston pump and accumulators) were compared to solutions based on BAT. Even machine tool auxiliary equipment suppliers autonomously developed their own eco-solutions: in some cases, quite relevant energy savings were achieved.

Focusing solely on energy consumption of machine auxiliaries is without doubts a too limiting approach. In fact, other groups of components can play a relevant role in the total consumption determination. This was demonstrated by Avram and Xirouchakis (2011) that quantified the energy shares of the machine sub-systems strictly connected to the cutting process. Although the studies showed that the spindle energy consumption can be relevant both in high and low cutting speed machining, only few literature research works were focused on the component enhancement. For instance, Abele et al. (2011) outlined some potential ways for increasing the efficiency of spindle systems. Even Harris et al. (2015) dealt with spindle system energy consumption reduction but focusing on a too narrow application (ultra-high spindles). In fact, in this research an electric and a pneumatic spindle were compared from the electric power demands perspective.

Since the topic seems quite unexplored, in this project it was decided to deeply analyze the energy saving opportunities of a novel spindle system conceptual design. More specifically, an innovative gear-less spindle solution suitable for multi-functional applications is studied from the energy consumption perspective. The development of such a solution was already indicated by Abele et al. (2010) as a future challenge in the development of a new generation of spindle systems. Moreover, the adoption of direct drive solutions is also promoted in ISO (2014) as an effective way for increasing the machine tool efficiency.

In the here presented research, the innovative spindle is compared with a classical spindle unit characterized by similar global performances but equipped with a gearbox-based module. The transmission makes the spindle adaptable to different applications (i.e. high torque, high speed cutting, drilling or threading). In the novel spindle solution, this adaptability is guaranteed by the electronic commutation of specifically designed stator winding circuits.

The elimination of the gearbox, together with the associated auxiliaries for lubricating and cooling, makes the novel solution particularly interesting from the energy saving point of view. On the contrary, the electrical motor is forced working over a wider range of spindle-torque combinations in which the best 150 electrical performances are probably not assured.

In this project, a methodology for performing the energy assessment of the two alternative spindle solutions was devised. The energy analysis was carried out using a combined experimental-modeling approach.

The two spindle units, equipped with the relative auxiliaries, were first experimentally characterized on a test rig. Experimental test results were used to develop empirical models that were successively exploited for inferring about the energy savings linked to the proposed direct drive spindle solution. In order to accomplish this task, a realistic scenario of use for the spindle was considered.

For making the study more general, a sensitive analysis changing the spindle working conditions used in the production batch emulation was carried out.

Methodology development

The relevance of the spindle system is demonstrated by numerous researches that were developed over the years for increasing performance and reliability of such a relevant machine tool component. In a key note paper, Abele et al. (2010) summarized the principal achieved results and outlined the main challenges in spindle future research:

- development of spindle technology for high torque and high-speed multifunctional applications
- energy consumption reduction focusing also on the peripheral equipment for drive, bearings, gearbox and on cooling system

- development of gear-less spindle solutions for high torque demanding applications (i.e. hard to cut materials like titanium alloys).

The listed challenges are also pulled by the market.

A spindle solution that fulfils the above reported specifications was developed in collaboration with a machine tool builder (Jobs) and a spindle manufacturer (HSD). The here presented report mainly focuses on the study of the energy saving opportunities linked the developed solution.

Spindle Test Case: system description

Since machine tools usually need to perform several machining operations on the same work-part, the spindle system has to be adequately designed for assuring the requested flexibility and the desired performances over such a wide range of working conditions. In modern machines, these challenging requirements are satisfied with consolidated design solutions. In most of the machine tools conceived for multiple applications, the spindle motor is connected to the cutting tool through a shiftable gearbox. In addition, sometimes a mechanical transmission can also be found. When high torque machining operations need to be carried out, the gearbox, reducing the rotating speed of the electrical

motor, provides the desired torque amplification. On the contrary, when high spindle speed operations need to be executed, the gearbox directly couples the electrical motor with the spindle shaft. This spindle solution is typically equipped with two chiller units and a hydraulic pump. The main chiller cools the electrical motor removing the losses related heat (i.e. bearing losses, viscous shear of air and electric motor losses). The pump assures an inlet flow of oil in the gearbox for lubrication and cooling purposes. The second chiller keeps the temperature of the motor oil within a suitable range. The schematic representation of the above described solution, for the studied Jobs machine (Jomax265), is reported in Figura 2-1, left side. Specifically, the spindle is equipped with an asynchronous AC Kessler motor and a Redex shiftable gearbox (transmission ratio $\tau = 1:5$). The motor and the gearbox chiller units (respectively KRA70J and KRO60J) are produced by Kelvin. Although this spindle system solution is widespread in modern machines, it exhibits some weak points. Indeed, the described solution is highly energy demanding. This is due to the auxiliary equipment (chillers and pump) requested for cooling the system. In addition, the losses associated to the gearbox contribute making this solution not particularly efficient. In order to overcome this issue, a novel gear-less spindle system solution was developed by Jobs and HSD. The new devised spindle system configuration is rather simplified: the gearbox, the oil pump and the gearbox chiller were eliminated (Figura 4-1, right side). The spindle is equipped with a HSD permanent magnet synchronous motor PMSM that assures, exploiting two different specifically designed stator windings, comparable performances in terms of the speed-torque characteristic curve.

Approach description

Although a rough estimation of the energy savings linked to the simplifications introduced to the auxiliary equipment can be easily envisaged, a comprehensive energy assessment of the two alternative spindle solutions is far from being an easy task and it requires a structured approach. In fact, several trade-offs need to be investigated. For example, the novel spindle solution, being based on a PMSM motor that is forced working over an extremely wide spindle speed range, could hardly achieve the motor efficiency assured by the AC asynchronous solution that exploits the amplification/reduction properties of the gearbox. Conversely, the gearbox is responsible for additional losses. Moreover, since the power absorbed by the chiller units strictly depends on the motor losses, as demonstrated by (Calvanese et al., 2013), a different chiller behaviour is expected in the compared spindle installations. In order to accomplish this task, a specific analysis approach was conceived, Figura 2-2. It is based on the development of reliable energy models for both the spindle systems. Even the auxiliaries were considered in the model. As suggested by Balogun and Mativenga (2013), an empirical approach was used in different phases of the model development (Paragraph 0): motor losses modeling, auxiliary equipment modeling, spindle efficiency modeling and spindle system global efficiency modeling.

Jomax 265
analyzed machine

ram and spindle system

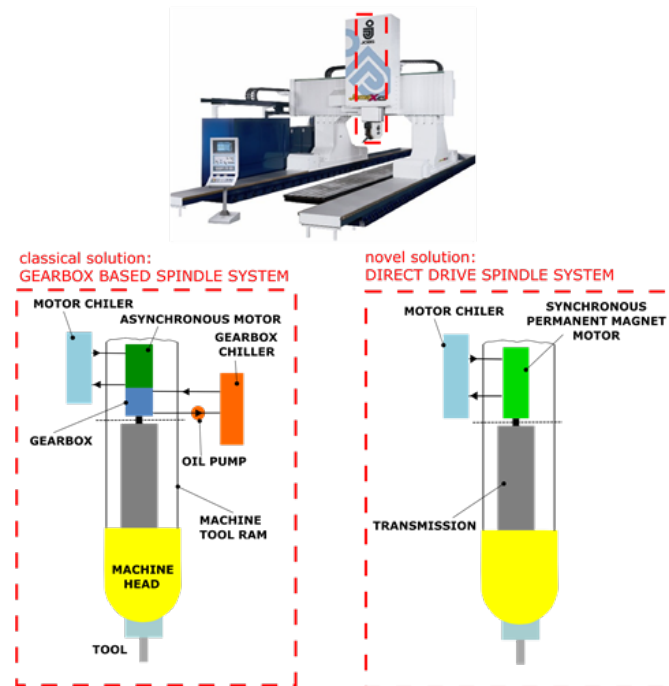


Figura 2-1 analyzed machine and spindle solutions comparison

The choice of adopting an empirical approach also for modeling the electrical motor losses was supported by a scientific literature analysis. In fact, although several studies on the motor losses modeling, both using analytical (i.e. Rahman and Zhou (1996)) or finite element FE approaches (i.e. Sizov et al. (2012)), have been done over the years, the empirical approach is still a largely diffused methodology for the electrical motors characterization. Moreover, the empirical approach allows taking into account the unknown losses such as the stray losses (Jimoh et al. (1985)). Since the necessity of considering the heat generated in the spindle and the role of the auxiliary equipment (chiller units and gearbox), the empirical approach seemed the sole suitable methodology for obtaining a reliable energy model of the overall spindle system. This is confirmed by the fact that the estimation of the heat generated through model is a challenging task and requires several experiments to identify the unknown model parameters, Bossmanns and Tu (1999).

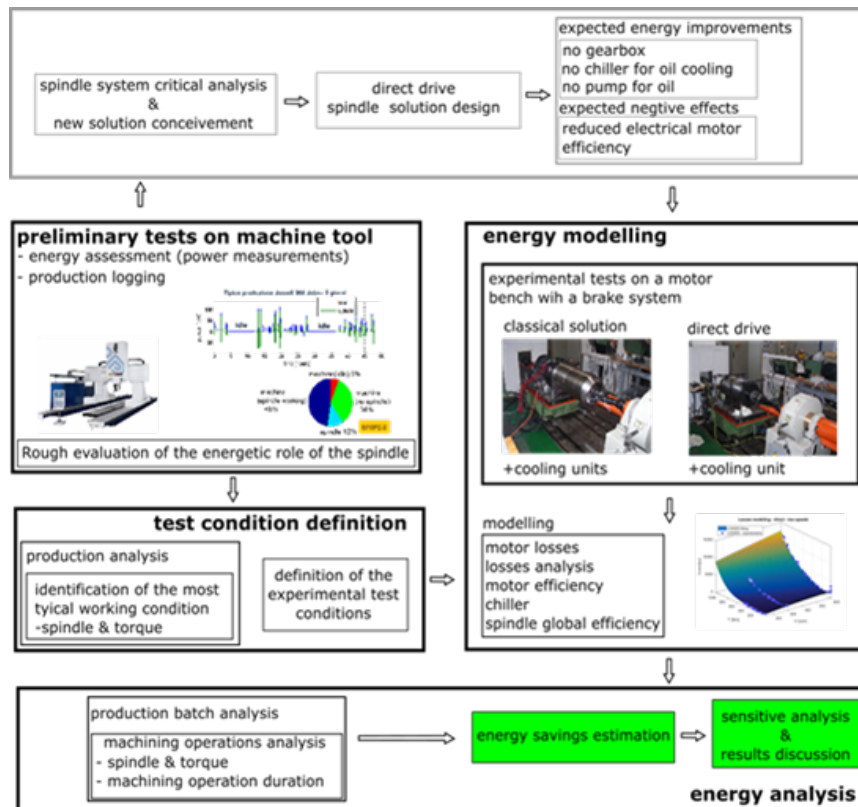


Figure 2-2 Approach used for the energy saving analysis

For identifying the described models, both the spindles were experimentally tested on a specific motor bench equipped with brakes (Paragraph 0). This allowed characterizing the spindles in different realistic cutting conditions, just reproduced setting the spindle speed and the braking torque (cutting torque) at the desired values. Further details on the adopted experimental procedure are reported. Suitable test conditions ("test condition definition") for the models development were defined (Subparagraph 0) analyzing the data acquired during two working (preliminary tests). These tests were also useful for performing a first rough machine tool energy assessment that put into evidence the role of the spindle in the overall machine tool energy consumption. The developed models were used for performing a meaningful energy assessment ("energy analysis") and a quantification of the achievable energy savings (Paragraph 0). This was done simulating the execution of a set of machining operations that belong to a real production batch. For sake of generality, sensitive analyses considering different machine task combinations were also carried out.

Spindle System experimental characterization

Preliminary tests on the machine during production

Power measurements and machine tool energy assessment

Some power measurements were carried out on the analyzed machine in order to obtain a preliminary energy characterization. In accordance with the guidelines under definition in (ISO, 2016), the energy assessment was done in the following machine configurations:

- machine in the "ready to operate" state
- machine during the execution of some production batches

For this purpose, the machine was equipped with a specifically designed power meter able to measure and storage power data of multiple electric loads. The following machine sub-systems were characterized: electrical cabinet, numerical controller NC, human machine interface HMI, machine drives, hydraulic unit, pumps and chillers. If a direct power measurement on a component was not possible, the absorbed power was estimated through differential power measurements. The active power of each considered machine subsystem $P_i(t)$ was computed considering $P_i(t) = i_{i1}(t)v_{i1}(t) + i_{i2}(t)v_{i2}(t) + i_{i3}(t)v_{i3}(t)$, where $v_{i1}(t)$, $v_{i2}(t)$, $v_{i3}(t)$ are the three-phases voltages and $(i_{i1}(t)$, $i_{i2}(t)$, $i_{i3}(t))$ are the corresponding absorbed currents. All the electrical quantities were acquired at a high sampling rate, $f_s = 30\text{kHz}$. The generic current $i_{ij}(t)$ was measured using a LEM ring based on the Hall's principle. The power absorbed by the machine and its main subcomponents in the "ready to operate" state are mapped in . The machine drives together with the NC unit absorb up to 30% (2.3kW) of the whole machine global power (7.78kW). Also the hydraulic unit plays a quite relevant role in terms of absorbed energy, 1.4kW (18%). It is worth of noting that the spindle auxiliary equipment (motor chiller (2.12kW), oil pump (0.26kW) and gearbox chiller (0.4kW)) accounted for 35% of the overall energy. For what concerns the energy assessment of the "shift regime" (according to ISO (2016) is a set of a representative tasks typically performed by the machine) it was decided to monitor mainly the global machine power and the spindle power. In this specific case, the powers were acquired for 48h, while the machine was processing real pieces. The production batches analysis brought to the conclusion that the machine was in the "idle" state for 34% of the analyzed time period T_p , the spindle was active for 35% of T_p and for the rest of the time the machine was active but without performing any machining operations. The map of the used energy is reported in **Figura 2-3**. This analysis was done in order to have an idea of the spindle contribution on the total absorbed energy. The overall machine energy E_{Mein} was computed integrating the measured machine power $P_{Mein}(t)$ over T_p , Eq. 1. It can be observed that the machine consumed about 6% of the overall energy E_{Mein} during the idle state, 34% when the spindle was not working and 48% when the the spindle was rotating.

$$E_{Mein} = \int_0^{T_p} P_{Mein}(t) dt \quad (1)$$

The spindle energy E_{sein} (computed integrating the measured spindle power $P_{sein}(t)$, Eq. 2) accounted for the 12% (178.8MJ) of the total energy (1.49GJ).

Although the spindle contribution E_{sein} (the sole linked to the electrical motor) was not the predominant one, it can be noted that the machine consumed a lot of energy (about 48%) when the spindle was active. This means that the spindle auxiliary equipment (chillers and the oil pump) played an important role from the energy consumption perspective.

This can be appreciated also looking at **Figura 2-4**, where both the spindle power and the power of the rest of the machine are reported for a portion of the analyzed production. It is clearly visible that when the spindle was working, even the rest of the machine was absorbing more power (+46%) with respect to the power absorbed when the spindle was not machining.

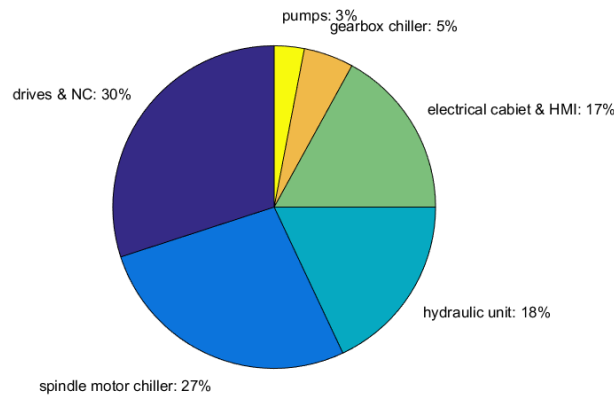


Figura 2-3 Ready to operate machine - power consumption distribution

This confirmed the importance of including the spindle related equipment in the energy analysis. This means that the power consumption of some machine tool subsystems (i.e. auxiliary equipment) is strongly related to the spindle losses. This relationship was not typically considered in almost all the papers on machine tool or spindle energy modeling.

Production analysis

A production logging system based on OPC server was set to monitor the machine during real production. In particular, the information about the tool code, the axes feed F , the spindle speed n and the spindle torque T were gathered. analyzing the acquired data, it was observed that the majority of the performed milling operations (mainly on steel and cast iron) were characterized by a spindle speed n that ranged from 180rpm to 510rpm and a spindle torque T that is within the 10-500Nm interval. These machining operations were executed with the spindle system set in the low speed-high torque configuration. For what concerns the machining operations carried out with the spindle in the high velocity configuration (i.e. drilling, threading), it was observed that the spindle speed n was set within the 2700-3200rpm interval while the requested torque T was extremely low (approximately negligible). This preparatory analysis was helpful for defining the experimental conditions to be reproduced on the spindle bench, Paragraph 0.

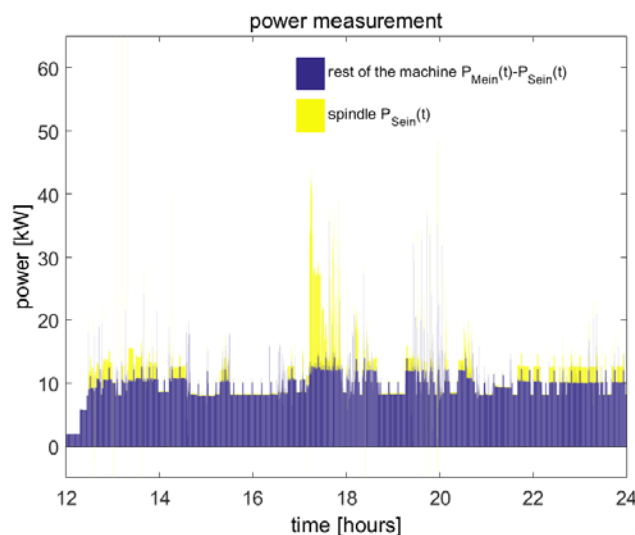


Figura 2-4: Power measurement during the execution of a production batch

Spindle system empirical energy characterization

In this report, a detailed description of the experimental procedure adopted for the spindle system energy characterization is provided. Data acquired during the experiments were used for the energy models development, Paragraph 0.

Energy model description

Before proceeding with the experimental procedure explanation, a general description of the adopted modeling approach is useful for a better comprehension of some performed choices. **Figura 2-1** accomplishes this task. Indeed, it shows a conceptual representation of the analyzed spindles with the system boundary definition and the considered energy flows. Moreover, the scheme shows how each spindle solution was experimentally characterized on the test bench.

The conceived model (Eq. 3) links the spindle global power consumption P_{Gein} to the requested mechanical power P_{Mout} that in this case stands for the requested cutting power P_{cutt} . The following relationship can be written defining the spindle speed n and torque T , $P_{Mout}(n, T) \equiv P_{cutt} = T \cdot n$.

$$P_{Gein} = f(P_{Mout}(\Omega, T)) \quad (3)$$

Using the model reported in Eq. 3 it would be possible to estimate the spindle power consumption for any cutting operation described by T and n .

As can be observed in Figura 2-5, P_{Gein} is the summation of the following contributions:

$$P_{Gein}(n, T) = P_{AUXein}(n, T) + P_{Sein}(n, T) \quad (4)$$

where P_{Sein} is the electrical power absorbed by the spindle motor while P_{AUXein} is the power consumption linked to the auxiliary equipment that depends on the analyzed spindle system configuration. For instance, if the gearbox-based solution is considered, P_{AUXein} can be computed through Eq. 5.

$P_{AUXein}(n, T) = P_{Scein}(n, T) + P_{Gcein}(n, T) + P_{Pein}(n, T)$ (5) where P_{Scein} is the electrical power absorbed by the motor chiller, P_{Gcein} is the electrical power absorbed by the gearbox chiller and P_{Pein} is the electrical power absorbed by the pump.

In terms of efficiency, according to Boglietti et al. (2003), the spindle efficiency can be therefore computed with Eq. 6

$$\eta_S(n, T) = \frac{P_{Mout}(n, T)}{P_{Sein}(n, T)} \quad (6)$$

Generalizing the concept to the overall spindle system, the global spindle efficiency η_{GS} can be computed through Eq. 7:

$$\eta_{GS}(n, T) = \frac{P_{Mout}(n, T)}{P_{Gein}(n, T)} \quad (7)$$

When a generic machining operation, performed at n , requires the cutting torque T , the overall spindle global power consumption can be estimated through Eq. 8

$$P_{Gein} = \frac{T \cdot n}{\eta_{GS}(n, T)} \quad (8)$$

The above equation cannot be used when the cutting power $P_{Mout} = 0$. In such a case, the spindle system global consumption needs to be calculated through Eq. 4.

The key point for developing the described model is the characterization of the overall spindle losses L_S as a function of n and T , Eq. 9:

$$L_S(n, T) = (P_{Sein}(n, T) - P_{Mout}(n, T)) \quad (9)$$

Focusing on the losses L_S , it was assumed that two main contributions are dominant, Eq. 10. One linked to friction $L_{SF}(n)$ that is affected mainly by the spindle speed n and another one associated to electric losses $L_{SE}(n, T)$. More details on the adopted friction model are provided in subparagraph 0.

$$L_S(n, T) = L_{SF}(n) + L_{SE}(n, T) \quad (10)$$

Eq. 4, Eq. 6 and Eq. 7 can be written in another way putting into evidence the losses L_S :

$$P_{Gein}(n, T) = P_{Mout}(n, T) + L_S(n, T) + P_{AUXein}(n, T) \quad (11)$$

$$\eta_S(n, T) = \frac{P_{Mout}(n, T)}{(P_{Mout}(n, T) + L_S(n, T))} \quad (12)$$

$$\eta_{GS}(n, T) = \frac{P_{Mout}(n, T)}{(P_{Mout}(n, T) + L_S(n, T) + P_{AUXein}(n, T))} \quad (13)$$

For being able to estimate η_{GS} , the auxiliary equipment power model $P_{AUXein}(n, T) = f(L_S(n, T))$ is therefore necessary.

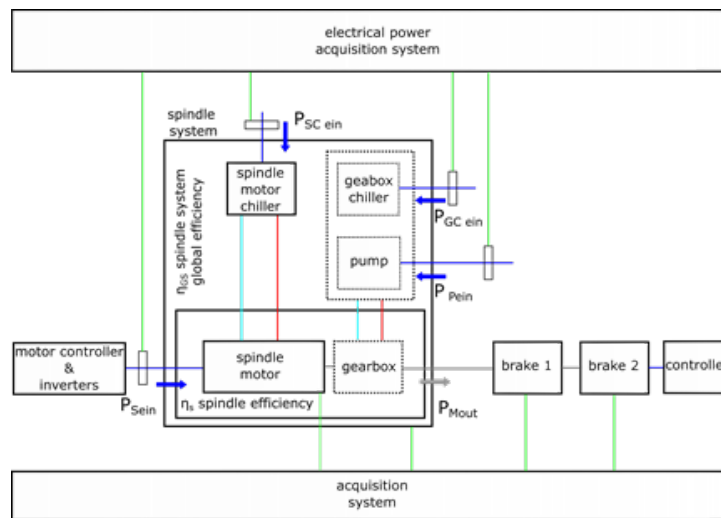


Figura 2-5: Schematic representation of the spindle on the bench - system boundaries and energy flows definition

Such a model puts into relationships the overall electrical power absorbed by the auxiliaries P_{AUXein} and the spindle losses L_S as defined in Eq. 9. In fact, the availability of $P_{AUXein}(n, T)$ and $L_S(n, T)$ allows computing P_{Gein} , η_S , η_{GS} .

It is worth of noting that both the losses $L_S(n, T)$ and the auxiliaries $P_{AUXein}(n, T) = f(L_S(n, T))$ models were empirically determined.

For this purpose, as shown in Figura 2-5, experimental tests were performed on the bench changing the spindle loading conditions ($n - T$) and monitoring the P_{GCein} , P_{SCein} , P_{Pein} and P_{Sein} powers. Moreover, in order to analyze the mechanisms that rule the spindle losses L_S (i.e. friction or electrical losses), some specific tests were carried out. More details can be found in Paragraph 0.

Experimental set-up description

The test bench used for the characterization of the spindle systems was depicted in Figura 2-6. It is composed of a spindle system bed that holds the spindle motor, two brakes connected in series with the control unit (Apicom VIBRU), a joint that mechanically connects the spindle shaft to the brakes and a module containing the spindle motor controller and the related drives (Siemens Simodrive 611). The test bench was also equipped with sensors and acquisition systems.

More specifically, the following quantities were measured during the tests:

overall torque T provided by the brakes (through Revere Transducers 363D3)

- spindle speed n through an encoder.
- currents and voltages of all the analyzed sub-units for the power computation of: P_{SCein} , P_{GCein} , P_{Pein} and P_{Sein} . The power computation of each unit was performed as described for the whole machine in the preliminary tests.
- temperatures (i.e. spindle and chiller temperatures). These quantities were acquired in order to monitor the thermal load of the spindle (especially spindle bearings) and of the chillers.

Tests description

For both the spindle system configurations two different test sessions were carried out.

- test A. According to Eq. 12, some tests were performed for the characterization of $\eta_S(n, T)$. For each selected spindle speed n , the overall brake load T (emulation of the cutting torque) was progressively increased up to the desired value that mainly depends on the technological requirements defined in subsection 3.1.2. Both P_{Mout} and P_{Sein} were measured during the tests. Spindle losses and consequently the η_S were computed respectively with Eq. 9 and Eq. 12. Such tests were repeated at different speeds both in the high torque and high velocity spindle configurations.

In Tabella 2-1 and Tabella 2-2 the experimental conditions used for the tests are reported.

- test B. This session was specifically conceived for the identification of the $P_{AUXein}(n, T) = f(L_S(n, T))$ relationship. The tests were carried out following the approach suggested in (Albertelli et al., 2016) where a linear model was proposed for the machine tool chiller units, Eq. 14.

$$P_{AUXein}(n, T) = P_{AUXein0} + m \cdot L_S(n, T) \quad (14)$$

The model parameters ($P_{AUXein0}$ and m) were identified through an experimental data regression procedure. More specifically, some tests were performed changing the loading conditions. For each test case, both the losses L_S and the P_{AUXein} were evaluated. In order to assure the achievement of the thermal stability, long run tests were carried out. For this purpose, some temperatures were measured during the tests. Since both

$P_{AUXein} = f(t)$ and $L_S = f(t)$ are time dependent (due to the chiller control strategy), the average values P_{AUXein} and L_S were computed before developing the energy model. For instance, focusing on the generic test performed with the $T_j - n_j$ combination, it was done using the following relationships.

$$\overline{P_{AUXein}}(n_j, T_j) = \frac{1}{t_{2j} - t_{1j}} \int_{t_{1j}}^{t_{2j}} P_{AUXein}(n_j, T_j, t) dt \quad (15)$$

$$\overline{L_S}(n_j, T_j) = \frac{1}{t_{2j} - t_{1j}} \int_{t_{1j}}^{t_{2j}} L_S(n_j, T_j, t) dt \quad (16)$$

where $t_{2j} - t_{1j}$ is the duration of the j^{th} long run test. The auxiliary equipment model was developed exploiting at least three different working conditions $L_S(n, T)$, see Tabella 2-1 and Tabella 2-2.

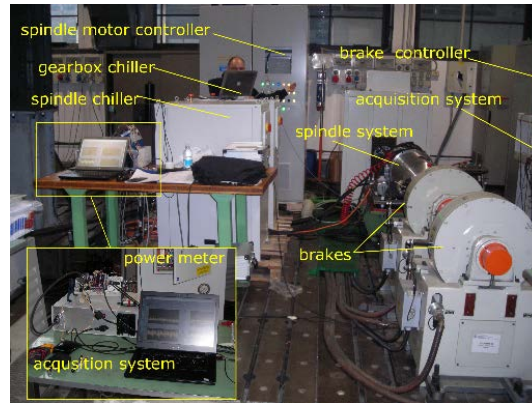


Figure 2-6: Test bench and instrumentation set-up

Test Type	Configuration	n [rpm]	T [Nm]
Type A	high torque	150	0; 35; 83; 110; 164; 224; 260; 304; 349; 407; 470
Type A	high torque	300	0; 56; 100; 148; 207; 282; 313; 409; 458; 511; 570; 611
Type A	high torque	600	0; 5; 10; 14; 25; 31; 57; 74; 99; 127; 152; 205; 255; 303; 344; 394; 412; 516; 573; 614; 666
Type A	high speed	2500	0; 3; 5; 9; 16; 32; 39; 47; 56; 64; 75; 101; 125; 136; 152
Type A	high speed	3000	0; 4; 18; 21; 38; 59; 80; 84; 100; 111; 121; 132; 144
Type A	high torque	3500	0; 5; 11; 13; 21; 40; 45; 50; 56; 68; 91; 100; 110; 120
Type B	high torque	300	800
Type B	high torque	600	210
Type B	high speed	1500	160

Tabella 2-1 Experimental test conditions for the gearbox-based spindle solution

- test C. According to Eq. 10, a specific experimental procedure was conceived for the spindle friction losses L_{SF} characterization. For this purpose, coast tests were carried out for both the spindle systems. The test consists in putting into rotation the spindle system at a certain rotation speed, unplug the motor from the drive and wait until the spindle naturally stops due to friction. Since the motor was not

connected to the drive, the adopted procedure assured to identify the sole contribution due to friction L_{SF} . A similar methodology was also used in (Bossmanns and Tu, 2001).

The relationship that describes the dynamic equilibrium of the system during the coast test is reported in Eq. 17. $J_m [kg \cdot m^2]$ is the overall spindle inertia reduced to the motor side, $\dot{\omega}_m [rad/s^2]$ the motor acceleration and $T_F [Nm]$ the overall present friction torque referred to the motor.

$$J_m \cdot \dot{\omega}_m(t) + T_F(\omega_m) = 0 \quad (17)$$

Since the overall inertia J_m can be easily identified using a specific procedure available on the motor drive, $\omega_m(t)$ is measured during the test and subsequently derived, the friction torque, at different speeds, can be computed using Eq. 17. Consequently, the friction power losses $L_{SF}(n)$ as a function of the spindle speed n can therefore be estimated:

$$L_{SF}(n) = T_F(n) \cdot \frac{60 \cdot n}{2\pi \cdot \tau} \quad (18)$$

Repeating the coast test with different spindle configurations (i.e. for the gearbox-based spindle system), it was also possible to characterize the friction contribution associated to the motor shaft (mainly due to the friction of bearings and the viscous shear of air), associated to the gearbox (for both the available gearbox shifts) and to the load (i.e. the friction⁵³⁰ introduced by the brake for the tests performed on the test-bench). The same characterization approach was used also for the direct drive spindle solution. In Eq. 18, depending on the analyzed configuration, the transmission ratio was set at $\tau = 1$ (i.e. for direct drive spindle system or for the gearbox-based spindle when used at high speeds) and at $\tau = 1/5$ when the gearbox-based spindle is used in the low speed range.

Test Type	Configuration	n [rpm]	T [Nm]
Type A	high torque	150	0; 6; 75; 100; 162; 200; 246; 298; 354; 401; 445; 469
Type A	high torque	300	0; 56; 100; 157; 198; 253; 315; 354; 397; 458; 498; 600; 633; 692
Type A	high torque	600	0; 50; 92; 102; 129; 203; 277; 302; 349; 398; 453; 498; 532; 599; 691
Type A	high speed	2500	0; 1; 29; 48; 54; 94; 103; 149; 173; 200; 211; 221; 242
Type A	high speed	3000	0; 2; 43; 49; 64; 90; 98; 125; 147; 149; 170; 189
Type A	high torque	3500	0; 3; 21; 43; 50; 99; 114; 147; 158
Type B	high torque	300	800
Type B	high torque	600	800
Type B	high speed	1500	210
Type B	high speed	3000	170

Tabella 2-2 Experimental test conditions for the gearbox-based spindle solution

Spindle system energy modeling

Spindle losses modeling

A multiple linear regression approach (Montgomery, 2001) was used for developing empirical models. The spindle losses models $L_S(n, T)$ were developed first. Polynomial functions were used for fitting the experimental data, Figura 2-7. A specific model was developed according to the analyzed spindle

system configuration (low/high speed). For instance, a 2nd-order function in the variable n and a 4th-order function in the variable T (Eq. 19) was used for modeling the losses when the spindle is in the low speed configuration. For the high spindle speed range, it was found that functions of the 2nd-order in the variable n and a 3rd-order function in the variable T (Eq. 20) fit quite well the experimental data of both the spindles. Referring to Eq. 19 and Eq. 20, p_{mn} are the regression coefficients that were estimated (\hat{p}_{mn}) through a least square minimization. ϵ is the error term in the models. For all the regressions quite high coefficients of determination ($R_{sqadj} > 0.98$) were found.

$$\begin{aligned}
 L_{S_{low\ speed}}(n, T) = & p_{00} + p_{10} \cdot n + p_{01} \cdot T + \\
 & p_{20} \cdot n^2 + p_{11} \cdot n \cdot T + p_{02} \cdot T^2 + \\
 & p_{21} \cdot n^2 \cdot T + p_{12} \cdot n \cdot T^2 + p_{03} \cdot T^3 + \\
 & p_{22} \cdot n^2 \cdot T^2 + p_{13} \cdot n \cdot T^3 + p_{04} \cdot T^4 + \epsilon
 \end{aligned} \quad (19)$$

$$\begin{aligned}
 L_{S_{high\ speed}}(n, T) = & p_{00} + p_{10} \cdot n + p_{01} \cdot T + \\
 & p_{20} \cdot n^2 + p_{11} \cdot n \cdot T + p_{02} \cdot T^2 + \\
 & p_{21} \cdot n^2 \cdot T + p_{12} \cdot n \cdot T^2 + p_{03} \cdot T^3 + \epsilon
 \end{aligned} \quad (20)$$

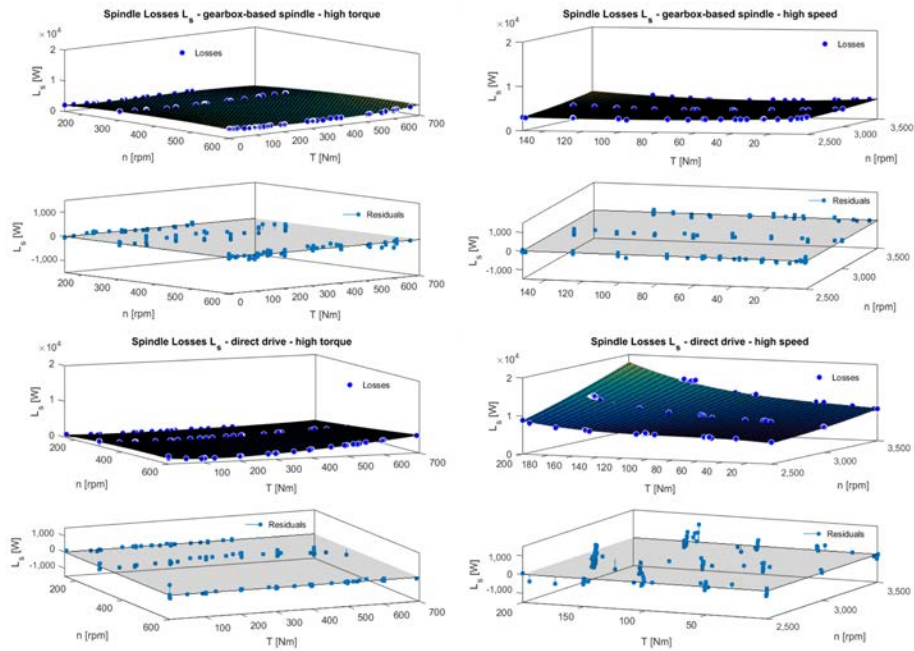


Figure 2-7: Spindle losses regression - spindle solutions comparison

In Figura 2-7, the residuals plots are also reported for each developed model. The identified parameters are reported below:

- gearbox-based spindle (high torque configuration): $p_{00} = 2,329$, $p_{10} = 123.5$, $p_{01} = 471.1$, $p_{11} = 86.62$, $p_{20} = -172.4$, $p_{02} = 546.1$, $p_{21} = -172.6$, $p_{12} = 298$, $p_{03} = 196.1$, $p_{22} = -176.7$, $p_{13} = 184.1$, $p_{04} = 123.9$ where n is normalized by mean $483.3rpm$ and standard deviation $183.6rpm$ and similarly T is normalized by mean $468.8Nm$ and standard deviation $269.6Nm$
- direct-drive spindle system (high torque configuration): $p_{00} = 2456$, $p_{10} = 931.3$, $p_{01} = 1,933$, $p_{11} = 536.6$, $p_{20} = 71.67$, $p_{02} = 800.2$, $p_{21} = -44.38$, $p_{12} = -11.15$, $p_{03} = 327.7$, $p_{22} =$

-54.75, $p_{13} = -57.44$, $p_{04} = 107.7$ where n is normalized by mean 356.1rpm and standard deviation 142.3rpm and similarly T is normalized by mean 628.7Nm and standard deviation 265.3Nm

- gearbox-based spindle (high speed configuration): $p_{00} = 3083$, $p_{10} = 278.4$, $p_{01} = -188.5$, $p_{11} = 110.7$, $p_{20} = 110$, $p_{02} = 287.9$, $p_{21} = 32.89$, $p_{12} = 100.6$, $p_{03} = -20.21$ where n is normalized by mean 2821rpm and standard deviation 402.3rpm and similarly T is normalized by mean 63.2Nm and standard deviation 49.08Nm
- direct-drive spindle (high speed configuration): $p_{00} = 9340$, $p_{10} = 2306$, $p_{01} = 2652$, $p_{11} = 1133$, $p_{20} = 243.9$, $p_{02} = 1260$, $p_{21} = 5.972$, $p_{12} = 2420$, $p_{03} = 268.1$ where n is normalized by mean 2922rpm and standard deviation 375.6rpm and similarly T is normalized by mean 153.3Nm and standard deviation 60.83Nm

Spindle losses analysis

Regarding the losses analysis, as anticipated in the previous section, specific tests were executed to identify the power losses due to friction. The model reported in Eq.17 was further developed assuming that the friction torque T_F is twofold, Eq. 21.

$$J_m \cdot \dot{\omega}_m(t) + c_{vF} \cdot \omega_m(t) + c_{sF} = 0 \quad (21)$$

Where c_{vF} is the viscous friction coefficient and c_{sF} the static friction coefficient. The parameters of the model can be identified through a regression procedure. More specifically, the experimentally measured motor speed $\omega_m(t)$ was fitted with the solution (Eq. 23) of the first order differential equation that describes the free spindle deceleration (Eq. 22).

$$\begin{cases} \dot{\omega}_m(t) + \frac{c_{vF}}{J_m} \cdot \omega_m(t) = -\frac{c_{sF}}{J_m} \\ \omega_m(0) = \omega_{m0} \end{cases} \quad (22)$$

Where ω_{m0} represents the initial condition.

$$\omega_m(t) = \omega_{m0} \cdot e^{-\frac{c_{vF}}{J_m} \cdot t} - \frac{c_{sF}}{c_{vF}} + \frac{c_{sF}}{c_{vF}} \cdot e^{-\frac{c_{vF}}{J_m} \cdot t} \quad (23)$$

Eq. 23 was rewritten (Eq. 24) just after having defined the following quantities: $p = -c_{vF}/J_m$ and $k = -c_{sF}/c_{vF}$.

$$\omega_m(t) = \omega_{m0} \cdot e^{-pt} + k - k \cdot e^{-pt} \quad (24)$$

p and k were estimated through the regression procedure. The friction model parameters c_{sF} and c_{vF} were further computed.

For sake of generality, the friction characterization procedure is here demonstrated for the gearbox-based spindle. Indeed, in such case the identification of the friction contribution due to the gearbox was also necessary.

Referring to **Figura 2-8**, the deceleration curves $\omega_m(t)$ of the spindle in three different configurations are reported. The motor with the coupled gearbox (*motor+gearbox*) was the first tested system. The gearbox was set in the high shift configuration. The test was also repeated mechanically connecting the load to the motor-gearbox group (*motor+gearbox+load*). The friction contribution due to the brake (*load*) resulted from the

subtraction of the previously identified friction parameters. The third test was executed with the gearbox in the low speed configuration.

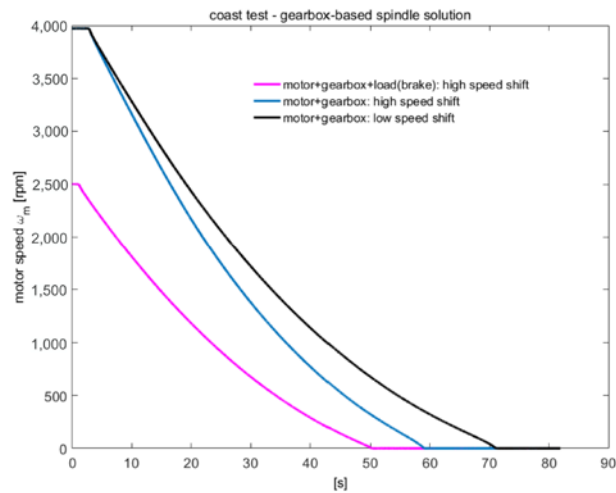


Figure 2-8: Coast test - gearbox-based spindle

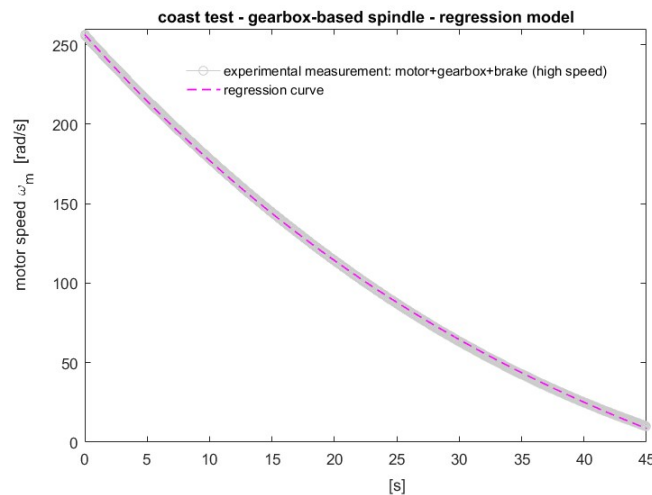


Figure 2-9: Coast test - example of regression curve

The identified friction parameters are reported in **Tabella 2-3**. Similar experiments were also carried out with the sole electrical motor in order to characterize the friction contribution L_{SFm} due to the bearings and due to the viscous shear of air, Bossmanns and Tu (2001).

The friction parameters estimation relies on (Eq. 23 and Eq. 24) a former system inertia J_m identification. It was carried out through a specific tool available on the Siemens drive. The identified moments of inertia are reported in **Tabella 2-4**. Just as an example, the regression of one of the deceleration curves is reported in Figure 2-9. The model shows a good agreement with the experimental measurements. For all the analyzed cases, quite high coefficients of determination ($R_{sq_{adj}} > 0.99$) were found.

Moreover, the comparison between the measured friction power (Eq. 17) and the friction power computed using the implemented model (Eq. 21) is reported in **Figure 2-10**.

The good matching between the curves shows that even a quite simple model can be used to predict the friction losses in a spindle system.

Eq. 10 can therefore be rewritten putting into evidence all the identified losses contribution. For what concerns the direct drive spindle solution, Eq. 10 becomes Eq. 25

$$L_S(n,T) = L_{SE}(n,T) + L_{SF}(n) = L_{SE}(n,T) + L_{SFml}(n) = L_{SE}(n,T) + L_{SFm}(n) + L_{SFfl}(n) \quad (25)$$

where the friction losses $L_{SF} \equiv L_{SFml}$ accounts for the contribution of the *motor* L_{SFm} and the contribution of the *load* L_{SFfl} . L_{SFm} can be neglected if compared to other terms, especially when the direct drive spindle is rotating at low speeds. For the gearbox-based spindle system, the following equation can be written:

$$L_S(n,T) = L_{SE}(n,T) + L_{SF}(n) = L_{SE}(n,T) + L_{SFmgl}(n) = L_{SE}(n,T) + L_{SFmg}(n) + L_{SFfl}(n) \quad (26)$$

where the friction losses $L_{SF} \equiv L_{SFmgl}$ accounts for the *motor+gearbox* friction losses L_{SFmg} and for the *load* L_{SFfl} contribution. It was found that L_{SFmg} is mainly due to the the contribution linked the gearbox rather than the one connected to the *motor* L_{SFm} .

test configuration	$c_{vF} [Nm/(rad/s)]$	$c_{sF} [Nm]$
<i>motor + gearbox + load</i> (high speed shift)	0.0144	1.8
<i>motor + gearbox</i> (high speed shift)	0.0074	1.1324
<i>motor + gearbox</i> (low speed shift)	0.0054	0.7924
<i>load</i>	0.007	0.6696

Tabella 2-3 Identified friction coefficients

test configuration	$J_m [kg \cdot m^2]$
<i>motor + gearbox + load</i> (high speed shift)	0.618
<i>motor + gearbox</i> (high speed shift)	0.312
<i>motor + gearbox</i> (low speed shift)	0.27

Tabella 2-4 Identified inertia

When the gearbox-based spindle rotates at low speed, L_{SFm} is higher than the corresponding one in the direct drive. This is linked to the fact that the motor, due to the role of the gearbox, is rotating at higher speeds if compared to the load. On the contrary, the friction losses L_{SFm} are similar in both the spindle systems for the high-speed rotating speeds.

Figura 2-11 and **Figura 2-12** underline the main losses contributions defined in Eq. 25 and Eq. 26 for both the low speed and high speed ranges. It can be observed that in the high speed range the direct drive spindle losses L_S are higher than in the traditional spindle system. This is mainly linked to the electric losses L_{SE} : they are close to be double if compared to the whole losses ($L_{Smg} + L_{SE}$) of the traditional spindle. This is mainly due to the control strategy used in the PMSM direct drive spindle. At low spindle speeds, on the contrary, the losses L_S observed in the traditional spindle solution are close to be double to the one of the direct drive spindle.

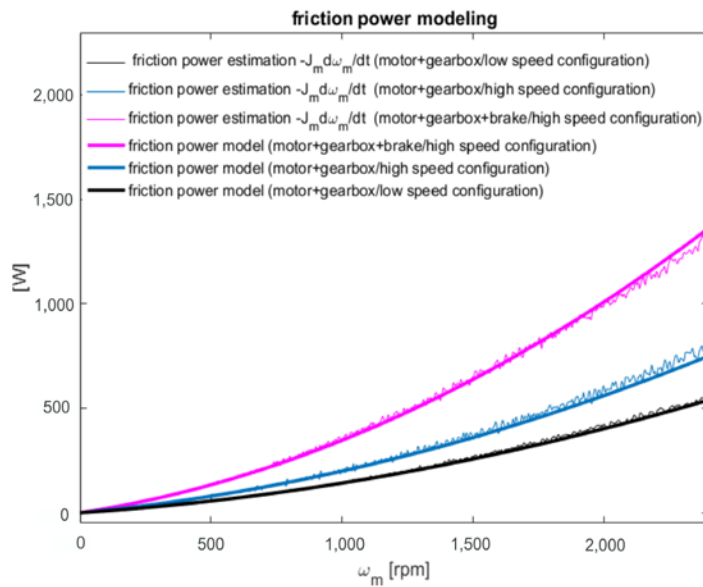


Figure 2-10: Friction power comparison - estimated through measurements Vs estimated through model

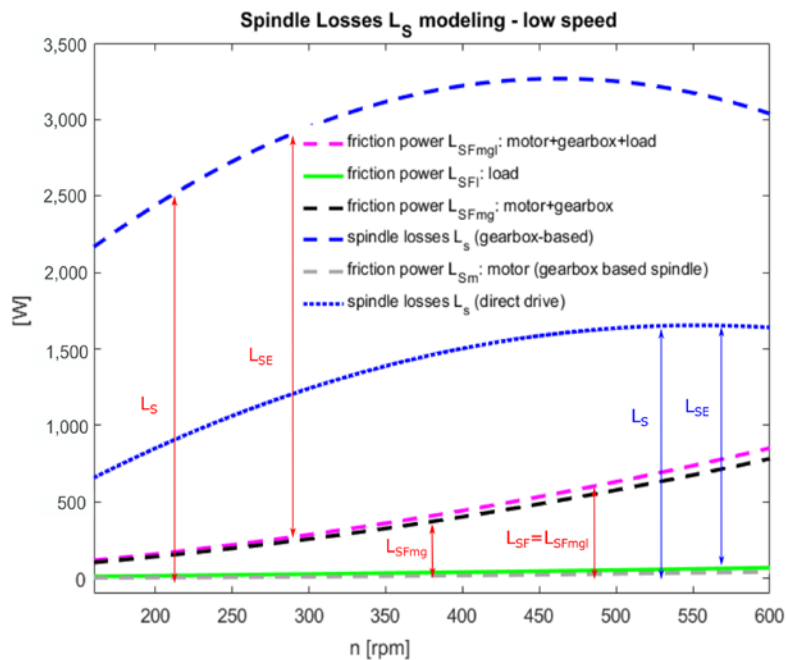


Figure 2-11: Spindle losses map - low speed configuration ($T = 0$)

This is surely due to the losses associated to the transmission but even more due to high electrical losses L_{SE} of the traditional spindle system. Since each spindle system has their own weak and strong points from the losses perspective, a more detailed analysis considering a realistic scenario of use is requested to infer about the two solutions.

Spindle efficiency modeling

In this Section the spindle efficiency models $\eta_S(n, T)$ were obtained using the methodology already presented in Section 4.1: experimental observations of $\eta_S(n, T)$ were first computed using Eq. 6 and then fitted with regression models.

For developing the $\eta_{GS}(n, T)$ models, it was necessary to identify the parameters (Tabella 2-5) of the model reported in Eq. 14.

As already anticipated, long run experimental tests were carried out for obtaining suitable data ($P_{AUXein}(n_j, T_j)$, $L_S(n_j, T_j)$) for the model development. It can be observed that for the gear-box based spindle, due to the presence of the oil pump and gearbox chiller, the identified model shows higher $P_{AUXein0}$ and m values.

Using Eq. 13 and Eq. 14 it was possible to compute $\eta_{GS}(n, T)$ for all the tested conditions, **Figura 2-13**.

The detrimental effect of the auxiliary equipment on the spindle efficiency ($\eta_S \rightarrow \eta_{GS}$) can be appreciated.

It strongly depends on the analyzed spindle system, on the spindle configuration (high torque or high speed) and on the working conditions.

Finally, a regression model was also developed for η_{GS} .

The comparison between the performance of the analyzed spindles in terms of global efficiency η_{GS} can be over-viewed in **Figura 2-14** where the percentage difference were reported for the analyzed n and T ranges.

When the spindle works at low spindle speeds, the efficiency of the novel spindle solution η_{GS} is higher (up to 14%) than the one observed for the classical solution. This is mainly due to the energy absorbed by the pump and the gearbox chiller.

For what concerns the spindle behaviour in the high speed range, the direct drive solution exhibits a worse global efficiency η_{GS} (up to -14%) although it strongly depends on the loading conditions.

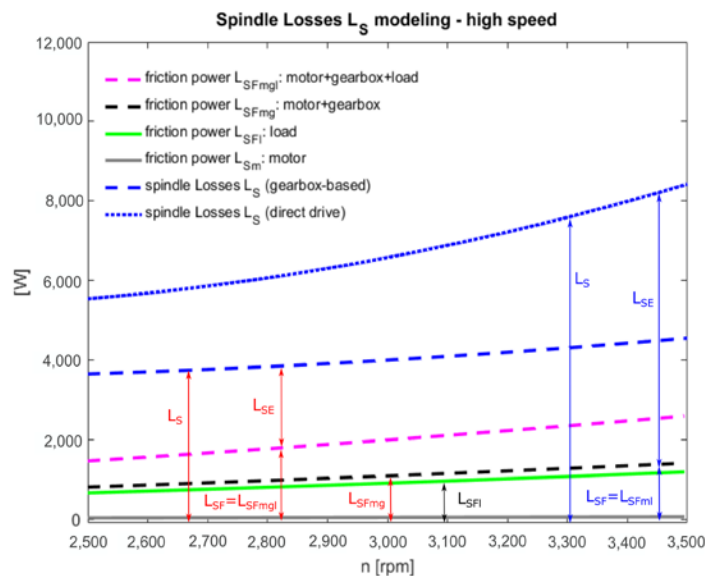


Figura 2-12: Spindle losses map - high speed configuration (T = 0)

Spindle system	$P_{AUXein0}$ [W]	m
----------------	-------------------	-----

Gearbox-based spindle	2808	0.117
Direct-drive spindle	2162.8	0.092

Tabella 2-5: Identified parameters of the auxiliary equipment energy model

This trade-off needs to be investigated. The direct drive spindle shows higher L_s but at the same time lower P_{AUX} .

Such high observed motor losses L_s are intrinsically connected to the motor type used for the direct drive solution (PMSM) that needs, when the speed increases, a weakened magnetic flux. The field weakening is obtained by increasing the motor direct current i_d that is typically set at $i_d = 0$ when the motor is rotating at low spindle speeds.

The i_d increment has a detrimental effect on the copper losses, Pillay and Krishnan (1989). The field weakening is a strategy that assures the reduction of the back-electromotive force (back-EMF) and consequently the prevention of the drive voltage limitation crossing, Liu (2005). Despite the high losses, the motor efficiency η_s values are within typical ranges for the considered motor type, Cavallaro et al. (2005).

This demonstrates that the PMSM was properly designed for the application.

On the contrary, in order to fulfil the drive voltage limitation when the asynchronous motor AC is put into rotation at high speed, the stator phase current is reduced. This makes the spindle losses increasing less with the velocity if compared to the direct drive solution.

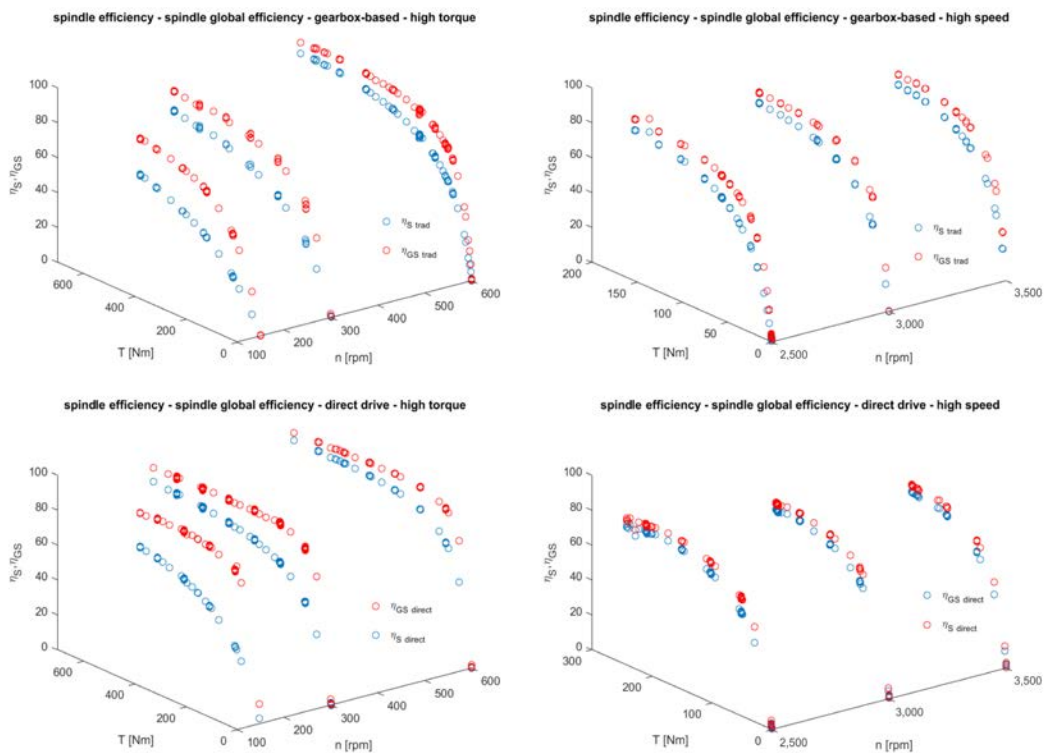


Figura 2-13: Spindle efficiency η_s - spindle global efficiency η_{GS} - experimental observations

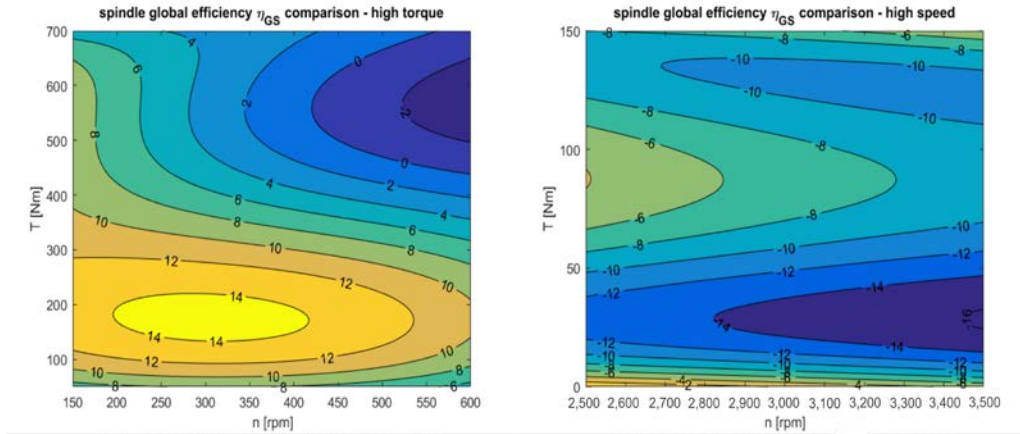


Figura 2-14: Spindle global efficiency η_{GS} modeling and comparison (percentage values)

It is worth of noting that a trivial evaluation of the energy assessment of both the solution is not adequate. In order to tackle this issue, it was decided to estimate the potential energy savings that could be achieved with the novel direct drive solution referring to realistic machine working conditions. The results of the analysis are reported in Paragraph 0.

Model Validation

In this section, the validation of the developed spindle energy model is reported. For this purpose, a real cutting test (a face milling operation) was carried out through the machine (*Jomax265*) equipped with the traditional gearbox-based spindle solution. The experimentally acquired spindle power P_{Sein} was compared to the power estimation performed through the developed model, Eq. 27.

For sake of generality, it was decided to focus on a machining operation with a not negligible contribution for what concerns the cutting power demand, P_{cutt} .

More specifically, in the model validation test, a portion of machine tool (Steel S355) basement was machined using the tool and the cutting parameters reported in **Tabella 2-6**. The power absorbed by the spindle P_{Sein} was estimated considering different contributions, as reported in Eq. 27.

Parameter	Value
processed material	steel S355
tool diameter D	160mm
number of teeth Z	8
lead angle	90degree
spindle speed n	600rpm
axes feed F	1200mm/min
axial depth of cut a_p	2mm
radial depth of cut	120mm
a_e	

Tabella 2-6: model validation - tool and cutting conditions

$$P_{Sein}(n, T) = L_S(n, T) + P_{cutt} = L_{SF}(n) + L_{SE}(n, T) + P_{cutt} \quad (27)$$

The cutting power P_{cutt} and the respective cutting torque ($T \approx 199Nm$), that depend on the processed material, tool properties and on cutting parameters, were estimated through the milling simulation software CutPro, (MAL, 2008).

Both the friction losses L_{SF} and the electrical losses L_{SE} were estimated through the developed models and knowing the spindle working conditions in terms of n and T .

As can be observed in **Figura 2-15**, the agreement between the spindle power P_{Sein} prediction and the measured value is good.

Indeed, the error in the estimation is about 2.7%. It was observed that in this specific cutting condition, the cutting power P_{cutt} accounts for the 84.2% of the spindle power P_{Sein} , the friction losses L_{SF} for the 5.7% and the electrical losses L_{SE} for the 10.1%.

The reported validation demonstrates that the developed spindle energy modeling approach can be reliably used for estimating the absorbed spindle power of real machining operations and that the model is an extremely useful instrument for performing the assessment of the energy savings presented in Paragraph 0.

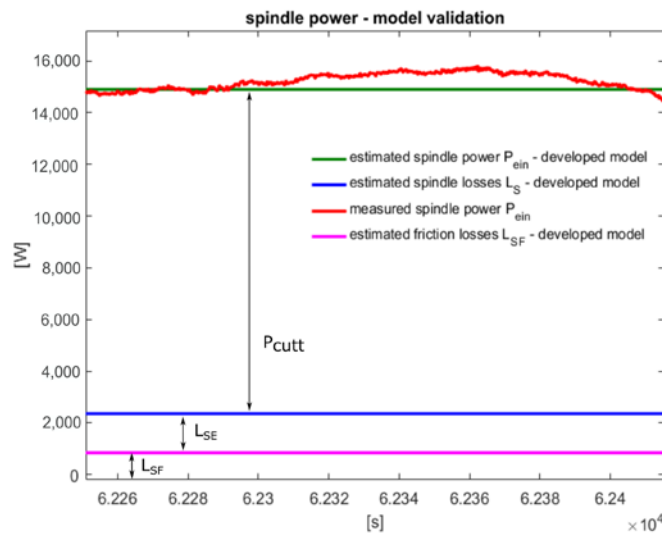


Figura 2-15: Spindle power P_{Sein} - comparison between experimental measurement and model estimation

Energy savings evaluation and results discussion

In the presented research, it was not possible to arrange proper cutting tests using both the analysed spindle systems. Indeed, it would have requested the substitution of the traditional spindle with the direct drive one on the analyzed machining centre (Jomax265) and this would have involved unacceptable drawbacks for the company that is still using the machine for its regular production. As already described, this limitation was fully overcome performing the experimental tests on the bench that is equipped with the brakes for emulating the cutting process.

This approach allowed testing and comparing both the spindles in several cutting conditions and it did not introduce any limitation or restriction for what concerns the validity of the energy evaluation. Indeed, the power consumption comparison between the traditional and direct drive spindles was done at the net of the cutting power that was identically extracted (intended as power flow) to both the spindle systems just setting the same value of torque T (through the brake) at the same rotational speed n . In addition, for being able to compare the power consumption and the efficiency of both the spindles in any generic working condition within the tested ranges of torque and speed, suitable models were developed and validated, Paragraph 0.

Although the results achieved in Paragraph 0 are intrinsically valuable they are not so useful because they are not contextualized from the manufacturing point of view. For this reason, a proper energy saving analysis was performed considering a realistic production scenario for the analyzed machine.

For sake of generality, in the selected reference production batch, the machine tool performed both low speed (roughing (high torque) - finishing (low torque)) operations and high speed-low torque (i.e. drilling and threading) operations. The machine was monitored for two real shifts (T_p ' 16h) and for each performed machining operation, the requested average spindle torque T_K , the spindle speed n_K and the duration Δt_K were gathered. Moreover, the global machine power $P_{Mein}(t)$ and the spindle power $P_{Sein}(t)$ were both experimentally measured.

The energy savings ΔE_{TOT} estimation was carried out with the support of the developed losses L_S models. As already anticipated, the comparison was done at null of the cutting power. ΔE_{TOT} was computed, as explained by Eq. 28, considering both the contribution due to the spindle ΔE_S and the one linked to the auxiliary equipment, that is twofold: ΔE_{AUX} and ΔE_{AUX_0} . Both the terms are strictly connected to the less energy demanding cooling system used in the direct drive spindle solution. More specifically, ΔE_{AUX} represents the energy saving that can be obtained when the spindle is performing a proper cutting while ΔE_{AUX_0} is the energy saved during the ready-to-operate state.

$$\Delta E_{TOT} = \Delta E_{AUX} + \Delta E_{AUX_0} + \Delta E_S \quad (28)$$

ΔE_{AUX} was estimated using Eq. 29, where $\Delta P_{AUXein}(n_K, T_K)$ is the difference, for each machining operation, between the electric powers absorbed by the two cooling systems.

$$\Delta E_{AUX} = \sum_{K=1}^n \Delta E_{AUX_K} = \sum_{K=1}^n \Delta P_{AUXein}(n_K, T_K) \cdot \Delta t_K \quad (29)$$

As can be observed, ΔE_{AUX} depends on the considered machining operations. Such a detailed analysis was possible thanks to the developed cooling system modeling that puts into relationship the chiller power with the spindle load, Eq. 14.

ΔE_{AUX_0} was computed using Eq. 30: it does not depend on the performed machining operations but it is strictly related to the time duration T_0 the machine is in the ready-to-operate state.

$$\Delta E_{AUX_0} = \Delta P_{AUXein_0} \cdot (T_p - \sum_{K=1}^n \Delta t_K) = \Delta P_{AUXein_0} \cdot T_0 \quad (30)$$

For what concerns the energy savings strictly connect to the spindle, they can be computed as reported in Eq. 31 where $\Delta L_S(n_K, T_K)$ represents the losses difference among

the two alternative spindle solutions. Even in this case, ΔE_S is spindle task dependent, **Figura 2-7**.

$$\Delta E_S = \sum_{k=1}^n \Delta E_{S_K} = \sum_{k=1}^n \Delta L_S(n_K, T_K) \cdot \Delta t_K \quad (31)$$

ΔE_S is evaluated at null of the cutting power P_{cutt} that is equal for both the analyzed spindle solutions.

The reported equations were used for estimating the potential energy savings in the following situations:

- the execution of a set of machining operations (taken as the reference case) extracted from a real production batch.
- the execution of fictitious production scenarios originated from the reference case. Indeed, a sensitive analysis was performed changing some parameters in order to generalize as much as possible the results. In particular the following simulations were done.

A sensitive analysis was performed changing the durations of all the considered machining operations (Δt_K). This roughly emulated the processing of similar workpieces (same requested n_K - T_K combinations) but with different dimensions. For doing that, each Δt_K was varied up to $\pm 40\%$ as reported in **Tabella 2-7**. For all the simulations, the same T_0 observed in the reference case was used because it was assumed that the same amount of time is approximatively requested for setting a new workpiece in the machine.

case	high torque configuration	high velocity configuration	scenario
a	$1.4 \cdot \Delta t_K$	$1.4 \cdot \Delta t_K$	different dimensions
b	$1.2 \cdot \Delta t_K$	$1.2 \cdot \Delta t_K$	different dimensions
n	$1 \cdot \Delta t_K$	$1 \cdot \Delta t_K$	reference condition
c	$0.8 \cdot \Delta t_K$	$0.8 \cdot \Delta t_K$	different dimensions
d	$0.6 \cdot \Delta t_K$	$0.6 \cdot \Delta t_K$	different dimensions

Tabella 2-7: Sensitive analysis considering different workpiece dimensions

Another sensitive analysis was performed considering a different balance between operations performed at low and high velocity. Even in this case, the analysis was accomplished changing the duration of each single operation as described in **Tabella 2-8**. The nominal T_0 was considered for all the simulated cases.

case	high torque configuration	high velocity configuration	scenario
a1	$1.4 \cdot \Delta t_K$	$0.6 \cdot \Delta t_K$	different usage
b1	$1.2 \cdot \Delta t_K$	$0.8 \cdot \Delta t_K$	different usage

n	$1 \cdot \Delta t_K$	$1 \cdot \Delta t_K$	reference condition
c1	$0.8 \cdot \Delta t_K$	$1.2 \cdot \Delta t_K$	different usage
d1	$0.6 \cdot \Delta t_K$	$1.4 \cdot \Delta t_K$	different usage
e1	$0.05 \cdot \Delta t_K$	$1 \cdot \Delta t_K$	different usage
f1	$1 \cdot \Delta t_K$	$0 \cdot \Delta t_K$	different usage

Tabella 2-8: Sensitive analysis considering a different balance between machining operations performed at low and high spindle speeds

Focusing first on reference production batch, **Figura 2-16** shows the potential cumulated energy saving. The sequence of analyzed operations, characterized by the corresponding T_K , n_K and Δt_K , is reported on the left side of **Figura 2-16**. The energy saving contributions due to the spindle ΔE_S and due to the auxiliary equipment (ΔE_{AUX}), according to the definition reported in Eq. 28-Eq. 31, can be appreciated. It can be observed that the role of the auxiliary equipment is more relevant than the contribution due to the spindle although it positively affects the global energy saving ΔE_{TOT} . As can be easily observed looking at **Figura 2-16**, ΔE_{S_k} is positive when the machining operation is performed with the spindle set in high torque configuration while is negative when high speed machining operations are carried out. The new conceived spindle direct solution shows a better global efficiency η_{GS} when it performs machining operation at low spindle speeds. On the contrary, when the spindle has to perform very light operations at quite high rotational speeds (i.e. threading and drilling) the spindle contribution to energy saving is negative $\Delta E_{S_k} < 0$.

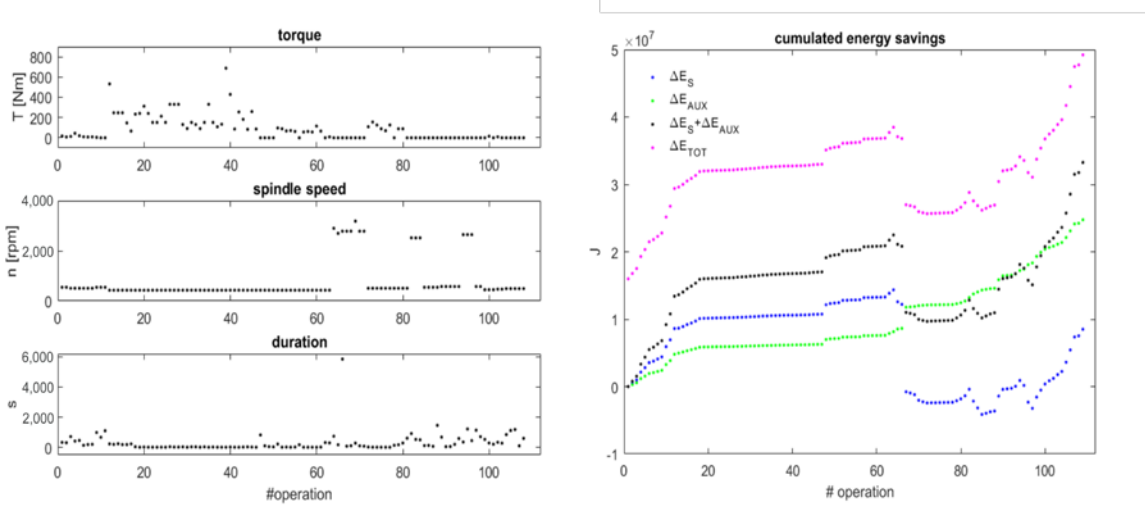


Figura 2-16: Composition of the reference production (TK, nK and Δt_K) on the left. Cumulated energy savings across the reference production execution - global ΔE_{TOT} and contributions linked to spindle ΔE_S , auxiliary equipment ΔE_{AUX} and $\Delta E_S + \Delta E_{AUX}$, on the right

Just for having an idea of energy enhancement, the energy saving percentage E_{SS-M} referred to the overall absorbed machined energy E_{Mein} and energy saving percentage E_{SS-S} referred to the absorbed spindle energy E_{Sein} were defined and computed according to Eq. 32 and Eq. 33 respectively.

$$\Delta E_{SS-M} = \frac{\Delta E_{TOT}}{E_{Mein}} = 7.4\% \quad (32)$$

E_{Mein} can be computed as done in Eq. 1 considering the experimentally measured machine power $P_{Mein}(t)$ and the production taken as the reference case.

$$\Delta E_{SS-S} = \frac{\Delta E_{TOT}}{E_{Sein}} = 63\% \quad (33)$$

E_{Sein} can be similarly computed through Eq. 2 considering the measured spindle power $P_{Sein}(t)$

Another meaningful metric is the energy saving percentage ΔE_{SS-CE} , defined with respect to the nominal cutting energy E_{CE} , Eq. 34.

$$\Delta E_{SS-CE} = \frac{\Delta E_{TOT}}{E_{CE}} = 147\% \quad (34)$$

And E_{CE} is computed through Eq. 35

$$E_{CE} = \sum_k (T_K \cdot n_K \cdot \frac{2\pi}{60} \cdot \Delta t_K) \quad (35)$$

According to the estimated energy saving indicators (ΔE_{SS-M} , ΔE_{SS-S} and ΔE_{SS-CE}) it can be concluded that considerable amount of energy can be ⁷⁶⁰ saved with the novel direct drive spindle solution.

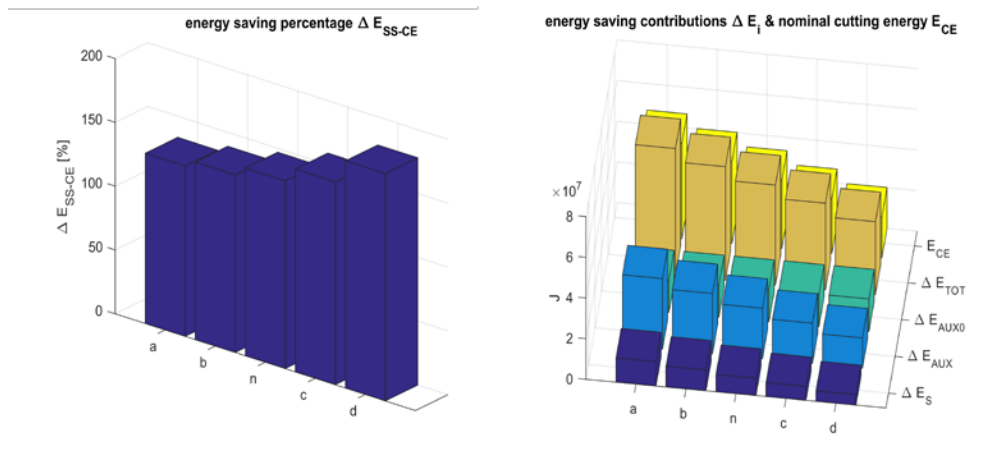


Figura 2-17: Sensitive analysis. Workpiece dimensions effect. Energy saving percentage Delta ESS-CE on the left, energy savings contributions ΔEi and nominal cutting energy ECE on the right

The performed additional analyses confirm the energy savings potentialities of the direct drive technology in spindle system design.

It is worth of noting that ΔE_{SS-CE} is more general than the previously defined indicators since it can be computed just knowing the sequence of machining operations to be executed. This property makes ΔE_{SS-CE} particularly suitable for performing the describes sensitive analyzes. The obtained results are reported in **Figura 2-17** and **Figura 2-18**.

Focusing first on **Figure 2-17**, it can be noted that ΔE_{SS-CE} increases with the decrement of the operation durations. What observed is due to a less relevant reduction of ΔE_{TOT} if compared to the one registered for E_{CE} . This depends on the fact that ΔE_{AUX_0} is kept constant.

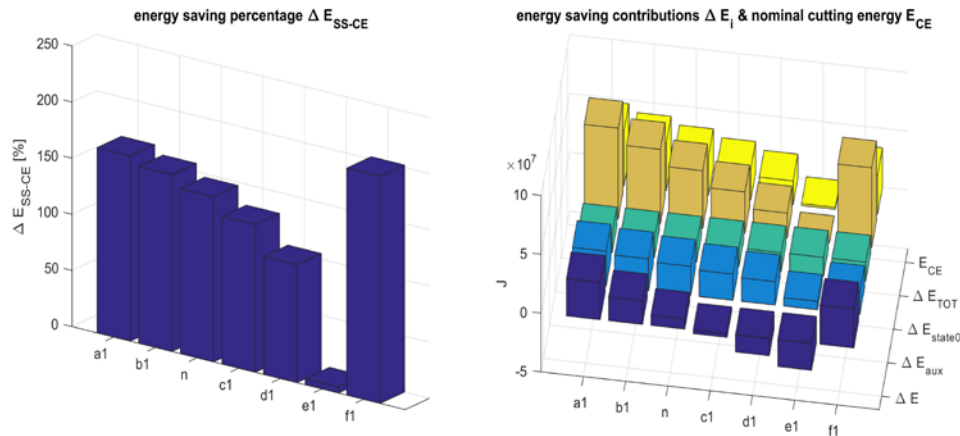


Figure 2-18: Sensitive analysis. Effects of different balances between low-high speed operations. Energy saving percentage Delta ESS–CE on the left, energy savings contributions ΔE_i and nominal cutting energy E_{CE} on the right

Similarity, the results of the other sensitive analysis are reported in **Figure 2-18**. It shows how ΔE_{SS-CE} and the energy saving contributions vary if a generic workpiece requires more machining operations performed at low spindle speed or vice-versa. The cases reported in **Tabella 2-8** were simulated.

It can be observed that if the workpiece processing needs more light machining operations performed at high spindle speeds, the ΔE_{SS-CE} tends to decrease. ΔE_{SS-CE} ' 105% in the "d1" case. While using such a multifunctional machine just for drilling and threading would be highly unlikely, the "e1" case was analyzed.

In this test case the machining operations performed at low spindle speeds are reduced of the 95%.

The simulation results show that ΔE_{SS-CE} is almost vanished. More in details, the energy savings strictly connected to the spindle ΔE_s moved to a negative value even if it is compensated by both ΔE_{AUX_0} and ΔE_{AUX} .

This is the most critical spindle working condition for what concerns the exploitation of the potential energy savings connected to the use of the direct drive solution.

On the contrary, if operations at low spindle speeds ("f1" case with roughing and finishing) are mainly performed, the energy savings can be considerable (ΔE_{SS-CE} ' 202%) high.

For the analyzed machine, production scenarios ascribable to "a1", "b1" or "f1" cases are surely more realistic.

Conclusions of the analysis

The effectiveness of the conceived methodology was demonstrated on a real test case. In particular, the potentialities, in terms of energy savings, of a spindle direct drive solution for a multi-functional machine centre were investigated. The energy assessment

was carried out with respect to a traditional spindle solution based on a gearbox that assures the possibility of executing both high torque–low speed and low torque–high speed machining operations.

A combined experimental-modeling procedure was opportunely conceived for performing this analysis. Both the spindle systems, together with the linked auxiliary equipment, were tested on a specific bench equipped with brakes in order to simulate real cutting conditions. The experimental data were used for developing energy models (losses L_s , spindle efficiency η_s and spindle system global efficiency η_{GS}) of the two spindle solutions.

A comprehensive energy assessment was carried out with the support of the developed models and defining a realistic scenario of use for the considered machine. More specifically, a set of many real machining operations was used for comparing the energy consumed by the alternative spindle systems. The energy analysis showed that considerable amount of energy can be saved substituting the traditional spindle with the novel direct drive solution. It was estimated that, for the considered reference production batch, up to 7% of the overall

machine tool energy consumption can be saved. This amount of saved energy corresponds to the $\Delta E_{SS-CE} = 147\%$ of the requested cutting energy. The analysis was also extended simulating other hypothetical production scenarios. For instance, this percentage ΔE_{SS-CE} ranges from 133% to 178% just changing the duration of each analyzed machining operation. Since it was found that the direct drive solution, for what purely concerns the electrical motor losses in the high spindle speed range, is less efficient than the classical solution, a second sensitive analysis was specifically conceived to study this potential critical aspect. The analysis was performed changing, in the set of machining operations used as a reference, the balance between roughing operations (high torque demanding) and the machining operations performed at high speeds (i.e. threading, drilling and finishing). The results showed that, even in the extreme and rather unlikely case in which most of the performed machining operations are finishing operations, the energy saving still remains positive even if the enhancement is practically negligible. The reported analysis does not only confirm the extremely positive impact of the direct drive spindle solution on the overall energy consumed by the machine but also shows that the achievable energy savings are quite robust to changes to the way the machine is used.

Outlook on the possible generalization and simplification of the proposed approach

Regardless of the results achieved in this specific analyzed case, the presented procedure for analysing machine tool spindle system (motor-transmission-chiller) has great potentialities to be generalized and further simplified. Indeed, as explained in the report for the project activity 1.3, the spindle represents one of the most relevant subsystems that needs to be characterized from the energy perspective.

The above-mentioned generalization/simplification is twofold. Firstly, the selection of the test conditions can be carried out considering, as standard, some spindle speed regions of the characteristic curve of the electrical motor. The same approach can be adopted even for the selection of the spindle torque values (i.e. see **Tabella 2-9**). As can be observed, some

fixed percentages of the nominal values of spindle speed n and spindle torque T can be selected for this purpose.

The second aspect is related to the possibility of performing the characterization of both the losses and the efficiency of the spindle system directly exploiting experimental measures on a real machine without carrying out neither specific test on the bench (as described in this report) nor real cutting tests. For this purpose, a fictitious methodology based on a continuous speed variation across the n_{nom} can be used to load the spindle (see activity 1.3). In this case the average power of the spindle and the average power of the chiller (or ventilation system) need to be measured.

	1	2	3
speed	50% n_{nom}	100 % n_{nom}	$(n_{nom}+n_{max})/2$
torque	75% T_{nom}	50% T_{nom}	10% T_{nom}

Tabella 2-9: Sensitive analysis considering different workpiece dimensions

The proposed simplification/generalization procedure obviously introduces approximations and makes the methodology less rigorous from the scientific point of view but, on the contrary, the advantages in terms of exploitability, especially in an industrial scenario, are clearly observable.

WP 1.4: TRL evolution

TRL4 → TRL 5

Bibliography

- Abele, E., Altintas, Y., Brecher, C., 2010. Machine tool spindle units. CIRP Annals - Manufacturing Technology 59, 781 – 802. doi:10.1016/j.cirp.2010.05.002.
- Abele, E., Sielaff, T., Schiffler, A., Rothenb cher, S., 2011. Analyzing Energy Consumption of Machine Tool Spindle Units and Identification of Potential for Improvements of Efficiency. Springer Berlin Heidelberg, Berlin, Heidelberg. pp. 280–285. doi:10.1007/978-3-642-19692-8_49.
- Albertelli, P., Keshari, A., Matta, A., 2016. Energy oriented multi cutting parameter optimization in face milling. Journal of Cleaner Production 137, 1602 – 1618. doi:10.1016/j.jclepro.2016.04.012.
- Altıntaş, R.S., Kahya, M., Unver, H. O., 2016. Modelling and optimization of energy consumption for feature based milling. The International Journal of Advanced Manufacturing Technology 86, 3345–3363. doi:10.1007/s00170-016-8441-7.
- Aramcharoen, A., Mativenga, P.T., 2014. Critical factors in energy demand modelling for cnc milling and impact of toolpath strategy. Journal of Cleaner Production 78, 63 – 74. doi:10.1016/j.jclepro.2014.04.065.
- Avram, O.I., Xirouchakis, P., 2011. Evaluating the use phase energy requirements of a machine tool system. Journal of Cleaner Production 19, 699 – 711. doi:10.1016/j.jclepro.2010.10.010.

Balogun, V.A., Mativenga, P.T., 2013. Modelling of direct energy requirements in mechanical machining processes. *Journal of Cleaner Production* 41, 179 – 186. doi:10.1016/j.jclepro.2012.10.015.

Boglietti, A., Cavagnino, A., Lazzari, M., Pastorelli, A., 2003. Induction motor efficiency measurements in accordance to iee 112-b, iec 34-2 and jec 37 international standards, in: *Electric Machines and Drives Conference*, 2003. IEMDC'03. IEEE International, pp. 1599–1605 vol.3. doi:10.1109/IEMDC.2003.1210664.

Borgia, S., Albertelli, P., Bianchi, G., 2016. A simulation approach for predicting energy use during general milling operations. *The International Journal of Advanced Manufacturing Technology*, 1–15doi:10.1007/s00170-016-9654-5.

Bossmanns, B., Tu, J., 2001. A power flow model for high speed motorized spindle sheat generation characterization. *Transaction of ASME* 123, 494–505.

Bossmanns, B., Tu, J.F., 1999. A thermal model for high speed motorized spindles. *International Journal of Machine Tools and Manufacture* 39, 1345–1366. doi:10.1016/S0890-6955(99)00005-X.

Brecher, C., Bäumler, S., Jasper, D., Trieb, J., 2012. *Energy Efficient Cooling Systems for Machine Tools*. Springer Berlin Heidelberg, Berlin, Heidelberg. pp. 239–244. doi:10.1007/978-3-642-29069-5_41.

Brecher, C., Jasper, D., Fey, M., 2017. Analysis of new, energy-efficient hydraulic unit for machine tools. *International Journal of Precision Engineering and Manufacturing-Green Technology* 4, 5–11. doi:10.1007/s40684-017-0001-6.

Calvanese, M., Albertelli, P., Matta, A., Taisch, M., 2013. Analysis of energy consumption in cnc machining centers and determination of optimal cutting conditions, in: *Re-engineering Manufacturing for Sustainability*, pp. 227–232.

Campatelli, G., Lorenzini, L., Scippa, A., 2014. Optimization of process parameters using a response surface method for minimizing power consumption in the milling of carbon steel. *Journal of Cleaner Production* 66, 309 – 316. doi:10.1016/j.jclepro.2013.10.025.

Cavallaro, C., Tommaso, A.O.D., Miceli, R., Raciti, A., Galluzzo, G.R., Trapanese, M., 2005. Efficiency enhancement of permanent-magnet synchronous motor drives by online loss minimization approaches. *IEEE Transactions on Industrial Electronics* 52, 1153–1160. doi:10.1109/TIE.2005.851595.

CECIMO, 2009. Self-regulation initiative. URL: www.cecimo.eu/site/ecodesign-and-self-regulatory-initiative/self-regulation-for-machine-tools/. (Date last accessed 2016-12-21).

Diaz, N., Helu, M., Jarvis, A., Tnissen, S., Dornfeld, D., Schlosser, R., 2009. Strategies for minimum energy operation for precision machining. *The Proceedings of MTTRF Annual Meeting*.

Draganescu, F., Gheorghe, M., Doicin, C., 2003. Models of machine tool efficiency and specific consumed energy. *Journal of Materials Processing Technology* 141, 9 – 15. doi:10.1016/S0924-0136(02)00930-5.

EU, 2009. Ecodesign requirements for energy-related products erp directive 2009/125/ec. *Official Journal of the European Union* 285, 10–35. URL: eur-lex.europa.eu/legal-content/EN/TXT/PDF/?uri=CELEX:32009L0125&from=EN. (Date accessed time 2016-12-21).

Fraunhofer-IZM, 2011. Energy-using product group analysis - lot 5 machine tools and related machinery. URL: www.ecomachinetools.eu/typo/home.html. (Date last accessed 2016-12-21).

Gtze, U., Koriath, H.J., Kolesnikov, A., Lindner, R., Paetzold, J., 2012. Integrated methodology for the evaluation of the energy- and cost-effectiveness of machine tools. *CIRP Journal of Manufacturing Science and Technology* 5, 151 – 163. doi:10.1016/j.cirpj.2012.04.001.

Guo, Y., Duflou, J.R., Qian, J., Tang, H., Lauwers, B., 2015. An operation-mode based simulation approach to enhance the energy conservation of machine tools. *Journal of Cleaner Production* 101, 348 – 359. doi:10.1016/j.jclepro.2015.03.097.

Gutowski, T., Dahmus, J., Thiriez, J., 2006. Electrical energy requirements for manufacturing processes., in: 13th CIRP International Conference of Life Cycle Engineering, Lueven, Belgium.

Hanafi, I., Khamlichi, A., Cabrera, F.M., Almansa, E., Jabbouri, A., 2012. Optimization of cutting conditions for sustainable machining of peek-cf30 using tin tools. *Journal of Cleaner Production* 33, 1 – 9. doi:10.1016/j.jclepro.2012.05.005.

Harris, P., Linke, B., Spence, S., 2015. An energy analysis of electric and pneumatic ultra-high speed machine tool spindles. *Procedia CIRP* 29, 239 – 244. doi:10.1016/j.procir.2015.02.046.

He, Y., Liu, F., Wu, T., Zhong, F.P., Peng, B., 2012. Analysis and estimation of energy consumption for numerical control machining. *Proceedings of the Institution of Mechanical Engineers, Part B: Journal of Engineering Manufacture* 226, 255–266. doi:10.1177/0954405411417673.

Huang, H., Ameta, G., 2014. Computational energy estimation tools for machining operations during preliminary design. *International Journal of Sustainable Engineering* 7, 130–143. doi:10.1080/19397038.2013.862580.

ISO, 2014. 14955-1 machine tools - environmental evaluation of machine tools - part 1: Design methodology for energy-efficient machine tools. URL: www.iso.org/iso/home/store/catalogue_tc/catalogue_detail.htm?csnumber=70035. (Date last accessed 2016-12-21).

ISO, 2016. 14955-2 machine tools - environmental evaluation of machine tools – part 2: Methods for measuring energy supplied to machine tools and machine tool components. URL: www.iso.org/iso/home/store/catalogue_tc/catalogue_detail.htm?csnumber=66354. (Date last accessed 2016-12-29).

Jayal, A., Badurdeen, F., Jr., O.D., Jawahir, I., 2010. Sustainable manufacturing: Modeling and optimization challenges at the product, process and system levels. *CIRP Journal of Manufacturing Science and Technology* 2, 144 – 152. doi:10.1016/j.cirpj.2010.03.006.

Jimoh, A.A., Findlay, R.D., Poloujadoff, M., 1985. Stray losses in induction machines: Part i, definition, origin and measurement. *IEEE Transactions on Power Apparatus and Systems* PAS-104, 1500–1505. doi:10.1109/TPAS.1985.319165.

Kant, G., Sangwan, K.S., 2014. Prediction and optimization of machining parameters for minimizing power consumption and surface roughness in machining. *Journal of Cleaner Production* 83, 151 – 164. doi:10.1016/j.jclepro.2014.07.073.

Kara, S., Li, W., 2011. Unit process energy consumption models for material removal processes. *CIRP Annals - Manufacturing Technology* 60, 37 – 40. doi:10.1016/j.cirp.2011.03.018.

Li, J.g., Lu, Y., Zhao, H., Li, P., Yao, Y.x., 2014. Optimization of cutting parameters for energy saving. *The International Journal of Advanced Manufacturing Technology* 70, 117–124. doi:10.1007/s00170-013-5227-z.

- Li, L., Yan, J., Xing, Z., 2013. Energy requirements evaluation of milling machines based on thermalequilibrium and empirical modelling. *Journal of Cleaner Production* 52, 113 – 121. doi:10.1016/j.jclepro.2013.02.039.
- Li, W., Zein, A., Kara, S., Herrmann, C., 2011. An Investigation into Fixed Energy Consumption of Machine Tools. Springer Berlin Heidelberg, Berlin, Heidelberg. pp. 268–273. doi:10.1007/978-3-642-19692-8_47.
- Liu, Q., 2005. Analysis, design and control of permanent magnet synchronous motors for wide-speed operation. Ph.D. thesis. National University of Singapore.
- MAL, 2008. Cut pro simulation software. URL: www.malinc.com/products/cutpro/. (Date last accessed 2017-05-17).
- Mativenga, P., Rajemi, M., 2011. Calculation of optimum cutting parameters based on minimum energy footprint. *CIRP Annals - Manufacturing Technology* 60, 149 – 152. doi:10.1016/j.cirp.2011.03.088.
- Montgomery, D.C., 2001. Design of Experiments. John Wiley.
- Neugebauer, R., Wabner, M., Rentzsch, H., Ihlenfeldt, S., 2011. Structure principles of energy efficient machine tools. *CIRP Journal of Manufacturing Science and Technology* 4, 136 – 147. doi:10.1016/j.cirpj.2011.06.017. energy-Efficient Product and Process Innovations in Production Engineering.
- Newman, S., Nassehi, A., Imani-Asrai, R., Dhokia, V., 2012. Energy efficient process planning for cnc machining. *CIRP Journal of Manufacturing Science and Technology* 5, 127 – 136. doi:10.1016/j.cirpj.2012.03.007.
- Pavanaskar, S., Pande, S., Kwon, Y., Hu, Z., Sheffer, A., McMains, S., 2015. Energy-efficient vector field-based toolpaths for cnc pocket machining. *Journal of Manufacturing Processes* 20, Part 1, 314 – 320. doi:10.1016/j.jmapro. 2015.06.009.
- Pillay, P., Krishnan, R., 1989. Modeling, simulation, and analysis of permanent magnet motor drives. i. the permanent-magnet synchronous motor drive. *IEEE Transactions on Industry Applications* 25, 265–273. doi:10.1109/28. 25541.
- Rahman, M.A., Zhou, P., 1996. Analysis of brushless permanent magnet synchronous motors. *IEEE Transactions on Industrial Electronics* 43, 256–267. doi:10.1109/41.491349.
- Rajemi, M., Mativenga, P., Aramcharoen, A., 2010. Sustainable machining: selection of optimum turning conditions based on minimum energy considerations. *Journal of Cleaner Production* 18, 1059 – 1065. doi:10.1016/j.jclepro.2010.01.025.
- Sizov, G.Y., Ionel, D.M., Demerdash, N.A.O., 2012. Modeling and parametric design of permanent-magnet ac machines using computationally efficient finite-element analysis. *IEEE Transactions on Industrial Electronics* 59, 2403– 2413. doi:10.1109/TIE.2011.2163912.
- Velchev, S., Kolev, I., Ivanov, K., Gechevski, S., 2014. Empirical models for specific energy consumption and optimization of cutting parameters for minimizing energy consumption during turning. *Journal of Cleaner Production* 80, 139 – 149. doi:10.1016/j.jclepro.2014.05.099.
- Wang, Q., Liu, F., Wang, X., 2014. Multi-objective optimization of machining parameters considering energy consumption. *The International Journal of Advanced Manufacturing Technology* 71, 1133–1142. doi:10.1007/ s00170-013-5547-z.
- Yan, J., Li, L., 2013. Multi-objective optimization of milling parameters the trade-offs between energy, production rate and cutting quality. *Journal of Cleaner Production* 52, 462 – 471. doi:10.1016/j.jclepro.2013.02.030.

- Yang, Y., Li, X., Gao, L., Shao, X., 2016. Modeling and impact factors analyzing of energy consumption in cnc face milling using grasp gene expression programming. *The International Journal of Advanced Manufacturing Technology* 87, 1247–1263. doi:10.1007/s00170-013-5017-7.
- Yi, Q., Li, C., Tang, Y., Chen, X., 2015. Multi-objective parameter optimization of cnc machining for low carbon manufacturing. *Journal of Cleaner Production* 95, 256 – 264. doi:10.1016/j.jclepro.2015.02.076.
- Yingjie, Z., 2014. Energy efficiency techniques in machining process: a review. *The International Journal of Advanced Manufacturing Technology* 71, 1123– 1132. doi:10.1007/s00170-013-5551-3.
- Zhou, L., Li, J., Li, F., Meng, Q., Li, J., Xu, X., 2016. Energy consumption model and energy efficiency of machine tools: a comprehensive literature review. *Journal of Cleaner Production* 112, Part 5, 3721 – 3734. doi:10.1016/j.jclepro.2015.05.093.

Attività WP 1.5: Modulo Polimerico: ottimizzazione del power factor e fabbricazione dei moduli (ICMATE)

Task 2.1.5: Modulo Polimerico: ottimizzazione del power factor e fabbricazione dei moduli [M1-M12] (CNR ICMATE)

Quadro generale di riferimento, obiettivi e stato dell'arte

L'utilizzo di generatori termoelettrici (TEG) trova applicazione principalmente nelle strategie di razionalizzazione dell'utilizzo dell'energia elettrica e di diminuzione dell'impatto ambientale della produzione. I TEG sono interessanti per applicazioni di piccola taglia dove si dimostra l'utilità dell'impiego di TEG come dispositivo ancillare nel miglioramento dell'efficienza complessiva del sistema per l'alimentazione di dispositivi e sensori non collegati alla rete elettrica. Si tratta di una tecnologia particolarmente interessante per tutte quelle applicazioni in cui il costo, la silenziosità, il basso peso e l'affidabilità siano tra le caratteristiche ricercate o comunque sufficientemente importanti per compensare la non elevata efficienza di questi dispositivi. L'impiego di un TEG è auspicabile in sistemi che richiedano basse potenze di alimentazione (μW - mW), soprattutto quando è possibile ottenere lavoro elettrico sfruttando il calore fornito dall'ambiente circostante a temperature prossime a quella ambiente. I generatori termoelettrici rientrano nella categoria dei cosiddetti *energy harvester*, ovvero di quei sistemi, metodi e processi che sfruttano fonti energetiche di bassa qualità e a bassa densità ma ampiamente disponibili, come elencato in tabella 1.

Tabella 1 Principali sistemi di energy harvesting e relative densità di potenza

energy harvesting methods	energy harvesting elements	power density
solar and light	photovoltaic solar panel	1500-15000 $\mu\text{W}/\text{cm}^2$
mechanical	wind turbine	3.5 mW/cm^2
	vibration piezoelectric wafer	500 $\mu\text{W}/\text{cm}^2$
	vibration electromagnetic	4.0 $\mu\text{W}/\text{cm}^2$
	vibration electrostatic	3.8 $\mu\text{W}/\text{cm}^2$
thermoelectric	TEG	40 $\mu\text{W}/\text{cm}^2$
		15 $\mu\text{W}/\text{cm}^2$ @10 ΔT
		100 $\mu\text{W}/\text{cm}^2$ ($\Delta\text{T} = 5^\circ\text{C}$)

Un discorso a sé stante meritano le applicazioni di bassissima potenza in condizioni di bassa exergia, come le reti wireless di sensori. In questo caso la ricerca è indirizzata verso lo sviluppo di moduli TE a base organica, costituiti da materie prime ampiamente disponibili e la cui sintesi può essere progettata per la produzione industriale di dispositivi termoelettrici relativamente a basso costo. Sono attualmente oggetto di indagine per lo sviluppo di moduli "indossabili", leggeri e meccanicamente flessibili a temperature prossime a quella ambiente con modeste differenze di temperatura tra lato caldo e lato freddo (qualche decina di $^\circ\text{C}$). Applicazioni operanti a bassa exergia, come le reti wireless di sensori (WSN-wireless sensor networks) o l'elettronica indossabile (wearable electronics), possono funzionare in maniera autonoma e durevole sfruttando la tecnologia termoelettrica. La comunicazione via internet fra sistemi di controllo e dispositivi presenti in case, edifici pubblici o isolati, piuttosto che fra macchinari presenti nelle industrie o fra veicoli in circolazione permette di avere in tempo reale

informazioni di varia natura con conseguente ottimizzazione del processo in corso (si pensi ad esempio al mondo dei trasporti, del commercio e dei processi industriali). In questo contesto, le reti WSN costituiscono parte dell'emergente tecnologia intelligente (smart technology) che getta le basi per la progettazione di sistemi complessi intelligenti quali, ad esempio le città intelligenti (smart cities). Gli scenari futuri prevedono la presenza di un numero sempre più alto di dispositivi di feedback che permettono di monitorare diversi tipi di parametri, dall'ambito domestico fino alla produzione industriale. I sensori integrati nelle WSN vengono attualmente alimentati da batterie che sfruttano fonti non rinnovabili e con durata limitata nel tempo. Le batterie funzionano bene con un numero limitato di sensori e non sono facilmente rimpiazzabili. L'utilizzo di generatori termoelettrici semplificherebbe la gestione dell'alimentazione poiché questi dispositivi possono operare teoricamente per periodi indefiniti, operano in assenza di fluidi di lavoro o componenti liquide, e hanno forma e dimensioni possono essere contenute e adattate al sistema che devono alimentare.

Sono stati fabbricati moduli termoelettrici a base di $(\text{Bi,Sb})_2(\text{Te,Se})_3$ per la microgenerazione partendo dal materiale massivo e su forma di film sottili. I composti a base di Bi_2Te_3 risultano essere i materiali termoelettrici più performanti a temperature prossime alla temperatura ambiente. Tuttavia, data la scarsità degli elementi costituenti (Te in particolare) e i costi legati alla sintesi, al *processing* e all'eventuale smaltimento, la ricerca si sta focalizzando sullo studio di materiali alternativi in grado di ridurre se non eliminare la presenza di elementi critici. I materiali organici, costituiti principalmente da C, N, H, O vengono considerati come una possibile alternativa ai tellururi inorganici. I polimeri conduttori PEDOT (poli(3,4-etilen-diossitiotofene)), PANI (polianilina), P3HT (poli-(3-esil-tiofene)) e Ppy (polipirrolo), già studiati per applicazioni in opto-elettronica, offrono buone potenzialità come materiali termoelettrici. Nonostante i valori di ZT dei polimeri conduttori siano di due ordini di grandezza inferiori rispetto agli analoghi inorganici, lo sviluppo di TEG a base polimerica è motivato dall'ampia disponibilità delle materie prime, dalla facilità nella fabbricazione per la grande versatilità di processo e dal peso contenuto dei moduli dovuto alla bassa densità dei materiali organici. Inoltre, la possibilità di processare i polimeri in soluzione o su forma di paste ne permette una facile integrazione sul dispositivo, massimizzando la superficie di assorbimento del calore e permettendo di ricoprire una vasta area, fattore importante nell'energy-(micro)harvesting. Ad oggi, lo studio dei materiali organici con proprietà termoelettriche è nella sua fase iniziale e molto resta ancora da sviluppare per quanto riguarda il materiale attivo e tutta la componentistica per l'assemblaggio del modulo termoelettrico. È dunque fondamentale seguire passo per passo la sintesi e caratterizzazione funzionale di nuovi materiali efficienti nonché la loro integrazione nei dispositivi finali.

Tra i principali polimeri conduttori, i più noti ed investigati come materiali termoelettrici di tipo *p* sono il poli(3,4-etilen-diossitiotofene) (PEDOT) e la polianilina (PANI). Quest'ultima, in particolare, si ottiene facilmente per ossidazione chimica o elettrochimica dell'anilina ed è presente in commercio con diversi pesi molecolari medi. Anche il PEDOT è disponibile commercialmente in sospensione ed in presenza del controione polistirenesolfonato (PSS). Per quanto riguarda i moduli termoelettrici organici sono in fase di commercializzazione TEG a base di PEDOT depositato e stampato con tecnica R2R (*roll to roll*), prodotti da OTEGO <http://www.otego.de/> con possibilità di ottenere TEG in forma di film sottile o di parallelepipedo massivo. Ad ora, non sono ancora stati commercializzati moduli a base di polianilina.

In tabella 2 sono riportate le proprietà termoelettriche di materiali a base di PEDOT e PANI dallo stato dell'arte.

Tabella 2 Proprietà termoelettriche di PANI e PEDOT e loro composti

matrix	filler	loading (wt%)	σ (S cm ⁻¹)	α (μ VK ⁻¹)	PF (Wm ⁻¹ K ⁻²)
PANI:CSA	-	-	160	5	2.7·10 ⁻⁴
PEDOT:PSS	-	-	890	74	4.7·10 ⁻⁴
PEDOT:PSS	PbTe	30	0.0023	-2500	1.44·10 ⁻⁶
PEDOT:PSS	Te	-	19	163	7·10 ⁻⁵
PANI:HCl	Bi ₂ Te ₃	30	11.6	40	2·10 ⁻⁴
PEDOT:PSS	Bi _{0.5} Sb _{1.5} Te ₃	4.1	1295	16	3.2·10 ⁻⁵
PANI:HCl	MoS ₂	85	0.8	8	
PEDOT:PSS	Au	0.01	241	27	1.8·10 ⁻⁵
PEDOT:PSS	SWCNT	35	400	23	2.4·10 ⁻⁵
PEDOT:PSS	SWCNT	85	4000	16	1.0·10 ⁻⁴
PANI:MeSO ₃ H	SWCNT	6.6	530	33	6·10 ⁻⁷
PANI:HCl	MWCNT	1	14	80	6·10 ⁻⁷
PANI:HCl	graphene	50	123	34	1.4·10 ⁻⁵
PANI:HCl	graphene oxide	10	7.5	28	6.0·10 ⁻⁷

1) Obiettivi

Obiettivo generale del progetto è lo sviluppo di procedure per l'integrazione intelligente dei sistemi produttivi con la rete di fornitura dell'energia elettrica con un miglioramento complessivo dell'efficienza, considerando anche l'impiego e messa a punto di moduli termoelettrici organici con matrice "attiva". La ricerca è stata focalizzata sull'individuazione di un opportuno materiale termoelettrico organico per la costruzione di moduli termoelettrici operanti a temperature prossime a quella ambiente. Il lavoro è stato articolato in una parte di sintesi e caratterizzazione funzionale del materiale attivo, individuando la composizione e il processo produttivo più idonei all'assemblaggio di un prototipo di generatore termoelettrico (TEG) e alla caratterizzazione del dimostratore. Gli obiettivi sono dunque stati:

- sintesi di un semiconduttore termoelettrico a base polimerica operante a temperature prossime alla temperatura ambiente e messa a punto di strategie sintetiche per l'aumento del *power factor* ($\alpha^2\sigma$) e il raggiungimento di $PF=0.3\mu WK^{-2}m^{-1}$
- estesa caratterizzazione composizionale e funzionale per verificare la riproducibilità e delle condizioni di sintesi e delle proprietà elettriche
- assemblaggio di un prototipo di generatore termoelettrico e valutazione delle prestazioni

2) Risultati conseguiti

- Sviluppo di materiali termoelettrici composti/ibridi a matrice conduttiva polimerica: sintesi green del composito PANI-DBSA/SWCNT e del corrispondente ibrido PANI-DBSA/SWCNT 30 vol%/Bi_{0.5}Sb_{1.5}Te₃ 17 vol% (PANI=polianilina, DBSA,(plasticizzante, = acido dodecilbenzen solfonico)

TRL 2 → TRL 3

- Progettazione, sviluppo e testing dei moduli: sono stati fabbricati quattro moduli flessibili uni-leg con connettori elettrici inglobati in matrice siliconica. Gli aspetti tecnologici di geometria e integrazione dei materiali impiegati nel dispositivo sono stati affrontati con l'ausilio di tecniche di simulazione multifisica (COMSOL Multiphysics), con la prospettiva di ottimizzarne le proprietà di scambio termico, di conduttività elettrica e di resistenza meccanica. $PF_{max} = 3 \mu W m^{-1} K^{-2} (\Delta T=10 \text{ } ^\circ C)$

TRL 2 → TRL 3

Avanzamenti rispetto allo stato dell'arte:

- È stato messo a punto un **processo solvent-free** per la preparazione di un materiale termoelettrico composito organico-inorganico a base polimerica
- Grazie alla procedura di preparazione, il composito ottenuto PANI-DBSA ha la consistenza di una pasta, e mostra **alta lavorabilità in tutte le fasi di fabbricazione del modulo**.

Descrizione delle procedure, della sperimentazione e dei risultati

Sintesi e caratterizzazione del materiale attivo per il modulo termoelettrico

Il polimero polianilina (PANI), un conduttore di tipo-*p*, è stato individuato come materiale di partenza per lo sviluppo di materiali termoelettrici organici. Lo studio del materiale ha riguardato solo la gamba *p* del modulo in quanti i polimeri conduttori di tipo *n* sono intrinsecamente instabili e tendono ad ossidarsi a condizioni ambiente.

Metodologia

Le proprietà termoelettriche di polimeri conduttori possono essere ottimizzate attraverso:

- 1) drogaggio del polimero per via chimica (reazioni di protonazione/deprotonazione) o elettrochimica (ossidazione/riduzione della catena polimerica)
- 2) formazione di *blend* con altre molecole o polimeri
- 3) sintesi di compositi usando *filler* inorganici quali metalli, semiconduttori o materiali a base di carbonio.

La polianilina è presente in diverse forme: *leucoemeraldina*, *emeraldina* e *pernigralina*, in ordine crescente di grado di ossidazione. La forma più stabile e utilizzabile è l'emeraldina. Quest'ultima non protonata è disponibile commercialmente a diversi valori di peso molecolare medio. Nonostante sia possibile sintetizzare la polianilina per via chimica (polimerizzazione ossidativa con ammonio-perossidossulfato) ed elettrochimica dal monomero anilina, per il suddetto studio è stato scelto di utilizzare polveri commerciali di PANI:EB. Le proprietà funzionali di PANI sono altamente dipendenti dalle condizioni di sintesi (temperatura, pH, tipo di acido usato) in scala di laboratorio. Infatti, e' stata misurata una variazione nei valori di conducibilità elettrica pari al 40% per più campioni di polianilina sintetizzati dallo stesso operatore con la stessa procedura. Il controllo della conducibilità elettrica (σ) si ottiene attraverso la protonazione/deprotonazione degli atomi di azoto imminici (figura 1) della forma emeraldina (emeraldine base-EB/emeraldine salt-ES).

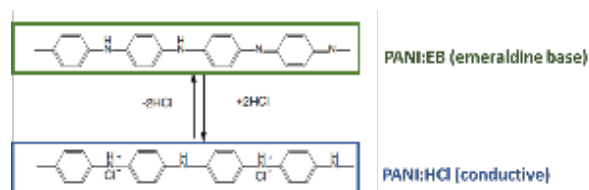


Figura 1 Reazione acido base della forma emeraldina della polianilina

Tutti gli acidi protici sono dunque possibili droganti per PANI.

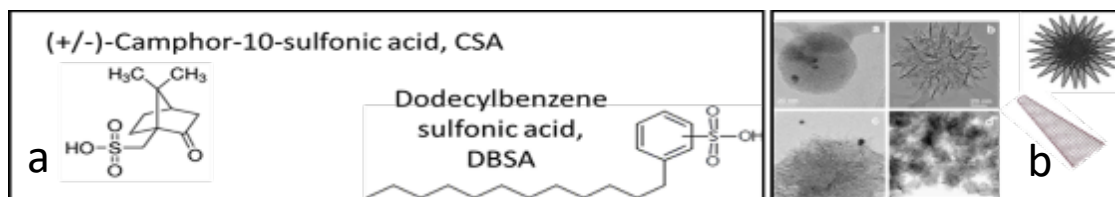


Figura 2 Struttura degli acidi CSA e DBSA (a) e immagini in microscopia TEM di Single Wall Carbon Nanohorn (SWCNH) In questo studio sono stati scelti l'acido canforsolfonico (CSA) e l'acido dodecilbenzen-solfonico (DBSA) (figura 2a). Contestualmente al drogaggio per protonazione, nella matrice PANI sono stati dispersi come filler nanostrutture di carbonio altamente conduttive, i *Single Wall Carbon Nanohorn* (SWCNH, figura 2b), e i semiconduttori termoelettrici di tipo-p $\text{Bi}_{0.5}\text{Sb}_{1.5}\text{Te}_3$ e $\text{Cu}_{12}\text{Sb}_4\text{S}_{13}$. La creazione di interfacce organico/inorganico nel caso dei compositi comporta, in linea di principio, l'aumento della conducibilità elettrica e del coefficiente di Seebeck del polimero. I compositi PANI/SWCNH sono stati ottenuti sia in forma di film sottile che in forma di pellet massivo, a seconda del processo utilizzato per la sintesi.

Sintesi e caratterizzazione di compositi a base di PANI-CSA/SWCNH

Film di PANI-CSA/SWCNH (SWCNH= 0, 15, 30 wt%) di spessore compreso fra 10 μm e 70 μm , sono stati ottenuti attraverso deposizione di sospensioni di SWCNH/PANI:EB in N-metil pirrolidone (NMP) su vetro. I film sono stati protonati tramite immersione in soluzioni acquose di CSA. In figura 3 sono riportati l'immagine digitale del campione PANI-CSA/SWCNH 15wt% e la micrografia FE-SEM dello stesso.



Figura 3 a) Film di PANI-CSA/SWCNH 15wt% b)micrografia FE-SEM in elettroni secondari di PANI-CSA/ SWCNH 15wt%.

I film risultavano molto flessibili al di sotto dei 50 μm di spessore. Come osservabile dall'analisi FE-SEM (figura 3b) i film depositati da NMP risultavano compatti, omogenei e senza buchi. Gli spot più luminosi sono attribuibili alle nanostrutture di carbonio disperse SWCNH, più conduttive. La stabilità termica dei campioni è stata valutata attraverso analisi termogravimetrica (TGA) accoppiata alla calorimetria a scansione differenziale (DSC) e analisi dei gas residui (RGA), figura 4. Dal confronto di campioni PANI-CSA (senza nanohorn) e PANI-CSA/SWCNH 15wt% è stata osservata una perdita di peso attorno al 5% nell'intervallo RT-200°C, attribuibile ad acqua e NMP residuo. L'analisi dei gas residui ha rivelato la presenza di SO_2 da 250°C-400°C (curve in basso figura 4), derivante dal drogante CSA (figura 2), con una perdita approssimativa poco marcata pari al 4.5%. I materiali dunque possono in linea di principio

essere operativi fino a 150°C. I diversi *step* di perdita di peso evidenziati dalla derivata TGA rispetto a T (curva DTG) sono stati attribuiti ai diversi processi di combustione del materiale. A circa 550°C, PANI-CSA mostra un solo massimo DTG mentre in PANI-CSA/SWCNH 15wt% due picchi DTG. Coerentemente con le curve DTG, a partire da 250°C le curve DSC hanno mostrato una serie di andamenti esotermici allargati, compatibili con la degradazione e l'ossidazione di PANI. Tra 550°C e 650°C il segnale esotermico relativo alla combustione del carbonio residuo è separato in due componenti per PANI-CSA/SWCNH 15wt%. La componente a temperatura più alta è stata attribuita alla combustione dei SWCNH.

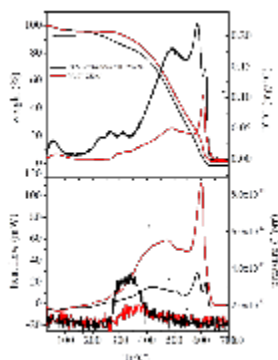


Figura 4. TGA, DSC e analisi dei gas residui (RGA) per PANI-CSA/SWCNH 15wt% (rosso) e PANI-CSA (nero). Con DSC in basso sono riportati i segnali $m/z=48$ (SO da SO_2). Condizioni: aria, 100ml/min, rampa 5°C/min, DSC EXO UP

Caratterizzazione funzionale di compositi a base di PANI-CSA/SWCNH

La conducibilità elettrica e il coefficiente di Seebeck sono stati misurati fino a 100°C su pellet ottenuti polverizzando i film in azoto liquido e pressando le polveri di PANI-CSA, PANI-CSA/SWCNH 15wt% e PANI-CSA/SWCNH 30wt%.

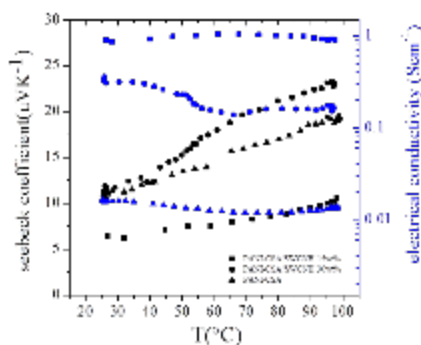


Figura 5 Coefficiente di Seebeck α (nero) e conducibilità elettrica σ (blu) in funzione della temperatura per i campioni PANI-CSA, PANI-CSA/SWCNH 15wt% e PANI-CSA/SWCNH 30wt%.

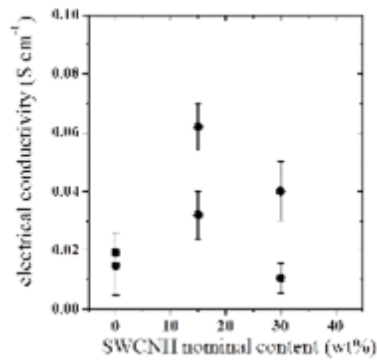


Figura 6 Conducibilità elettrica vs. contenuto di SWCNH di film PANI-CSA, PANI-CSA/SWCNH 15wt% e PANI-CSA/SWCNH 30wt%.

L'aggiunta di SWCNH ha condotto ad un aumento dei valori di σ pari a 0.91 S cm^{-1} per PANI-CSA/SWCNH 15 wt% , $\sigma = 0.36 \text{ S cm}^{-1}$ per PANI-CSA/SWCNH 30 wt%. Questi valori sono circa un ordine di grandezza maggiori rispetto a PANI-CSA ($\sigma = 0.016 \text{ S cm}^{-1}$). Per PANI-CSA/SWCNH 15wt% è stato misurato il massimo valore di σ a temperatura ambiente. A concentrazioni maggiori, i SWCNH perturbano lo *stacking* delle catene polimeriche, minimizzando l'interazione $\pi - \pi$ intercatena. Inoltre, le nanostrutture di carbonio tendono ad una maggiore aggregazione

con l'aumento della loro concentrazione, diminuendo il volume di interazione fra SWCNH e PANI, con conseguente aumento della resistenza all'interfaccia.

Sono stati misurati valori di conducibilità elettrica anche sui film (figura 6).

La conducibilità elettrica per film contenenti SWCNH risultavano di circa un ordine di grandezza inferiori ai valori determinati sui pellet derivati dalla frammentazione dei film. Questo può essere dovuto ad un effetto omogeneizzante di macinazione e pressatura dei film permettendo il redistribuirsi degli aggregati PANI/SWCNH e migliorando il contatto ohmico all'interfaccia. Lo stato dell'arte riporta $\sigma = 6.7 \times 10^{-2} \text{ S cm}^{-1}$ per pellet di PANI/SWCNH ottenuti per polimerizzazione di anilina in presenza di SWCNH, coerentemente con i film qui descritti.

Per quanto riguarda α , a temperatura ambiente è stato misurato per PANI-CSA/SWCNH 30wt% un valore pari a $12 \mu\text{VK}^{-1}$, simile a PANI-CSA senza SWCNH mentre per PANI-CSA/SWCNH 15wt% α era circa la metà. Il più alto valore di *power factor* ($\text{PF} = \alpha^2 \sigma$) di $3.2 \times 10^{-3} \mu\text{Wm}^{-1}\text{K}^{-2}$ è stato calcolato per il campione PANI-CSA/SWCNH 15wt% . Nonostante il modesto PF, l'aggiunta di SWCNH ha comunque comportato un aumento sensibile della conducibilità elettrica senza particolari variazioni del coefficiente di Seebeck, soprattutto se si confrontano le composizioni PANI-CSA e PANI-CSA/SWCNH 30 wt%. Una serie di fattori tra cui il controllo dell'aggregazione dei SWCNH e il grado di protonazione della polianilina hanno influito sui valori di σ . Per via della sua basicità, N metil pirrolidone può competere con la polianilina nelle reazioni acido base diminuendo il grado di protonazione in PANI, con conseguente riduzione della conducibilità elettrica. Inoltre, è stato dimostrato che in NMP le catene di PANI si avvolgono su se stesse in una conformazione meno distesa e l'interazione $\pi - \pi$ è meno favorita. Per contro, nei film depositati da m-cresolo, la distensione delle catene è favorita con conseguente

aumento dello stacking π - π intercatena e aumento di σ . Non a caso, in letteratura i valori più elevati di conducibilità elettrica sono stati misurati in film di PANI-CSA depositati da m-cresolo..

Sintesi e caratterizzazione di compositi a base di PANI-DBSA/SWCNH

Alla luce di quanto appena discusso, è stata messa a punto una seconda via di sintesi per i compositi a base di PANI/SWCNH, sfruttando un processo senza solvente di doping termico attraverso l'acido dodecilbenzensolfonico (DBSA). Per confronto sono state comunque condotte delle prove depositando film di polianilina per evaporazione da solvente. Polveri di PANI:EB sono state mescolate a SWCNH e polveri nanostrutturate dei semiconduttori termoelettrici $\text{Bi}_{0.5}\text{Sb}_{1.5}\text{Te}_3$ (BiSbTe) e $\text{Cu}_{12}\text{Sb}_4\text{S}_{13}$ (tetraedrite, CuSbS) ottenendo quattro tipi di materiali le cui composizioni nominali (% in peso) in SWCNH e semiconduttore termoelettrico sono indicate in seguito

1) PANI-DBSA

2) PANI-DBSA/SWCNH 11-15 wt% -(PANI-DBSA/SWCNH)

3) PANI-DBSA/SWCNH 4-7 wt%+ BiSbTe 60-62wt% -(PANI-DBSA/SWCNH+BiSbTe)

4) PANI-DBSA/SWCNH 6 wt%+ CuSbS 41 wt%-(PANI-DBSA/SWCNH+CuSbS)

Il tellururo di bismuto e antimonio- $\text{Bi}_{0.5}\text{Sb}_{1.5}\text{Te}_3$, commercialmente presente come polvere micrometrica, è stato macinato via *ball milling* per ottenere una riduzione della dimensione dei grani. La tetraedrite $\text{Cu}_{12}\text{Sb}_4\text{S}_{13}$ nano-cristallina è stata sintetizzata tramite un metodo in soluzione. Le percentuali dei filler sono variabili, data la difficoltà nel pesare in maniera accurata i SWCNH per la loro densità estremamente bassa.

Il DBSA è stato aggiunto alla miscela di polveri fino ad ottenere una consistenza pastosa. La pasta è stata depositata sotto forma di film su vetro o su stampi per ottenere pellet di varie forme. Il doping della polianilina avviene per via termica, scaldando a 100°C . Dopo trattamento termico in forno a 150°C , i substrati ove posano i film o le pastiglie sono stati staccati previa immersione in acqua, ottenendo film spessi dai $50\ \mu\text{m}$ ai $300\ \mu\text{m}$ e pellet con diametri vari e spessori ottimali massimi di circa 2 mm. In figura 7 viene riportata la curva DSC per una miscela PANI:EB-DBSA dalla quale sono state scelte le condizioni di trattamento termico per il doping e la solidificazione del materiale.

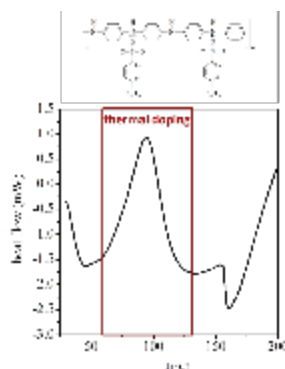


Figura 7 Curva DSC di una miscela PANI-DBSA per lo studio del processo di doping termico. Condizioni: aria 100ml/min, rampa $5^\circ\text{C}/\text{min}$. Sopra il termogramma viene riportata la struttura della polianilina protonata e complessata con DBSA, $\text{PANI}(\text{DBSA})_x$

I compositi sono stati sintetizzati con un eccesso di DBSA pari a $\text{DBSA}/\text{PANI} \approx 3.17$ (mol). Intorno ai 100°C (figura 7 curva DSC), è stato osservato il picco DSC esotermico relativo al processo di protonazione della polianilina da parte di DBSA e successiva coordinazione della base coniugata all'azoto imminico di PANI, con formazione del complesso $\text{PANI}(\text{DBSA})_x \cdot n\text{DBSA}_{\text{free}}$. ($\text{DBSA}_{\text{free}}$ è l'acido in eccesso). Successivamente è stato osservato un andamento della curva simile ad una transizione vetrosa con

una temperatura di soglia di circa 156°C, attribuibile alla transizione del materiale da sospensione pastosa a solido semirigido. Una volta raffreddati i campioni, DBSA_{free} è stato rimosso lasciando in immersione i campioni in acqua.

L'eccesso di DBSA agisce da emulsionante e plasticizzante. La pasta a base di PANI-DBSA prima del trattamento termico facilmente processabile, può essere spalmata su vetrini o iniettata su stampi come quello raffigurato in figura 8 a. Stampi di diverse dimensioni e forme possono essere facilmente ottenuti usando paste siliciche resistenti alle alte temperature. La base in silicone può essere formata su di un templatato negativo, in questo caso acido polilattico, ottenuto attraverso stampa 3D.

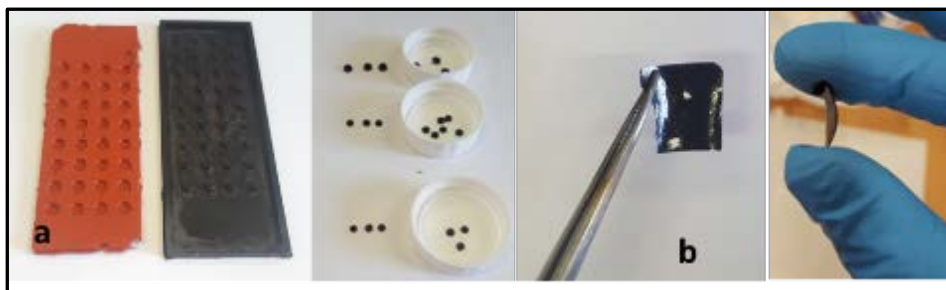


Figura 8 a) pellet di PANI-DBSA/SWCNH ottenuti per deposizione della pasta su stampo b). film PANI-DBSA/SWCNH ottenuti per deposizione su vetrino.

Per confronto con il metodo senza solvente appena descritto, film di PANI-DBSA/SWCNH sono stati ottenuti per deposizione dei precursori sospendendo i SWCNH in presenza di DBSA in CHCl₃ e aggiungendo successivamente la polianilina nella forma emeraldina (figura 9). Essendo la polianilina solubile nella forma protonata in CHCl₃, era ragionevole prevedere una migliore omogeneità della dispersione e un'incrementata interazione polimero/filler rispetto ad un composito ottenuto per mescolamento meccanico delle polveri. Il cloroformio è stato scelto per il suo basso punto di ebollizione (61.2°C) rispetto ai solventi normalmente utilizzati per depositare film a base di polianilina (202°C per NMP e 203°C per m-cresolo), nonostante la minore solubilità. La sospensione in CHCl₃ di SWCNH-DBSA è stabile e non è stata osservata la presenza di precipitati nelle 24 ore successive alla preparazione.

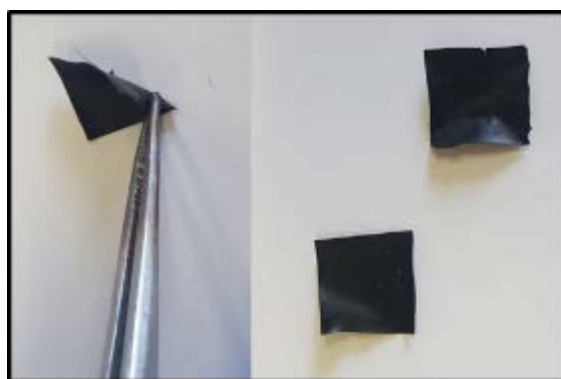


Figura 9. Film a base di PANI-DBSA/SWCNH ottenuti per deposizione da CHCl₃

Dei film così ottenuti sono stati misurati spessori non eccedenti i 60 µm. I materiali, inoltre, hanno mostrato un maggior grado di flessibilità rispetto a quelli ottenuti per doping termico. Per quanto riguarda la stabilità termica dei compositi PANI-DBSA/SWCNH, sono state registrate le curve TGA e DSC in aria per il polimero drogato senza (PANI-DBSA) e con SWCNH (PANI-DBSA/SWCNH 11-15wt%).

Per entrambi PANI-DBSA e PANI-DBSA/SWCNH è stata osservata una perdita di peso compresa fra 1.5 %-4% dovuta al rilascio di acqua fra temperatura ambiente e 150°C. A circa 260°C una seconda marcata variazione di peso di circa il 20%, evidenziata dalla forma stretta del picco della derivata del peso (DTG), è stata attribuita alla decomposizione del drogante DBSA.

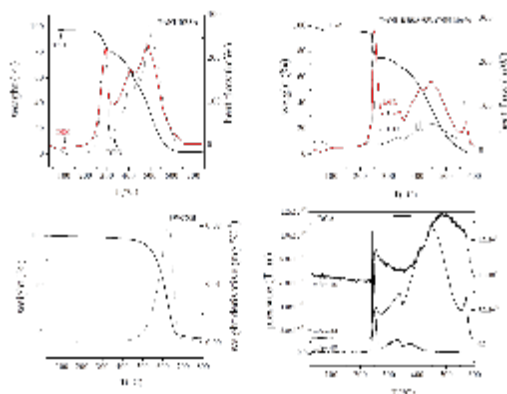


Figura 10 Analisi termogravimetrica (TGA) e calorimetria a scansione differenziale (DSC): confronto fra PANI-DBSA (in alto a sinistra), PANI-DBSA/SWCNH 11-15 wt% (in alto a destra) e SWCNH. L'analisi dei gas residui (RGA) è stata condotta per PANI-DBSA/SWCNH 30v%, dove vengono riportati i segnali $m/z=48$, $m/z=44$ e $m/z=30$ (in basso a destra). CONDIZIONI: aria, 100ml/min con rampa di riscaldamento di 5°C/min ad eccezione di PANI-DBSA dove la rampa usata è di 10°C/min

L'analisi dei gas residui, infatti, ha rivelato in questo intervallo di temperature un picco nell'andamento del segnale $m/z=48$, relativo al frammento SO derivante dai gruppi $-SO_3^-$ di DBSA. Le variazioni dei segnali $m/z=30$ (frammenti CH_2-O e CH_3CH_2) e $m/z=44$ (CO_2) sono compatibili con la degradazione del drogante. I materiali dunque possono essere in linea di principio utilizzabili fino ad una temperatura massima di 150°C, dopodiché avviene la degradazione e del drogante e del polimero. La presenza dei SWCNH non è facilmente visibile considerando solo la TGA. Le curve DSC, DTG e RGA ($m/z=44$) mostrano dopo i 550°C un picco ben distinto in PANI-DBSA/SWCNH 30v%, assente nel polimero non caricato con SWCNH. In questo intervallo di temperature avviene solitamente la combustione molto esotermica e netta delle nanostrutture di carbonio, come si può osservare confrontando con la TGA-DTG dei SWCNH puri.

La quantità di DBSA che complessa la polianilina è stata ricavata attraverso l'analisi termogravimetrica di un campione a composizione nominale PANI-DBSA/SWCNH 11-15 wt% mostrata in figura 11 assieme al metodo utilizzato

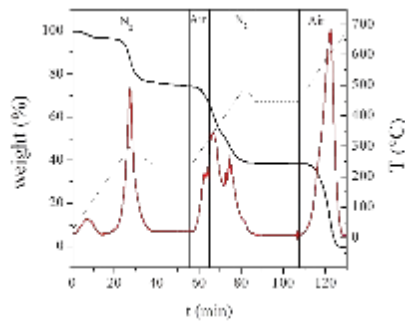


Figura 11 Analisi termogravimetrica per PANI-DBSA/SWCNH 11-15wt% per la determinazione del contenuto di DBSA. Curva TGA (nero), derivata DTG in funzione del tempo (rosso) e programma di temperatura utilizzato (tratteggiato). La misura è stata fatta alternando azoto-aria come gas carrier.

La prima perdita di peso è relativa alla decomposizione del drogante (stretto picco DTG in figura 11 visibile anche in figura 10) mentre i successivi stadi di decomposizione/ossidazione sono relativi al polimero e ai SWCNH. E' stato ricavato un valore di $x=0.36$ per PANI(DBSA)_x coerentemente con quanto già osservato in letteratura. Il contenuto di SWCNH è stato stimato tramite confronto delle analisi termogravimetriche di più campioni PANI-DBSA e PANI-DBSA/SWCNH 11-15wt% come mostrato in figura 12.

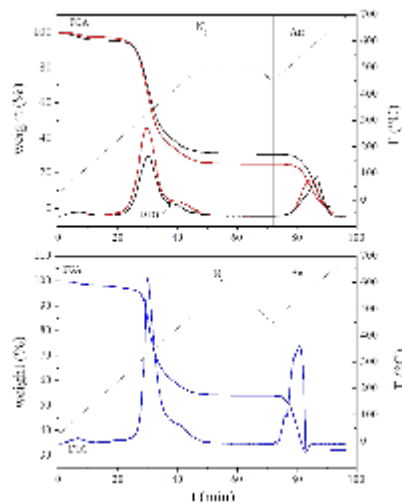


Figura 12. Curve TGA e DTG per PANI-DBSA (rosso), PANI-DBSA/SWCNH 11-15wt% (nero) PANI-DBSA/SWCNH 4-7wt%+BiSbTe 60-62wt% (blu) in funzione del tempo. La curva tratteggiata è il programma di temperatura utilizzato La misura è stata fatta alternando azoto e-aria come gas carrier

L'ultima perdita di peso era pari a circa 30.5% per i campioni contenenti SWCNH mentre per i campioni PANI-DBSA ammontava a circa 24.5-25% (curve rosse e nere figura 12). La differenza è stata ragionevolmente attribuita alla presenza di SWCNH che bruciano dopo i 550°C (picco DTG per PANI-DBSA/SWCNH 11-15wt% a 600°C). Al netto del peso di DBSA, il rapporto SWCNH/PANI misurato è pari a circa 8%, valore che si discosta leggermente dalla composizione nominale ma comunque soddisfacente.

Per quanto riguarda il contenuto di $\text{Bi}_{0.5}\text{Sb}_{1.5}\text{Te}_3$ in PANI-DBSA/SWCNH 4-7 wt%+ BiSbTe 60-62wt%, il residuo di 31.9% in peso nella TGA corrisponde a una quantità di BiSbTe del 62% in peso rispetto a PANI/SWCNH, calcolo fatto trascurando l'ossidazione di Bi ($T=400^\circ\text{C}$) e la possibile sublimazione di Te. E' stata infatti riportata in letteratura una sensibile attenuazione dei fenomeni di ossidazione di Bi e sublimazione di Te per polveri di $\text{Bi}_{0.5}\text{Sb}_{1.5}\text{Te}_3$ inglobate in materici polimeriche. Il valore è prossimo alla

composizione nominale. Per i compositi contenenti le tetraedriti PANI-DBSA/SWCNH 6 wt%+ CuSbS 41 wt%. non è stato possibile determinare la percentuale di $\text{Cu}_{12}\text{Sb}_4\text{S}_{13}$ data la degradazione termica di quest'ultimo dopo i 400°C.

La presenza di $\text{Cu}_{12}\text{Sb}_4\text{S}_{13}$ è stata verificata attraverso microscopia a scansione di elettroni a effetto di campo (FE-SEM) come si vede in figura 13.

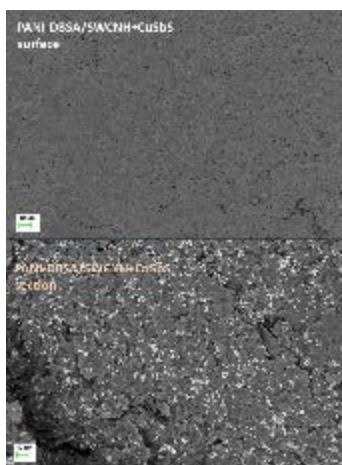


Figura 13. FE-SEM in piano e in sezione di un campione di PANI-DBSA/SWCNH 6 wt%+ CuSbS 41 wt%

Nelle immagini acquisite sulla sezione del campione in elettroni retrodiffusi è visibile il filler $\text{Cu}_{12}\text{Sb}_4\text{S}_{13}$ disperso e inglobato nella matrice polimerica. Per quanto riguarda le altre composizioni, le immagini SEM di figura 14 mostrano la differenza di morfologia fra il semplice PANI-DBSA e gli altri campioni contenenti i filler inorganici.

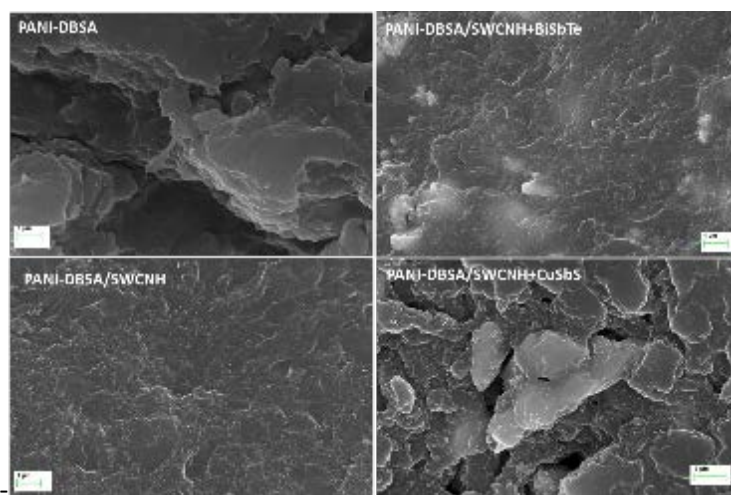


Figura 14. Micrografie FE-SEM su sezioni dei campioni PANI-DBSA, PANI-DBSA/SWCNH, PANI-DBSA/SWCNH+BiSbTe e PANI-DBSA/SWCNH+CuSbS

I campioni contenenti SWCNH presentano una maggiore rugosità nella morfologia, dovuta alla presenza delle nanostrutture di carbonio avvolte nella matrice polimerica. Anche i semiconduttori $\text{Cu}_{12}\text{Sb}_4\text{S}_{13}$ e $\text{Bi}_{0.5}\text{Sb}_{1.5}\text{Te}_3$ sono visibili come spot più chiari nelle immagini FE-SEM. Per PANI-DBSA/SWCNH+BiSbTe, le analisi EDS condotte su diversi punti del campione hanno confermato la presenza di $\text{Bi}_{0.5}\text{Sb}_{1.5}\text{Te}_3$ come visibile in figura 15. Nonostante le polveri siano state meccanicamente agitate assieme al polimero prima di aggiungere DBSA e formare la pasta, esse risultano disperse in

maniera omogenea in tutta la matrice polimerica. In figura 16 sono riportate le immagini FE-SEM dei film PANI-DBSA/SWCNH ottenuti per deposizione da CHCl_3

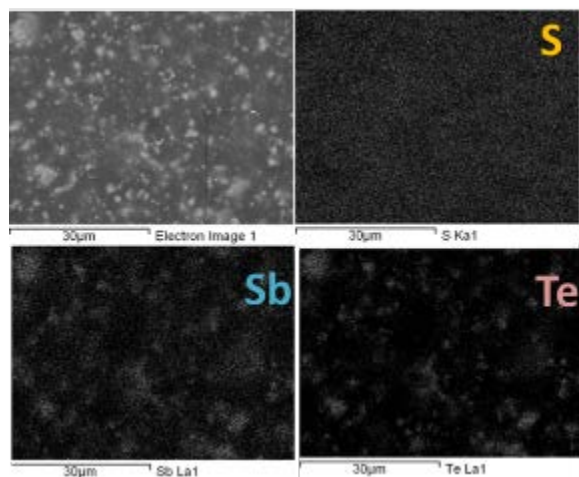


Figura 15 Analisi EDS su sezioni dei campioni PANI-DBSA, PANI-DBSA/SWCNH, PANI-DBSA/SWCNH+BiSbTe e PANI-DBSA/SWCNH+CuSbS. Lo zolfo è dovuto alla presenza di DBSA.

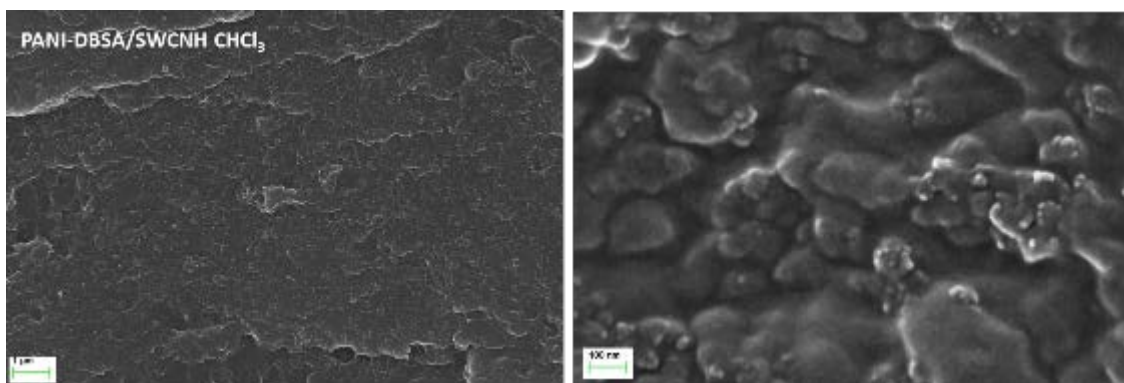


Figura 16 Immagini FE-SEM in sezione su film ottenuto per deposizione di PANI-DBSA/SWCNH da CHCl_3

I film risultano compatti e densi. Si notano aggregati visibili come punti più chiari per i campioni ottenuti dal metodo senza solvente, dovuti alla presenza di SWCNH nella matrice polimerica. Il grado di cristallinità dei materiali polimerici ottenuti per doping termico è pari a circa 11-12%. Questo valore è stimato attraverso la deconvoluzione dello spettro di diffrazione dei raggi X su polveri di PANI-DBSA e PANI-DBSA/SWCNH. In figura 17 è riportato il diffrattogramma per PANI-DBSA. SWCNH non influisce sul grado di cristallinità del polimero.

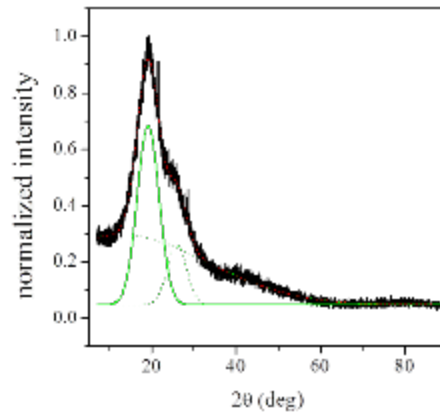


Figura 17 Diffrazione dei raggi-X per PANI-DBSA. In nero i dati sperimentali, in verde i picchi di deconvoluzione del pattern.

Caratterizzazione funzionale di compositi a base di PANI-DBSA/SWCNH

Il coefficiente di Seebeck (α) e la conducibilità elettrica (σ) sono stati misurati in funzione della temperatura per i compositi PANI-DBSA, PANI-DBSA/SWCNH, PANI-DBSA/SWCNH CHCl_3 , PANI-DBSA/SWCNH+BiSbTe e PANI-DBSA/SWCNH+CuSbS (figura 18)

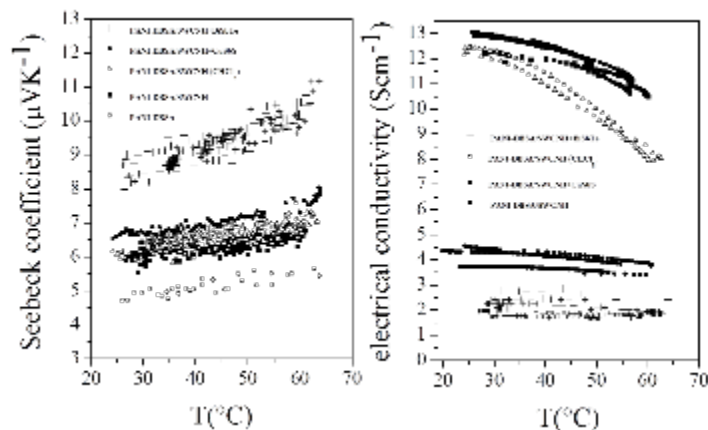


Figura 18 Coefficiente di Seebeck (α) e conducibilità elettrica (σ) da temperatura ambiente fino a 60°C per i campioni PANI-DBSA, PANI-DBSA/SWCNH, PANI-DBSA/SWCNH+BiSbTe e PANI-DBSA/SWCNH+CuSbS

Le misure sono state condotte sia su pellet formati direttamente per deposizione della pasta a base di PANI-DBSA su appositi stampi che su pastiglie ottenute per pressatura dei film spessi 50 μm polverizzati in azoto liquido. L'aggiunta di SWCNH a PANI-DBSA ha condotto ad un aumento del coefficiente di Seebeck di circa il 30% rispetto a PANI-DBSA in tutto l'intervallo 25°C-60°C, con α compreso fra 6-7 μVK^{-1} . I valori di α del campione ottenuto per deposizione da CHCl_3 di PANI-DBSA/SWCNH sono risultati leggermente superiori a quelli misurati per PANI-DBSA/SWCNH. L'aggiunta del semiconduttore termoelettrico $\text{Bi}_{0.5}\text{Sb}_{1.5}\text{Te}_3$ a PANI-DBSA/SWCNH ha contribuito ad un ulteriore aumento del coefficiente di Seebeck con valori compresi fra 8-11 μVK^{-1} da temperatura ambiente a 60°C, quasi il doppio di α del polimero drogato con DBSA, coerentemente con l'alto valore di figura di merito di $\text{Bi}_{0.5}\text{Sb}_{1.5}\text{Te}_3$ a temperatura ambiente ($ZT \approx 1.8$). La presenza del termoelettrico $\text{Cu}_{12}\text{Sb}_4\text{S}_{13}$, ha comportato un lieve aumento di α (<10%) rispetto al campione contenente solo SWCNH.

Per quanto riguarda la conducibilità elettrica le differenze fra i valori delle varie composizioni sono più marcate e hanno tendenza inversa rispetto all'andamento di α . I valori di σ diminuiscono rispetto a quanto misurato per PANI-DBSA/SWCNH con la presenza di $\text{Bi}_{0.5}\text{Sb}_{1.5}\text{Te}_3$ e di $\text{Cu}_{12}\text{Sb}_4\text{S}_{13}$. In PANI-DBSA/SWCNH+BiSbTe sono stati misurati σ compresi fra 1.8 Scm^{-1} e 2.7 Scm^{-1} mentre in PANI-DBSA/SWCNH+CuSbS $\sigma \approx 3.8 \text{ Scm}^{-1} - 4.5 \text{ Scm}^{-1}$. Per le composizioni PANI-DBSA/SWCNH e PANI-DBSA/SWCNH da CHCl_3 i valori sono compresi fra 8 Scm^{-1} e 12.5 Scm^{-1} , compatibilmente con l'elevata conducibilità elettrica dei SWCNH.

I valori più bassi misurati per i compositi contenenti i semiconduttori termoelettrici possono essere ragionevolmente dovuti ad un effetto di rottura dello stacking π - π delle catene di polianilina dovuto alle polveri inorganiche intercalate fra le catene polimeriche. Nonostante le dimensioni dei cristalliti siano state stimate essere comprese fra 300-500nm, le polveri una volta disperse nella matrice polimerica tendono ad aggregare influenzando sulle interazioni inter catena della polianilina. La conducibilità elettrica e il coefficiente di Seebeck dei film PANI-DBSA/SWCNH ottenuti per deposizione da CHCl_3 e di PANI-DBSA/SWCNH ottenuto per trattamento termico della pasta PANI-DBSA sono simili. In particolare, σ tende a diminuire in maniera più marcata a $T > 40^\circ\text{C}$ per i film ottenuti da CHCl_3 . E' stato calcolato il fattore *power factor* ($\text{PF} = \alpha^2\sigma$) di $0.05 \mu\text{VK}^{-2}\text{m}^{-1}$ a $T = 30^\circ\text{C}$ per PANI-DBSA/SWCNH mentre per PANI-DBSA/SWCNH+BiSbTe e PANI-DBSA/SWCNH+CuSbS $\alpha^2\sigma$ è pari a $0.02 \mu\text{VK}^{-2}\text{m}^{-1}$. I valori sono coerenti con quanto riportato in letteratura per sistemi simili PANI/nanostrutture di carbonio (TAB1). La diffusività termica dei campioni PANI-DBSA, PANI-DBSA/SWCNH e PANI-DBSA/SWCNH+BiSbTe è stata misurata per $T = 30^\circ\text{C}$ e $T = 60^\circ\text{C}$ (figura 19).

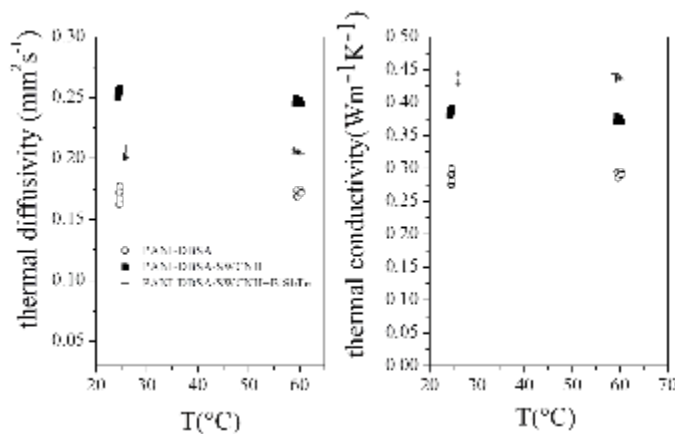


Figura 19 Valori di diffusività termica (λ) e conducibilità termica (κ) rispettivamente misurati e calcolati per PANI-DBSA, PANI-DBSA/SWCNH e PANI-DBSA/SWCNH+BiSbTe

La conducibilità termica è stata successivamente calcolata moltiplicando i valori di diffusività termica per la densità di ciascun campione e per il calore specifico determinato sperimentalmente per PANI-DBSA. L'andamento di λ è coerente con i valori di conducibilità elettrica stimati per i tre campioni considerati, con $\lambda = 0.26 \text{ mm}^2\text{s}^{-1}$ per PANI-DBSA/SWCNH, $\lambda = 0.20 \text{ mm}^2\text{s}^{-1}$ per PANI-DBSA/SWCNH+BiSbTe e $\lambda = 0.17 \text{ mm}^2\text{s}^{-1}$ per PANI-DBSA a $T = 30^\circ\text{C}$. A parità di calore specifico per i tre campioni e per la maggiore densità di PANI-DBSA/SWCNH+BiSbTe rispetto agli altri due campioni, la conducibilità di quest'ultimo è maggiore rispetto a quella di PANI-DBSA/SWCNH, con $\kappa = 0.43 \text{ Wm}^{-1}\text{K}^{-1}$ a $T = 30^\circ\text{C}$. Alla luce di quanto sopra discusso, le proprietà termoelettriche non hanno mostrato una forte dipendenza con la temperatura nell'intervallo $25^\circ\text{C} - 60^\circ\text{C}$.

La riproducibilità dei valori di σ , α e λ a parità di composizione è stata reputata soddisfacente, soprattutto se si considera il fatto che nei materiali polimerici le proprietà di trasporto sono molto sensibili al metodo di preparazione.

3.1.2 Prototipo di modulo termoelettrico

I compositi a base di PANI-DBSA/SWCNH e PANI-DBSA/SWCN+BiSb sono stati selezionati come materiale attivo per un prototipo di generatore termoelettrico (TEG). Essendo i termoelettrici polimerici quasi esclusivamente dei conduttori di tipo p, i prototipi sono stati concepiti come *uni-leg*, usando nichel come elettrodo e gamba n.

Dopo aver individuato i componenti ancillari del modulo e misurato la resistenza di contatto elettrico all'interfaccia composito/nichel, è stato condotto uno studio preliminare per prevedere la prestazione in termini di potenza teorica del modulo, considerando i dati ottenuti dalle caratterizzazioni funzionali sopra riportate.

I moduli sono stati successivamente testati ottenendo i valori della potenza in uscita a diversi ΔT .

Misure di resistenza di contatto elettrica

La resistenza di contatto specifica misurata in $\Omega \text{ cm}^2$ è la resistenza elettrica alla giunzione tra il materiale termoelettrico e l'elettrodo nei moduli termoelettrici. Essa è una quantità parassita in serie alla resistenza dei singoli elementi dei moduli termoelettrici per cui ne riduce le prestazioni.

L'apparato per la misura (figura 20) è costituito da un supporto per il campione a quattro contatti: due blocchi di argento tra i quali mettere il campione per la corrente, un terzo contatto per la misura nella tensione fisso sull'elettrodo del campione e un quarto contatto costituito da un sottile ago in carburo di tungsteno mobile.

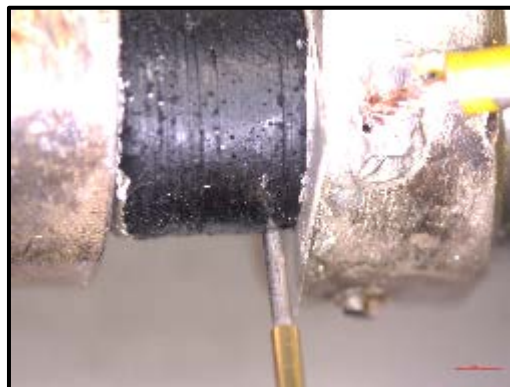


Figura 20 Pellet di PANI-DBSA/SWCNH fra i due blocchetti di argento nell'apparato per la misura della resistenza di contatto.

In figura 21 sono riportati due esempi di misure ottenute con risoluzione di $10 \mu\text{m}$ per due pellet di PANI-DBSA/SWCNH a cui è stata applicata ai lati la pasta di argento con l'elettrodo di nichel. La resistenza di contatto all'interfaccia viene ricavata come intercetta dell'asse delle resistenze.

E' stato determinato un valore medio di $10.1 \pm 4.5 \text{ m}\Omega \text{ cm}^{-2}$ di resistenza di contatto elettrico all'interfaccia polimero/nichel. La tecnica di misura permette di verificare la presenza di disomogeneità nei materiali. Come si vede nell'immagine in basso, infatti, la resistenza misurata ha un andamento a step ovvero la pendenza della retta aumenta improvvisamente per certi valori di spostamento dall'interfaccia. Nel caso di materiali compositi ciò può essere attribuito a disomogeneità puntuali nella dispersione dei filler ma anche a rotture locali dovute all'effetto della pressione dei cilindri d'argento sul pellet misurato. E' inoltre da sottolineare il fatto che l'elettrodo di nichel aderisce al polimero attraverso una pasta d'argento ed è quindi ragionevole attendersi una non perfetta distribuzione della pasta.

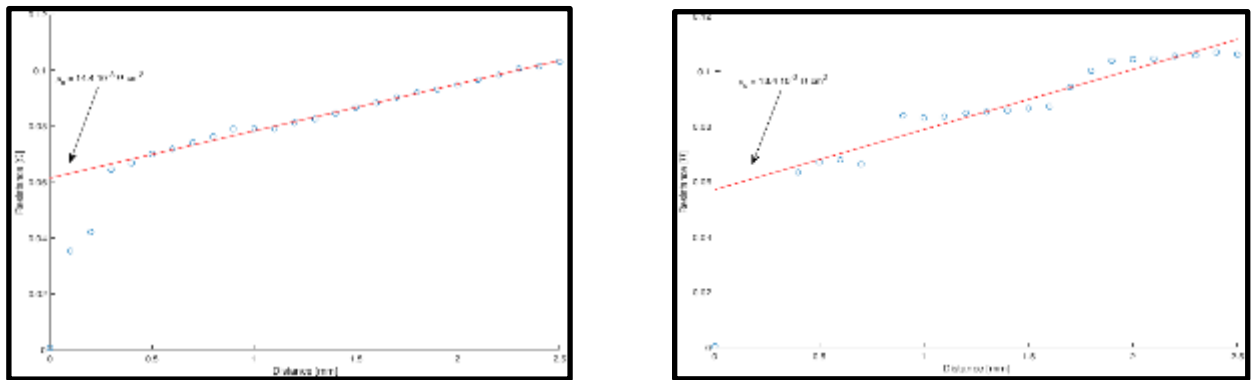


Figura 21. Misure di resistenza di contatto su un campione di PANI-DBSA/SWCNH con elettrodo in Ni e pasta di argento. La resistenza di contatto è ricavata come intercetta nell'asse delle resistenze.

Alla luce di quanto appena discusso era ragionevole prevedere valori di resistenza di contatto dell'ordine dei $\text{m}\Omega \text{ cm}^{-2}$, comparabili con la resistenza dei singoli elementi del modulo, fattore di cui tener conto nella stima della potenza in uscita.

Analisi numeriche per la valutazione delle prestazioni di moduli termoelettrici a base polimerica

La valutazione delle performance di un modulo termoelettrico può esser fatta risolvendo numericamente il sistema accoppiato di equazioni differenziali alle derivate parziali in T (temperatura) e V (potenziale elettrico) che governa il funzionamento dei moduli. In regime stazionario il sistema può essere descritto come

$$\nabla \cdot \mathbf{q} = Q \quad (1.1)$$

$$\nabla \cdot \mathbf{j} = 0 \quad (1.2)$$

dove flusso termico \mathbf{q} [W/m^2] e densità di corrente \mathbf{j} [A/m^2] sono legate ai gradienti di temperatura (∇T) e di potenziale (∇V) dalle seguenti relazioni costitutive, che comprendono flusso di Peltier e potenziale di Seebeck (effetti termoelettrici):

$$\mathbf{q} = P\mathbf{j} - k\nabla T \quad [2.1]$$

$$\mathbf{j} = \sigma(\mathbf{E} - \alpha\nabla T) = \sigma(-\nabla V - \alpha\nabla T) \quad [2.2]$$

dove P è il coefficiente di Peltier [V] e α è il coefficiente di Seebeck [V/K]; \mathbf{E} è l'intensità di campo elettrico [V/m]; in [1.1] la sorgente interna di calore $Q[\text{W}/\text{m}^3]$ è data da $Q=\mathbf{j}\cdot\mathbf{E}$. Le equazioni (1.1), (1.2)

definiscono un problema accoppiato termico ed elettrico di natura non lineare (effetto Joule, oltre alla dipendenza delle proprietà termoelettriche dalla temperatura), la cui soluzione si può ottenere per via numerica grazie a procedure di discretizzazione. Il metodo degli elementi finiti (FEM) si presenta come strumento versatile per sviluppare simulazioni multifisiche. Il metodo fornisce la soluzione del problema tramite il calcolo dei valori di temperatura e potenziale elettrico sui nodi di una mesh con la quale vengono discretizzate (figura 22a) le parti del modulo (elementi termoelettrici, connettori, eventuali componenti accessorie). Date in input la geometria del modulo, le proprietà dei materiali e le condizioni al contorno (valori di temperatura e potenziale e/o flussi termici in entrata e intensità di corrente), l'algorithmo permette di calcolare le distribuzioni di temperatura e potenziale elettrico come interpolazione dei valori nodali, tramite funzioni di forma polinomiali definite sugli elementi della mesh (gli *elementi finiti*). Da qui, vengono poi valutate le prestazioni dei moduli, in termini di potenza elettrica prodotta ed efficienza. Eventuali resistenze termiche / elettriche di contatto possono essere introdotte nel modello come proprietà di superficie all'interfaccia tra elemento termoelettrico e connettori (figura 22b).

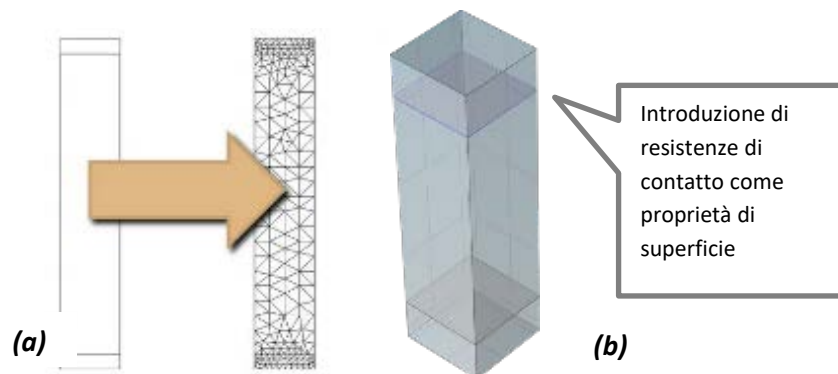


Figura 22: (a) Discretizzazione (mesh) di un elemento termoelettrico e dei connettori; (b) introduzione nel modello di resistenze di contatto alle interfacce per evitare layer sottili che renderebbero inutilmente fitta la mesh di calcolo.

Nel caso di moduli a base polimerica, considerazioni di compatibilità termoelettrica portano la progettazione del modulo ad una configurazione di tipo *uni-leg*, usando PANI come materiale di tipo p e connettori in Ni in sostituzione di semiconduttori di tipo n. Le proprietà termoelettriche (k , ρ , α) del polimero sono quelle del PANI-DBSA/SWCNH+BiSbTe; per gambe n / connettori si assumono le proprietà riportate in figura 23.

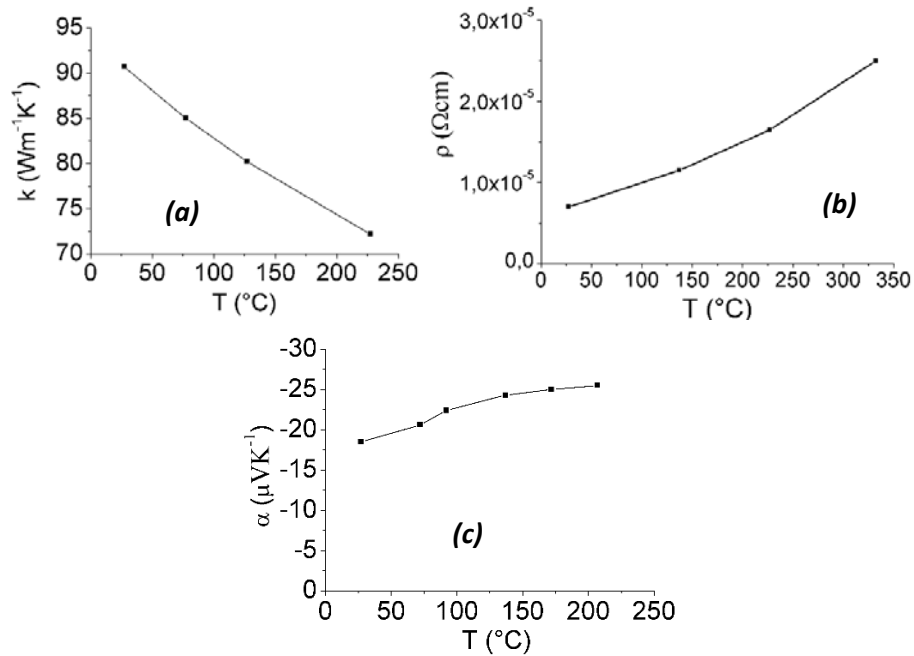


Figura 23: Conducibilità termica (a), resistività elettrica (b) e coefficiente di Seebeck (c) degli elementi in Ni.

La procedura numerica descritta permette di calcolare le distribuzioni di T e V nelle parti del modulo; in figura 24, tali distribuzioni vengono riportate per una singola coppia (sezione gamba p 4.0 mm x 4.0 mm, altezza 1.0 mm; sezione connettore 0.125 mm x 4.0 mm) in condizioni di circuito aperto, con $\Delta T=20$ K.

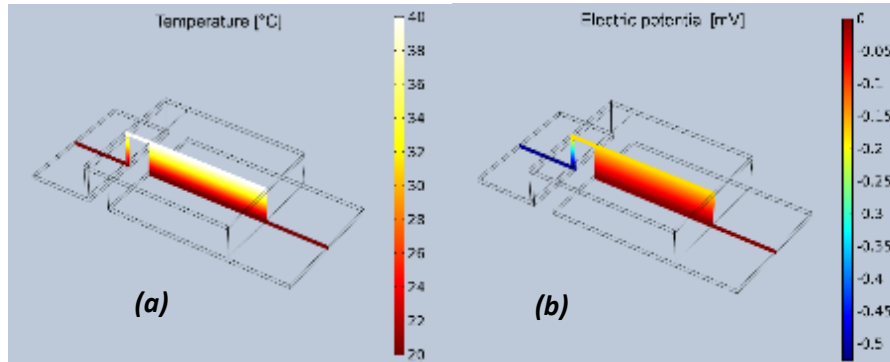


Figura 24: Distribuzione di temperatura (a) e potenziale elettrico (b) in una singola coppia polimero – connettore in Ni.

Lo sviluppo dell'analisi al variare della resistenza di carico applicata permette di valutare la potenza del modulo, tenendo conto anche delle resistenze elettriche di contatto. In tabella 3 vengono riportate le densità di potenza di un modulo unileg con fill factor $f=0.44$, per vari gradienti di temperatura (20 K, 40 K, 60 K, 80 K) e per due valori di resistenza di contatto ($6 \times 10^{-3} \Omega \text{cm}^2$ e $14.4 \times 10^{-3} \Omega \text{cm}^2$).

Tabella 3: Valori di densità di potenza ($\mu\text{W}/\text{cm}^2$) per diversi gradienti termici e con due differenti valori di resistenza di contatto elettrico. Potenza p_{out} [$\mu\text{W}/\text{cm}^2$], modulo unileg $f=0.44$

	$\Delta T = 20$ K	$\Delta T = 40$ K	$\Delta T = 60$ K	$\Delta T = 80$ K
$\rho_{\text{cc}} = 6 \times 10^{-3} \Omega \text{cm}^2$	0.6	2.6	5.8	10.3

$\rho_{cc} = 14.4 \times 10^{-3}$ Ωcm^2	0.5	2.0	4.4	7.8
--	-----	-----	-----	-----

I valori presentati in tabella 3 sono da considerarsi come limiti teorici, essendo presenti nella realtà resistenze di contatto termico non considerate nelle simulazioni presentate. Tali resistenze dovranno essere caratterizzate in un ulteriore studio.

Costruzione del prototipo di generatore termoelettrico

Gli elementi p del prototipo TEG sono stati ottenuti per deposizione su stampi della pasta a base di polianilina e acido dodecilbenzensolfonico, come descritto nella parte di sintesi dei materiali compositi PANI-DBSA. Il modulo a base di PANI-DBSA/SWCNH+BiSbTe è stato costruito a partire da elementi quadrati 4x4 mm di lato con spessore di circa 1.0 ± 0.3 mm. Ogni elemento è stato connesso attraverso una lamina di nichel dello spessore di 0.125 mm per un totale di 16 elementi connessi (4x4 elementi) utilizzando pasta di argento per far aderire la superficie del materiale attivo all'elettrodo (figura 25)

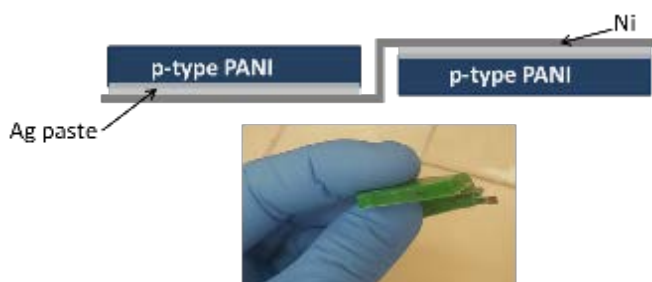


Figura 25 Rappresentazione schematica del modulo uni-leg ottenuto connettendo attraverso una lamina di nichel due gambe p di materiale a base di PANI-DBSA e fotografia del modulo inglobato in matrice siliconica.

Il modulo è stato poi inglobato in una matrice siliconica protettiva per conferire un certo grado di flessibilità al TEG, come mostrato in figura 24, ottenendo un quadrato di 2.5x2.5 cm di lato con spessore 3.5 mm. Il TEG costituito da PANI-DBSA/SWCNH è stato fabbricato in maniera simile, ma con differenti dimensioni e geometria delle gambe p : 3x3 pellet tondi del diametro di 4mm con spessore 1.8 ± 0.3 mm. Le dimensioni del modulo inglobato in matrice siliconica sono 2.5x2.5cm di lato con spessore 3.9 mm.

Test dei prototipi

Le potenze in uscita dei due dimostratori a base di PANI-DBSA/SWCNH e PANI-DBSA/SWCNH+BiSbTe sono state misurate per mezzo di un'apposita stazione di test schematizzata in figura 26

La stazione di test si compone essenzialmente di una camera da vuoto che comprende il riscaldatore, il modulo da testare e il parallelepipedo di alluminio utilizzato per la misura del flusso termico, oltre che dell'elettronica necessaria per il controllo, la misura e l'archiviazione dei dati. Sono state determinate le curve corrente-potenziale (I-V) e corrente-potenza in uscita (I-P) per ciascun prototipo mantenendo il lato freddo a temperatura ambiente e variando progressivamente la temperatura del lato caldo. In figura 27 sono riportati gli andamenti di I-V e I-P a diversi valori di ΔT . per il modulo a base di PANI-DBSA/SWCNH e in figura 28 il voltaggio a circuito aperto (V_{oc}) e la corrente di corto circuito (I_{sc}) per entrambi i prototipi.

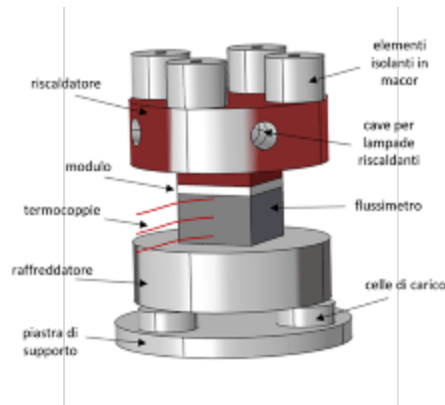


Figura 26 Rappresentazione schematica della stazione di test utilizzata per misurare la potenza in uscita dei due prototipi di TEG

Il TEG a base di PANI-DBSA/SWCNH+BiSbTe è stato testato fino a $\Delta T=80^{\circ}\text{C}$ ($T_{\text{max}}=100^{\circ}\text{C}$) mentre PANI-DBSA/SWCNH a temperature prossime a quella ambiente, con $\Delta T_{\text{max}}=18.1^{\circ}\text{C}$ e temperatura massima del lato caldo di 35°C . Per PANI-DBSA/SWCNH, V_{oc} è pari a 2mV con resistenza $R= 1.66 \Omega$ e potenza massima $P= 0.63 \mu\text{W}$ a $\Delta T=18.1^{\circ}\text{C}$. In PANI-DBSA/SWCNH+BiSbTe, per $\Delta T=19.5^{\circ}\text{C}$, $V_{\text{oc}}= 1.6\text{mV}$, $R= 6.17 \Omega$ e $P=0.01 \mu\text{W}$. La resistenza interna è maggiore di quasi 4 volte rispetto al modulo non contenente $\text{Bi}_{0.5}\text{Sb}_{1.5}\text{Te}_3$, coerentemente con i valori di conducibilità elettrica di circa 5 volte maggiori misurati nel materiale PANI-DBSA/SWCNH. Inoltre si deve tener conto anche dell'alta resistenza di contatto elettrico all'interfaccia elettrodo/polimero misurata. In figura 29 sono riportate le potenze massime in uscita per unità di area dei due prototipi in funzione di ΔT . In PANI-DBSA/SWCNH per $\Delta T=9.6^{\circ}\text{C}$ è stata misurata una potenza di $31\text{nW}/\text{cm}^2$ mentre a $\Delta T=18.1^{\circ}\text{C}$ $P= 100\text{nW}/\text{cm}^2$. In PANI-DBSA/SWCNH+BiSbTe le potenze per $\Delta T=10^{\circ}\text{C}$ e $\Delta T=19.5^{\circ}\text{C}$ risultavano essere rispettivamente di $4\text{nW}/\text{cm}^2$ e $16\text{nW}/\text{cm}^2$ mentre a $\Delta T=80^{\circ}\text{C}$ $P=280\text{nW}/\text{cm}^2$. Rispetto ai valori teorici calcolati considerando le proprietà termoelettriche dei materiali qui proposti e riportati in tabella 3, i valori di potenza per PANI-DBSA/SWCNH+BiSbTe sono di circa un ordine di grandezza inferiori. Questo è dovuto alle alte resistenze di contatto termico ed elettrico all' interfaccia elettrodo-gamba del modulo. Inoltre bisogna tener conto della deformazione e compressione che le gambe subiscono per la pressione applicata nella stazione di test che possono portare ad eventuali rotture del contatto elettrico.

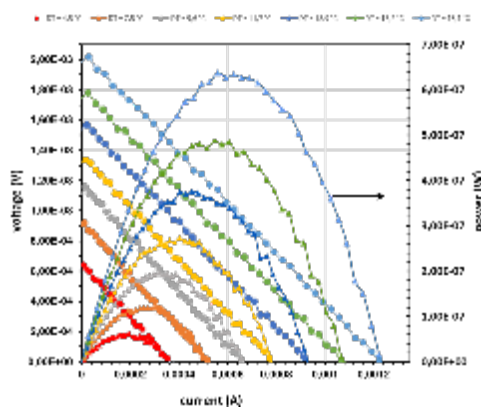


Figura 27 Curve I-V e I-P a diversi valori di ΔT per il modulo costituito da 3x3 elementi di PANI-DBSA/SWCNH connessi con lamina di nichel in matrice silconica

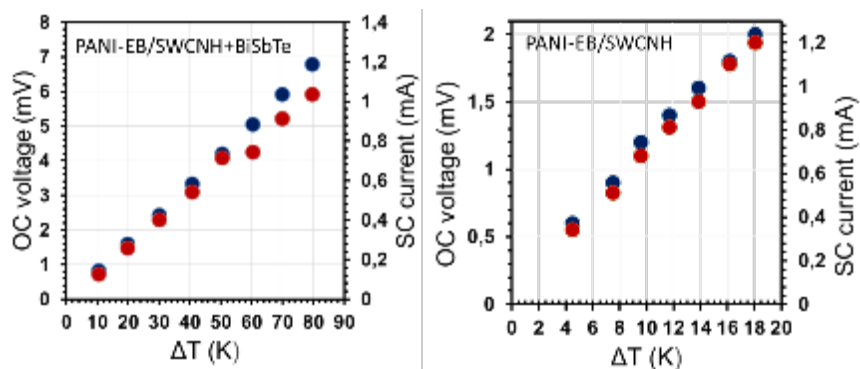


Figura 28 Voltaggio a circuito aperto (OC Voltage, blu) e corrente di corto circuito (SC current, rosso) in funzione della differenza fra lato caldo e lato freddo per PANI-DBSA/SWCNH (modulo con 9 gambe) e PANI-DBSA/SWCNH+BiSbTe (modulo con 16 gambe)

In letteratura è stato riportato un valore di potenza per unità di area pari a circa 400 nW/cm^2 a $\Delta T=20\text{K}$ per un TEG a geometria pi-greco costituito da 35 termocoppie con *packing density* di 0.40 dove il materiale attivo è a base dei composti di coordinazione con leganti tetratiolato poly[Na_x(Ni-ett)] poly[Cu_x(Cu-ett)] come gambe p e n rispettivamente. Un altro esempio in letteratura è costituito dal TEG ottenuto assemblando 55 termocoppie con gambe di spessore pari a $30 \mu\text{m}$ di PEDOT-Tos dal derivato del tetratiafulvalene /TTF-TCNQ avente *packing density* di 0.47 e densità di potenza a $\Delta T=10\text{K}$ pari a 22 nW/cm^2 .

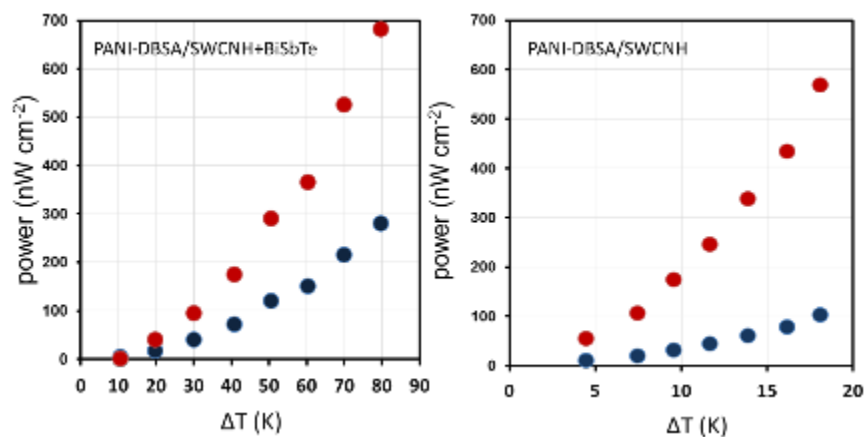


Figura 29 Potenza massima in uscita per i due prototipi PANI-DBSA/SWCNH e PANI-DBSA/SWCNH+BiSbTe costituiti rispettivamente da 9 gambe tonde di diametro 4mm x 1.8 mm di spessore e 16 gambe quadrate 4mmx4mm x1 mm. In rosso sono i valori estrapolati considerando il parametro *packing density* definito come il rapporto fra la sommatoria dell'aria di tutte le gambe e l'area totale del modulo.

3.2) Confronto con i risultati attesi

I risultati attesi sono stati ampiamente conseguiti.

Sono stati sintetizzati due tipi di compositi a base del polimero polianilina con due droganti differenti: acido canforsulfonico (CSA) e acido dodecilbensulfonico (DBSA). In seguito ad un'estensiva caratterizzazione termoelettrica, i materiali del tipo PANI-DBSA hanno mostrato migliori prestazioni in termini di *power factor* ($\alpha^2\sigma$). Un valore di $0.05 \mu\text{Wm}^{-1}\text{K}^{-2}$ è stato infatti ottenuto per il composito PANI-DBSA/SWCNH, valore prossimo al target di $0.1 \mu\text{Wm}^{-1}\text{K}^{-2}$. Inoltre, è stata verificata la riproducibilità sia dei valori del coefficiente di Seebeck che della conducibilità elettrica per diversi campioni con uguale composizione, parametro molto importante quando si lavora con materiali termoelettrici organici. Uno degli obiettivi era l'individuazione di un processo di sintesi dei suddetti compositi che fosse semplice e

veloce. La procedura di sintesi testata, che non prevedeva l'utilizzo di solventi ma il semplice mescolamento meccanico dei precursori e loro dispersione in acido dodecilbenzensolfonico, ha soddisfatto tali requisiti. Attraverso tale metodo infatti, è stato possibile ottenere il materiale su forma di pellet di diverse dimensioni estrudendo la pasta su stampi o spalmandola su substrati rigidi in vetro, teflon o allumina per ottenere film di poche decine di μm . Per migliorare l'interazione ohmica polimero/filler, i precursori SWCNH, DBSA e PANI sono stati processati in solvente organico in maniera tale da rendere più omogenea la distribuzione dei SWCNH nella matrice polimerica, prevedendo ragionevolmente un'aumento del *power factor*. Per i compositi così sintetizzati sono state osservate una morfologia e microstruttura molto simili ai materiali ottenuti senza solvente come anche i valori di α e σ misurati. Il processo in soluzione non ha dunque portato un aumento di $\alpha^2\sigma$. Una volta ottimizzata la parte di sintesi e caratterizzazione del materiale, l'attività prevedeva l'assemblaggio di un dimostratore termoelettrico. Dopo l'individuazione dei componenti ancillari (nichel come elettrodo/gamba n e pasta di argento per il contatto nichel/PANI), è stata valutata la resistenza di contatto elettrico all'interfaccia polimero/elettrodo. Tenendo conto dei valori di resistenza di contatto e dei dati ottenuti nella parte di caratterizzazione elettrica, sono stati calcolati i limiti teorici di potenza in uscita tramite modellazione FEM effettuata con Comsol. Per un modulo a base di PANI-DBSA/SWCNH+BiSbTe è stata prevista una densità di potenza compresa fra $0.5\text{-}0.6\mu\text{W}/\text{cm}^2$ a $\Delta T=20\text{K}$ mentre per gradienti termici più alti i valori calcolati sono $> 1\mu\text{W}/\text{cm}^2$, **in linea con gli obiettivi prefissati**.

Calcolata la potenza teorica, sono stati assemblati con successo **due dimostratori** a base di PANI-DBSA/SWCNH+BiSbTe e PANI-DBSA/SWCNH. La densità di potenza in uscita per il TEG a base di PANI-DBSA/SWCNH misurata era pari $0.1\mu\text{W}/\text{cm}^2$ per $\Delta T=18.1\text{ }^\circ\text{C}$, mentre nel caso di PANI-DBSA/SWCNH+BiSbTe $P=0.02\mu\text{W}/\text{cm}^2$ a $\Delta T=20\text{ }^\circ\text{C}$. I valori ottenuti sono migliorativi rispetto a quanto riportato in letteratura.

3.3) Criticità

Non sono state evidenziate criticità rispetto agli obiettivi previsti.

3.4) Eventuali scostamenti rilevanti e aggiustamenti

Non si sono evidenziati scostamenti o aggiustamenti necessari.

3.5) Deliverables

D_1.5: Report Tecnico contenente tutti i risultati delle attività di ricerca condotte:

Moduli termoelettrici a base polimerica leggeri, con discreto grado di flessibilità per l'integrabilità in dispositivi nell'ambito della wearable electronics-wireless sensor networks, con power factor compreso tra 1 e $3\mu\text{Wm}^{-1}\text{K}^{-2}$.

3) Conclusioni

È stato messo a punto con ottimi risultati un **processo solvent-free** per la preparazione di un materiale termoelettrico composito organico-inorganico a base polimerica.

Grazie alla procedura di preparazione, il composito ottenuto PANI-DBSA ha la consistenza di una pasta, e mostra **alta lavorabilità in tutte le fasi di fabbricazione del modulo**.

Per quanto riguarda la parte di sintesi del materiale, il metodo di fabbricazione è veloce e potenzialmente scalabile, e potrebbe essere ulteriormente migliorato modificando a livello molecolare i precursori al fine di incrementare ulteriormente il parametro $\alpha^2\sigma$. Per aumentare α e σ è necessario migliorare l'interazione all'interfaccia polimero/filler inorganico. Il contatto ohmico fra i SWCNH e le catene di polianilina può essere migliorato polimerizzando direttamente l'anilina in presenza delle nanostrutture di carbonio che fungono da template. Nonostante questo passaggio allunghi i tempi di fabbricazione del materiale e richieda l'utilizzo di ulteriori precursori e la messa a punto di un nuovo processo di produzione, l'aumento della conducibilità elettrica può portare a valori di PF superiori al target di $0.1-0.5 \mu\text{VK}^{-2}\text{m}^{-1}$. Per diminuire ulteriormente la resistenza interna, può essere migliorato il contatto elettrico fra l'elettrodo e gli elementi a base polimerica. Una delle strategie è quella di impiegare elettrodi più flessibili della lamina di nichel. Una possibilità consiste nell'utilizzare strisce di kapton su cui depositare layer metallici altamente conduttivi. Alla maggiore flessibilità delle strisce, che si traduce in una migliore adattabilità alla superficie del pellet polimerico e ad una conseguente migliore adesione al materiale polimerico, si accoppierebbe una desiderabile diminuzione della densità del modulo.

*Si sottolineano i seguenti risultati come **industrializzabili** per la tecnologia «wearable TEG» :*

- *processo di formatura facile e veloce* → si ottiene un materiale flessibile e lavorabile per grandi superfici (decine di cm^2)
- *materiale leggero* → composito p-type PANI-DBSA = 30v % + 17v % $\text{Bi}_{0.5}\text{Sb}_{1.5}\text{Te}_3 \approx 0,3 \text{ g/cm}^2$
- $PF = 1.5 \cdot 10^{-2} \mu\text{Wm}^{-1}\text{K}^{-2}$ → in linea con i migliori risultati di letteratura

4) Apparecchiature utilizzate

- Glove box (MBraun UniLab);
- Mulino planetario (Pulverisette 5, Fritsch);
- Termogravimetria e calorimetria a scansione differenziale (TG-DSC, SDT Q 600 Apparatus TA Instrument)
- Sistema di analisi dei gas residui (RGAHPR20 QIC-Hiden Analytical)
- Microscopio elettronico a scansione (FE-SEM Sigma Zeiss) con sistema di analisi EDS (Oxford X-Max);
- Laser Flash per analisi di conducibilità termica (Netzsch LFA 457 MicroFlash®);
- Stazione di misura della resistività elettrica e del coefficiente di Seebeck
- Stazione di misura della resistività in piano su film col metodo Van Der Pauw
- Stazione di misura per il test dei moduli termoelettrici
- Stazione di misura della resistenza elettrica di contatto

5) Profili delle risorse umane impegnate

- Ricercatore con laurea in Chimica
- Ricercatore con laurea in Fisica
- Ricercatore con Laurea in Scienza dei Materiali
- Collaboratore tecnico/tecnico laureato con laurea in Chimica o Ingegneria Meccanica
- Ricercatore con laurea in Ingegneria
- Dirigente di Ricerca con laurea in Chimica

6) Diffusione dei risultati

Pubblicazioni

- 1) A. Famengo, A. Ferrario, S. Boldrini, S. Battiston, S. Fiameni, C. Pagura, M. Fabrizio, 9th ECNP International Conference on Nanostructured Polymers and Nanocomposites, Rome 2017, 19-21 September *Polyaniline – carbon nanohorn composites as thermoelectric materials*. (Poster)
- 2) A. Famengo, A. Ferrario, S. Boldrini, S. Battiston, S. Fiameni, C. Pagura, M. Fabrizio *Polyaniline – carbon nanohorn composites as thermoelectric materials* Polym. Int (2017) 66, 1725
- 3) A. Famengo, A. Ferrario, S. Boldrini, S. Battiston, S. Fiameni, C. Pagura, M. Fabrizio, Giornate sulla Termoelettricità GiTe, Torino, 2017 22-23 February *Polyaniline – carbon nanohorn composites as thermoelectric materials (Presentazione orale, premio Associazione Italiana Termoelettricità come miglior presentazione-giovani ricercatori)*
- 4) A. Famengo, A. Ferrario, S. Boldrini, S. Battiston, L. Crociani, S. Fiameni, C. Pagura, M. Fabrizio, EMRS-Spring Meeting, Strasbourg 2017, 21-26 May *Polyaniline-based composites as thermoelectric materials*. (Poster)
- 5) A. Famengo, S. Rossi, P. Bison, S. Boldrini *Thermal conductivity characterization of polyaniline doped material for thermoelectric applications Proc. of SPIE (2017) 10214. (Proceeding di conferenza SPIE- The International Society for Optical Engineering)*
- 6) A. Famengo, A. Ferrario, S. Boldrini, S. Battiston, S. Fiameni, C. Pagura, M. Fabrizio, 15th European Conference on Thermoelectrics, Padova , 2017, September 25-27 *Polyaniline-carbon nanohorn composites as thermoelectric materials* (Presentazione orale)
- 7) A. Famengo, A. Ferrario, S. Boldrini, S. Battiston, S. Fiameni, C. Pagura, M. Fabrizio, Conferenza di Dipartimento DSCTM Department of Chemical Sciences and Materials Technology , Alghero, 2017, October 19-20 *Polyaniline-carbon nanohorn composites as thermoelectric materials* (Presentazione orale)

Organizzazione di eventi

- 1) 15th European Conference on Thermoelectrics , Padova 25-27 settembre 2017. *Program Co-Chair*: M. Fabrizio, S. Boldrini, S. Battiston, S. Fiameni. *Local committee* (CNR-ICMATE): S. Battiston, S. Boldrini, M. Fabrizio, S. Fiameni, A. Famengo, C. Fanciulli, A. Ferrario, A. Miozzo. *International committee*: A. Weidenkaff (Stuttgart Univ.), F. Gascoin (Cristmat), D. Narducci (Univ. of Milan-Bicocca), J. König (Fraunhofer), A. Burkov (Ioffe Phys. Technic Inst.), M. Fabrizio (CNR-ICMATE), A.P. Gonçalves (Lisbon Univ.), J. Grin (Max Planck), B. Lenoir (Inst. J. Lamour), A. Maignan (Cristmat), G. Min (Univ. of Cardiff), E. Müller (DLR), P. F. Rogl (Wien Univ.), K. Wojciechowski (AGH UST).